IN-18
84730
p.257
NAS8-36426

D180-30550-1

Final Report

SPACE STATION INTEGRATED WALL DESIGN AND PENETRATION DAMAGE CONTROL

by

A.R. Coronado, M.N. Gibbins, M.A. Wright, and P.H. Stern

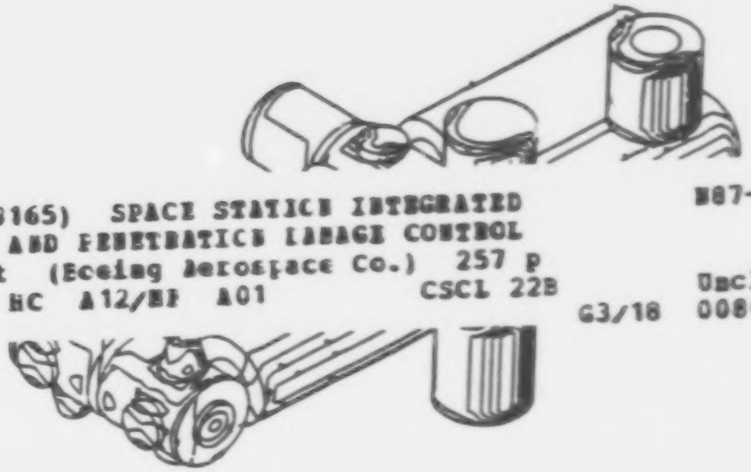

(NASA-CR-179165) SPACE STATION INTEGRATED WALL DESIGN AND PENETRATION DAMAGE CONTROL Final Report (Boeing Aerospace Co.) 257 p Avail: NTIS HC A12/MF A01 CSCL 22B
N87-28581
Unclas
G3/18 0084730

Prepared for

National Aeronautics and Space Administration

July 1987

Contract NAS8-36426

Technical Management
NASA George C. Marshall Space Flight Center
Marshall Space Flight Center, Alabama
Structures and Dynamics Laboratory
Sherman L. Avans

Boeing Aerospace Company
Seattle, Washington

D180-30550-1

Final Report

SPACE STATION INTEGRATED WALL DESIGN AND PENETRATION DAMAGE CONTROL

by

A. R. Coronado, M. N. Gibbins, M. A. Wright, and P. H. Stern

Prepared for

National Aeronautics and Space Administration

July 1987

Contract NAS8-36426

Technical Management
NASA George C. Marshall Space Flight Center
Marshall Space Flight Center, Alabama
Structures and Dynamics Laboratory
Sherman L. Avans

Boeing Aerospace Company
Seattle, Washington

SPACE STATION INTEGRATED WALL DESIGN AND PENETRATION DAMAGE CONTROL

by

A. R. Coronado, M. N. Gibbins, M. A. Wright, and P. H. Stern

ABSTRACT

A methodology has been developed to allow a designer to optimize the pressure wall, insulation, and meteoroid/debris shield system of a manned spacecraft for a given spacecraft configuration and threat environment. The threat environment consists of meteoroids and orbital debris, as specified for an arbitrary orbit and expected lifetime. An overall probability of no penetration is calculated, as well as contours of equal threat that take into account spacecraft geometry and orientation. Techniques, tools, and procedures for repairing an impacted and penetrated pressure wall have been developed and tested. These techniques are applied from the spacecraft interior and account for the possibility of performing the repair in a vacuum. Hypervelocity impact testing has been conducted to (1) develop and refine appropriate penetration functions and (2) determine the internal effects of a penetration on personnel and equipment.

KEY WORDS

Design Optimizing
Hypervelocity Impact
Meteoroids
Modeling
Orbital Debris
Penetration Analysis
Penetration Codes
Regression
Repair Techniques
Space Station
Testing
Threat Analysis

FOREWORD

This report presents the work accomplished by The Boeing Company from 3 June 1985 to 5 August 1987 on "Space Station Integrated Wall Design and Penetration Damage Control," NAS8-36426. The work was administered under the direction of Mr. Sherman L. Avans, Structures Development Branch of the Structures and Dynamics Laboratory, NASA George C. Marshall Space Flight Center.

We want to express our appreciation to Mr. Avans for his encouragement and contributions on this contract, and to Ms. Jennifer Horn for her support. We also wish to thank Mr. Roy Taylor for his efficient direction of the MSFC hypervelocity impact test laboratory. His help was instrumental in enabling us to modify and expand our testing program as the need arose.

CONTENTS

Page

SUMMARY 1

INTRODUCTION 3

1.0 REFERENCE CONFIGURATION 5
- 1.1 Representative Baseline 5
- 1.2 Module Pattern 5
- 1.3 Integrated Wall Design 5

2.0 ENVIRONMENT 9
- 2.1 Debris Environment 9
- 2.2 Meteoroid Environment 12
- 2.3 Uncertainties in the Environment Definition 15
- 2.4 Environment Sensitivity Studies 16
- 2.5 Flux Definition Uncertainty 16
- 2.6 Debris Penetration Function Uncertainty 16
- 2.7 Exposure Duration Sensitivity 18
- 2.8 Impact Angle and Velocity Probability Distribution 18
- 2.9 PNP Requirement 18
- 2.10 Future Flux Environment 21
- 2.11 Conclusions 23

3.0 HYPERVELOCITY IMPACT TESTING 25
- 3.1 Data Base From Preceding Studies 25
- 3.2 Additional Testing for Penetration Analysis - Task 1 25
- 3.3 Task 2 Testing for Effects of Penetration 28

4.0 WALL DAMAGE CHARACTERIZATION AND PENETRATION CRITERIA 37
- 4.1 Task 1 Data Analysis 37
- 4.2 Lexan Projectiles 47
- 4.3 Multiple Variable Linear Regression 53
- 4.4 Backwall Failure Definition 63
- 4.5 Impact Testing of Alternative Shield Materials 68
- 4.6 Single and Double Shield Test Results Comparison 74

Page

4.7 Total Penetration Function 80
4.8 Phenomenological Penetration Function - PEN4 84
4.9 Single Plate Penetration Function 88

5.0 INTERNAL EFFECTS OF PENETRATION 91

5.1 Task 2 Data Analysis - Transient Effects 91

5.2 Physiological Effects of Pressure Loss 91

6.0 REPAIR TECHNIQUES 95

6.1 Patch Methods Developed and Their Applications 97
6.2 Repair Tools Developed 101
6.3 Patch Application Demonstrated 103
6.4 Rubber Ring Patch Application 107
6.5 Conclusions of Laboratory Patch Demonstration 114
6.6 Neutral Buoyancy Simulations 116
6.7 Patch Materials 116

7.0 DESIGN EVALUATION COMPUTER CODE 119

7.1 Building the Space Station Model 121
7.2 Hidden Surface Algorithm 121
7.3 Approach to Modeling Orbital Debris 123
7.4 Approach to Modeling Meteoroids 125
7.5 Penetration Function 126
7.6 Design Analysis Computer Code 128
7.7 Model Generation 128
7.8 GEOMETRY Module 128
7.9 RESPONSE Module 130
7.10 BUMPER Module 130
7.11 CONTOUR Module 130
7.12 Analysis Results 132
7.13 Orientation Sensitivity Study 132
7.14 Theory 135

Page

8.0 DESIGN GUIDE 137

8.1 Integrated Wall Design 137
8.2 Module Configuration 142
8.3 Module Pattern 144

9.0 CONCLUSIONS 147

REFERENCES 151

APPENDIX A - Test Data Summary A1

APPENDIX B - Test Report - Neutral Buoyancy Simulation of Pressure Wall Repair B1

APPENDIX C - Data Base for Linear Regression C1

APPENDIX D - Test Specimen Hardware Drawings D1

APPENDIX E - Physiological Effects of Decompression E1

APPENDIX F - Effectiveness of Composites as Meteoroid/Debris Shields F1

APPENDIX G - Mathematical Derivations of Analysis Method G1

APPENDIX H - Sensitivity Analyses From Linear Regression Penetration Function H1

APPENDIX I - Physiological Significance of Sound and Noise Data I1

APPENDIX J - Test Data Compared With Regression Function J1

FIGURES

Page

1.1-1 Reference Configuration Module Pattern 6
1.3-1 Space Station Common Module Reference Configuration 6

2.1-1 Debris Flux Equation Environment 10
2.1-2 Debris Velocity Probability Distribution 10
2.1-3 Transforming Velocity Distribution to Angle Distribution 11
2.1-4 Comparison of Angle Density Functions 11
2.2-1 Meteoroid Environment Model 13
2.2-2 Corrections for Geocentric Meteoroid Model 13
2.2-3 Meteoroid Impact Velocity Distribution Relative to Space Station 14
2.5-1 Flux Uncertainty Sensitivity Study 17
2.6-1 Penetration Function Sensitivity Study 17
2.7-1 Orbit Time Sensitivity Study 19
2.7-2 Orbit Time versus Weight Sensitivity Study 19
2.8-1 Impact Angle Probability Distribution 20
2.8-2 Impact Velocity Probability Distribution 20
2.10-1 Comparison of Current and Future Debris Environment 22
2.10-2 Effect of Proposed Flux and Baseline Design Configuration 22
2.10-3 Comparison of Weight for Constant Probability of No Penetration 24

3.2-1 Module Design Data Comparison With Test Data 26
3.2-2 Task 1 Test Summary 27
3.2-3 Task 1 Test Configuration and Definition 29
3.2-4 Task 1 Test Article in the Test Chamber 29
3.2-5 Normalized Penetration Witness Plates Penetrated Converted to Equivalent Back Wall Thickness 30
3.2-6 Task 1 Test Series 201 31
3.2-7 Task 1 Test Series 202 31
3.3-1 Effects of Penetration Test Chamber and Setup 33
3.3-2 Task 2 Test Configuration Summary 34

Page

3.3-3 Task 2 Effects of Penetration Testing Instrumentation 34
3.3-4 Task 2 Instrumentation Setup Inside the Large Test Chamber Behind the Witness Panel 35
3.3-5 Task 2 Test Article, Pressure Transducers, and Photodiodes Inside Large Test Chamber 35

4.1-1 Test Results Comparison for Effect of Impact Angle on Damage to Backwall 38
4.1-2 Impact Angle Effect on Backwall Damage for Tests With 0.063-in Shields, 4-in Spacing, 0.125-in Backwall, and MLI; 0.250-in Diameter Projectile 39
4.1-3 Impact Angle Effect on Backwall Damage for Tests With 0.063-in Shields, 4-in Spacing, 0.125-in Backwall, and MLI; 0.300-in Diameter Projectile 40
4.1-4 Impact Angle Effect on Backwall Damage for Tests with 0.063-in Shields, 4-in Spacing, 0.125-in Backwall, No MLI; 0.250-in Diameter Projectile 42
4.1-5 Test Results Comparison for Effect of Shield Thickness on Damage to Backwall 44
4.1-6 Shield Thickness Effect on Backwall Damage for Tests With 4-in Spacing, 0.125-in Backwall, and MLI; 0.250-in Diameter Projectile at 45-deg Impact Angle 45
4.1-7 Shield Thickness Effect on Backwall Damage for Tests With 4-in Spacing, 0.125-in Backwall, With MLI; 0.300-in Diameter Projectile at 65-deg Impact Angle 46
4.1-8 Test Results Comparison for Effect of MLI on Damage to Backwall 48
4.1-9 MLI Effect on Backwall Damage for Tests With 0.080-in Shields, 4-in Spacing, 0.188-in Backwall, 0.313-in Diameter Projectile at 0-deg Impact Angle 49
4.1-10 MLI Effect on Backwall Damage for Tests With 0.080-in Shields, 4-in Spacing, 0.188-in Backwall, 0.313-in Diameter Projectile at O-deg Impact Angle 50
4.1-11 Multilayer Insulation (MLI) Damage From Hypervelocity Impact, Test 210B 51
4.1-12 Shield Blowback During Impact Tests With MLI 51
4.2-1 Lexan Projectile Impacts, 0.040-in Shields, 4-in Spacing, 0.125-in Backwall, No MLI 52
4.3-1 Development and Use of a Multiple Variable Linear Regression Penetration Function 54
4.3-2 Assessment of the Multiple Linear Regression Technique 55

Page

4.3-3 A Sample of Variables Used in the Multiple Linear Regression Studies 55
4.3-4 Variables Included in Best Fit Penetration Functions as Determined by BMDP 9R 57
4.3-5 Analysis for Optimum Number of Regression Variables 58
4.3-6 BMDP-Derived Penetration Function in 11 Variables 59
4.3-7 MLI Advantage As Indicated by Linear Regression Penetration Function 60
4.3-8 Early Regression Equation 64
4.4-1 Spall Factor Derived From Nonpenetrating Hypervelocity Impact Tests 66
4.4-2 Penetration Threshold Factor Derived From Near Penetration Threshold Data 67
4.5-1 Comparison Between Test Damage and Analysis Predictions for Alternative Shield Materials 69
4.5-2 Kevlar Shield Penetration Resistance Compared to Aluminum Shield Penetration Resistance 71
4.5-3 Comparison Between Test Damage and Analysis Predictions for Kevlar Shield Material 72
4.5-4 Damage Comparison - Kevlar Versus Aluminum Shields 73
4.6-1 Double Shield Versus Single Shield Configuration Penetration Resistance Comparison 75
4.6-2 Double Shield Versus Single Shield With MLI Penetration Resistance Comparison 77
4.6-3 Double Shield Versus Single Shield Configuration Penetration Resistance Comparison 78
4.6-4 Double Shield Versus Single Shield Configuration Penetration Resistance Comparison 79
4.6-5 Configuration Comparison 81
4.7-1 Overview of Single and Double Wall Penetration Functions Available in BUMPER 82
4.7-2 Ballistic Range (PEN4) Penetration Function 83
4.7-3 Shatter Range (Burch Equations) Penetration Function 85
4.7-4 Melt/Vaporize Range (Wilkinson) Penetration Function 86
4.7-5 Normal Impact Correlation 87
4.8-1 Analytical Hypervelocity Impact Penetration Function Prediction/Test Data Comparison 89
4.9-1 Comparison of Penetration Resistance to Meteoroids of Single Wall and Double Wall Structures 90

Page

5.1-1 Transient Effects of Penetration Within a Pressurized Cabin 93
5.2-1 Effects of Pressure Wall Penetration on Crew Physiology 94

6.0-1 On-Orbit Repair of Integrated Common Module Wall 96
6.1-1 Space Station Pressure Wall Repair Concept Summary 98
6.1-2 Space Station Layered Patch Repair Technique 99
6.1-3 Alternative Concept Multilayered Patch 99
6.1-4 Rubber Ring Patch Design 100
6.1-5 Rubber Ring Patch Alternative Application Methods 100
6.2-1 Repair Tools and Patches 102
6.2-2 Required Existing Tools From the Space Transportation System Inventory 102
6.2-3 Organization of Space Station Wall Repair Tools 104
6.3-1 Preliminary Task Analysis Interior (PGA) Patch Application Task Analysis 105
6.3-2 Hypervelocity Impact Damage for Repair Demonstration 108
6.3-3 Abrade the Wall Surface With the Cleaning Tool to Remove Loose Material 108
6.3-4 Collect Loose Material With Adhesive Surface on Cleaning Tool 109
6.3-5 Center Alignment Template Over Hole 109
6.3-6 Verify Fit of Selected Patch Against Wall Markings 110
6.3-7 Press Patch Firmly Into Place 110
6.3-8 Burnish Bubbles, Folds, and Creased Edges With Patch Handle 111
6.3-9 The Completed Layered Patch 111
6.4-1 Rubber Ring Patch Application Task Timeline 112
6.4-2 Rubber Ring Patch Applied to a Curved Panel 113
6.7-1 Potential Repair Materials 117

7.0-1 Wall Response Function 120
7.1-1 Space Station Geometry Model, 5000 Elements 120
7.2-1 Output of Hidden Surface Algorithm for Meteoroid Threat Angle 123
7.3-1 Debris Impact Analysis Approach 124
7.3-2 Debris Impact Analysis of Space Station Elements 124
7.4-1 Meteoroid Analysis Threat Angle Generation 127
7.4-2 Effect of Meteoroid Velocity on Total Space Station PNP 127
7.4-3 Effect of Space Station Orbital Velocity on Total Space Station PNP 127
7.6-1 Design Analysis Computer Code - Data Flow 129

Page

7.11-1 Design Contours 131
7.12-1 Debris Threat Distribution 133
7.12-2 Meteoroid Threat Distribution, Side View 133
7.13-1 Results of Orientation Sensitivity Study 134

8.1-1 Space Station Integrated Wall Structure 139
8.1-2 Review of Potential Space Station Integrated Wall Materials 141
8.1-3 Shield Materials Penetration Resistance Trade Study 143
8.3-1 Self-Shielding of Space Station Module Pattern 145
8.3-2 Space Station Module Pattern Vulnerable Areas 146

9.0-1 Compliance With Contract Objectives and Requirements 148

GLOSSARY

AO	atomic oxygen
BAC	Boeing Aerospace Company
BUMPER	(design analysis computer code developed under this contract)
backwall	(the primary plate of a multiplate wall system. In this report the pressure wall of a Space Station module is the backwall.)
BMDP	(statistical analysis software for multiple linear regression analysis by BMBP Statistical Software, Los Angeles, California)
critical diameter	(the diameter of a particle that just penetrates a configuration for a given impact velocity and angle)
EB	electron beam
EVA	extravehicular activity
flux	(number of particles passing through a unit area per unit time)
HULL	(a hydrocode used for modeling hypervelocity impact)
IVA	intravehicular activity
JSC	Johnson Space Center
LEO	low Earth orbit
MLI	multilayer insulation
MMA	Martin Marietta Aerospace
MSFC	Marshall Space Flight Center
N	(a normalized penetration value for expressing the amount of impact damage in a multiplate system)
NASA	National Aeronautics and Space Adminstration
NASTRAN	NASA Structural Analysis finite element code
NBS	neutral buoyancy simulator
NORAD	North American Aerospace Defense

PEN4	(a multiplate hypervelocity penetration code)
PGA	pressure garment assembly
PNP	probability of no penetration
RFP	request for proposal
shield	(the first plate of a multiplate wall system; also known as a bumper)
spacing	(the distance between the shield and backwall)
SSCE	Space Station critical element
SUPERTAB	registered trademark of Structural Dynamics Research Corporation, a division of General Electric CAE International, Inc.
threshold	(impact damage on the verge of penetrating the element in question)
UFF	Universal File Format
UV	ultraviolet

D180-30550-1

SPACE STATION INTEGRATED WALL DESIGN AND PENETRATION DAMAGE CONTROL

by A. R. Coronado, M. N. Gibbins, M. A. Wright, and P. H. Stern

The Boeing Company

SUMMARY

A methodology, in the form of a computer code, has been developed that will allow a designer to optimize the pressure wall, insulation, and meteoroid/ debris shield of a manned spacecraft of arbitrary configuration and orientation. This design analysis code, BUMPER, uses a geometry model similar to a NASTRAN structural model to define the geometry and orientation. The geometry model is analyzed from all possible threat angles, for either meteoroids or debris, to determine which elements are exposed to a threat and which are hidden and therefore shielded by other elements. The wall configuration for each of the model elements is defined and, through the use of the penetration function, the diameter of a threat projectile that just penetrates that configuration is calculated. These diameters are calculated for the entire range of expected velocities and impact angles. Using the NASA flux models for debris and/or meteoroids, the probability of no penetration (PNP) for any time period can be calculated. The probability of penetration for each element is calculated and can be used to identify the spacecraft areas at greatest risk. A companion code, CONTOUR, can produce design contour plots of equal PNP for any combination of shield and wall thicknesses, spacing, and insulation. These plots allow designers to conduct rapid trade studies of differing wall configurations.

Hypervelocity impact testing was conducted at the NASA/MSFC facility using a two-stage, light-gas gun. A total of 118 tests were conducted to verify and improve the penetration function of a two-plate target array impacted by spherical aluminum projectiles. Test parameters were varied widely; (1) spacings varied between 101.6 to 203.2 mm (4 to 8 in), (2) shield thicknesses varied from 0.813 to 2.032 mm (0.032 to 0.08 in), (3) wall thicknesses varied from 1.60 to 4.775 mm (0.063 to 0.188 in), (4) impact angles varied from normal to 65 deg from normal, (5) impact

velocities varied from 2.0 to 7.8 km/s (6500 to 25,600 ft/s), and (6) the majority of the specimens had 30 layers of multilayer insulation (MLI) between the shield and the second plate. In addition, 24 tests were conducted to investigate the internal effects of a penetration (i.e., flash, noise, and spall). These tests were conducted in a large, highly instrumented pressure vessel to simulate a common module.

Repair techniques, including patches, application tools, and procedures for applying the patches in a vacuum while wearing a pressure suit, were developed. These procedures have been tested in the neutral buoyancy tank at NASA/MSFC, and recommendations by the test engineers have been incorporated. Prototype patches have been applied to impacted panels, which were then tested for their ability to hold pressure. A patent application has been submitted for these repair techniques.

INTRODUCTION

The work performed under this contract was divided into four tasks. Task 1 was the development of an integrated module wall design guide. Under this task we developed a module wall design methodology allowing designers to evaluate alternative wall configurations, conduct trade studies, and determine which design is optimum for a given orbit, spacecraft configuration and orientation, and threat environment. We also demonstrated technology readiness of the design guide. This design guide is in the form of a computer code, named BUMPER, which uses a geometry model similar to that used by NASTRAN to account for the effects of spacecraft geometry and orientation such as self-shielding. BUMPER also uses equations to define a penetration function defining the projectile size that just penetrates the defined wall configuration for a given velocity and impact angle combination. A hypervelocity impact testing program, conducted by NASA at MSFC, was used to verify and improve the empirical penetration function and demonstrate our technology readiness.

Task 2 was the development of a penetration control plan to assess the effects of a primary wall penetration and for module repair or replacement following an impact. To fulfill the requirements under this task, we developed an effects of penetration test program, again conducted by NASA/MSFC, to quantitatively measure what happens during the penetration of a large chamber simulating a common module. The results of these tests will be used to define the instrumentation requirements for later tests and should not be considered definitive. We developed repair criteria and requirements for determining when and how repairs should be made. We also developed repair concepts, fabricated prototype patches, repaired and pressure-tested actual penetrated aluminum plates, and determined procedures for performing these repairs while wearing a space suit. These procedures were later demonstrated and verified in the neutral buoyancy simulator at MSFC under a separate program.

Task 3 was the development of a phenomenological penetration function, PEN4, used to complement our empirical penetration function. PEN4 was originally developed under a Navy contract to determine the ability of a warhead fragment to penetrate a multiple aluminum array and destroy critical components within. It has since been modified to determine the penetration resistance of an arbitrary aluminum target array to impacts by aluminum projectiles and therefore can be applied to Space Station wall designs.

Task 4 was the development of an acoustic impact/penetration system that used acoustic transducers, digital recording equipment, and appropriate software to the determine the location of impacts. Initial experiments were conducted on flat aluminum plates to demonstrate proof of concept; later tests were conducted on a large, curved, aluminum panel with an isogrid rib reinforcement system.

Tasks 3 and 4 were added to the contract in March 1987.

1.0 REFERENCE CONFIGURATION

1.1 REPRESENTATIVE BASELINE

The development of a design tool required that a Space Station module configuration be available to measure development progress and to provide a standard for alternative design comparison. The design chosen for the purposes of the contract is referred to as the reference configuration and is shown in figure 1.1-1. However, it does not represent a specific design by any organization but rather a representative baseline that incorporates features expected to be found in a Space Station design. When comparisons are made to test or analysis results later in this document, they will generally be made to the reference configuration. This may refer to either the Space Station design configuration, the wall configuration, or both. In any case, the reference configuration is meant to be only representative of features found in Space Station designs.

1.2 MODULE PATTERN

The module pattern is based on the twin-keel, horizontal figure-eight configuration with nodes and tunnels proposed by NASA/MSFC in 1985. The long axis of the reference configuration is parallel to the velocity vector (X-axis). All center lines of Space Station elements (modules, connecting tunnels, and nodes) lie in the orbital plane, which is defined by the X- and Y-axes. The Z-axis is parallel to the Earth normal vector and positive away from Earth.

1.3 INTEGRATED WALL DESIGN

The reference wall configuration chosen was proposed by Boeing Aerospace Company (BAC) for the Space Station Phase B RFP and is shown in figure 1.3-1 along with details of the reference common module. This configuration is representative only of expected wall designs and may not represent an optimized design. It incorporates all major integrated wall elements such as a shield, MLI, and a backwall. The shield is 7075-T6 aluminum 1.016 mm (0.040 in) thick and stands off 101.6 mm (4.0 in) from the backwall. The backwall, which is the pressure wall, is 2219-T87

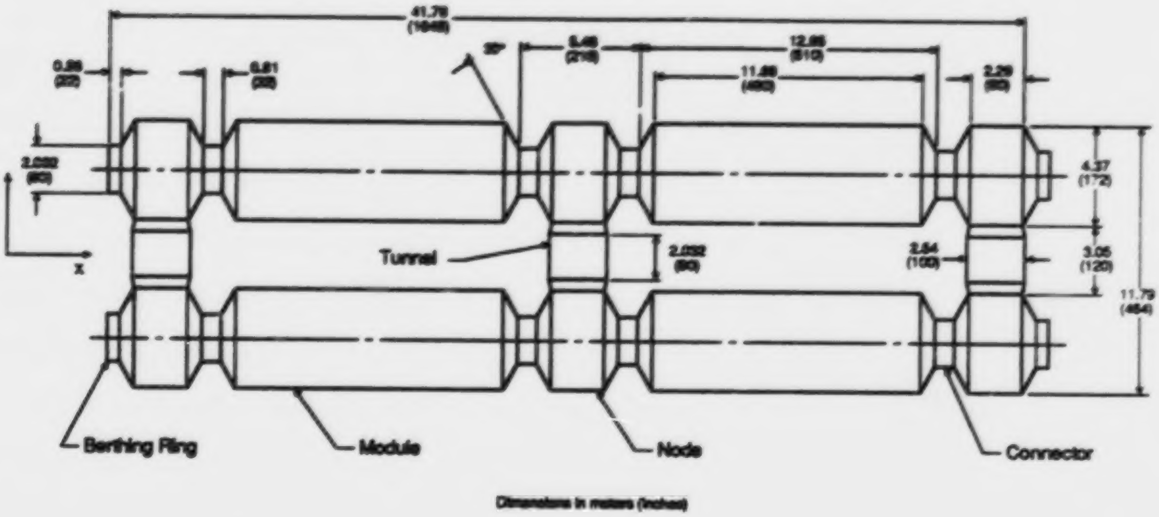
41.78 (1645)
0.56 (22)
0.81 (32)
30°
5.48 (216)
12.95 (510)
11.89 (468)
2.29 (90)
2.032 (80)
y
x
4.37 (172)
Tunnel
2.032 (80)
2.54 (100)
3.05 (120)
11.79 (464)
Berthing Ring
Module
Node
Connector
Dimensions in meters (inches)

Figure 1.1-1. Reference Configuration Module Pattern.

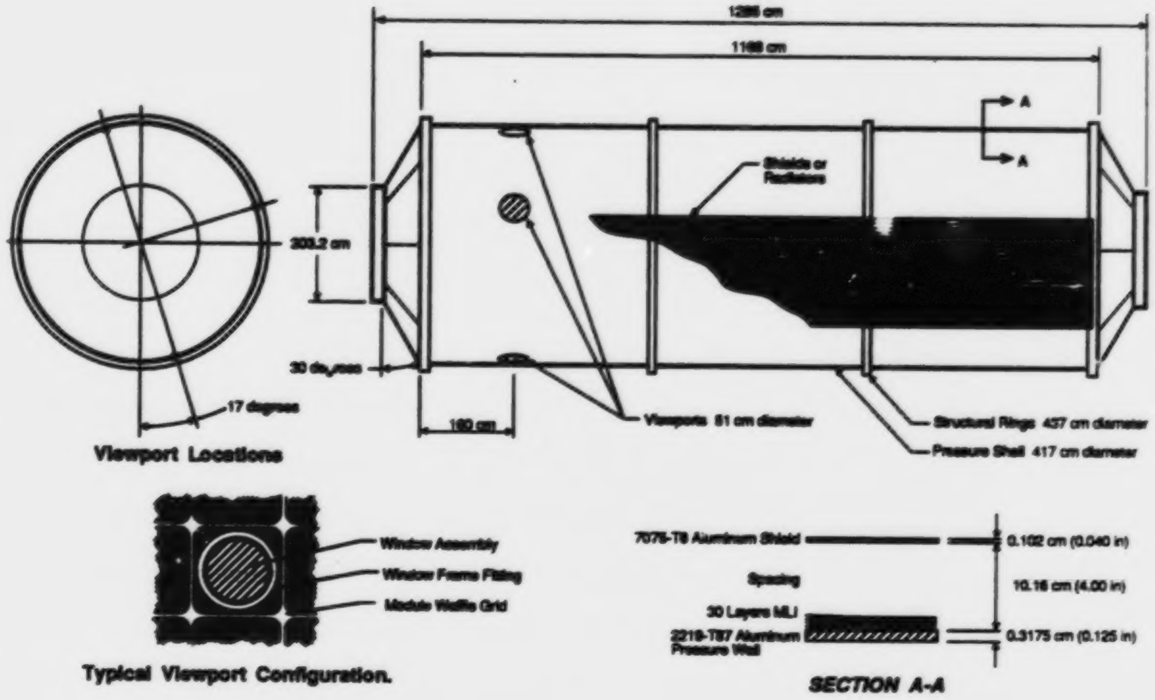
1285 cm
1168 cm
A
A
Shields or Radiators
303.2 cm
30 deg max
17 degrees
160 cm
Viewports 81 cm diameter
Structural Rings 437 cm diameter
Pressure Shell 417 cm diameter
Viewport Locations
Window Assembly
Window Frame Fitting
Module Waffle Grid
Typical Viewport Configuration.
7075-T6 Aluminum Shield
0.102 cm (0.040 in)
Spacing
10.16 cm (4.00 in)
30 Layers MLI
2219-T87 Aluminum Pressure Wall
0.3175 cm (0.125 in)
SECTION A-A

Figure 1.3-1. Space Station Common Module Reference Configuration

aluminum 3.175 mm (0.125 in) thick. The multilayer insulation consists of 30 layers 1/2 mil kapton aluminized on one side, 29 layers of Dacron mesh between each kapton layer, and 1 layer of beta cloth (coated s-glass) on the side nearest the shield for durability. The areal weight of this combination is 1.074 kg/m^2. There is no differentiation between wall configurations such as waffle grid or T-stiffened monocoque, and stress in either wall is not considered.

2.0 ENVIRONMENT

2.1 DEBRIS ENVIRONMENT

The document defining the debris environment for this contract is JSC 20001 (ref. 2-1). The flux equation and distribution for debris is shown in figure 2.1-1. The debris velocity probability distribution in figure 2.1-2 shows that the expected impact velocity ranges from 0.1 to 16.0 km/s. The angle distribution is derived from the velocity distribution using the vector diagram and equation shown in figure 2.1-3. Important assumptions are that the orbits for Space Station and threatening debris are circular and at the same altitude, (i.e., that they have the same velocity). While analyzing these data we determined that the angle and velocity distributions given in reference 2-1 were inconsistent. The author later confirmed that the two distributions were derived from North American Aerospace Defense (NORAD) data from different years. Because of this inconsistency we used the velocity distribution, the more fundamental form of data, and derived a consistent angle distribution (fig. 2.1-4) for use under this contract. This figure shows that the majority of debris approaches Space Station from approximately 45 deg on either side of the orbital velocity vector. This implies that the Space Station orientation is an important factor in determining PNP. This was later shown to be correct.

The debris flux is a highly directional phenomenon; however, the flux equation in figure 2.1-1 has been modified to conform to the definition of an omnidirectional flux. This was done by the author of reference 2-1 to be consistent with the definition and usage of the meteoroid flux equation described in the following section. The debris flux equation as defined in JSC 20001 is for a random-tumbling plate. Appendix G defines the Space Station probability model using an orientated plate. To account for the differences between the two definitions, the debris flux equation must be multiplied by a factor of four. A more rigorous explanation may be found on page G-6 of this report.

PRECEDING PAGE BLANK NOT FILMED

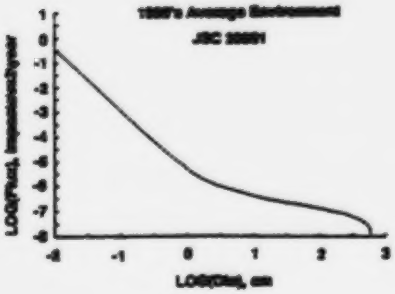

Flux Equation:

$\text{Log } F = -2.52 \text{ Log } D - 5.46$
D = diameter in centimeters; $D < 1.0$ cm

$\text{Log } F = -5.46 - 1.78 \text{ Log } D + 0.0889 (\text{Log } D)^2 - 0.194 (\text{Log } D)^3$
D = diameter in centimeters; $1.0 \text{ cm} \leq D \leq 200 \text{ cm}$

where:

F = Number of impacts of objects with diameter D or greater per square meter per year

Log = Logarithm base 10

Orbital Altitude = 500 km

Figure 2.1-1. Debris Flux Environment

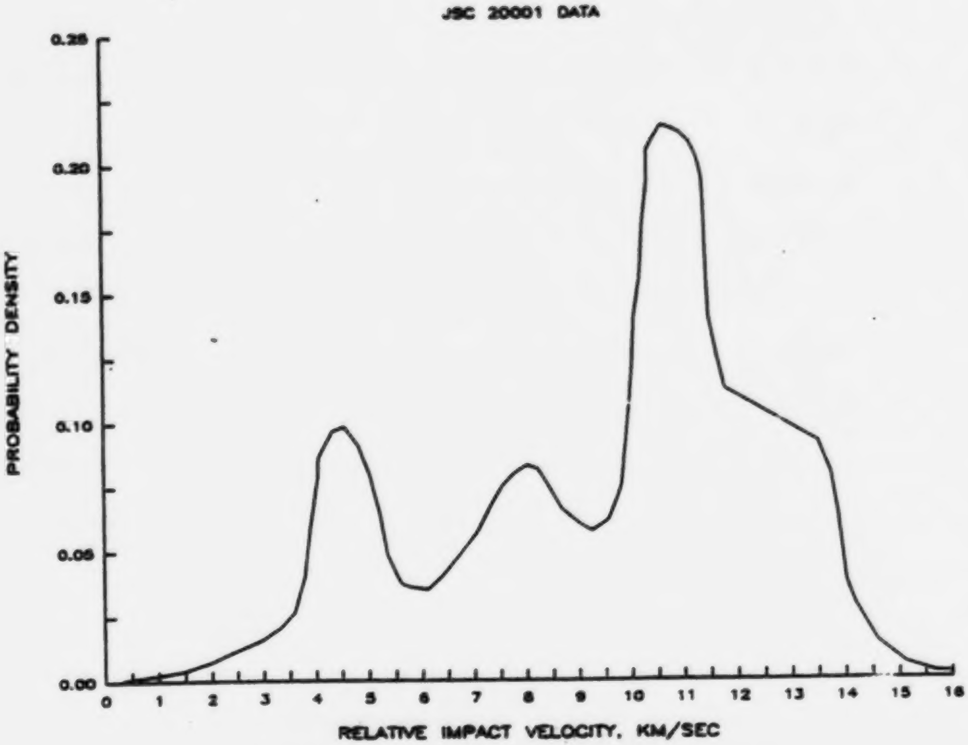

Figure 2.1-2. Debris Velocity Probability Distribution

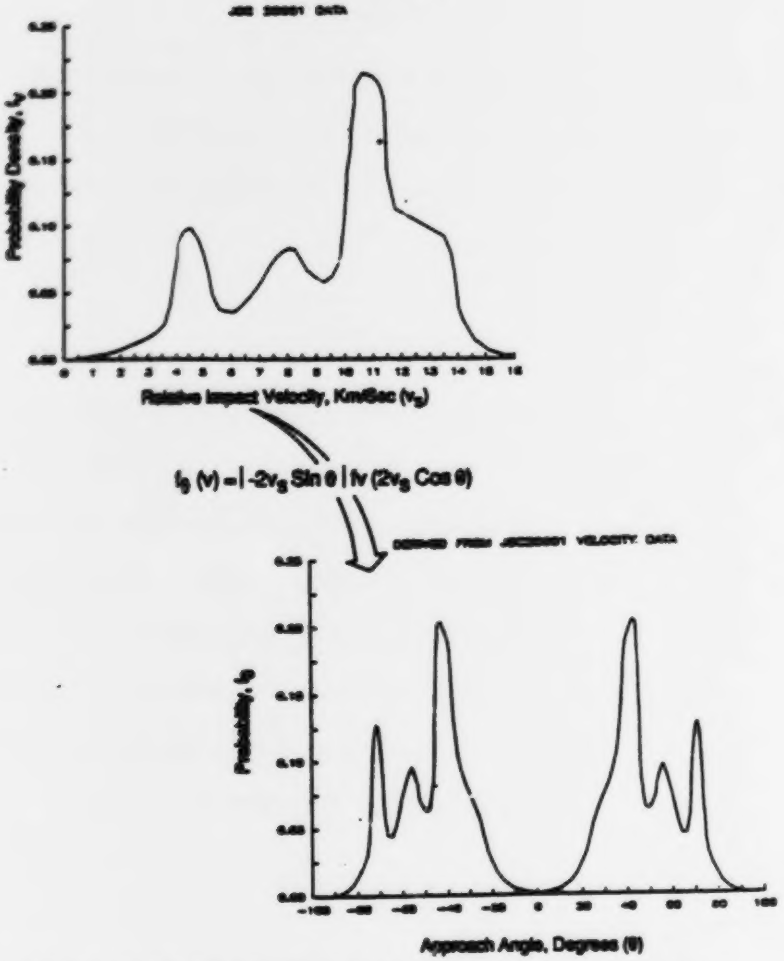

Figure 2.1-3. Transforming Velocity Distribution to Angle Distribution

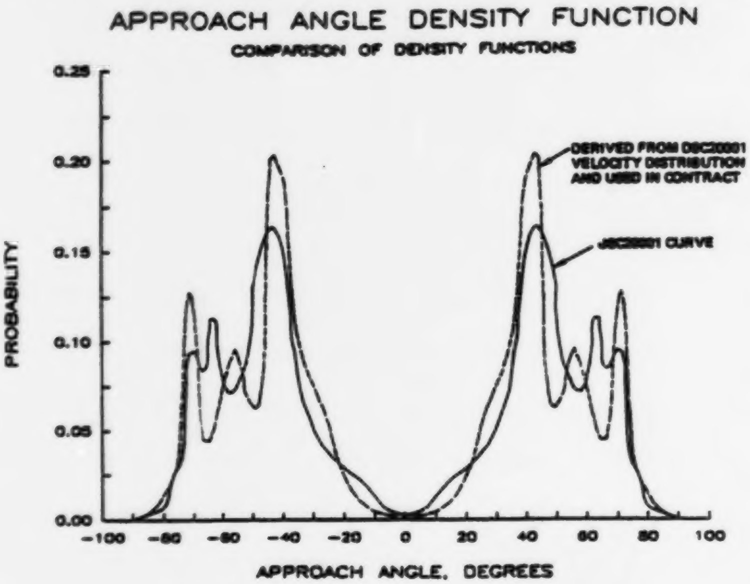

Figure 2.1-4. Comparison of Angle Density Functions

Several important assumptions have been made about the character of orbital debris. JSC 20001 states that the average mass density for debris objects less than 1 cm in diameter is 2.8 g/cm^3, approximately the same as aluminum. Predicted average densities are less for larger objects. For consistency and repeatability, testing is performed with spherical aluminum projectiles. Limited testing was done with cylindrical projectiles to estimate how much more penetration capability they have, and with lexan projectiles to simulate meteoroid impacts.

As stated previously, all orbital debris that threatens Space Station is assumed to be in the same orbit as Space Station and therefore has the same orbital velocity. We expect few, if any, debris impacts will occur to rearward facing structure because, in general, debris cannot catch up. Additionally, all threatening debris approachs Space Station in the orbital plane, so few debris impacts are expected to occur to structure not facing the orbital plane (i.e., toward or away from the Earth). Some debris are in noncircular orbits and could strike Space Station from slightly above or below the plane of the orbit; however, due to atmospheric drag these particles tend to circularize or reenter the atmosphere more quickly and therefore pose a lesser threat.

2.2 METEOROID ENVIRONMENT

The document defining the meteoroid environment for this contract is NASA SP-8013 (ref. 2-2). It recommends a design density of 0.5 g/cm^3 for meteoroids. A small percentage of particles are stony with much higher densities; however, the majority of particles are assumed to be sporadic and stream meteoroids of cometary origin with low densities. The velocity probability distribution and flux model given in reference 2-2 are shown in figure 2.2-1. Meteoroid velocities range from 10 to 72 km/s with an average of 20 km/s.

The velocity distribution and flux model are geocentric and must be corrected for the effects of orbital velocity as shown in figure 2.2-2. This effect increases the apparent flux and impact velocity for surfaces facing toward the Space Station velocity vector and decreases it for surfaces that face away. The increase in impact velocities for forward-facing surfaces is caused by the vector summation of Space Station's orbital velocity and meteoroid's geocentric velocity. This

ORIGINAL PAGE IS
OF POOR QUALITY

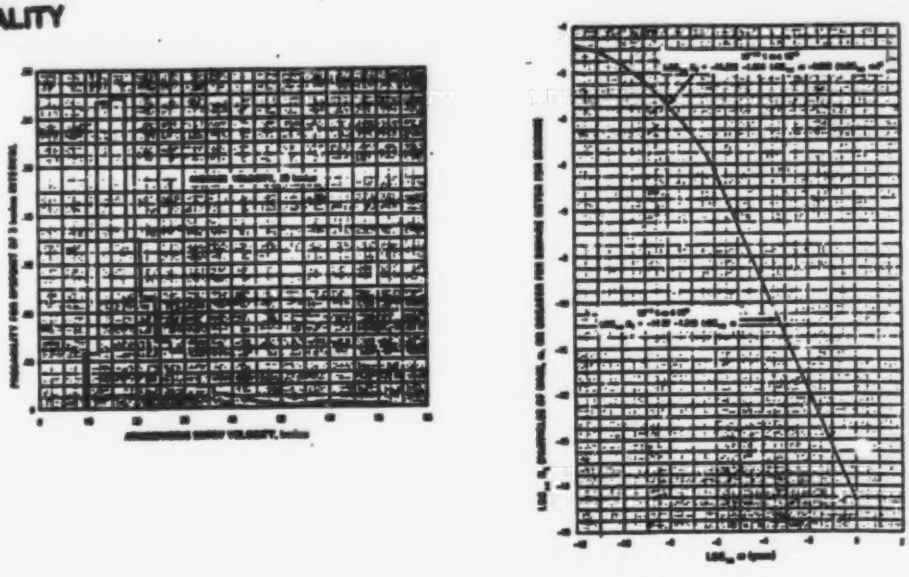

Figure 2.2-1. Meteoroid Environmental Model

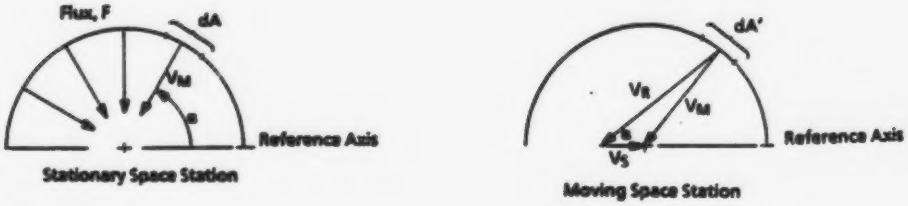
Flux, F
dA
V_M
α
Reference Axis
Stationary Space Station
dA'
V_R
V_M
V_S
Reference Axis
Moving Space Station

"Uniform" flux

- **Directional distribution = constant**
- **Velocity distribution = constant**

$V_M = V_R$

$F = \dfrac{\text{Particles}}{\text{unit area} \times \text{unit time}}$

Relative Velocity, VR

$V_R = V^* + V \cos \alpha$

where $V^* = (V_M^2 - V_S^2 \sin^2 \alpha)^{1/2}$

Magnification:

Area: $\dfrac{dA'}{dA} = \dfrac{V_R^2}{V^* V_M}$

Flux: $\dfrac{F'}{F} = \dfrac{V_R^3}{V^* V_M^2}$

Figure 2.2-2. Corrections for Geocentric Meteoroid Model

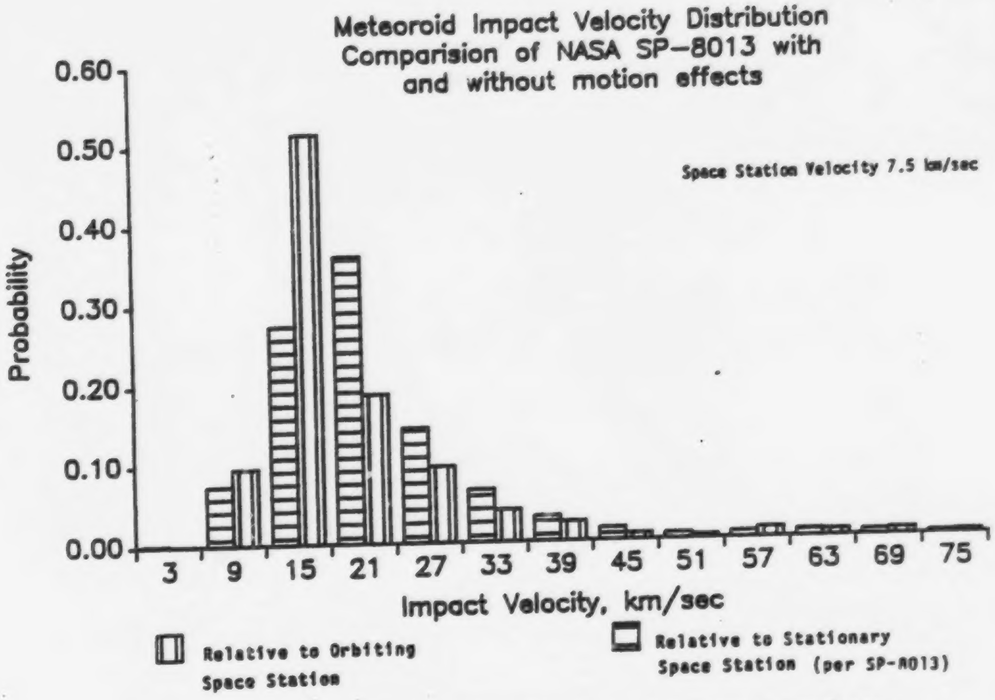

Figure 2.2-3. Meteoroid Impact Velocity Distribution Relative to Space Station

lowers the apparent impact angle for forward-facing surfaces and increases it for rearward-facing surfaces. This in turn leads to a higher apparent flux impacting forward-facing surfaces and a lower apparent flux impacting rearward-facing surfaces. Figure 2.2-3 shows the changes in the impact velocity distribution when the Space Station orbital velocity (7.5 km/s) is taken into account. Our studies, summarized in section 7.0, show that using an average meteoroid velocity of 20 km/s and accounting for Space Station orbital velocity allows us to accurately calculate PNP and distribution of impacts on Space Stations' surface.

Generally two correction factors must be applied to a meteoroid flux distribution when the area of interest is a low-Earth orbit: defocusing and body shielding. The defocusing factor is an apparent increase in flux near the Earth due to gravity. Body shielding is due to shielding of the meteoroid flux by the Earth and increases as orbital altitudes decreases. Defocusing has been applied to the flux equation used in this contract. Body shielding is accounted for during the generation of meteoroid threat angles, which is described more fully in section 7.4. An assumed orbital altitude of 500 km is used to determine the geometry of the threat angle generation. Threat angles below the Earth's horizon are not considered in the analysis.

2.3 UNCERTAINTIES IN ENVIRONMENT DEFINITIONS

JSC 20001 describes uncertainties in the debris flux equation that range from a factor of 3 for debris 1.0 cm in diameter and larger to a factor of 10 for debris 1.0 mm in diameter and smaller. For this contract the flux equation, as described in reference 2-1, was considered nominal, and no attempt was made to incorporate the uncertainties into the analysis. However, sensitivity studies were conducted to determine what effect these possible variations in the flux would have on PNP. These results are reported in the following paragraphs.

SP-8013 indicates that there may be greater uncertainties in the meteoroid environment, both with the flux model and with the density estimates. As with the debris environment, the meteoroid flux equation is used as nominal with no attempt to account for the uncertainties. Sensitivity studies show that meteoroid impacts are a much smaller problem than debris impacts, and therefore the meteoroid environment uncertainties have much less effect.

2.4 ENVIRONMENT SENSITIVITY STUDIES

As stated previously, sensitivity studies were conducted to determine how much of an effect changes in the environment definitions, penetration function, or time in orbit had on PNP. The computer code and technique used to conduct these analyses is described in more detail in section 7.0. The configuration and orientation used was the reference configuration described previously with the reference wall design.

2.5 FLUX DEFINITION UNCERTAINTY

The first study determined the effect uncertainties in the debris flux definition have on PNP. This was done by multiplying the calculated flux by a factor ranging from 0.5 to 10. The results in figure 2.5-1 show PNP decreasing as the multiplier on the flux (flux factor) approaches 10. We conclude from this figure that an accurate flux definition is necessary for an accurate PNP calculation.

2.6 DEBRIS PENETRATION FUNCTION UNCERTAINTY

The second study determined how uncertainties in the debris penetration function affect PNP. The penetration function is the calculation of projectile diameters that just penetrate a wall configuration for any given velocity and impact angle combination. This was done by multiplying the diameter of a debris particle that would just penetration the reference configuration by an adjustment factor. Figure 2.6-1 shows how PNP varies for adjustment factors between 0.65 and 1.5, an uncertainty larger than we expect. Only a 3.4% change in PNP is demonstrated for a plus and minus 10% change in the penetration function. This could represent, however, a significant weight impact for Space Station.

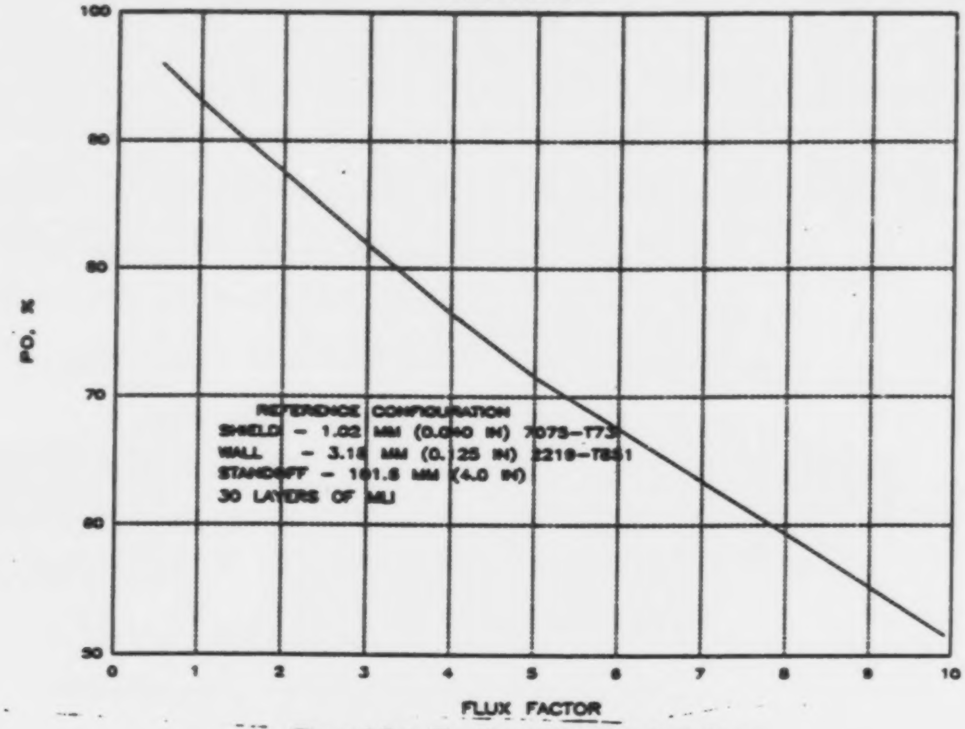

Figure 2.5-1. Flux Uncertainty Sensitivity Study

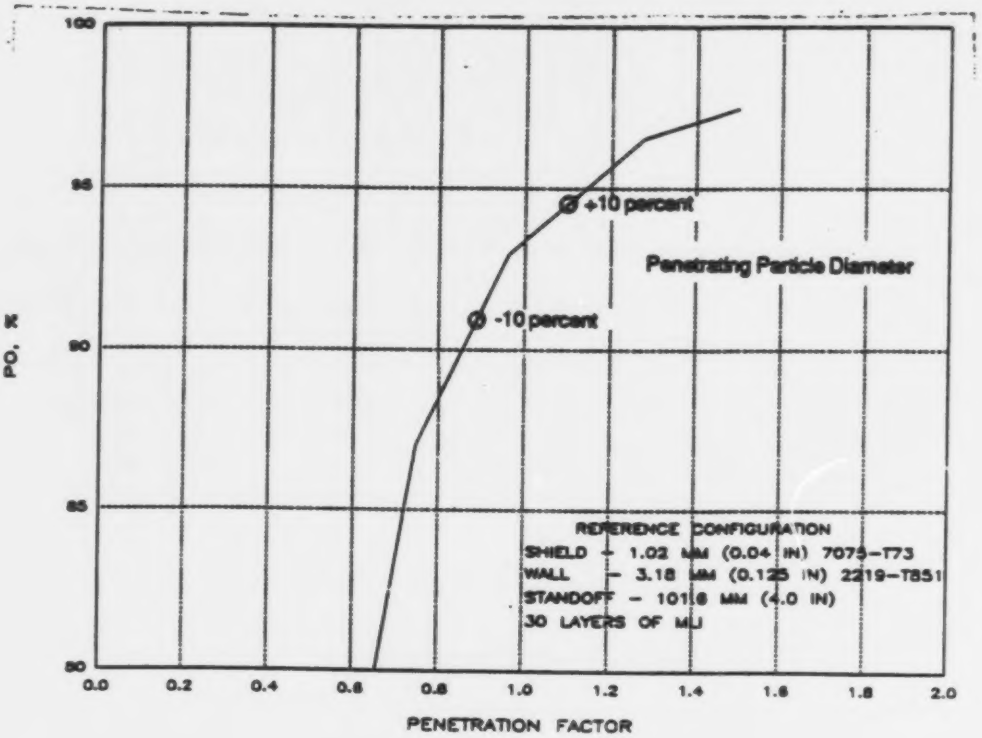

Figure 2.6-1. Penetration Function Sensitivity Study

2.7 EXPOSURE DURATION SENSITIVITY

During the course of this contract, estimates for expected exposure duration for Space Station have varied from 10 to 30 years. To determine what affect this would have PNP for debris, we varied the time in orbit while holding all other variables constant (i.e., no change in configuration, shielding, or flux). Figure 2.7-1 shows a significant decrease in PNP with exposure duration, indicating additional shielding will be needed over time to maintain the required PNP. The second exposure duration study determined the resulting weight increase if the shield and wall thickness were increased to maintain a constant PNP. Figure 2.7-2 shows that a doubling of weight is required to maintain the required PNP. This assumes a constant debris environment and no additional shielding

2.8 IMPACT ANGLE AND VELOCITY PROBABILITY DISTRIBUTION

During the course of the sensitivity studies we developed probability distributions for impact angle and velocity as shown in figures 2.8-1 and 2.8-2, respectively. These proved to be useful in developing a test matrix, described in section 3.0, and in developing a penetration function. Figure 2.8-1 shows that the median impact angle for debris is between 45 and 50 deg, although most of the available test data was for normal (0-deg) impacts. Figure 2.8-2 reveals a more disturbing trend: a two-stage, light-gas gun can achieve a maximum impact velocity of approximately 8 km/s for useful projectile sizes. Fully 70% of expected impact velocities are outside of our ability to test and verify experimentally. Analytic methods used to predict results of impacts in this region are described in section 4.0.

2.9 PNP REQUIREMENT

The original requirement for PNP was set in NASA TM-82585 (ref. 2-3), which stated that Space Station program elements will be designed for at least a 0.95 total probability of no penetration during the 10-year, on-orbit design life. Therefore, most comparisons in this report will give a single overall PNP value, which represents the PNP for the entire habitable portion of

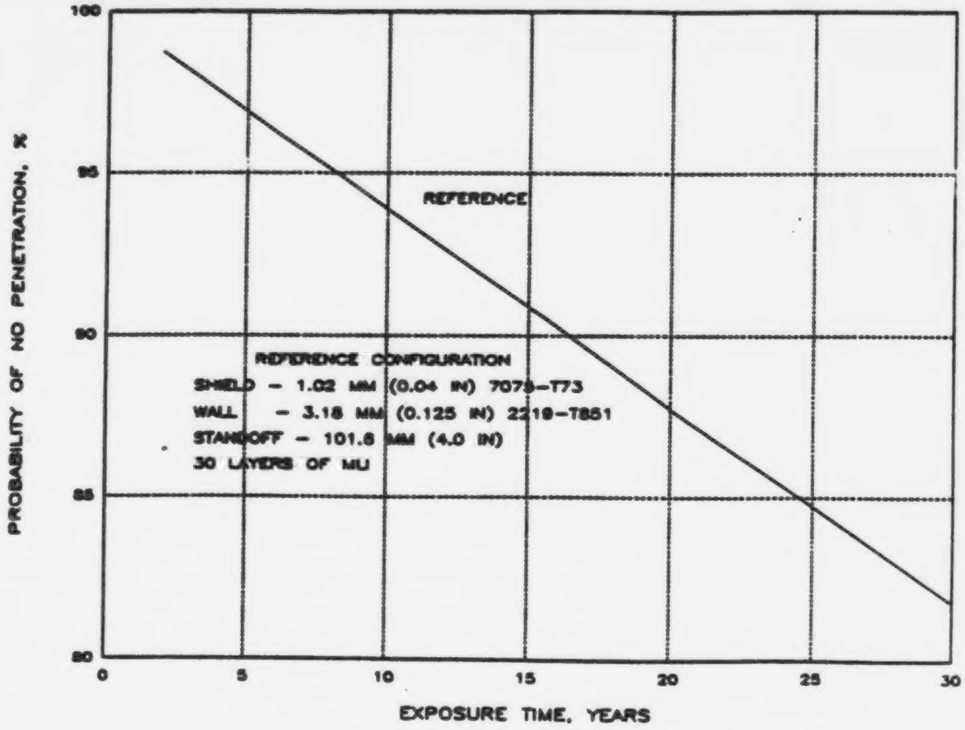

Figure 2.7-1. Orbit Time Sensitivity Study

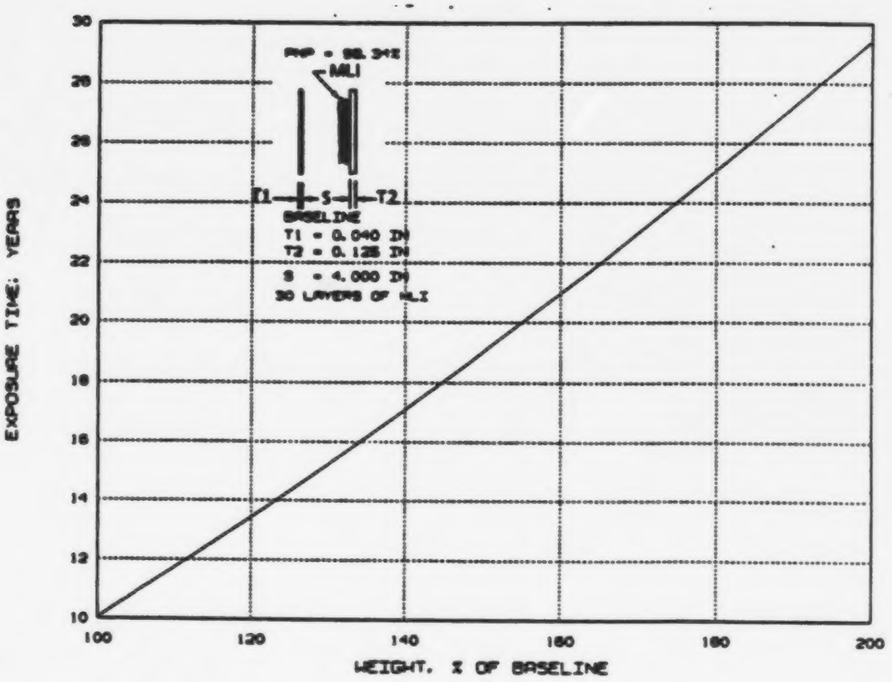

Figure 2.7-2. Orbit Time versus Weight Sensitivity Study

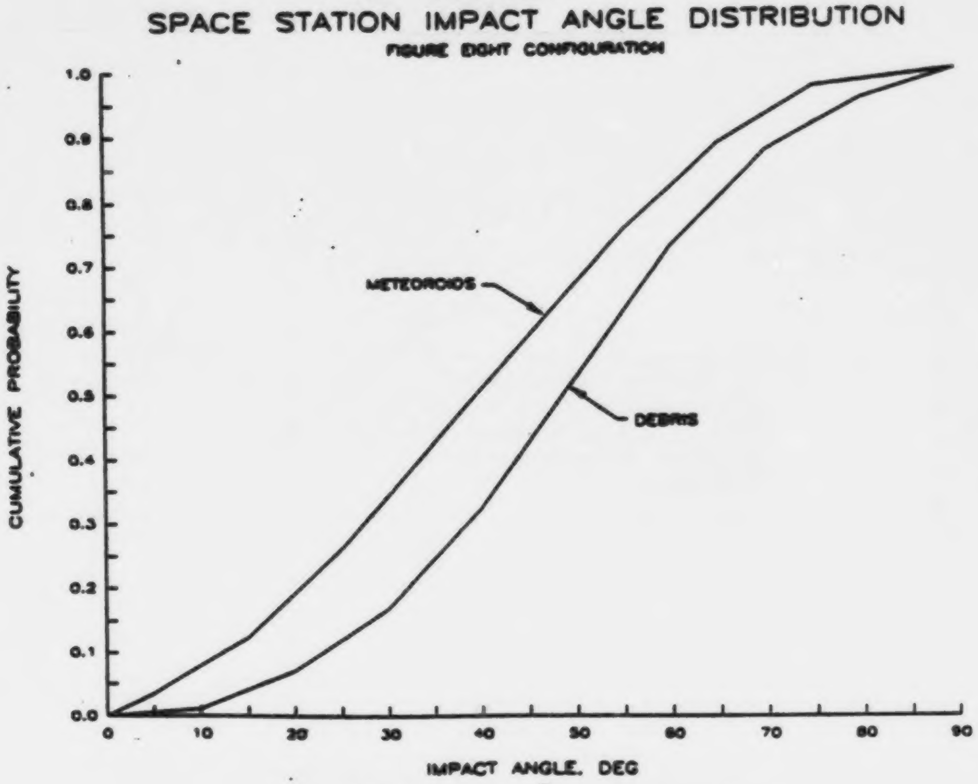

Figure 2.8-1. Impact Angle Probability Distribution

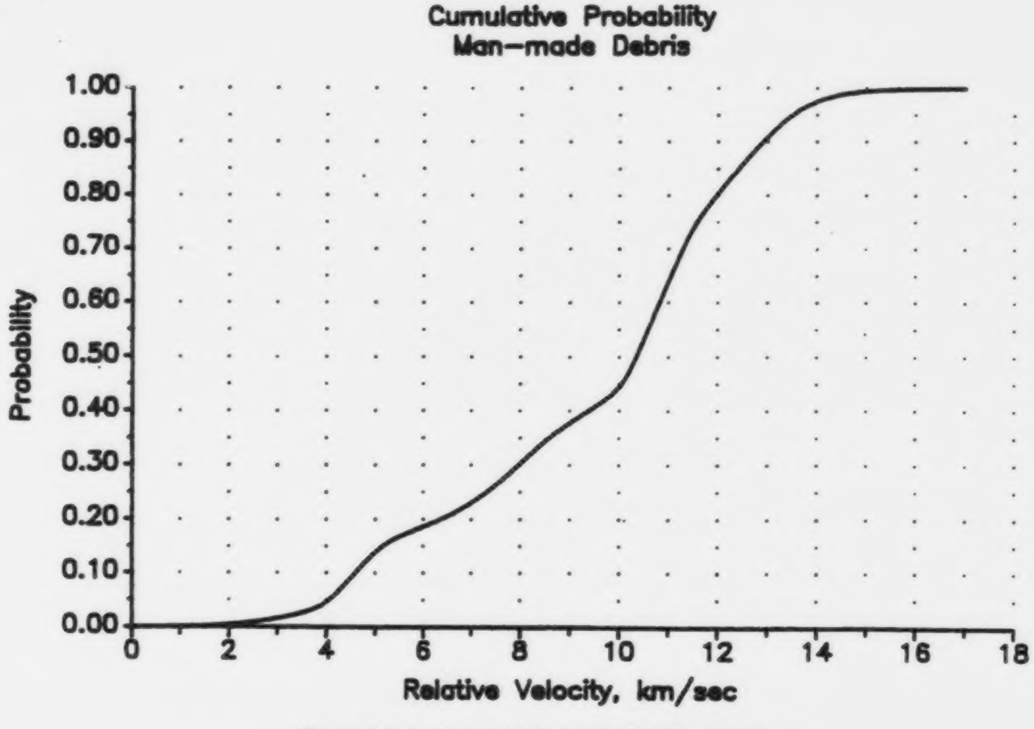

Figure 2.8-2. Impact Velocity Probability Distribution

Space Station. However, in November 1986, the Space Station Control Board issued a directive (ref. 2-4) that changed these requirements significantly. First, it requires that each Space Station critical elements (SSCE) such as modules, nodes, and tunnels be considered individually, and, second, that they must separately and individually meet a PNP of 0.9955. These requirements were further expanded and clarified during the second Space Station RFP by NASA document SS-SRD-001 (ref. 2-5). Analyses and comparisons after that date are done by either on an individual basis or multiplying individual PNPs together for comparison with earlier results.

The reference design used in this contract, at an assumed orbital altitude of 500 km, does not meet the requirement of 0.95 PNP. It did, however, provide a basis with which to compare changes in design, flux, and altitude and in this manner proved itself to be very useful.

2.10 FUTURE FLUX ENVIRONMENT

In response to a request from NASA/MSFC, a future environment proposed by Mr. Don Kessler of NASA/JSC was evaluated and compared with the JSC 20001 environment. These specific questions were addressed:

a. What is the change in the probability of no penetration on existing designs under the future flux?

b. What is the weight increment required to provide the existing level of protection for the future environment?

Figure 2.10-1 shows a comparison of the equations describing the current debris environment as given in JSC 20001 and the suggested environment for the year 2000. The configuration that was analyzed is the reference configuration described in section 1.0. Figure 2.10-2 shows the PNP as a function of design life for both the current and future environment. The PNP for the entire reference configuration and 10-year life is 93.4%. This value applies to the entire habitable portion of the Space Station. For each curve, we have assumed that the environment remains

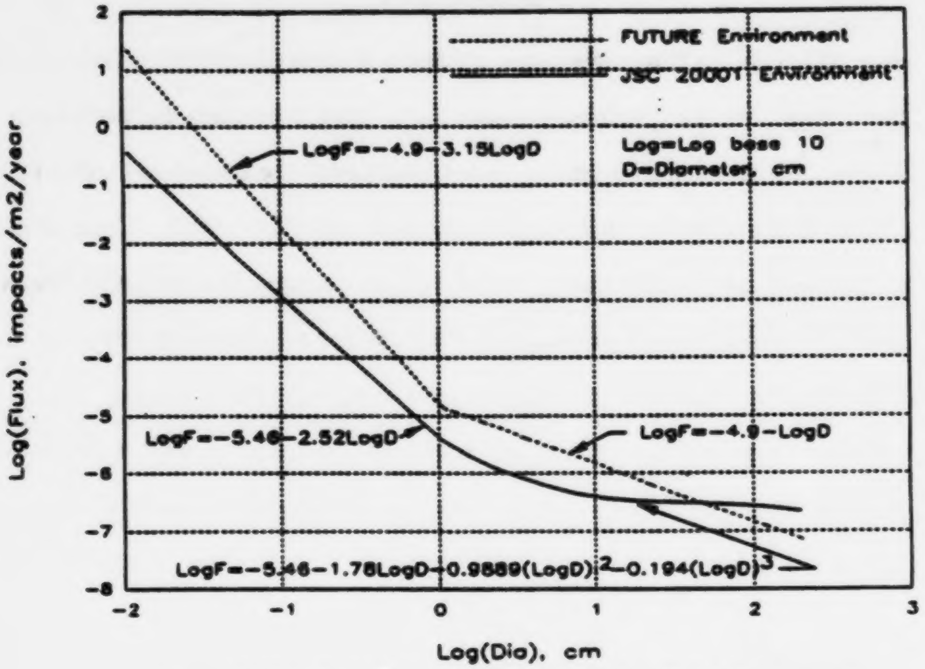

Figure 2.10-1. Comparison of Current and Future Debris Environment

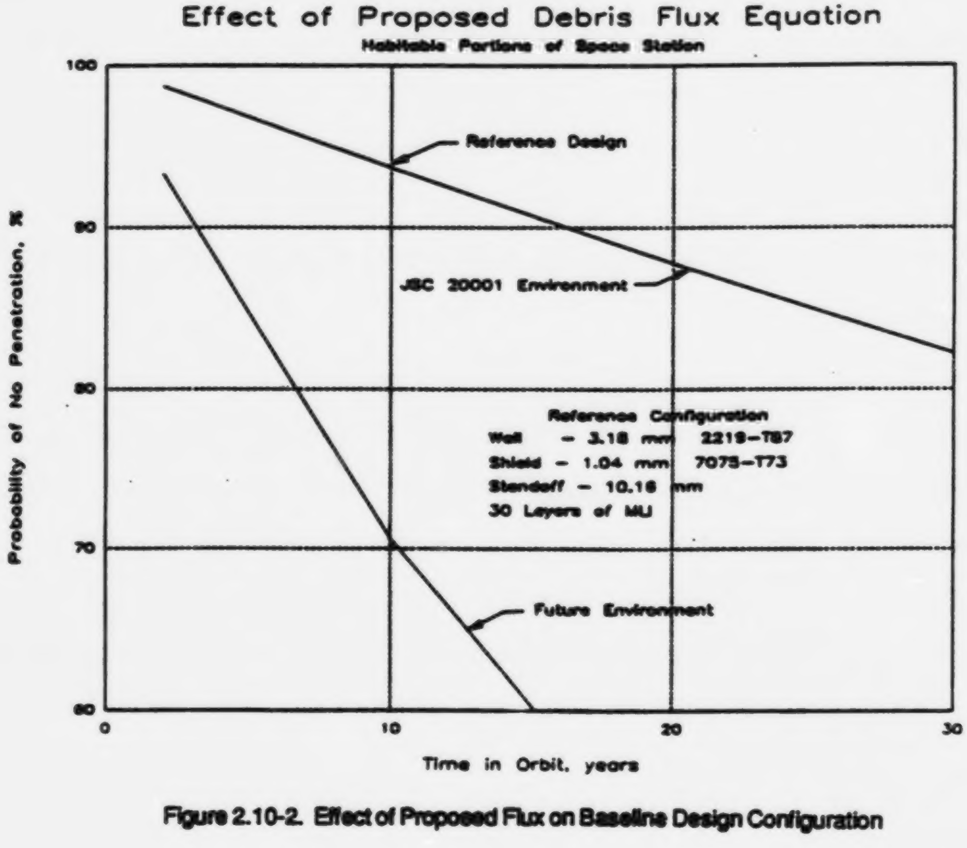

Figure 2.10-2. Effect of Proposed Flux on Baseline Design Configuration

constant over the life of the station. The effect of a time-varying environment is to change the nearly linear relationship shown in the graphs to curves.

Figure 2.10-3 shows the Space Station weight increase as a function of exposure time for both the current and the future environment, assuming that PNP was held constant at the reference design value of 95.4% by increasing only shield and backwall thickness. Thus, these estimates are not for an optimized structure and tend to overestimate the weight.

2.11 CONCLUSIONS

The conclusion reached during these studies was that confidence in calculated PNP for Space Station depends on confidence in the debris flux definition.

The complete environment model including meteoroids was brought together in one document, JSC 30000 (ref. 2-6), as part of Space Station system requirements. The environment specifications in JSC 30000 correspond to JSC 20001 and SP-8013.

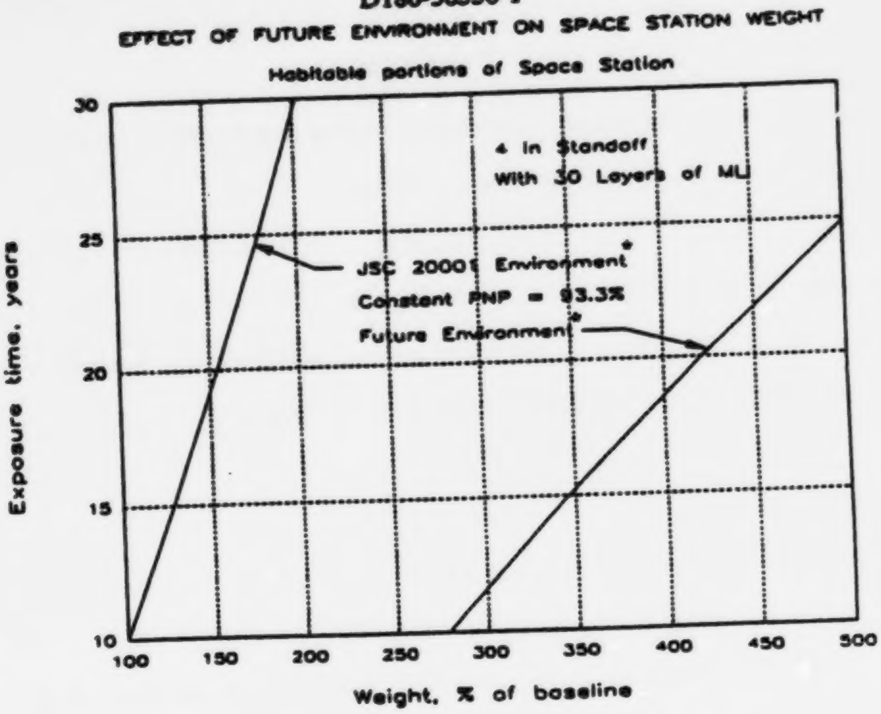

*calculations assume that the environment does not change for the time period shown

Figure 2.10-3. Comparison of Weight for Constant Probability of No Penetration

3.0 HYPERVELOCITY IMPACT TESTING

3.1 DATA BASE FROM PRECEDING STUDIES

As a basis for preliminary analysis and for developing a test program we used data from four sources (refs. 3-1, 3-2, and 3-3) plus data from Martin Marietta Aerospace (MMA) testing performed at MSFC during 1985 and 1986. Testing reported in references 3-1 and 3-2 used relatively thin aluminum plates. Thin backwalls tend to perform differently than thick backwalls; most notable is spallation vulnerability of thick backwalls. More recent testing at MSFC has reflected plate thicknesses representative of Space Station pressure wall (backwall) and shield requirements. The majority of these tests were at 0-deg impact angles; however most Space Station impacts are expected to occur above 45 deg.

3.2 ADDITIONAL TESTING FOR PENETRATION ANALYSIS - TASK 1

Test Facility. All contract hypervelocity impact testing was performed on the two-stage, light-gas gun at MSFC, which is capable of velocities between 1 and 8 km/s depending on the projectile mass. This facility is fully described in reference 3-4.

Rational for Testing. Testing was designed to build on the available data base and to increase confidence in the penetration function. Figure 3.2-1 shows the relationships among the reference Space Station design, the optimum integrated wall design as determined by our analysis, and the primary test parameters. The optimum weight line represents the optimum ratio of shield and backwall thickness to maximize PNP and minimize structural weight.

Task 1 test program details are outlined in figure 3.2-2. Test cases were specified to increase the range of key test variables in the data base, while keeping the variables within expected Space Station design boundaries. Selected shield and backwall thicknesses were limited to readily available sizes. Although this testing was primarily performed at oblique impact angles, some tests were done at 0 deg for direct comparison to previous testing. To effectively model the expected Space Station configuration, approximately half the tests included MLI between the shield and

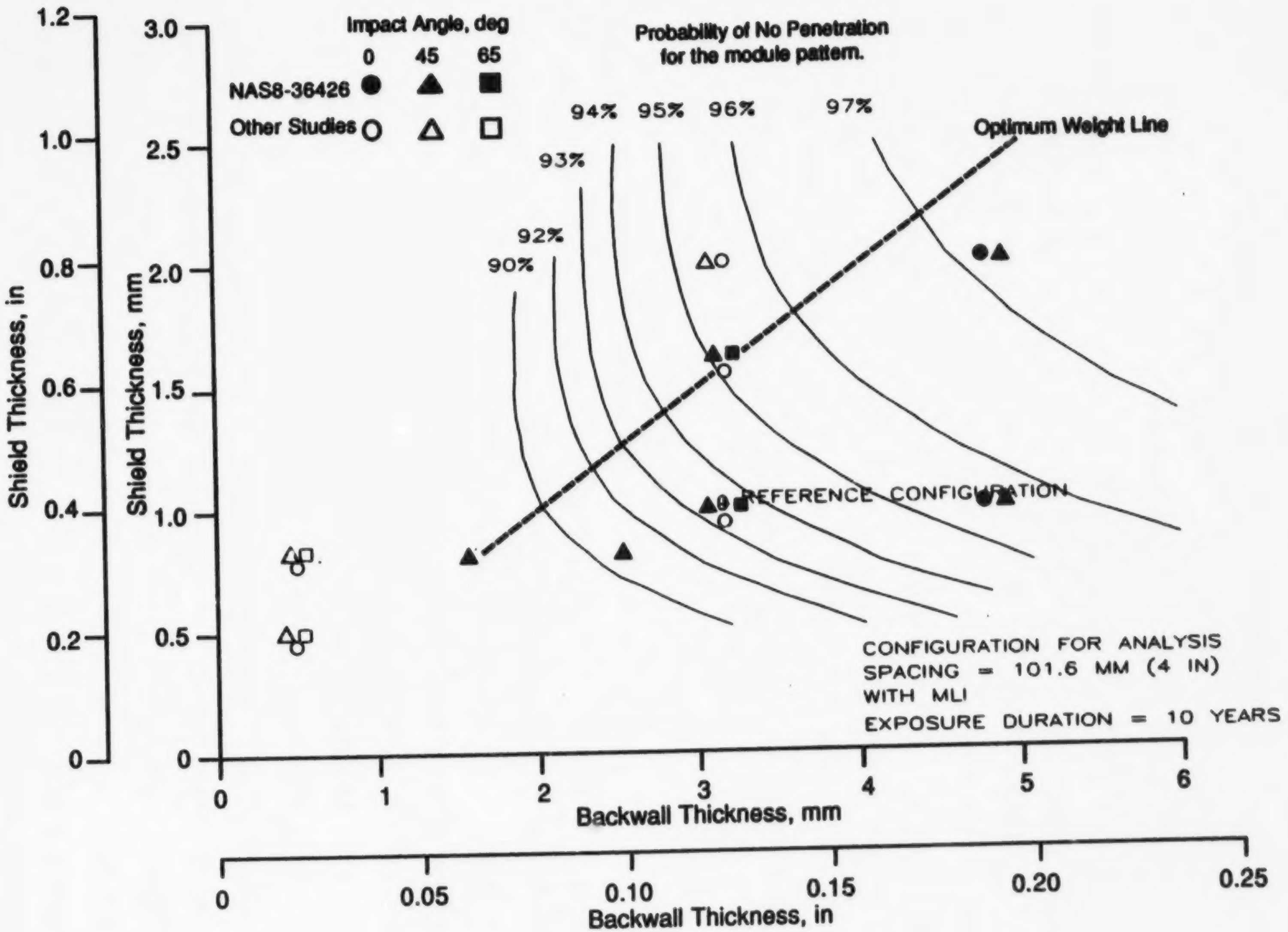

Figure 3.2-1. Module Design Data Comparison With Test Data.

Test Number	201	202	203	204	205	206	207	208	213	214	215	216	217	218
MLI														
Yes	●		●		●		●				●			●
No		●		●		●		●	●	●		●	●	
Shield														
0.032														
0.040	●	●	●	●						●	●		●	●
0.063					●	●	●	●						
0.080									●			●		
Wall														
0.063														
0.100														
0.125	●	●	●	●	●	●	●	●						
0.188									●	●	●	●	●	●
Spacing														
4	●	●	●	●	●	●	●	●	●			●		
6														
8										●	●		●	●
Impact Angle														
0-deg									●	●	●			
45-deg	●	●			●	●						●	●	●
65-deg			●	●			●	●						

Unless otherwise noted:
Shield - 6061-T6
Wall - 2219-T87
Projectile - 1100 sphere

All dimensions in inches.

Test Number	219	220	223	224	225	226	227	228	229	230	231
MLI											
Yes			●	●		●	●		●	●	
No	●	●			●			●			●
Shield											
0.032						●	●	●			
0.040			●	●	●						
0.063	●	●								●	●
0.080									●		
Wall											
0.063							●				
0.100						●					
0.125	●	●	●	●	●					●	●
0.188								●	●		
Spacing											
4					●			●	●	●	●
6	●	●	●	●		●	●				
8											
Impact Angle											
0-deg	●	●			●			●	●		
45-deg			●	●		●	●			●	
65-deg											●
	(1)	(2)	(3)	(4)	(5)						

Unless otherwise noted:
Shield - 6061-T6
Wall - 2219-T87
Projectile - 1100 sphere

All dimensions in inches.

(1) LiAl shield material

(2) dSiC shield material

(3) Cylinder projectile

(4) Cylinder projectile

(5) Lexan projectile

Figure 3.2-2. Task 1 Test Summary.

backwall. Several shots employed cylindrical projectiles at oblique impact angles to enhance the data base available on nonspherical impacts. Two advanced material systems, discontinuous silicon carbide reinforced aluminum and lithium aluminum, were tested as shields to screen their performance under hypervelocity impact.

Test Design. The basic test configuration is diagrammed in figure 3.2-3, and a test article in the test chamber is shown in figure 3.2-4. Oblique impact tests produce several effects different from normal impact: ricochet from the shield, and two components of damage – normal and flightpath. The ricochet particles were detected with a witness sheet situated as shown in the figure. Normal and flightpath damage can usually be distinguished on the backwall by following the projectile line of flight for flightpath damage and following a line normal from the point of shield penetration for normal damage.

This test program used witness sheets to measure the residual damage of projectiles penetrating the backwall. This technique was employed in all the testing included in our data base. Comparable values for degree of penetration are the important data in determining a penetration function from the test results. The impact test results provide the maximum crater depth in partial backwall penetrations, and the number of thin witness plates penetrated in tests penetrating the backwall. This information is converted to the number of equivalent backwall plates penetrated, N, by the method shown in figure 3.2-5.

Test Results. Test data are plotted diameter versus velocity in appendix J. The first two of these are also shown in figures 3.2-6 and 3.2-7. The line appearing in the figures is the alternative regression analysis penetration function described in section 4.3 and demonstrates the shallow slope of the penetration function at 45-deg impact angles. The data points shown bracket the penetration function in both figures. Section 4.0 contains a more detailed data analysis.

3.3 TASK 2 TESTING FOR EFFECTS OF PENETRATION

Rationale for Testing. Pressure wall penetration by orbital debris or meteoroids will produce a pressure pulse and a light flash, followed by pressure decay within the Space Station

ORIGINAL PAGE IS OF POOR QUALITY

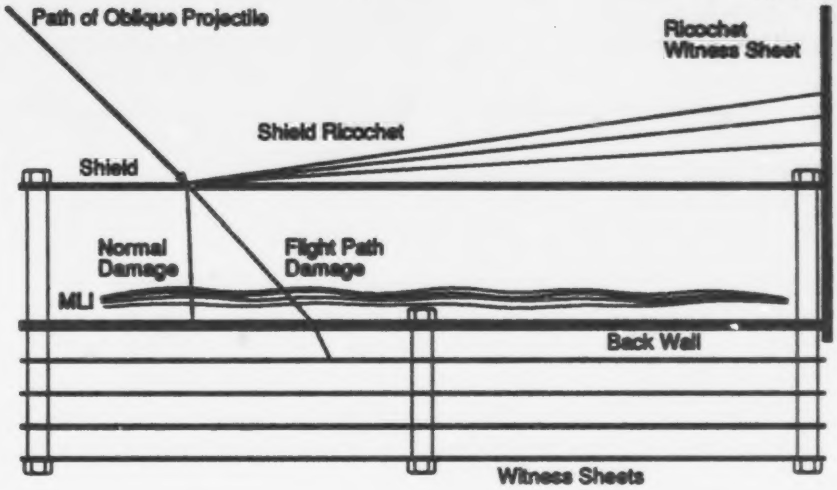
Path of Oblique Projectile
Ricochet Witness Sheet
Shield Ricochet
Shield
Normal Damage
Flight Path Damage
MLI
Back Wall
Witness Sheets

Figure 3.2-3. Task 1 Test Configuration and Definitions.

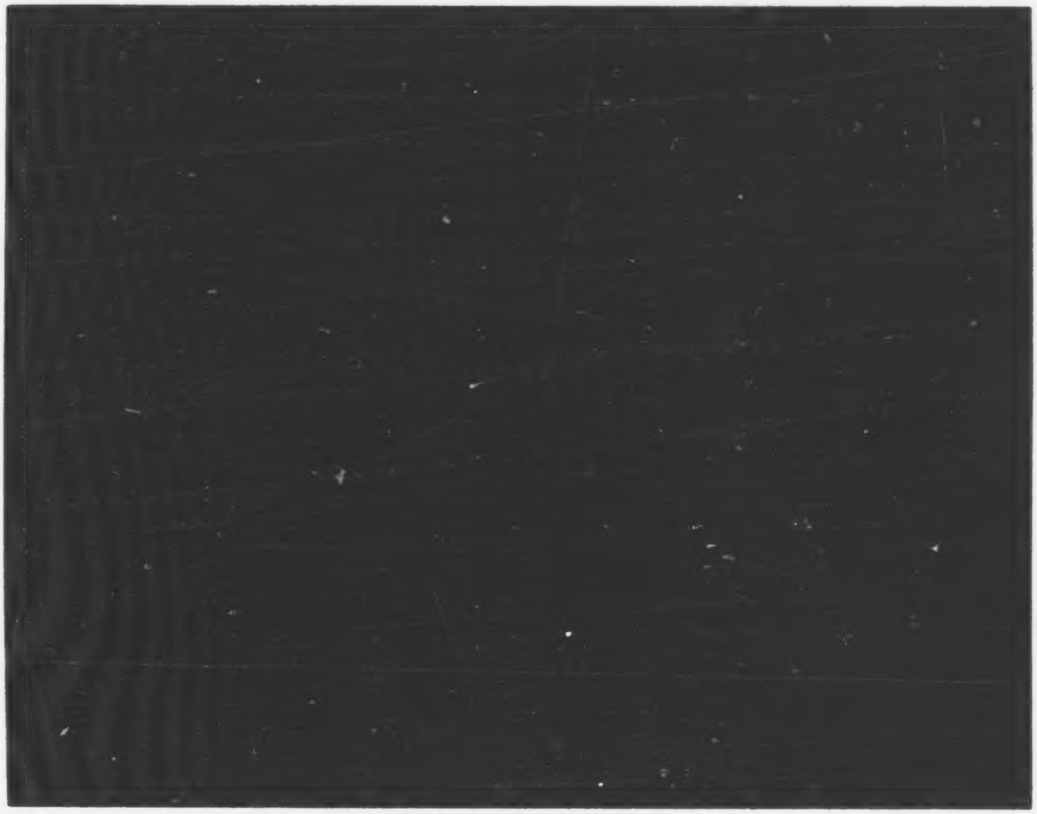

Figure 3.2-4 Task 1 Test Article in the Test Chamber.

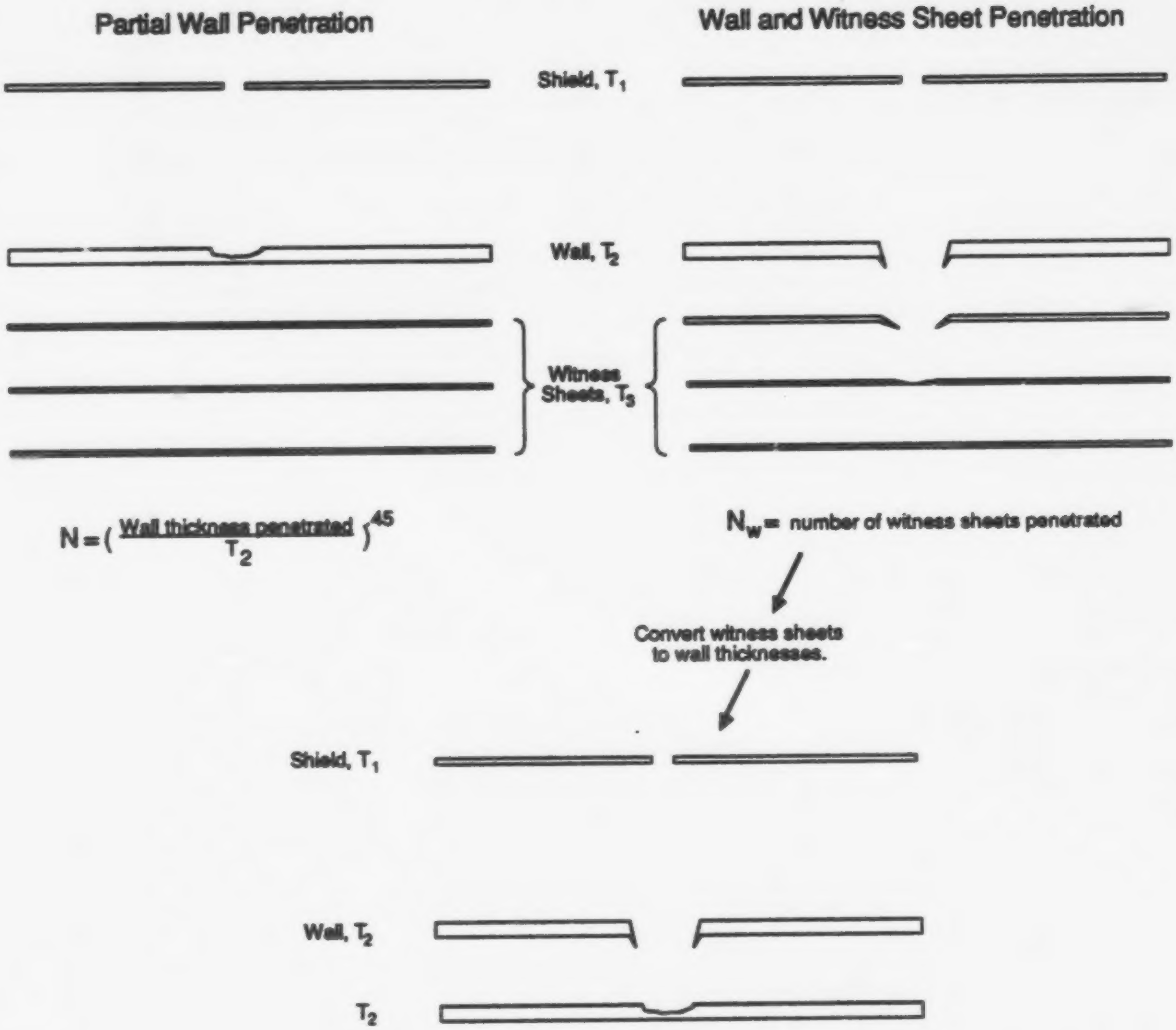
Partial Wall Penetration
Wall and Witness Sheet Penetration
Shield, T1
Wall, T2
Witness Sheets, T3
Convert witness sheets to wall thicknesses.
Shield, T1
Wall, T2
T2

$$N = \left(\frac{\text{Wall thickness penetrated}}{T_2} \right)^{45}$$

N_w = number of witness sheets penetrated

$$N = 1 + N_w \left(\frac{T_3}{T_2} \right)^{7/12}$$

N = Normalized Penetration

(equivalent number of plates penetrated (other than T_1) of thickness T_2. Therefore, $N > 1$ represents wall penetration.)

Reference: G.T. Burch, Air Force Armament Laboratory Technical Report AFATL-TR-67-116, Boeing, 1967.

Figure 3.2-5. Normalized Penetration – Witness Plates Penetrated Converted to Equivalent Back Wall Thickness.

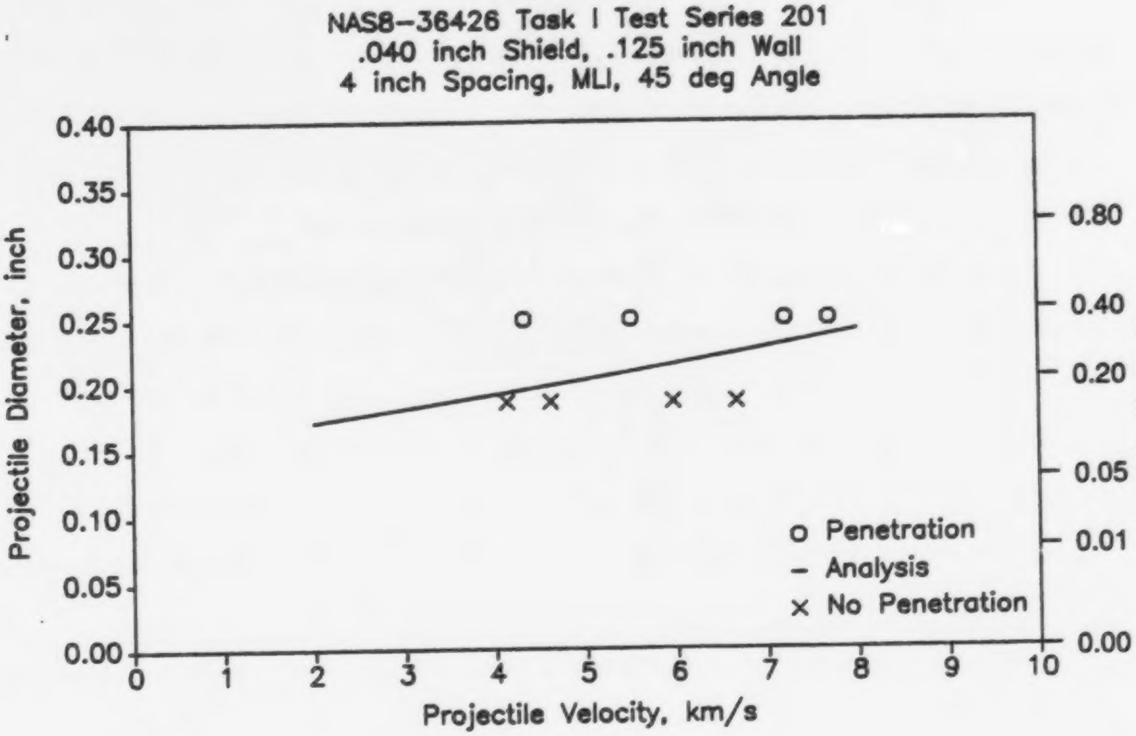

Figure 3.2-6. Task 1 Test Series 201.

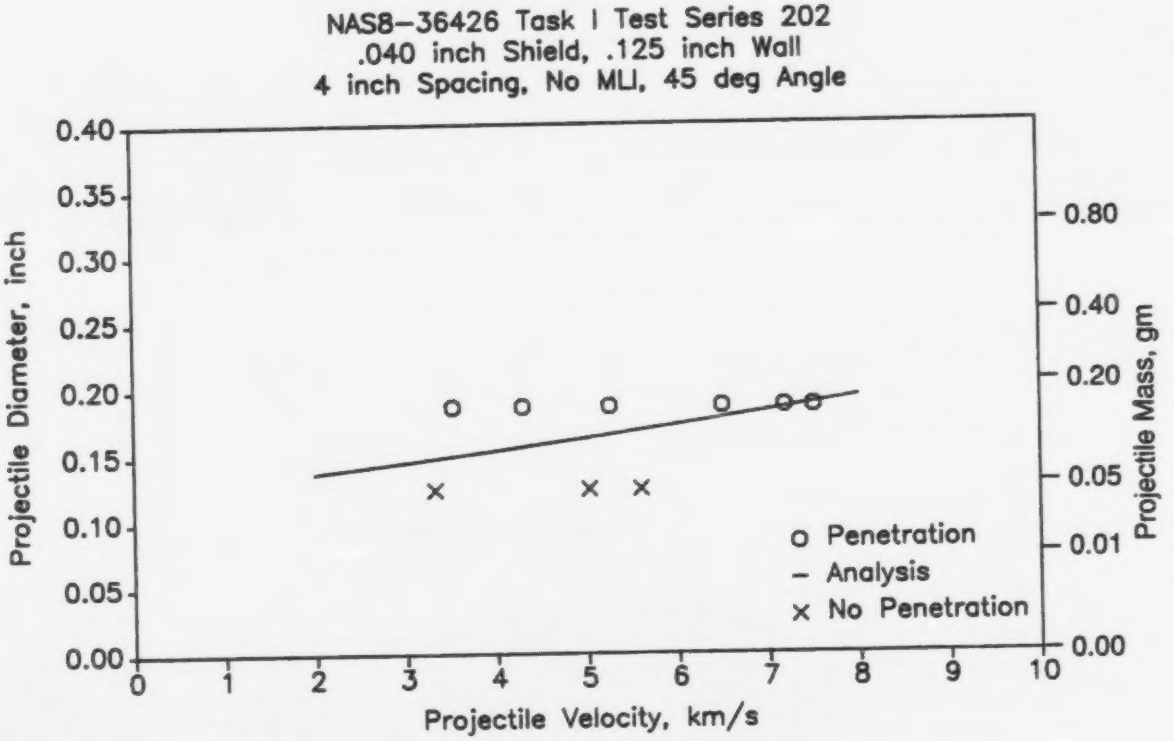

Figure 3.2-7. Task 1 Test Series 202.

module. Most previous testing for transient effects concentrated on small test chambers, and often used high percentages of oxygen in the atmosphere. This program used a large chamber containing a standard atmosphere. A primary intent of our test program was to identify instrumentation and systems required for an improved test program to follow.

Test Design. Testing was conducted at the MSFC hypervelocity facility to measure the transient effects in a large chamber at 1 atm as illustrated in figure 3.3-1. The test summary is shown in figure 3.3-2. Most test configurations are dual wall (shield and backwall) with and without MLI because we expect the module to use this construction in most areas. Four tests were performed on a single wall with and without MLI to measure any variation in response resulting from lack of a shield. Projectile sizes ranged from 0.125- to 0.350-in diameter to produce a variety of penetration severities.

The instrumentation used during testing is outlined in figure 3.3-3 and is diagrammed in figure 3.3-1. The figure 3.3-4 photograph shows the witness plate used to represent internal structure and the pressure transducers mounted on a support behind it. Figure 3.3-5 shows the test article bolted to the flange inside the chamber and the pressure transducers and photodiodes mounted close to the penetration site.

Test Results. Results of task 2 testing is discussed in section 5.0 and appendix I.

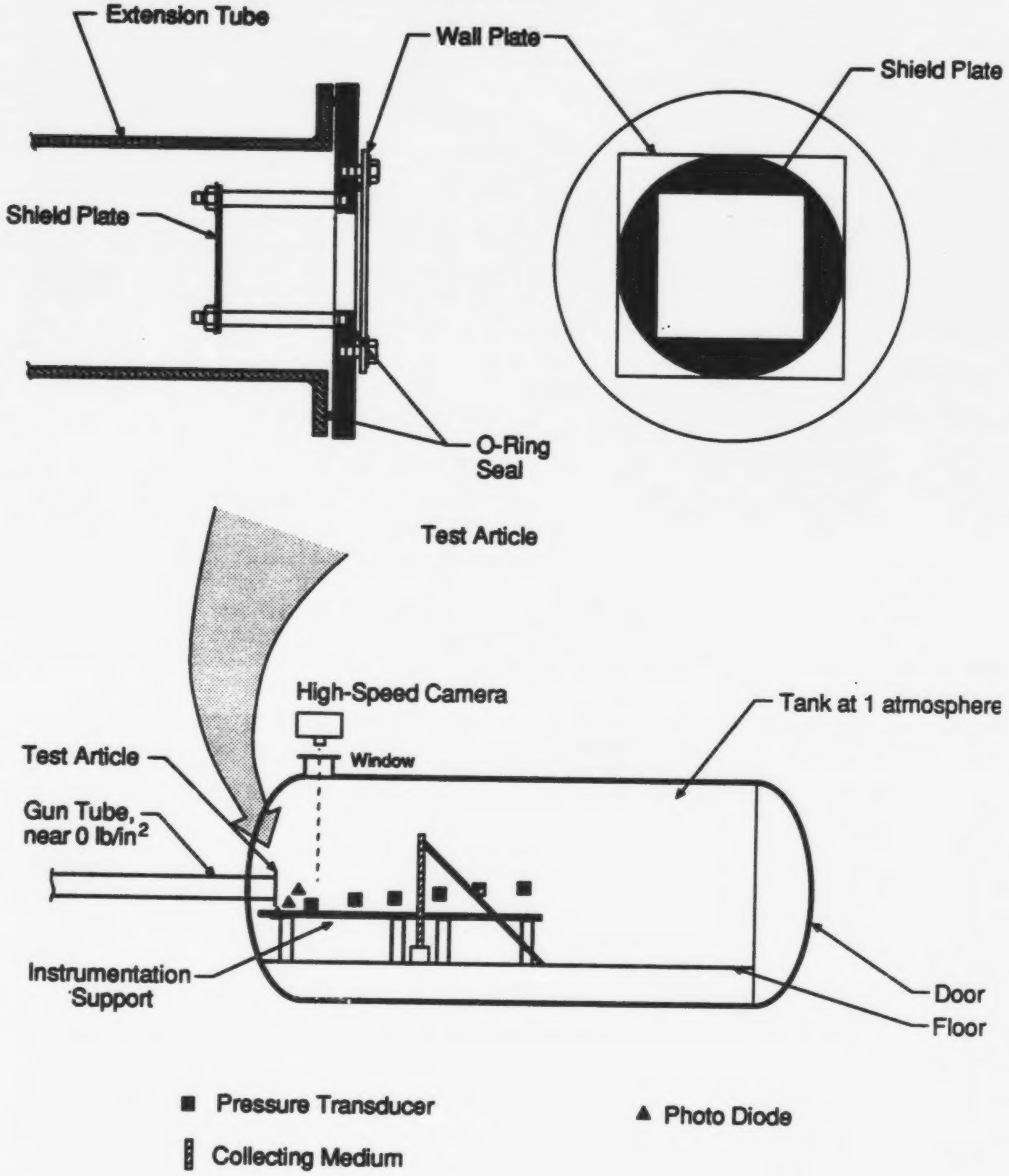
Extension Tube
Wall Plate
Shield Plate
Shield Plate
O-Ring Seal
Test Article
High-Speed Camera
Tank at 1 atmosphere
Window
Test Article
Gun Tube, near 0 lb/in²
Instrumentation Support
Door
Floor
■ Pressure Transducer
▲ Photo Diode
Collecting Medium

Figure 3.3-1. Effects of Penetration Test Chamber and Setup.

]

Test Number	1	2	3	4	5	6	7	8	9	10	11	12	13	14	15	16	17	18	19	20	21	22	23
MLI																							
Yes	●		●		●		●		●		●		●	●	●		●		●		●		●
No		●		●		●		●		●		●				●		●		●		●	
Shield																							
0.040	●	●			●	●								●	●	●					●	●	
0.063			●	●			●	●					●				●	●	●	●			●
none									●	●	●	●											
Projectile Dia																							
sphere 0.125									●	●													
0.187	●	●																					
0.250			●	●							●	●											
0.313					●	●	●	●															
0.350															●	●	●	●	●	●	●	●	●
cylinder 0.200													●	●									
Spacing																							
4	●	●	●	●	●	●	●	●	●	●	●	●	●	●	●	●	●	●			●	●	●
6																			●	●			
Impact Angle																							
0-deg	●	●	●	●	●	●	●	●	●	●	●	●	●	●	●	●	●	●	●	●	●	●	●
45-deg																							

All dimensions in inches; all wall thicknesses = 0.125 inch.

Figure 3.3-2. Task 2 Test Configuration Summary.

Instrument	Commercial Type	Environmental Effect	Response Range	Number Required
Photodiode	EG&G HD - 1100	Flash Intensity and Temperature	Wavelength 400 to 1100 nanometers	2
Pressure Transducer	DCB H109/A02	Pressure Pulse	125,000 lb/in^2 0.0005 Hz to 500 kHz	6
High Speed Camera	HYCAM	Visual Effects	8000 frames per sec	1
H Field Sensor	Wire coil with RF amplifier and oscilloscope	Electro Magnetic Pulse	100 MHz	1
Witness Plates/ Collecting Medium	To include materials used in module interiors and calibrated geletin.	Effects on Materials		1

Figure 3.3-3. Task 2 Effects of Penetration Testing Instrumentation.

Figure 3.3-4. Task 2 Instrumentation Setup Inside the Large Test Chamber Behind the Witness Panel.

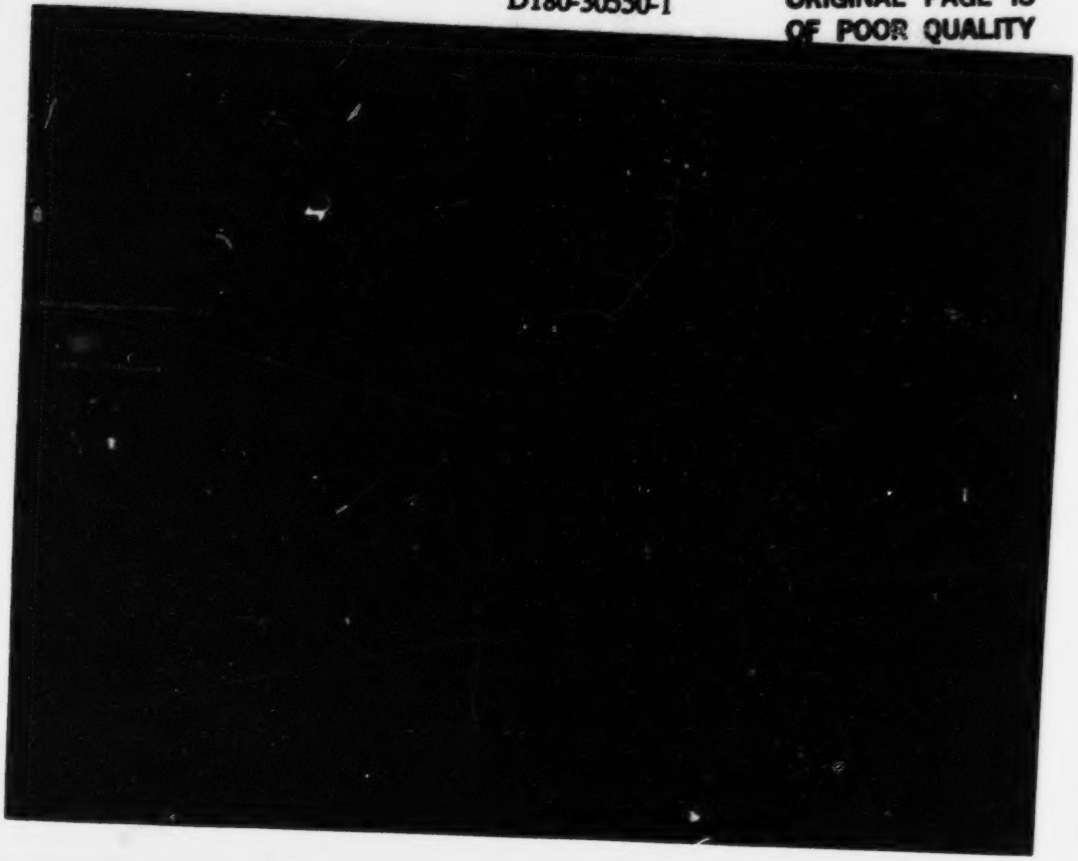

Figure 3.3-5. Task 2 Test Article, Pressure Transducers, and Photodiodes Inside Large Test Chamber.

4.0 WALL DAMAGE CHARACTERIZATION AND PENETRATION CRITERIA

4.1 TASK 1 DATA ANALYSIS

Data Analysis for Penetration Prediction. Pressure wall (backwall) damage can occur in several ways, such as cratering, spalling, fracture, crack propagation, perforation, and combinations of these. A definition of acceptable damage level in the pressure wall is required to ensure structural integrity and crew safety. The criteria for identifying pressure wall failure due to an impact is crucial in calculating an accurate penetration function and ultimately a probability of no penetration (PNP) for Space Station design. The criterion used in data analysis on this contract is light visible through the backwall constitutes a penetration. Quantification of damage is described in section 3.2.

Effect of Incident Angle. Data gathered on this and other programs show the range in damage produced by different incident angles. Figure 4.1-1 summarizes closely comparable tests varying only in angle, with other test variables held approximately constant. Reproducibility of impact velocity is difficult in hypervelocity testing, so the tests do not have precisely equal velocities. Nevertheless, we feel the velocities are close enough to draw meaningful conclusions. Damage as measured with witness plates and with the normalized penetration value indicates impacts at 45-deg incidence angles are more damaging than impacts at either 0-deg or 65-deg.

This conclusion is also supported by the photographs in figures 4.1-2 and 4.1-3, representing two pairs of tests appearing in figure 4.1-1. These photographs show the normal and flightpath backwall damage modes for two pairs of tests. (See fig. 3.2-3 for a definition of normal and flightpath.) The photographs show the damage mode has an angle dependency. The 45-deg impacts demonstrate a greater degree of damage in the flightpath direction, while the 65-deg impacts show a greater degree of damage in the normal direction. Flightpath damage caused the penetration in the 45-deg impacts. In these tests the flightpath damage of 65-deg impacts is less severe and does not penetrate. While normal damage increases for 65-deg impact, the increase in this case is not enough to penetrate. Both normal and flightpath modes are presumed to coincide

Test ID (6)	MLI	Projectile Diameter, in	Impact Velocity, km/s	Hole Depth, in	Witness Plates Penetrated	Normalized Penetration (5)	Impact Angle, deg
12 C (7)	Yes	0.250	4.33	0.100 (1)	0	0.904	0
205 A	Yes	0.250	4.20	0.125 (3)	0.25 (4)	1.086	45
209 A	Yes	0.250	4.37	0.061 (2)	0	0.722	65
21C (7)	Yes	0.300	6.60	0.01 (1)	0	0.317	0
212 B	Yes	0.300	6.38	0.125 (3)	2.75 (4)	1.944	45
207 B	Yes	0.300	6.47	0.125 (3)	0.1 (4)	1.034	65
230 D	No	0.250	5.51	0.125 (3)	2.5	1.858	45
136 A (8)	No	0.250	6.25	0.125 (3)	1	1.343	55
208 D	No	0.250	5.63	0.125 (3)	0	1.000	65

T_1 = 0.063 in
S = 4 in
T_2 = 0.125 in

(1) Estimated value
(2) Measured value
(3) Complete wall penetration
(4) Fractional value estimated
(5) Normalization procedure explained in figure 3.2-5.
(6) Test IDs refer to NAS8-36426 test program except as noted.
(7) SM-1 Test Program performed at MSFC.
(8) Martin Marietta Aerospace Test Program performed at MSFC.

Figure 4.1-1. Test Results Comparison for Effect of Impact Angle on Damage to Backwall.

ORIGINAL PAGE IS
OF POOR QUALITY

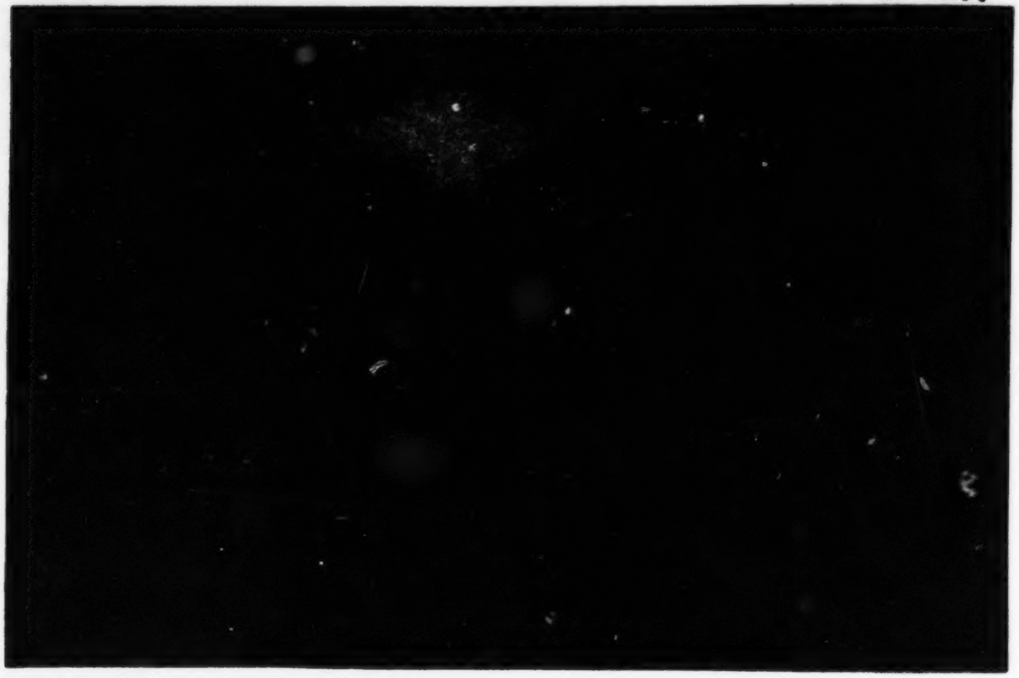

(a) 45-deg Impact Angle, 4.20 km/s (205 A)

(b) 65-deg Impact Angle, 4.37 km/s (209 A)

Figure 4.1-2. Impact Angle Effect on Backwall Damage for Tests With 0.063 in Shields, 4-in Spacing, 0.125-in Backwall, and MLI; 0.250-in Diameter Projectile.

ORIGINAL PAGE IS
OF POOR QUALITY

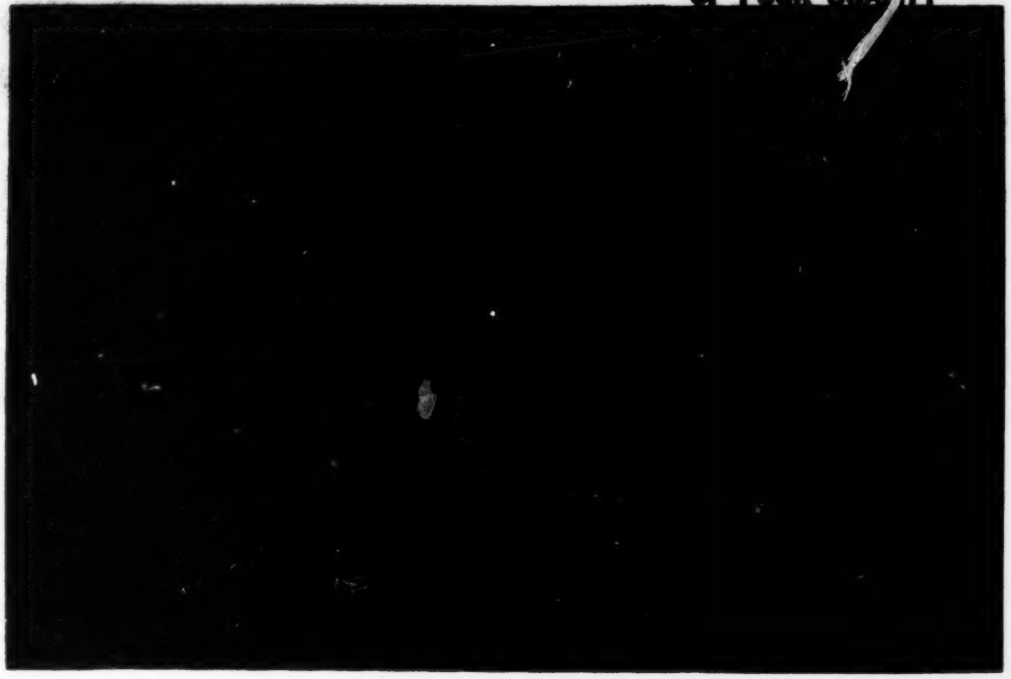

(a) 45-deg Impact Angle, 6.38 km/s (212 B)

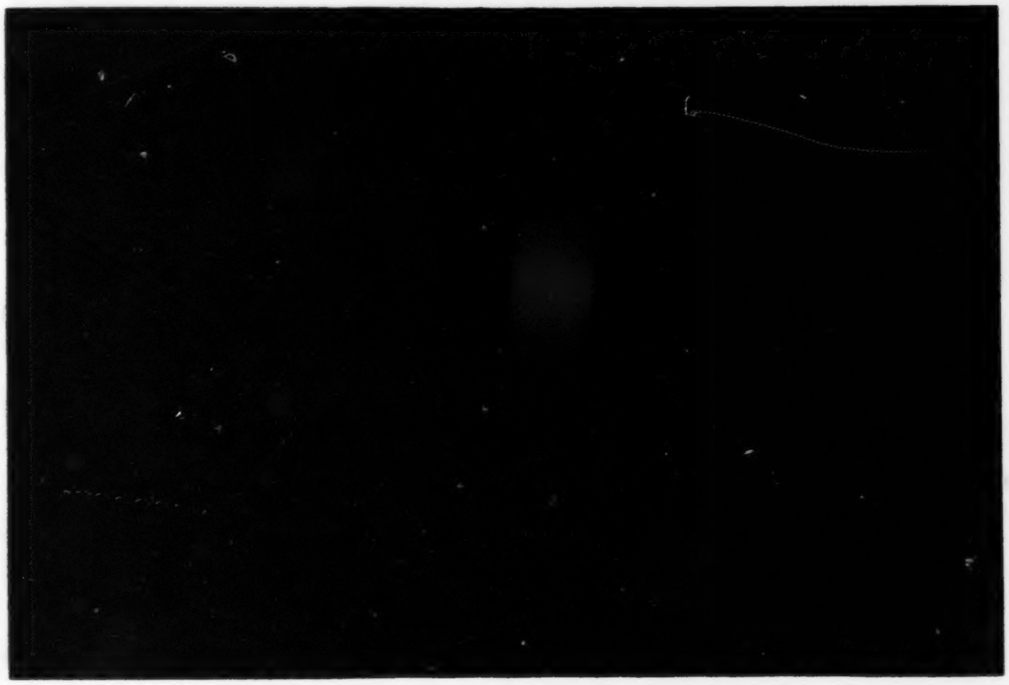

(b) 65-deg Impact Angle, 6.47 km/s (207 B)

Figure 4.1-3. Impact Angle Effect on Backwall Damage for Tests With 0.063-in Shields, 4-in Spacing, 0.125-in Backwall, and MLI; 0.300-in Diameter Projectile.

for 0-deg impacts. A phenomenological explanation for why 45-deg impacts are more damaging than 0-deg impacts is not yet available.

This discussion demonstrates, for incidence angles between 45 and 65-deg, that the damage mode crosses over from flightpath dominated to normal dominated. Figure 4.1-4 shows this transition as incidence angle increases from 45 through 55 to 65-deg. Figure 4.1-1 shows, for these tests, quantitatively measured damage (normalized penetration) decreasing as the incidence angle increases from 45 to 65-deg. This discussion also reinforces the argument for additional testing at these incidence angles.

Shield Thickness. Shields of differing thickness shatter the projectile in differing ways. Some investigators (ref. 3-1) have identified optimum ratios between shield thickness and projectile diameter. Our approach is to determine the lowest weight integrated wall (shield and backwall) design to achieve the required penetration-resistance level. Nevertheless, test data demonstrate that impact damage characteristics vary for different shield thicknesses and impact angles.

Figure 4.1-5 compares tests showing the effect shield thickness has on backwall and witness plate damage. At 0- and 45-deg incidence angles, damage is less severe for the thicker shield. The reverse is true at 65-deg, with the thinner shield resulting in less damage. This effect is also evident by observing damage on the test panels. The photographs in figure 4.1-6 show the normal and flightpath damage on the backwall for 45-deg impact and two different shield thicknesses. More severe damage is evident in the flightpath area with the thinner (0.040-in) shield (a), while normal damage (in the form of craters) is greater with the thicker (0.063-in) shield (b).

Conversely, figure 4.1-7 shows the damage modes of higher incidence angles (around 65-deg) crossover, with the normal damage component more severe than the flightpath damage component for both thick and thin shield configurations. Because normal damage controls for 65-deg and thick shields produce greater normal damage, thick shields are less efficient for high impact angles. The crossover impact angle occurs in the region between 45- and 65-deg.

ORIGINAL PAGE IS
OF POOR QUALITY

(a) 45-deg Impact Angle, 5.51 km/s (230 D)

(b) 55-deg Impact Angle, 6.25 km/s (136 A)

Martin Marietta Aerospace

Figure 4.1-4. Impact Angle Effect on Backwall Damage for Tests With 0.063-in Shields, 4-in Spacing, 0.125-in Backwall, No MLI; 0.250-in Diameter Projectile.

ORIGINAL PAGE IS
OF POOR QUALITY

(c) 65-deg Impact Angle, 5.63 km/s (208 D)

Figure 4.1-4. (Continued). Impact Angle Effect on Backwall Damage for Tests With 0.063-in Shields, 4-in Spacing, 0.125-in Backwall, No MLI; 0.250-in Diameter Projectile.

Test ID (6)	Shield Thickness, in	MLI	Projectile Diameter, in	Impact Velocity, km/s	Hole Depth, in	Witness Plates Penetrated	Normalized Penetration (5)	Impact Angle, deg
205 A	0.063	Yes	0.250	4.20	0.125 (3)	0.25 (4)	1.086	45
201 A	0.040	Yes	0.250	4.33	0.125 (3)	2.5 (4)	1.858	45
207 B	0.063	Yes	0.300	6.47	0.125 (3)	0.1 (4)	1.034	65
203 A	0.040	Yes	0.300	6.45	0.042 (2)	0	0.609	65
206 C	0.063	No	0.187	5.40	0.080 (1)	0	0.816	45
202 C	0.040	No	0.187	5.26	0.125 (3)	2.5 (4)	1.858	45
102 A(8)	0.080	Yes	0.300	5.35	0.020	0	0.435	0
21 D(7)	0.063	Yes	0.300	5.85	0.125	1	1.343	0

$S = 4$ in
$T_2 = 0.125$ in

(1) Estimated value
(2) Measured value
(3) Complete wall penetration
(4) Fractional value estimated

(5) Normalization procedure explained in Monthly Progress Report No. 19.
(6) Test IDs refer to NAS8-36426 test program except as noted.
(7) SM-1 Test Program performed at MSFC.
(8) Martin Marietta Aerospace Test Program performed at MSFC.

Figure 4.1-5. Test Results Comparison for Effect of Shield Thickness on Damage to Backwall.

ORIGINAL PAGE IS
OF POOR QUALITY

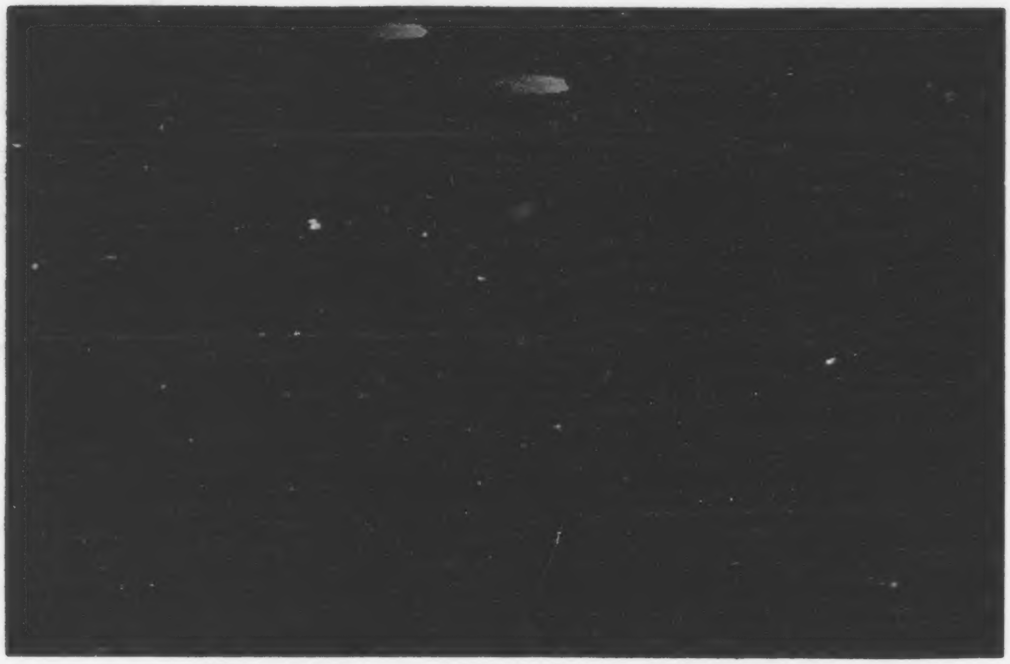

(a) 0.040-in Shield, 4.33 km/s (201 A)

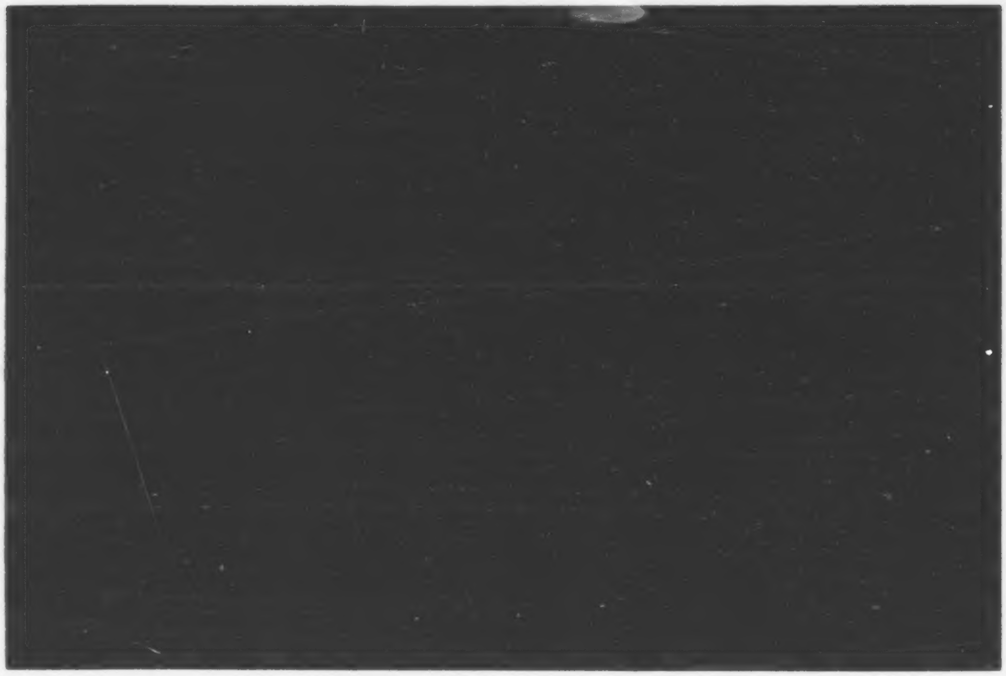

(b) 0.063-in Shield, 4.20 km/s (205 A)

Figure 4.1-6. Shield Thickness Effect on Backwall Damage for Tests With 4-in Spacing, 0.125-in Backwall, and MLI; 0.250-in Diameter Projectile at 45-deg Impact Angle.

(a) 0.040-in Shield, 6.45 km/s (203 A)

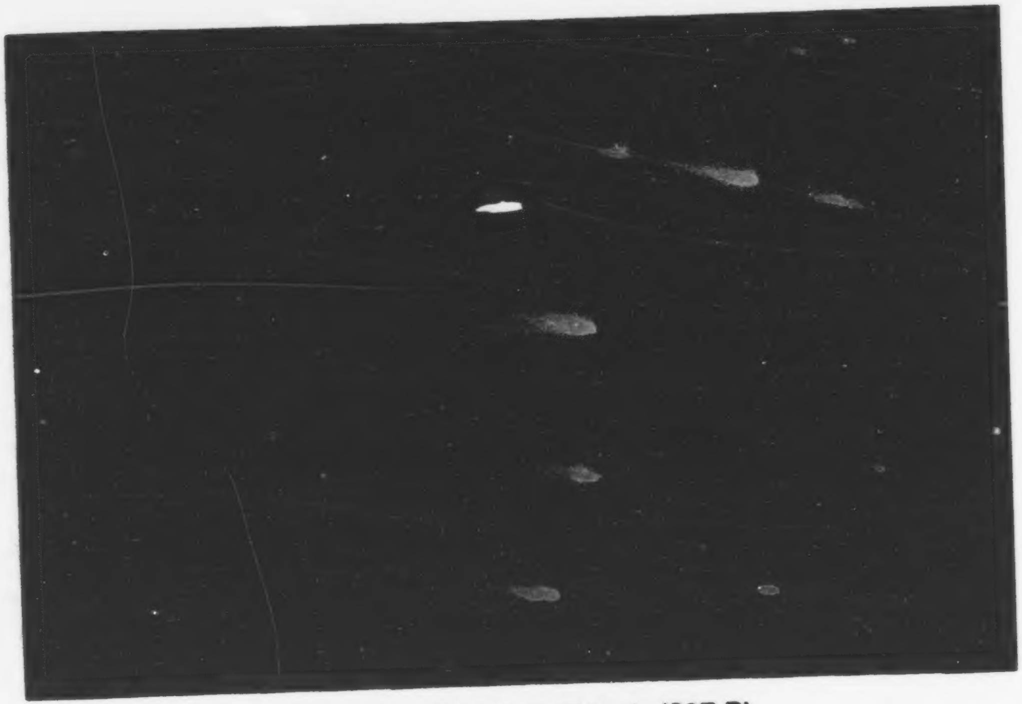

(b) 0.063-in Shield, 6.47 km/s (207 B)

Figure 4.1-7. Shield Thickness Effect on Backwall Damage for Tests With 4-in Spacing, 0.125-in Backwall, With MLI; 0.300-in Diameter Projectile at 65-deg Impact Angle.

The previous discussion has demonstrated the interrelationships among impact angle, shield thickness, and damage to the backwall. Because many impacts occur on the Space Station at angles in and above the region where damage modes cross over (see sec. 2.0 for the distribution of impact angles), an optimum shield thickness may exist for Space Station integrated wall designs. To determine the optimum shield thickness, the penetration function must correctly model the crossover effect. Additional test data in the high impact angle region will increase confidence in our penetration function.

Effect of Multilayer Insulation. Testing under this and other studies has demonstrated the effect multilayer insulation (MLI) has in inhibiting impact damage. Figure 4.1-8 shows the effect for normal impact by comparing damage for tests with and without MLI. The effect of MLI is to remove the smallest fragments from the cloud of fragments created by shield impact and thereby reduce damage to the backwall, as shown in figure 4.1-9. This means fewer small craters and fewer overlapping craters occur in the backwall. Dissipating the energy hitting the backwall also reduces spalling from backwall back side surface, as shown in figure 4.1-10. While the backwall unprotected by MLI is badly spalled, the backwall covered by MLI is only bulged. The damage mode is often a bulge with cracks for an MLI-covered backwall rather than the cratering and spallation experienced without MLI.

The MLI blanket can be severely damaged during an impact as shown in figure 4.1-11, which views the test article inside the test chamber immediately after the shot. Reinforcing the MLI with a scrim, performing like rip-stop nylon, would reduce the amount of damage. This photograph also illustrates that MLI tends to explode upon impact. In some tests using MLI, this explosion has deformed the shield against the flightpath direction as shown in figure 4.1-12.

4.2 LEXAN PROJECTILES

Four tests were conducted using lexan projectiles (spheres and cylinders) to investigate meteoroid-like (icy) impacts against Space Station structure. Lexan was chosen as a representative material because its density is close to water. Representative backwall damage is shown in figure

Test ID (6)	Shield Thickness, in	Wall, inch	MLI	Projectile Diameter, in	Impact Velocity, km/s	Hole Depth, in	Witness Plates Penetrated	Normalized Penetration (5)	Impact Angle, deg
213 B	0.080	0.188	No	0.313	5.90	0.188 (3)	0.25 (4)	1.086	0
229 A	0.080	0.188	Yes	0.313	5.30	0.090	0	0.718	0
202 D	0.040	0.125	No	0.187	6.50	0.125 (3)	2	1.687	45
221 A	0.040	0.125	Yes	0.187	6.67	0.056 (2)	0	0.694	45

Spacing = 4 in

(1) Estimated value
(2) Measured value
(3) Complete wall penetration
(4) Fractional value estimated
(5) Normalization procedure explained in Monthly Progress Report No. 19.
(6) Test IDs refer to NAS8-36426 test program.

Figure 4.1-8. Test Results Comparison for Effect of MLI on Damage to Backwall.

(a) Without MLI, 5.90 km/s (213 B front side)

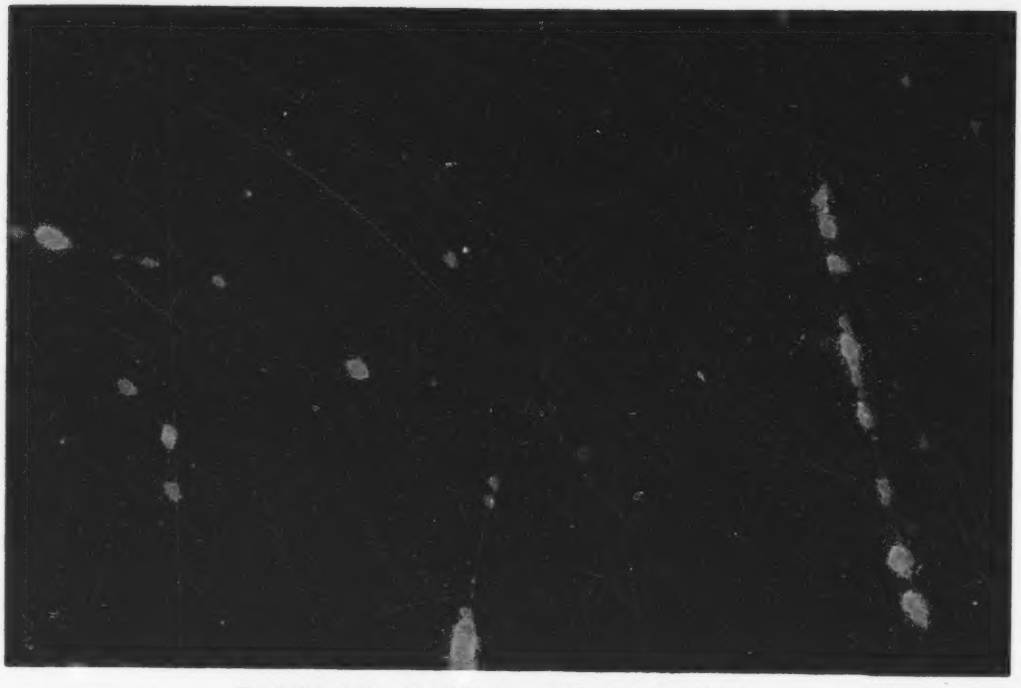

(b) With MLI, 5.30 km/s (229 A front side)

Figure 4.1-9. MLI Effect on Backwall Damage for Tests With 0.080-in Shields, 4 in Spacing, 0.188-in Backwall, 0.313-in Diameter Projectile at 0-deg Impact Angle.

ORIGINAL PAGE IS
OF POOR QUALITY

(a) Without MLI, 5.90 km/s (213 B back side)

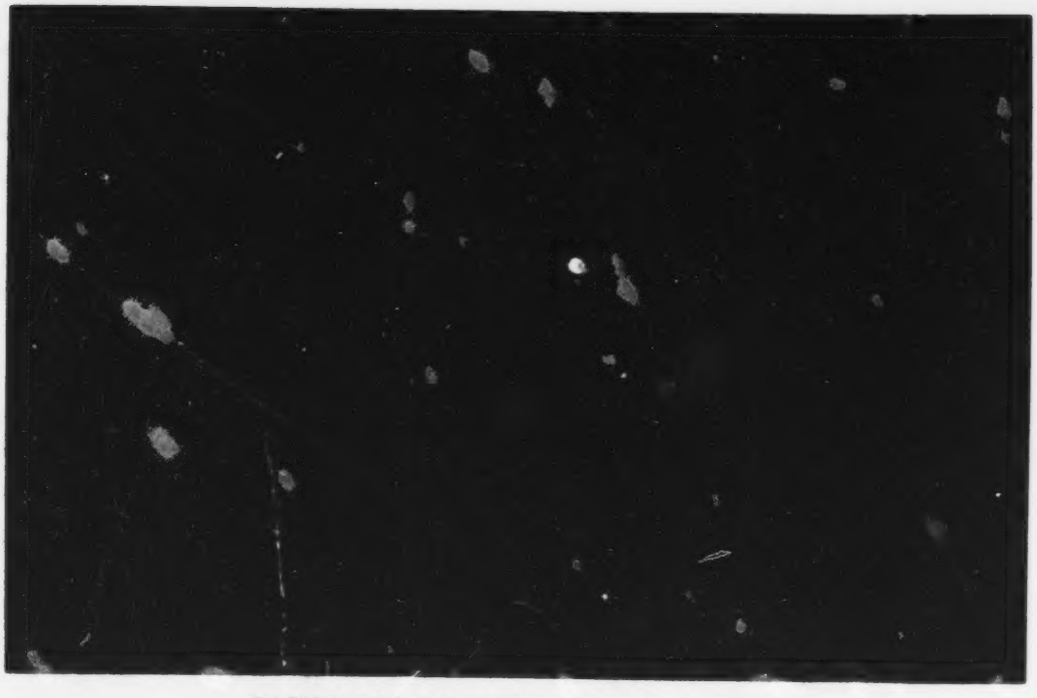

(b) With MLI, 5.30 km/s (229 A back side)

Figure 4.1-10. MLI Effect on Backwall Damage for Tests With 0.080-in Shields, 4 in Spacing, 0.188-in Backwall, 0.313-in Diameter Projectile at 0-deg Impact Angle.

ORIGINAL PAGE IS
OF POOR QUALITY

Figure 4.1-11. Multilayer Insulation (MLI) Damage From Hypervelocity Impact, Test 210 B.

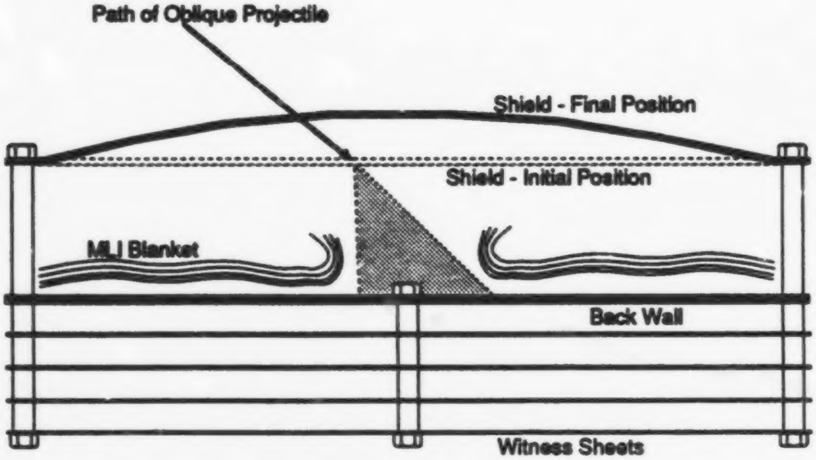
Path of Oblique Projectile
Shield - Final Position
Shield - Initial Position
MLI Blanket
Back Wall
Witness Sheets

Figure 4.1-12. Shield Blowback During Impact Tests With MLI.

(a) 0.368-gm Projectile, 5.80 km/s (225 A)

(b) 0.475-gm Projectile, 6.41 km/s (225 D)

Figure 4.2-1. Lexan Projectile Impacts, 0.040-in Shields, 4-in Spacing, 0.125-in Backwall, No MLI.

ORIGINAL PAGE IS
OF POOR QUALITY

4.2-1. The smaller spherical lexan projectiles failed to penetrate in three tests, so the fourth test used a larger mass cylindrical lexan sabot. The sabot penetrated four witness sheets as well as the backwall.

4.3 MULTIPLE VARIABLE LINEAR REGRESSION

An Empirical Penetration Function. Penetration functions represent critical projectile diameters as a function of projectile velocity for a specific integrated wall design. A critical projectile just barely penetrates the backwall. Empirical penetration functions are possible for impacts below 8 km/s because testing can be performed for these velocities. Previously developed empirical penetration functions are presented in references 3-1 and 3-2 for velocities between 3 and 8 km/s known as the shatter regime, and reference 4-1 for velocities below 3 km/s known as the ballistic regime. Test data from this contract, and other testing performed from 1985 to 1987 at MSFC, reflect plate thicknesses and spacings typically specified in Space Station integrated wall designs. Many of these tests also include MLI between the shield and backwall, and have oblique impact angles. We used these test data to evaluate the existing empirical penetration functions and to develop an alternative penetration function in the shatter range with multiple variable linear regression as outlined in the task flow diagram in figure 4.3-1.

Linear Regression. Advantages and disadvantages of the regression technique are outlined in figure 4.3-2. Primary advantages center on the quantitative results obtainable from the final penetration function developed. The penetration function can be used to assess the relative penetration resistance of proposed integrated wall designs and can be applied in the BUMPER code to determine an overall PNP estimate for the module group. Disadvantages of the technique extend from the problems of choosing appropriate variables to constitute the function and from the quality of available test data. These disadvantages can be minimized by planning test programs to provide a meaningful range of all design variables. All values in the range should be evenly represented to maximize confidence in the trends. Also, variables can be chosen to reflect hypothesized physical effects.

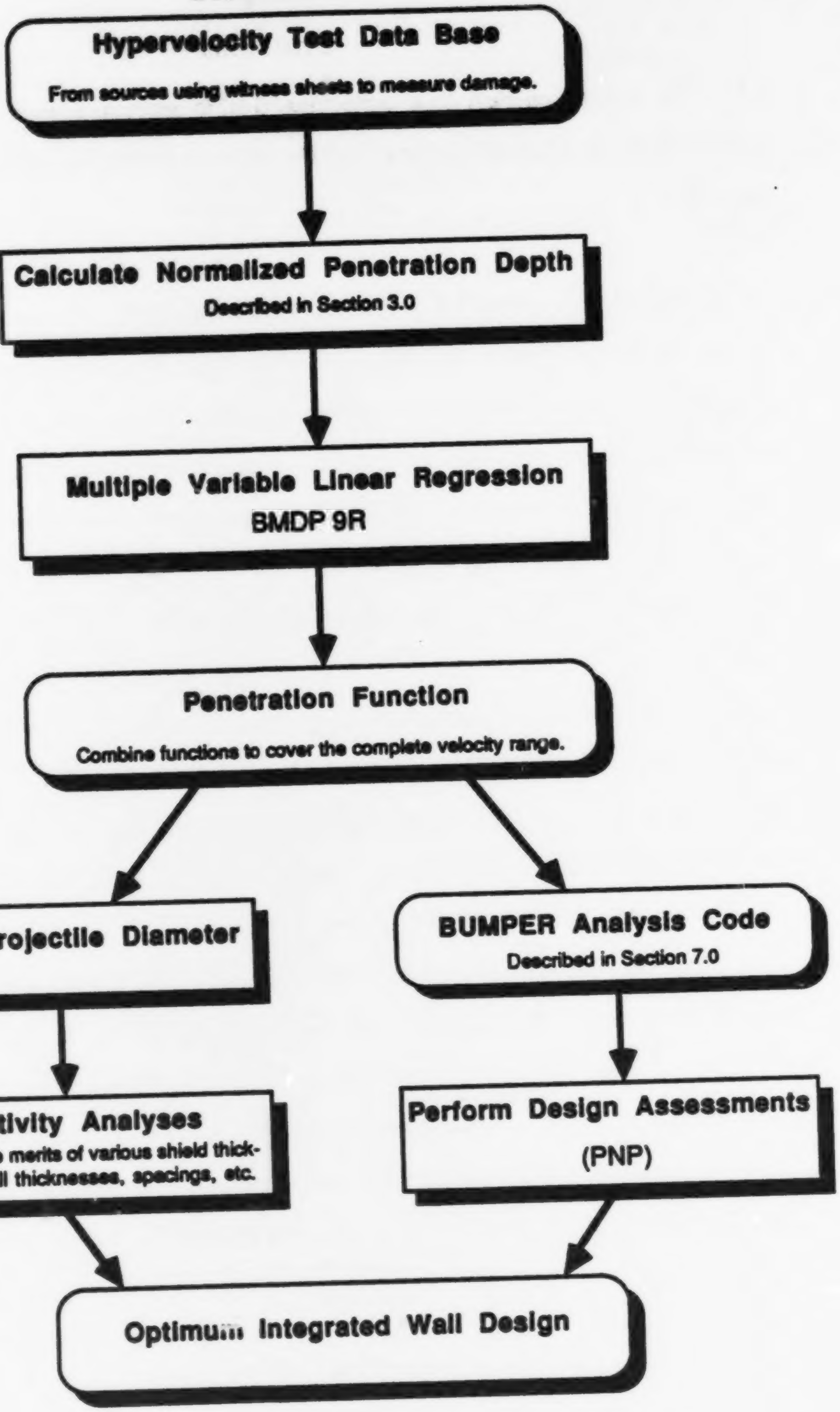
Hypervelocity Test Data Base
From sources using witness sheets to measure damage.
Calculate Normalized Penetration Depth
Described in Section 3.0
Multiple Variable Linear Regression
BMDP 9R
Penetration Function
Combine functions to cover the complete velocity range.
Critical Projectile Diameter
BUMPER Analysis Code
Described in Section 7.0
Sensitivity Analyses
Compare relative merits of various shield thicknesses, backwall thicknesses, spacings, etc.
Perform Design Assessments
(PNP)
Optimum Integrated Wall Design

Figure 4.3-1. Development and Use of a Multiple Variable Linear Regression Penetration Function.

Advantages	**Disadvantages**
• Results are quantitative. • Penetration function is objectively derived. • Leads to sensitivity studies. • Can use function to evaluate hypothetical designs. • Function can reveal and quantify trends not apparent from 2D data plots. • Global trends can be revealed that may not appear in subsets of the data base.	• Results are data base dependent.† • Results depend somewhat on the variables chosen. • Function may not model physical processes. • Agreement between function and all data may not be achieved. † 1. Large and consistent data spread required in all test variables for confidence in the results. 2. All important variables may not show significance and therefore may not be represented in the penetration function. 3. The degree of penetration must be quantified in a way useful to the eventual application of the penetration function.

Figure 4.3-2. Assessment of the Multiple Linear Regression Technique.

Basic Test Variables	T_1 T_2 S D MLI V θ
Multiplicative Combinations of Test Variables	T_1^2 T_2^2 S^2 $D \times T_1$ $MLI \times T_1$ $T_1 \times T_2$ $\sin\theta$ $\cos\theta$ $\tan\theta$ $V \times \cos\theta$ $V \times T_2$ $T_2 \times \cos\theta$ $MLI \times T_1 \times \cos\theta$ $MLI \times T_2 \times \cos\theta$
Ratios of Test Variables	$\frac{S}{D}$ $\frac{T_1}{D}$ $\frac{V}{T_2}$ $\frac{T_2}{D}$

T_1 = Shield Thickness, T_2 = Backwall Thickness, S = Spacing, D = Projectile Diameter
θ = Impact Angle, MLI = Multilayer Insulation (1 if included, 0 if not included),
V = Projectile Velocity

Figure 4.3-3. A Sample of Variables Used in the Multiple Linear Regression Studies.

Data Base. The data base included only test data employing witness sheets (see fig. 3.2-3), which provide a consistent method for measuring damage. In addition to testing performed under this contract, data sources include references 3-1, 3-2, and 3-3 plus data from MMA testing performed at MSFC during 1985 and 1986. Shield thicknesses ranged from 0.51 to 4.06 mm (0.020 to 0.160 in), spacings ranged from 25.4 to 305 mm (1 to 12 in), backwall thicknesses ranged from 0.25 to 5.72 mm (0.010 to 0.225 in), impact angles ranged from 0- to 75-deg, and impact velocities ranged form 1.40 to 7.83 km/s. This data base is weak in some areas such as shield thicknesses above 2.03 mm (0.080 in), spacings above 203 mm (8 in), and backwall thicknesses above 4.78 mm (0.188 in). The complete data base is listed in appendix C.

A single numerical quantity (normalized penetration depth, N) specified the amount of damage depending on the depth of the deepest crater or the number of witness sheets penetrated. The technique for calculating this normalized penetration depth is described in section 3.2. N is the regression-dependent variable. The penetration function value is therefore the normalized penetration depth, N. The penetration function takes the general form: $N = f(D, V, \text{other test parameters})$. Solving the penetration function for $N = 1$ produces projectile diameter, D, and velocity, V, pairs describing the line between penetrating and nonpenetrating projectiles. This line is also termed the penetration function and is illustrated in the figures of appendix J.

The Form of the Function. Regression variables were chosen from three categories: (1) geometric dimensions of the basic test parameters, (2) multiplicative combinations of these geometric dimensions, and (3) ratios of the geometric dimensions suggested in previous studies. Some of these variables are shown in figure 4.3-3. An approach to solving the problem of determining the appropriate combination of these variables is to apply a microcomputer statistical software package, BMDP (ref. 4-2). One of the subprograms of BMDP, 9R, was used to develop penetration functions with various combinations of the regression variables. Starting with a list of potential penetration function variables, the 9R subprogram forms all possible subsets of variables, performs multiple variable linear regressions on these subsets, and searches the results for the best

T_1															
T_1^2										●	●	●	●	●	●
T_2		●	●	●	●	●	●	●	●	●	●	●	●	●	●
T_2^2		●	●	●	●	●	●	●	●	●	●	●	●	●	●
S															●
D			●	●	●	●	●	●	●	●	●	●	●	●	●
$\cos\theta$															
$\sin\theta$						●	●	●	●	●	●	●	●	●	●
V^2												●	●		
MLI							●		●	●	●	●	●	●	●
$\tan\theta$						●	●	●	●	●	●	●	●	●	●
$T_1 \times T_2$											●	●			
$V \times \cos\theta$								●	●	●	●		●	●	●
MLI $T_1 \cos\theta$					●										
MLI $T_2 \cos\theta$															
MLI $T_1 \sin\theta$															
MLI $T_2 \sin\theta$															
D T_1								●	●	●	●	●	●	●	●
V/T_2				●	●	●	●								
V T_2									●	●	●	●	●	●	●
S/D														●	
T_1/D															
T_2/D	●														
Number of Variables Included	1	2	3	4	5	6	7	8	9	10	11	11	11	11	11
R^2	.561	.633	.718	.755	.775	.793	.812	.827	.837	.842	.848	.845	.844	.843	.843

Best overall

Alternative 11 variable penetration functions.

Figure 4.3-4. Variables Included In Best Fit Penetration Functions as Determined by BMDP 9R.

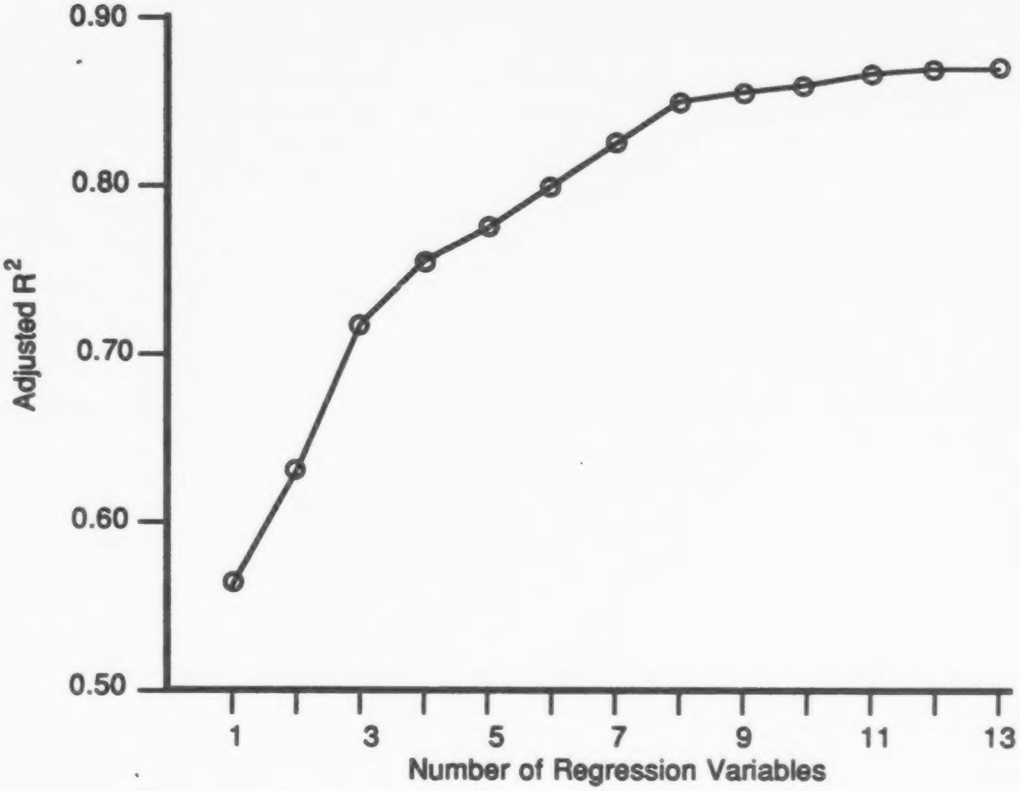

Figure 4.3-5. Analysis for Optimum Number of Regression Variables.

Variable	Coefficient Estimate	t - test	Significance Level
Intercept	3.685		
T_1^2	122.4	4.27	<.0001
T_2	-51.88	-15.74	<.0001
T_2^2	103.8	9.37	<.0001
D	15.19	11.50	<.0001
$\sin\theta$	1.421	6.70	<.0001
MLI	-0.5174	-7.22	<.0001
$\tan\theta$	-1.119	-10.39	<.0001
$T_1 \times T_2$	99.78	3.31	<.001
$V \times \cos\theta$	-0.3490	-6.45	<.0001
$D \times T_1$	-128.8	-5.72	<.0001
$V \times T_2$	1.767	4.31	<.0001

Coefficient of determination, $R^2 = 0.849$ 254 Data points

N = Number of equivalent thickness back walls (T_2) penetrated:

$$N = 3.685 + 122.4T_1^2 - 51.88\,T_2 + 103.8\,T_2^2 + 15.19\,D + 1.421\sin\theta - 0.5174\,(MLI) - 1.119\tan\theta + 99.78\,T_1T_2 - 0.3490\,V\cos\theta - 128.8\,D\,T_1 + 1.767\,V\,T_2$$

T_1, T_2, and D in inches, V in km/s. MLI = 1 if included, 0 if not included.

Figure 4.3-6. BMDP-Derived Penetration Function in 11 Variables.

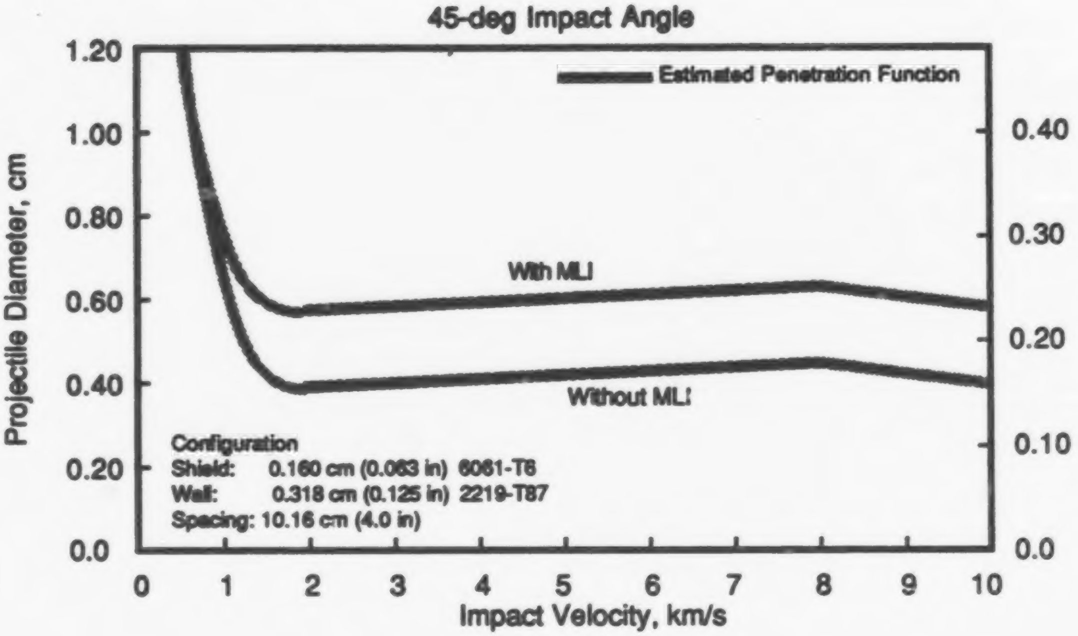

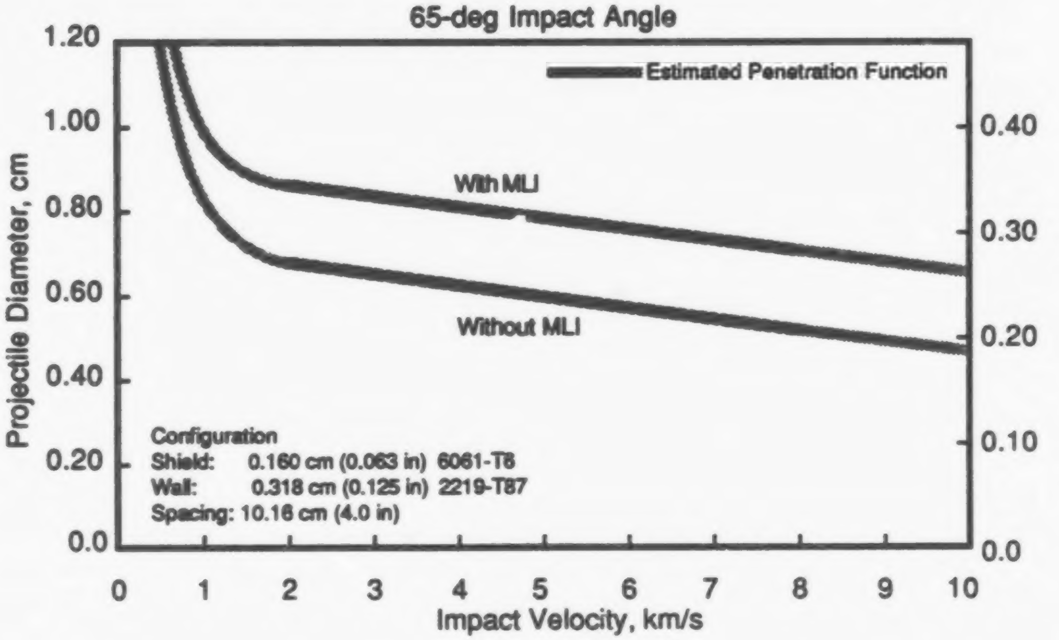

Figure 4.3-7. MLI Advantage as Indicated by Linear Regression Penetration Function.

fitting subsets. Best fit is judged with the coefficient of determination, R^2. The coefficient of correlation is the square root of the coefficient of determination or R.

Figure 4.3-4 represents a 9R analysis performed using the 23 variables in the left-hand column. These variables were selected because they were considered fundamental to impact mechanics, or they performed well in earlier BMDP studies. (Some combinations of variables were never included in any functions.) The bullets in figure 4.3-4 indicate the best fit functions for a specific number of variables. The coefficients of determination corresponding to these best fits are listed in the bottom row. The left four columns list alternative functions to the best fit 11 variable function. This method of presentation also shows how specific variables enter and exit the best fit penetration function as the total number of variables increases.

A surprising development was that spacing, S, did not appear in a best fit penetration function, but appeared only in the fourth and fifth best function for 11 variables. When included, spacing had weak significance, often in excess of 0.05 as measured by the Student t statistic. This result indicates spacing has a weak effect on penetration resistance in the velocity range between 2 and 8 km/s. Similarly, several ratios (S/D, T_1/D, T_2/D) appearing in penetration functions from other studies (refs. 3-1 and 3-2) are not significant in figure 4.3-4.

Many variables can be included in one penetration function, although there is usually a limit to the number of significant variables. As variables are added to a particular penetration function, the R^2 continues to increase, but at an ever-diminishing rate. This effect is shown in figure 4.3-5. We therefore limit the number of variables in a penetration function to approximately 12.

The best fit penetration function off figure 4.3-4 (for 11 variables) is listed in figure 4.3-6. All variables are well within the required significance level of 0.05. When plotted, this penetration function shows expected integrated wall performance based on trends in the entire data base. Figure 4.3-7 shows the relative performance of MLI in raising the critical projectile diameter. This function is valid only between 2 and 8 km/s. Estimated critical projectile lines are included below 2 km/s and above 8 km/s to represent the role played by linear regression in determining the complete penetration function. The estimated functions represent trends revealed by other analytical techniques but are not numerically precise.

Results. The common way to present a penetration function is by plotting diameter versus velocity. Appendix H contains plots of the figure 4.3-6 penetration function for various shield thicknesses, backwall thicknesses, and impact incidence angles. The function plots as a straight line unless it contains a power term in either diameter or velocity.

No combination of variables was clearly superior to another. Selection of the best penetration function is therefore difficult. Nevertheless, some trends were consistent:

a. Some variables are consistently included in the highest scoring combinations; some variables are never included in any combinations. T_2 has the strongest role in most penetration functions.

b. Sensitivity studies on most of the penetration functions plotted showed 45-deg incident angles are more penetrating than 0-deg, and 65-deg incident angles are less penetrating than either 45- or 0-deg.

c. Penetration functions for 0-deg incident angles had less slope than previously thought (i.e. less velocity dependency). For 45-deg incident angles, the functions were essentially flat, and for 65-deg incident angles the functions were negatively sloped.

These conclusions must be considered with caution because the data base still lacks broad coverage in some areas, such as spacing and backwall thickness. More testing is required to make the regression technique completely satisfactory. Data are especially needed at high impact angles (40- to 75-deg.)

Alternative Approach to Linear Regression. Independent of and earlier than the effort previously described, a penetration function was assembled by trial and error. The specific variables were chosen to reflect expected performance in the integrated wall design and were included only if their t-test exceeded 2.00 (significance < 0.05.) Overall the functions were compared to one another by the coefficient of determination, R^2.

The best function obtained using this method is listed in figure 4.3-8. This is the penetration function depicted in the figures of appendix J and leads to alternative conclusions on the effect of impact angle. The slope of the critical diameter line decreases with increasing impact angle but does not become negative. In addition, this penetration function does not show a drop in critical diameter for 45-deg impacts.

Final Selection of a Regression Penetration Function. The alternative regression penetration function was the first to produce acceptable results and, because it maintains a positive slope, is more easily integrated into the BUMPER analysis described in section 7.0. Appropriate application of either the BMDP function or the alternative function depends on the task at hand.

4.4 BACKWALL FAILURE DEFINITION

Onset of Spallation Definition. When a hypervelocity particle impacts a plate, a compression wave propagates from the front surface toward the back surface. The compression wave is reflected from the back surface as a tensile wave. Spalling occurs when when this tensile wave exceeds the ultimate dynamic tensile yield strength of the material (ref. 4-3).

To account for penetrations caused by a combination of cratering and spalling, we use a spall factor in our penetration analysis code. One option for this spall factor is a constant 0.85 (i.e., failure is assumed to occur when the calculated crater depth reaches 85% of the plate thickness). This estimate was based on a few normal impact tests that resulted in penetrations, which were performed early in the Space Station Advanced Development SM-1 Test Program (ref. 3-3.) The spall factor provides a margin of safety over a perforation criterion.

Analysis of available test data shows the onset of spalling varies with the projectile velocity component normal to the backwall. Figure 4.4-1 shows only nonpenetrating tests from our data base to determine the minimum penetration depth where spallation occurs. The penetration fraction or normalized penetration is plotted against normal projectile velocity (velocity times the cosine of the impact angle). The penetration fraction is the ratio of the deepest crater depth in the backwall to the original backwall thickness raised to the 0.45 power, as described in figure 3.2-4. This

Variable	Coefficient Estimate	t - test	Significance Level, %
Intercept	1.52	2.03	<.05
$T_1^{1/3}$	-6.18	-7.03	<.0001
T_2	-18.8	-18.52	<.0001
$\frac{\log S}{D}$	-0.146	-2.40	<.05
$(MLI)(T_1)$	-14.0	-8.63	<.0001
$D^{1/3}$	10.8	9.79	<.0001
$V\cos^2\theta$	-0.287	-8.00	<.0001
$\tan\theta$	-0.713	-7.66	<.0001

Coefficient of determination, $R^2 = 0.77$ 234 Data points

N = Number of equivalent thickness back walls (T_2) penetrated:

$$N = 1.52 - 6.18\,T_1^{1/3} - 18.8\,T_2 - 0.146\,\frac{\log S}{D} - 14.0\,(MLI)(T_1) + 10.8\,D^{1/3} - 0.287\,V\cos^2\theta - 0.713\,\tan\theta$$

T_1, T_2, S, and D in inches, V in km/s. MLI = 1 if included, 0 if not included.

Figure 4.3-8. Early Regression Equation.

exponent correlates the predictions based on tests penetrating multiple, thin (0.020-in) witness sheets versus nonpenetrating thick backwall test data developed in reference 3-1. Figure 4.4-1 indicates the spalling factor varies from 0.90 at 2.6 km/s to approximately 0.43 at 6.1 km/s. This is consistent with the value of 0.476 at 7.4 km/s derived in reference 4-4. The spall factor is assumed equal to 1.0 (i.e., no spalling) at velocities below 2.0 km/s and equal to 0.43 above 6.1 km/s.

The data in figure 4.4-1 include results from tests performed at velocities between 1 and 7.4 km/s and aluminum shield thicknesses ranging from 1.02 to 2.03 mm (0.040 to 0.080 in). The backwall material was 2219-T87 aluminum in each test. The spacing between shield and backwall varied between 102 and 152 mm (4 and 6 in). The results may be configuration dependent and, although probably adequate for comparable aluminum configurations, may not be valid for materials other than aluminum.

We define the onset of spallation as the point where an impact causes deformation (bulging) and cracks on the backwall back side but no penetration occurs and no backwall material is released. (A velocity slightly faster would produce spalling.) This is a conservative approach to defining the backwall failure criterion because all the nonpenetrating, nonspalling tests shown above the assumed spall line in figure 4.4-1 would be considered failures.

Penetration Threshold Definition. A less conservative alternative approach is to define failure as the penetration threshold. The penetration threshold occurs when the bottom of the deepest impact crater on one side of the backwall and the bottom of the deepest spall formation on the other side just meet. Applying this criterion to test data requires some judgement because few tests actually achieve the penetration threshold. Tested backwalls judged near the penetration threshold were included in the sample. These test data are plotted in figure 4.4-2. The penetration fraction is defined the same as in figure 4.4-1. Many test specimens represented in figure 4.4-2 experienced spallation (those above the line), but the extent of spallation is not used directly in defining the penetration threshold.

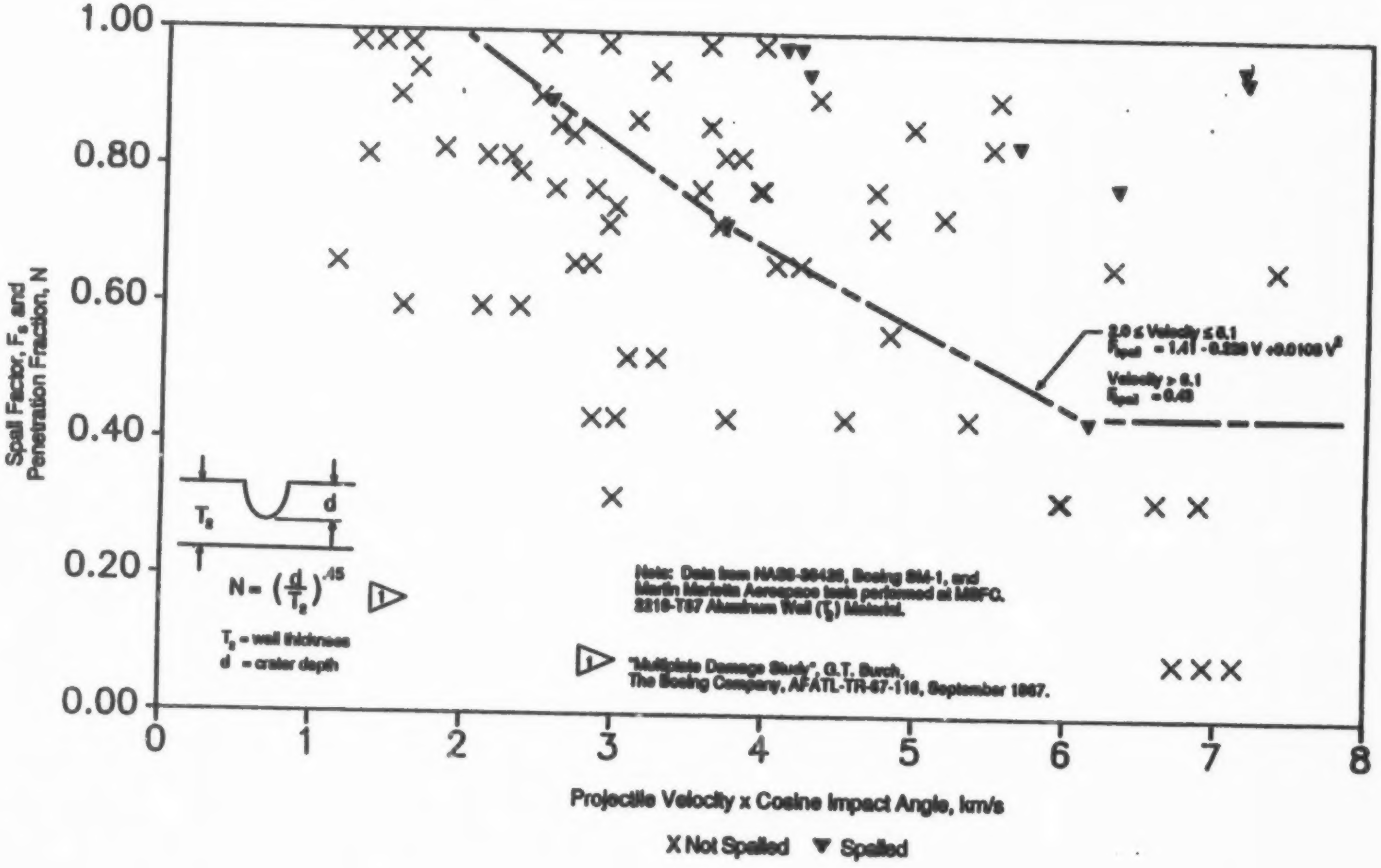

Figure 4.4-1. Spall Factor Function Derived from Nonpenetrating Hypervelocity Impact Tests

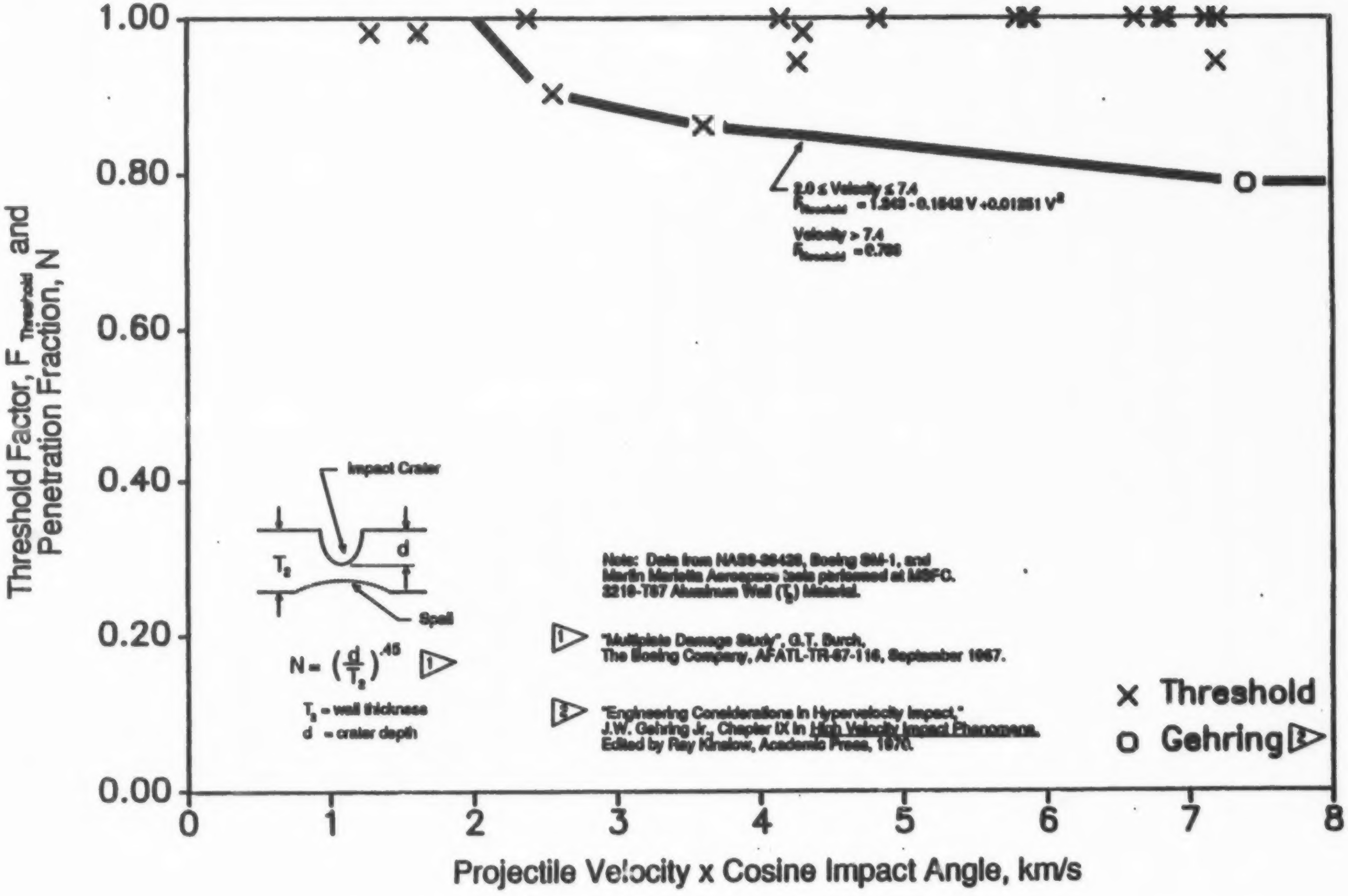

Figure 4.4-2. Penetration Threshold Factor Derived from Near Penetration Threshold Data

The threshold failure curve for the all-aluminum configurations tested is defined as follows: below 2.0 km/s the curve is set equal to 1.0 because spalling cannot occur below this velocity; above 7.4 km/s the factor is assumed to remain constant at 0.786 (ref. 4-4) to prevent failure due to perforation. The intermediate region is determined by the data points with the smallest penetration fraction (the lower boundary of the data in fig. 4.4-2) and defines the lower limit for nonpenetrating damage where the impact crater and spall damage just meet.

Failure Definition Comparisons. The reference Space Station configuration and integrated wall design, shown in figures 1.0-1 and 1.0-2, was analyzed using these two failure definitions in BUMPER (described in sec. 7.0) for comparison. The constant 0.85 spall factor produces a 93.4% PNP with the penetration analysis code. Substituting the curve in figure 4.4-1 for the constant quantitatively shows the effect of defining failure as the onset of spalling; PNP was 90.0%. In a similar manner we can substitute the threshold equation shown in figure 4.4-2 into a second version of our penetration analysis code; PNP was 92.2%. The absolute value of PNP is dependent on the penetration function, configuration, and environment definition used; nevertheless, the 2.2% difference is significant. A 10% increase in backwall thickness is required to raise the PNP from 90.0% to 92.2% using the operational (constant spall factor) code. All parametric data reported under this contract are based on the operational version of BUMPER.

For a constant PNP, integrated walls designed to the onset of spallation failure criterion expose personnel and equipment to less potential danger. The penalty, however, is increased shielding weight. The threshold failure criterion saves weight but may expose personnel and equipment to spall fragments traveling at hypervelocities.

4.5 IMPACT TESTING OF ALTERNATIVE SHIELD MATERIALS

Metallics. The contract test program included two metallic shield materials as potential alternatives to 6061-T6: (1) a lithium aluminum alloy (Li-Al) and (2) discontinuous silicon carbide reinforced aluminum metal matrix composite (dSiC/Al). The thicknesses available for test samples of Li-Al and dSiC could not be compared directly to 6061-T6 on an equal areal weight basis.

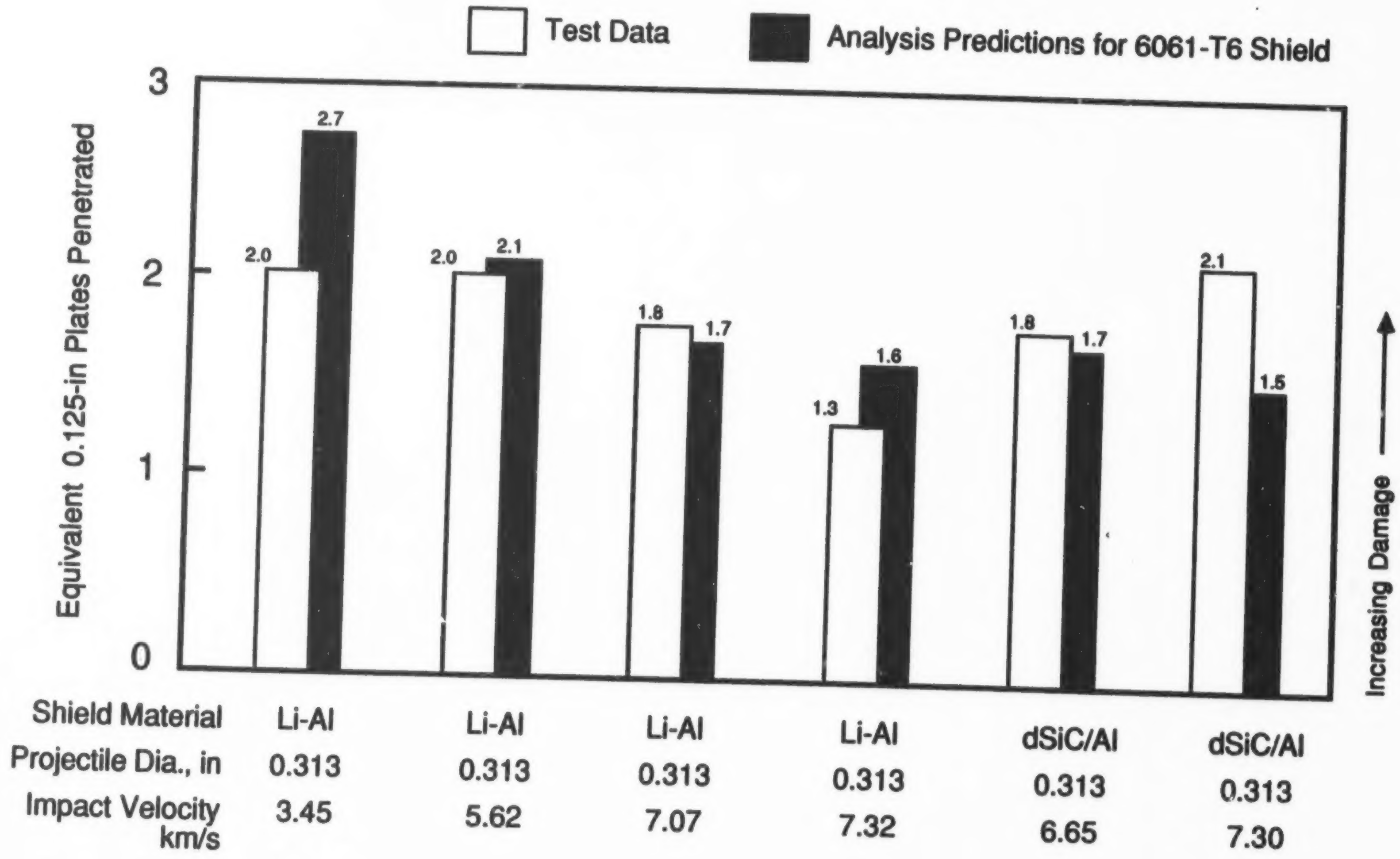

Li-Al - Lithium Aluminum dSiC/Al - Discontinuous Silicon Carbide / Aluminum

Wall thickness = 0.125-in; spacing = 4-in; no MLI present.

Figure 4.5-1. Comparison Between Test Damage and Analysis Predictions for Alternative Shield Materials.

Therefore, these data were compared in figure 4.5-1 using our penetration analysis for an equivalent configuration with a 6061 shield of areal weight equal to the Li-Al or dSiC/Al shields. The analysis calculates N, the number of equivalent backwall plates penetrated; shorter bars indicate less penetration. Li-Al performed better than the predicted performance for aluminum in three out of four tests, while dSiC/Al performed worse in both tests. Although the results for Li-Al appear encouraging, they are only preliminary indications for material evaluation. A complete test program incorporating various projectile diameters, impact angles, and target thicknesses would be required to quantify the performance of these materials.

Kevlar. Kevlar was tested as a shield material by MMA at MSFC. Figure 4.5-2 shows the results of hypervelocity impact tests of configurations with Kevlar and aluminum shields having approximately equal areal densities. The predicted performance of all aluminum configurations as determined by the regression analysis (described in sec. 4.3) is also shown for comparison. The data appear to indicate Kevlar and aluminum shields with equal area density have approximately equal penetration resistance. The results also show alternating penetration and no penetration with increasing velocity for the all aluminum specimens. This condition is not uncommon when using shields that are thick compared to the backwall. Previous testing has shown thick shields produce massive fragments that in turn become lethal projectiles on the backwall.

In figure 4.5-3, results for Kevlar shield testing are compared to predictions for aluminum shield configurations of approximately equivalent areal density. The methodology used for this comparison is the same as used in figure 4.5-1. These results also indicate that on an equal areal density basis, Kevlar and aluminum shields are equally effective in resisting penetration. Nevertheless, the data as presented in figures 4.5-2 and 4.5-3 do not reflect the relative severity of damage to the backwall.

The important difference between aluminum and Kevlar shields is revealed by comparing backwall damage test-to-test as shown in figure 4.5-4. Three pairs of tests were grouped according to approximately equivalent shield areal weight, projectile diameter, spacing, and backwall thickness. Impact velocities could not be duplicated exactly but are closely paired in each

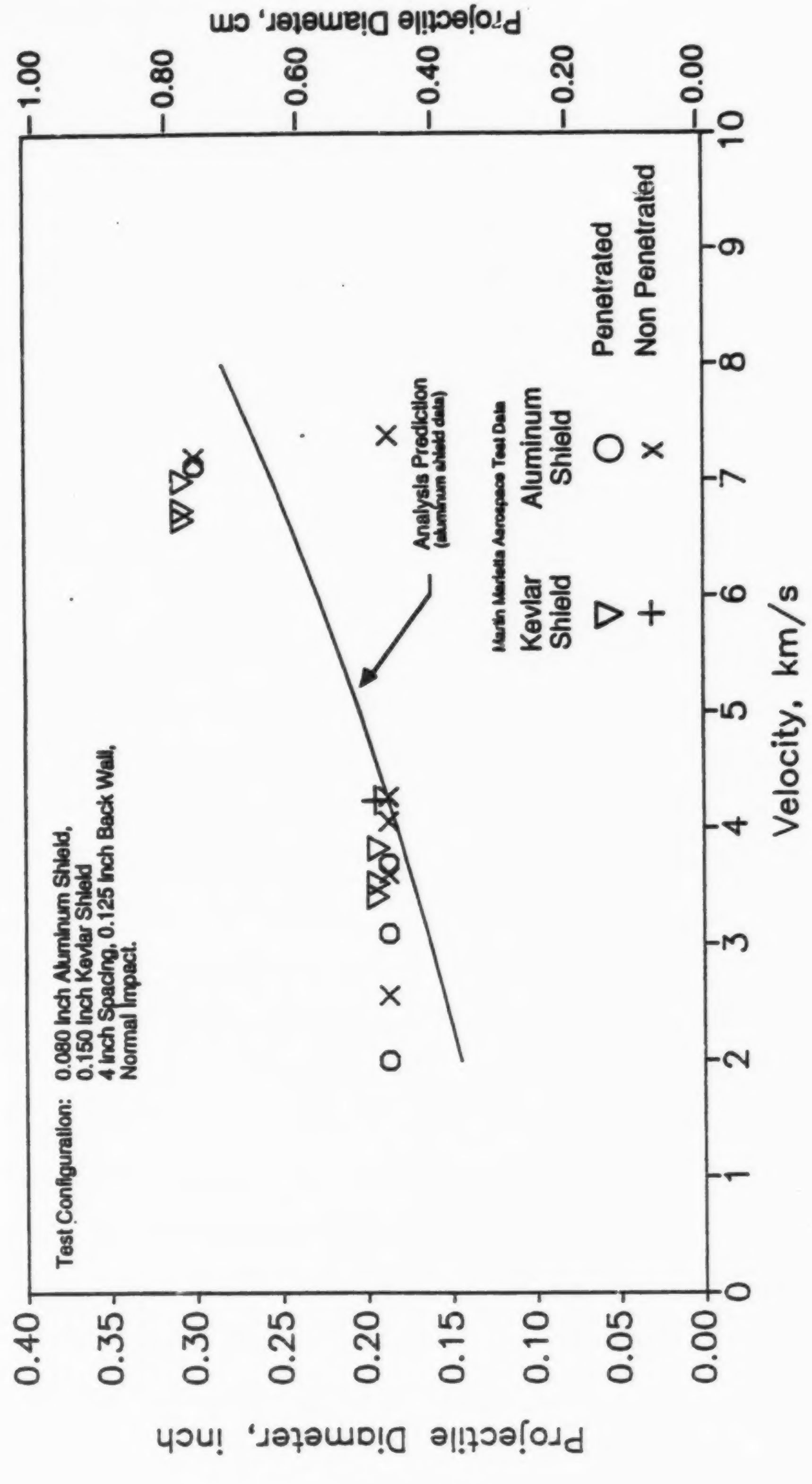

Figure 4.5-2. Kevlar Shield Penetration Resistance Compared to Aluminum Shield Penetration Resistance

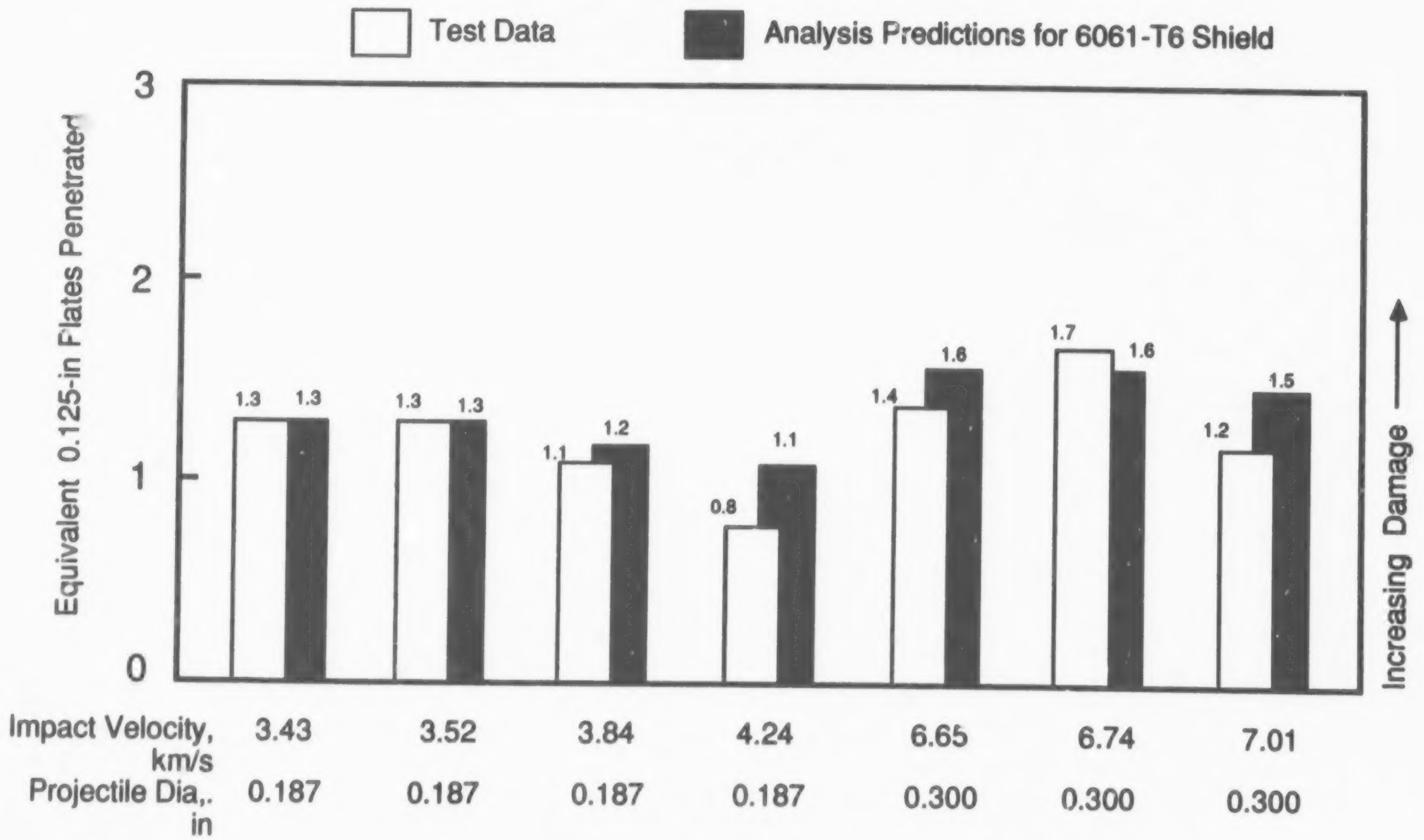

Martin Marietta Aerospace test data.

0.150-in thick Kevlar shields and equivalent areal mass 0.075-inch thick aluminum shields.
Wall thickness = 0.125-in; spacing = 4-in; no MLI present.

Figure 4.5-3. Comparison Between Test Damage and Analysis Predictions for Kevlar Shield Material.

Shield		Kevlar/Aluminum Areal Density Ratio	Projectile		Pressure Wall Hole Size, in	Kevlar/Aluminum Hole Area Ratio
Thickness, in	Material		Velocity, km/s	Diameter, in		
0.063	Aluminum	N/A	7.01	0.300	0.75 dia	N/A
0.110	Kevlar	0.87	7.15	0.300	2.2 x 2.7	10.5
0.080	Aluminum	N/A	7.13	0.300	0.1 x 0.01	N/A
0.150	Kevlar	0.94	7.01	0.300	2 dia	4000
0.080	Aluminum	N/A	3.70	0.187	0.18 x 0.3	N/A
0.150	Kevlar	0.94	3.52	0.187	0.35 dia	2.26

Kevlar data from Martin Marietta Aerospace Tests.

N/A = Not Applicable

Wall thickness = 0.125-in; spacing = 4-in; No MLI present.
Kevlar is half the density of aluminum, therefore comparisons shown are for Kevlar shields approximately twice as thick as aluminum shields.

Figure 4.5-4. Damage Comparison - Kevlar vs. Aluminum Shields.

case. The backwall hole sizes were measured directly from the test article. The relatively large hole sizes produced in the Kevlar tests can be explained by a mismatch in shock impedance between shield and projectile materials (see app. F). This mismatch prevents the dispersion of impact fragments, from both projectile and shield, over as large an area on the backwall as would occur with an aluminum shield.

Comprehensive experimental programs for various shield materials were reported in references 3-2 and 4-5. These investigations show structural grade aluminum is as good or better than other structural materials. No composite materials were considered in these programs.

The foregoing discussion presents results from some preliminary screening tests comparing alternative composite shield materials. Based on this limited investigation no significant advantage appears for Kevlar and dSiC over aluminum in terms of weight or penetration resistance. In fact, these composite materials appear significantly worse from the standpoint of residual damage potential to the backwall and interior components for those combinations of projectile mass and velocity causing a penetration.

4.6 SINGLE AND DOUBLE SHIELD TEST RESULTS COMPARISON

Most testing performed under this contract has used a single shield protecting the backwall. A portion of these tests also included 30 layers of multilayer insulation (MLI) between the shield and backwall to more accurately simulate the proposed Space Station module design. MMA has conducted tests at MSFC using two aluminum shields. We have compared these test results with our single shield test data and analysis results to assess differences in performance.

Data for single and double shield configurations are superimposed in figure 4.6-1. Here, both configurations have equal areal weight of shielding. A penetration function estimated from the double shield data is shown for comparison to the single shield penetration function developed from the regression analysis. These data indicate that dividing a single shield into two spaced shields each half as thick as the single shield significantly increases the penetration resistance. These data confirm the results from reference 3-2, where three or more spaced elements

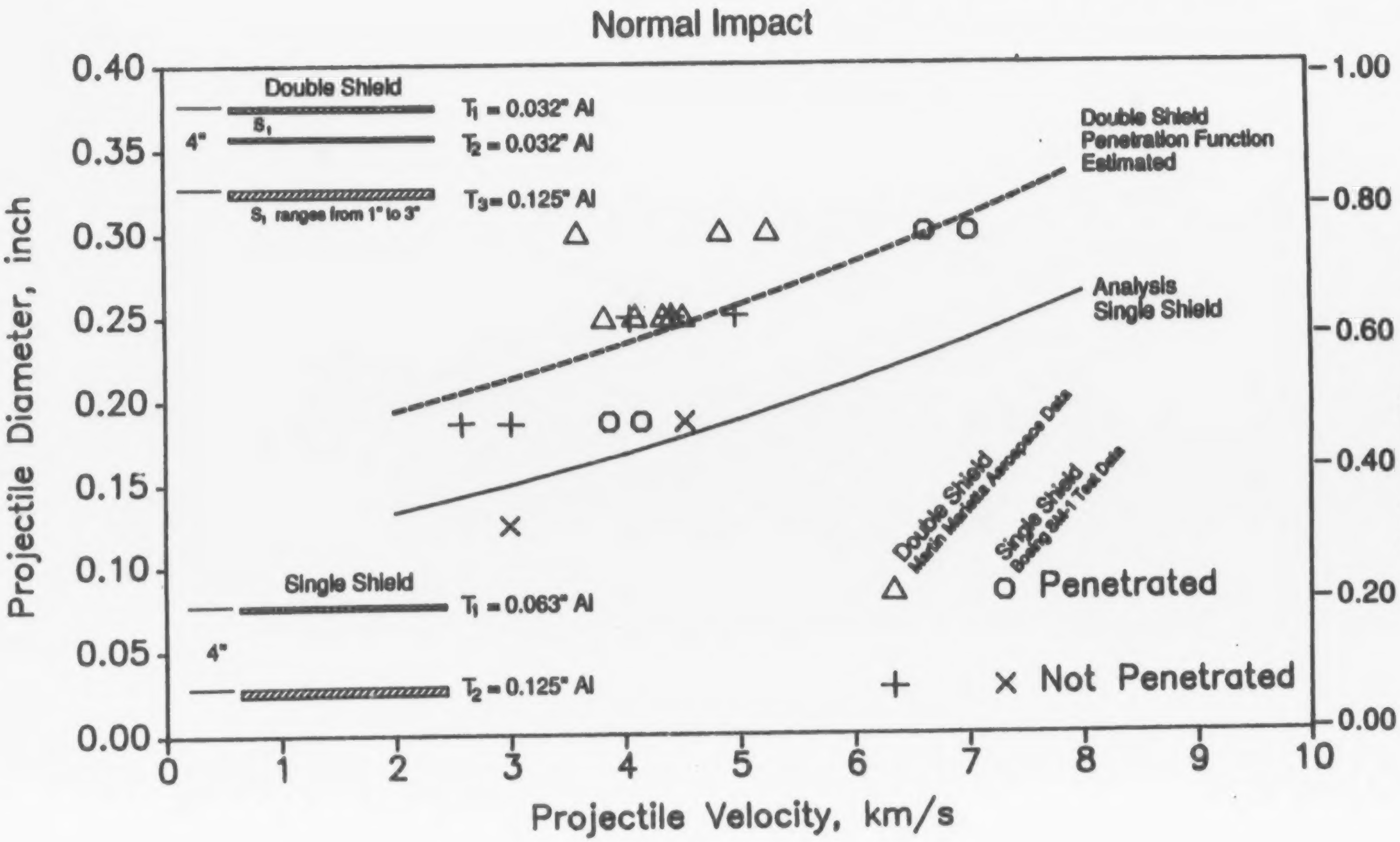

Figure 4.6-1. Double Shield versus Single Shield Configuration Penetration Resistance Comparison

consistently provided better protection than equivalent two element (shield plus backwall) configurations.

Data for both double and single shield with MLI configurations are superimposed in figure 4.6-2 along with the linear regression penetration function for single shields. Both configurations have 1.60-mm (0.063-in) shields, 102-mm (4-in) spacing, and 3.18-mm (0.125-in) backwalls; however, an MLI blanket (1185 g/m^2) is used in the single shield configuration instead of a 0.032-in-thick aluminum intermediate shield (2200 g/m^2.) These data indicate the MLI provides the same level of penetration resistance as a second shield of 0.81-mm (0.032-in) aluminum.

Our test data have shown MLI enhances the shields effectiveness; therefore, we also compared the double shield data to a hypothetical single shield (with MLI) configuration in figure 4.6-3. The single shield capability was determined by the alternative regression analysis function (see sec. 4.3) using a 1.19-mm (0.047-in) aluminum shield configuration with an MLI blanket. The single shield and MLI combination have a total areal weight equal to the tested double shield. The figure also shows an estimated penetration function for the double shield data. This comparison indicates a double shield is superior to a single shield with MLI.

Figure 4.6-4 shows the results of MMA tests of double shield configurations at 45-deg impact angles along with comparable single shield data and associated analysis obtained under this contract. Also included in this figure is an analysis for an equivalent weight single shield configuration with MLI. Because no nonpenetrating test results are available for the two-shield configuration, we cannot determine the capability of this configuration. Nevertheless, this analysis shows a shield of 1.19-mm (0.047-in) aluminum plus MLI, which has an equal area weight as a 1.60-mm (0.063-in) aluminum shield without MLI, provides at least as good protection as the double shield.

The foregoing discussion illustrates the difficulty encountered when comparing the results of hypervelocity impact tests on different configurations. The results from tests conducted under controlled conditions are subject to considerable scatter particularly at oblique impact angles. For

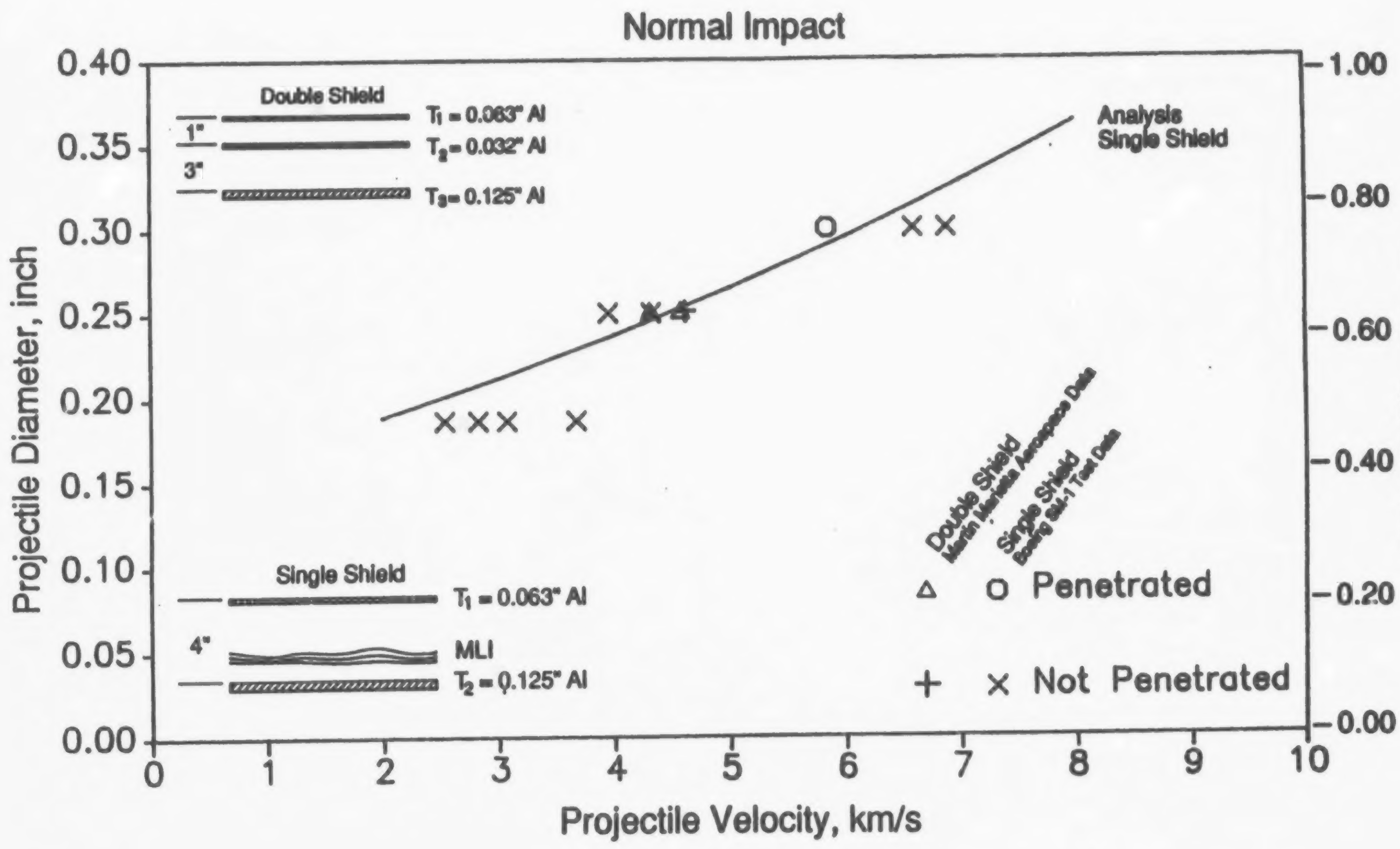

Figure 4.6-2. Double Shield versus Single Shield with MLI Penetration Resistance Comparison

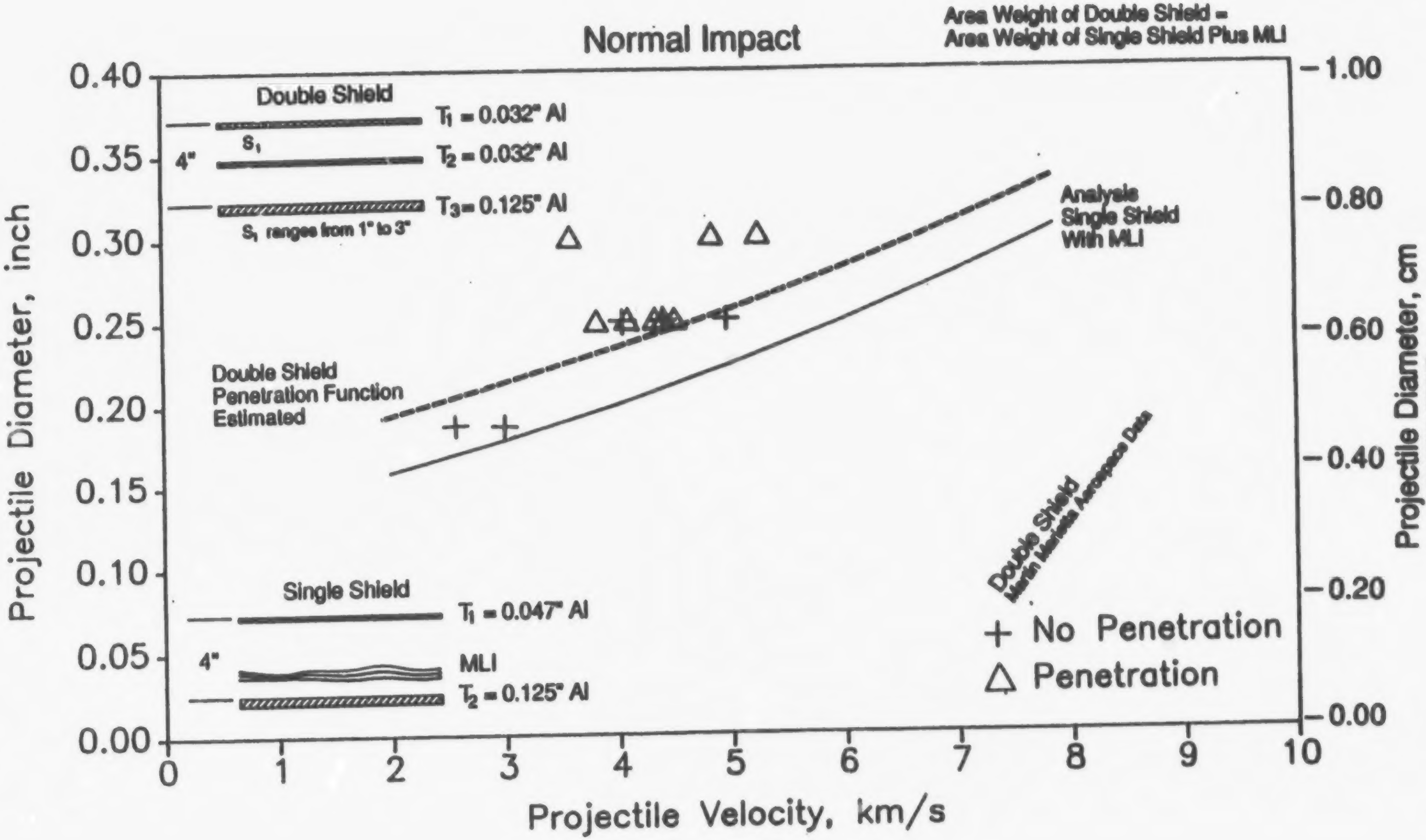

Figure 4.6-3. Double Shield versus Single Shield Configuration Penetration Resistance Comparison

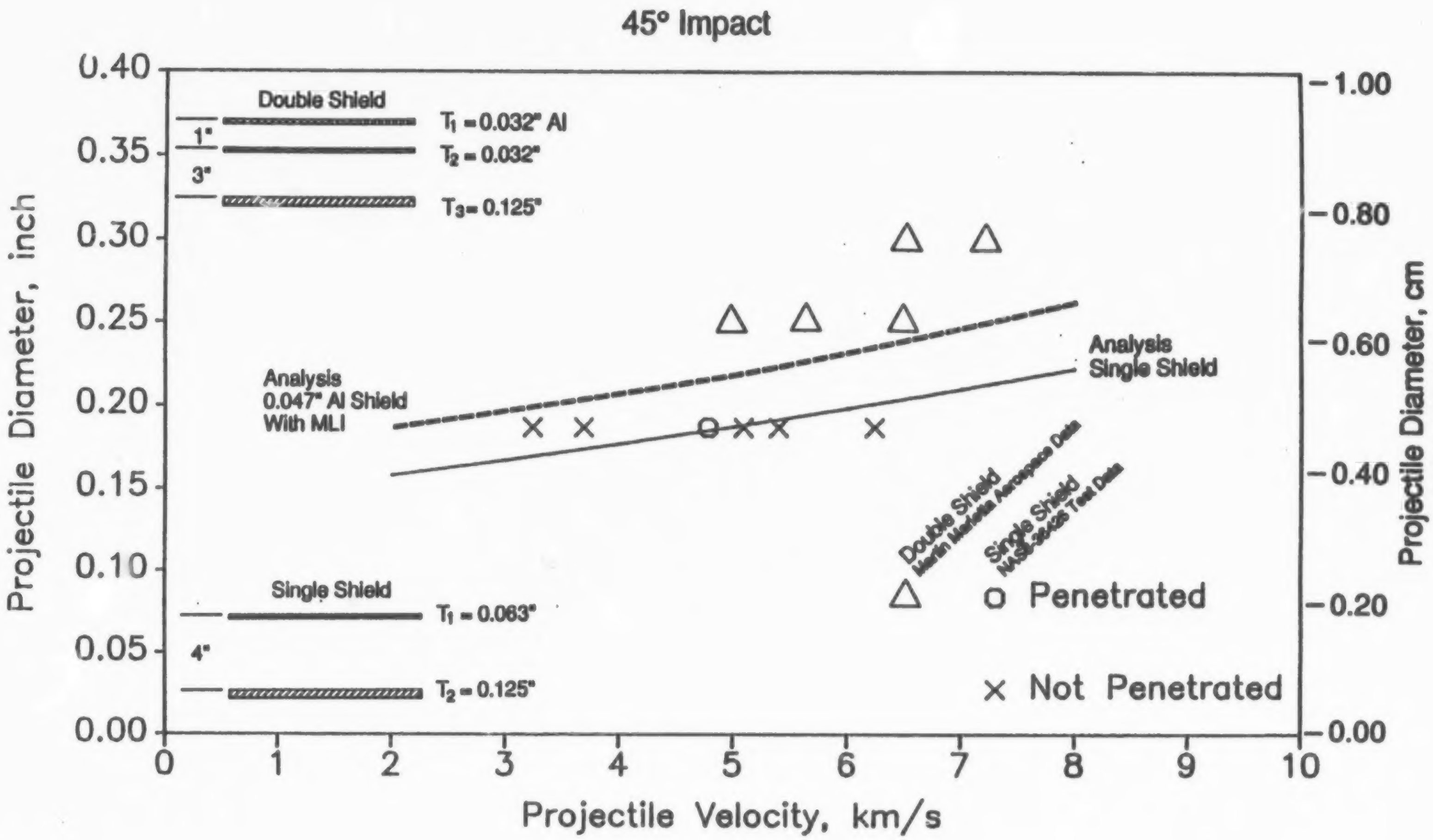

Figure 4.6-4. Double Shield versus Single Shield Configuration Penetration Resistance Comparison

this reason we have relied on the results of linear regression analysis and a large experimental data base.

In figure 4.6-5 the analysis curves from figures 4.6-1 through 4.6-4 are superimposed and all the test data points deleted. This comparison indicates the following trends:

a. A single shield approximately half as thick as the backwall provides the least protection that is acceptable.

b. Replacing the single 1.60-mm (0.063-in) aluminum shield with an equivalent areal weight combination of 1.19-mm (0.047-in) aluminum plus MLI increases the penetration resistance.

c. Replacing the single 1.60-mm (0.063-in) aluminum shield with two shields each 0.81-mm (0.032-in) thick provides still more protection.

d. The most dramatic improvement for a modest increase in weight is obtained by adding MLI to the basic shield.

e. With a relatively thick shield (1.60-mm [0.063-in] aluminum), there is virtually no improvement by substituting a metallic shield of greater weight for the MLI (see fig. 4.6-2.) When two lighter shields (0.81-mm [0.032-in] aluminum) are used, the all-aluminum configuration appears superior to the aluminum plus MLI combination (see fig. 4.6-3.)

f. Advantages of a double metallic shield over a shield-plus-MLI combination are partially offset by the greater attach structure weight required for the intermediate metallic shield over the structure weight required to restrain the MLI.

4.7 TOTAL PENETRATION FUNCTION

A penetration function defines the relationship between projectile velocity and critical projectile diameter. Four alternative penetration functions are available in our analysis code, BUMPER, as shown in figure 4.7-1. Penetration function number 1 combines three partial functions from the ballistic, shatter, and melt/vaporize velocity ranges. In the low-velocity range the ballistic portion of PEN4 is used as presented in figure 4.7-2. This is an earlier version of PEN4 than described in section 4.8 but is maintained for continuity with the configuration and design studies using this

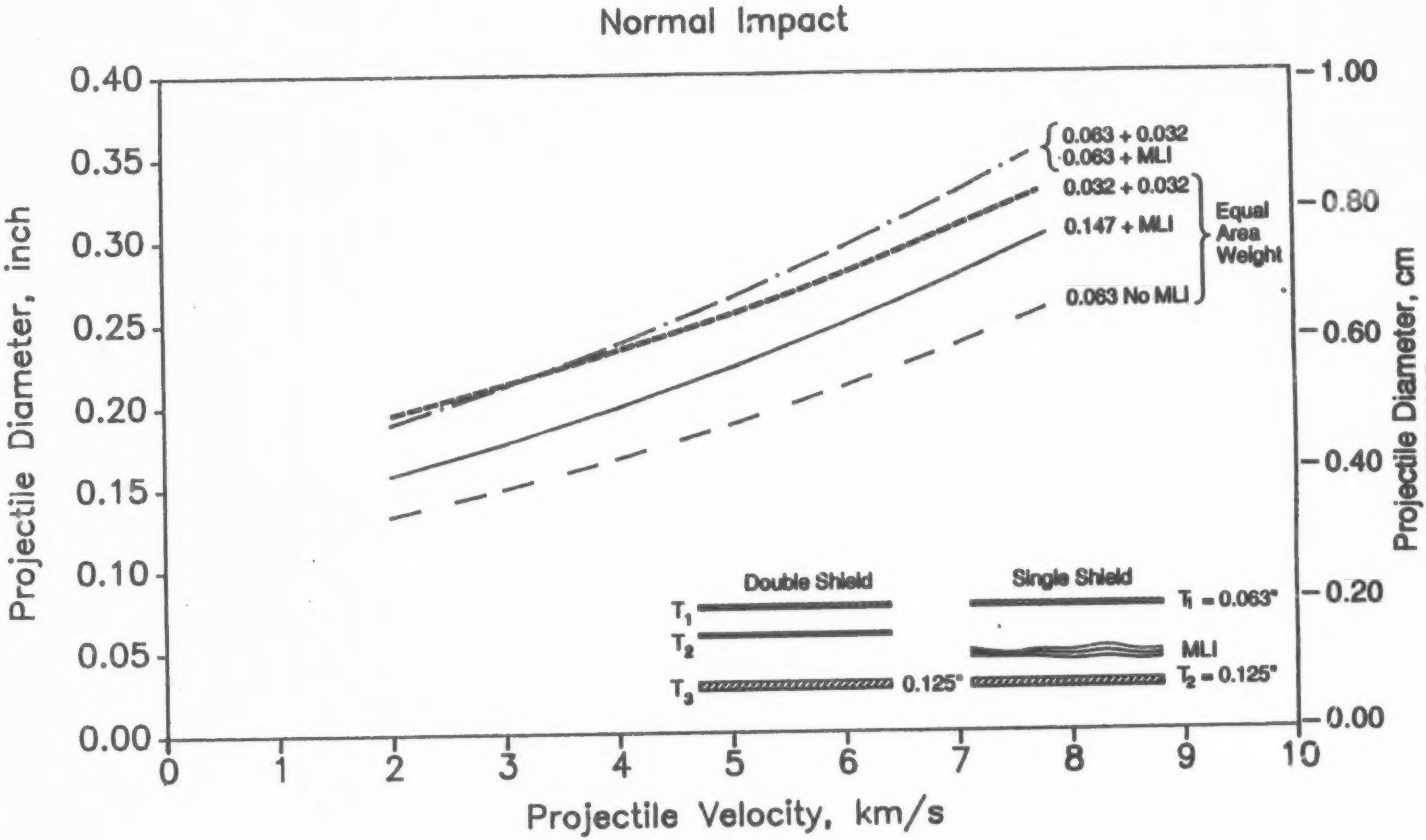

Figure 4.6-5. Configuration Comparison

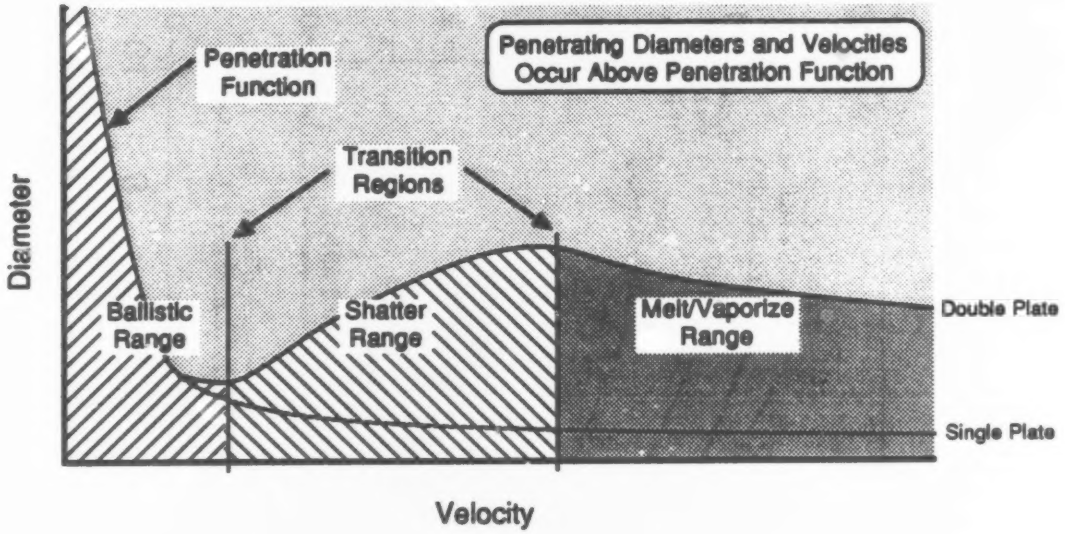

Four Alternative Penetration Functions

1	Ballistic - PEN4 Section 4.8 Reference 4-6. Shatter - Burch Section 4.7 Reference 3-1. Melt/Vaporize - Wilkinson Section 4.7 Reference 4-3.
2	Ballistic - PEN4 Section 4.8 Reference 4-6. Shatter - Regression Section 4.3 Figure 4.3-8. Melt/Vaporize - Wilkinson Section 4.7 Reference 4-3.
3	Complete Function - PEN4 Section 4.8 Reference 4-6.
4	Single Plate Function - Schmidt-Holsapple Section 4.9 Reference 4-5. (See figure 4.9-1 for single plate penetration function diagram and equation.)

All penetration functions assume aluminum on aluminum impacts. For penetration functions 1 and 2 above, transitions must be made between the ranges. Between ballistic and shatter, critical diameters are calculated for both and the larger diameter controls. Between shatter and melt/vaporize, critical diameters are calculated for both and the smaller diameter controls.

Figure 4.7-1. Overview of Single and Double Wall Penetration Functions Available in BUMPER.

$$V_{50_i} = \left[\left[\frac{0.6\,T_i}{\left(\frac{0.281\,D\rho_p}{\rho_i} \right)^{1/3} \cos\theta} \right]^{1/.31} \frac{2\,S_{Y_i}}{\rho_p} \right]^{1/2}$$

$i = 1$ for shield
$i = 2$ for wall

Shield is penetrated only if $V > V_{50_{i=1}}$

If $V \geq Vf + 4000$ Impact occurs in shatter regime » use Burch equation.

$$Vf = \begin{cases} 4100 \text{ if } \frac{T_1}{D} < 0.40 \\ 4986 \left(\frac{T_1}{D}\right)^{0.21} \text{ if } \frac{T_1}{D} \geq 0.40 \end{cases}$$

Residual Velocity

$$V_R = \left[\frac{1.33\,V^2\,R_p^2\,\rho_p - (8\,S_{Y_i}\,T_i\,e^{-V\,3.125 \times 10^{-4}})/\cos\theta}{1.33\,R_p^2\,\rho_p + R_p\,T_i\,\rho_i\,/\cos\theta} \right]^{1/2}$$

Wall is penetrated only if $V_R > V_{50i=2}$

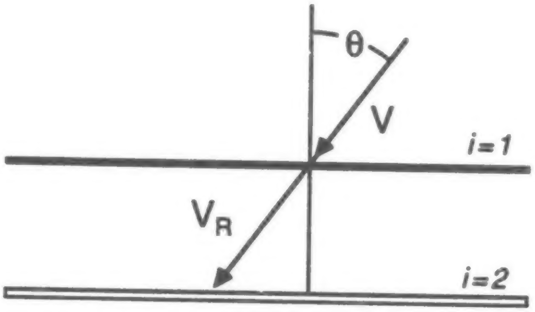

Dual Wall

V = particle velocity, ft/s

T_i = plate thickness, ft

D = particle diameter, ft

R_p = particle radius, ft

ρ_p = particle density, slugs/ft

ρ_i = plate density, slugs/ft

θ = impact angle, from the normal

S_{Y_i} = yield strength, lb/ft^2

Figure 4.7-2. Ballistic Range (PEN4) Penetration Function

function. In the shatter range the *Burch* equations (ref. 3-1) shown in figure 4.7-3 are used. In the transition region between ballistic and shatter ranges, BUMPER calculates the critical diameter with both PEN4 and the Burch, and chooses the larger as the controlling critical diameter. The Wilkinson equations (ref. 4-6) are used for the melt/vaporize range. In the transition region between shatter and melt/vaporize, BUMPER calculates the critical diameter with both Burch and Wilkinson). The velocity where Wilkinson produces the smaller critical diameter demarks the transition from shatter to melt/vaporize. Wilkinson then predicts the critical projectile diameter for greater velocities. Wilkinson is a theoretically derived penetration function for impacts at velocities above where testing is possible and is outlined in figure 4.7-4. Wilkinson is also used in analyzing meteoroid impacts, which can reach very high velocities. (See sec. 2.0 for meteoroid velocity distribution.)

Penetration function 2 of figure 4.7-1 is formed similarly to 1 above except the regression equation for the shatter range (as described in sec. 4.3) replaces the Burch equations and the latest version of PEN4 is used.

As a verification of our analysis, we compared penetration function 2 to results from a HULL hydrocode analysis performed for MSFC by Dr. Robert Becker of the Army Corps of Engineers (ref. 4-7). The comparison is for normal impacts only and is shown in figure 4.7-5. All penetrating HULL runs are above the penetration function, and all nonpenetrating HULL runs are below the penetration function. This serves as independent support for our penetration function. Uncertainties in this verification may be eliminated with more HULL runs.

4.8 PHENOMENOLOGICAL PENETRATION FUNCTION - PEN4

Penetration function 3 in figure 4.7-1 is an improved phenomenological penetration code originally developed to determine the ability of warhead fragments to penetrate multiple aluminum arrays and destroy critical components within (ref. 4-8.) It has since been modified to determine the penetration resistance of an arbitrary aluminum target array to impacts by aluminum projectiles

Flight Path Penetration: $N_F = (F_1 + 0.63 F_2)\left(\frac{V}{C}\right)^{-4/3}\left(\frac{S}{D}\right)^{-5/12}\left(\frac{T_2}{D}\right)^{-7/12}$

Normal Path Penetration: $N_N = F_3\left(\frac{D}{T_2}\right)\left(\frac{V}{C}\right)^{-4/3}$

$$F_1 = 2.42\left(\frac{T_1}{D}\right)^{1/3} + 4.26\left(\frac{T_1}{D}\right)^{1/3} - 4.18$$

$$F_2 = 0.5 - 1.87\left(\frac{T_1}{D}\right) + \left(5\frac{T_1}{D} - 1.6\right)\chi^3 + \left(1.7 - 12\frac{T_1}{D}\right)\chi$$

$$F_3 = 0.32\left(\frac{T_1}{D}\right)^{5/6} + 0.48\left(\frac{T_1}{D}\right)^{1/3}\sin^3\theta$$

$$\chi = \tan\theta - 0.5$$

C = speed of sound in shield, ft/s
V = projectile velocity, ft/s
S = spacing, in
D = projectile diameter, in
T_i = plate thickness, in

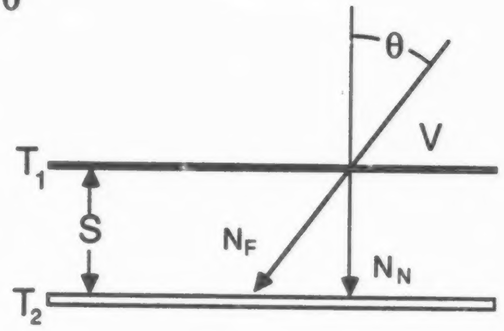

For T_2 penetration, set $N = 1$ and solve for D which will be the critical diameter. To account for spallation of T_2, solve for $N = 0.85$.

Reference: G.T. Burch, Airforce Armament Laaboratory Technical Report AFATL-TR-67-116, Boeing, 1967.

For Normal Impact: $N = F_1\left(\frac{V}{C}\right)^{-4/3}\left(\frac{S}{D}\right)^{-5/12}\left(\frac{T_2}{D}\right)^{-7/12}$

Implemented through November 1985

Reference: Lundeberg, Stern, and Bristow, "Meteoroid Protection for Spacecraft Structure, NASA CR-54201, October 1965.

Equivalent Aluminum T_2 Thickness of 30 Layers of MLI

When MLI is included in the dual wall design, it is equivalent to an amount of aluminum added to the backwall T_2 as follows:

$T_{MLI} = 3.045 \times 10^{-6}\ V^{3.42}$ cm ($V \leq 10$ km/s)
$T_{MLI} = 0.008$ cm ($V > 10$ km/s)

Ref. B.G. Cour-Palais, ESA SP -153, 1979.

Figure 4.7-3. Shatter Range (Burch Equations) Penetration Function.

For $M_1/(\rho_p D) > 1.0$ $\quad M_p = 1.44\, L_2 M_2 S^2 / V_N$

For $M_1/(\rho_p D) < 1.0$ $\quad M_p = \left[\dfrac{1.44\, (\pi/6)^{1/3} L_2 M_1 M_2 S^2}{(\rho_p)^{2/3}\, V_N} \right]^{3/4}$

Projectile diameter, cm $\quad D = \left[\dfrac{6\, M_p}{\pi\, \rho_p} \right]^{1/3}$

1. Calculate critical projectile mass with one of the above equations.
2. Calculate projectile diameter.
3. If initial equation does not apply for that diameter, use other equation.

M_p = critical projectile mass, gm

M_1 = mass per unit area for shield, gm/cm^2

M_2 = mass per unit area for wall, gm/cm^2

V_N = normal component of velocity vector, km/s

L_2 = vessel wall material constant (0.401 for Al - 2219)

S = spacing, cm

ρ_p = projectile density, gm/cm^3

Reference: J.P.D. Wilkinson, "A Penetration Criterion for Double Walled Structures Subject to Meteoroid Impact," AIAA Journal, October 1969.

Figure 4.7-4. Melt / Vaporize Range (Wilkinson) Penetration Function.

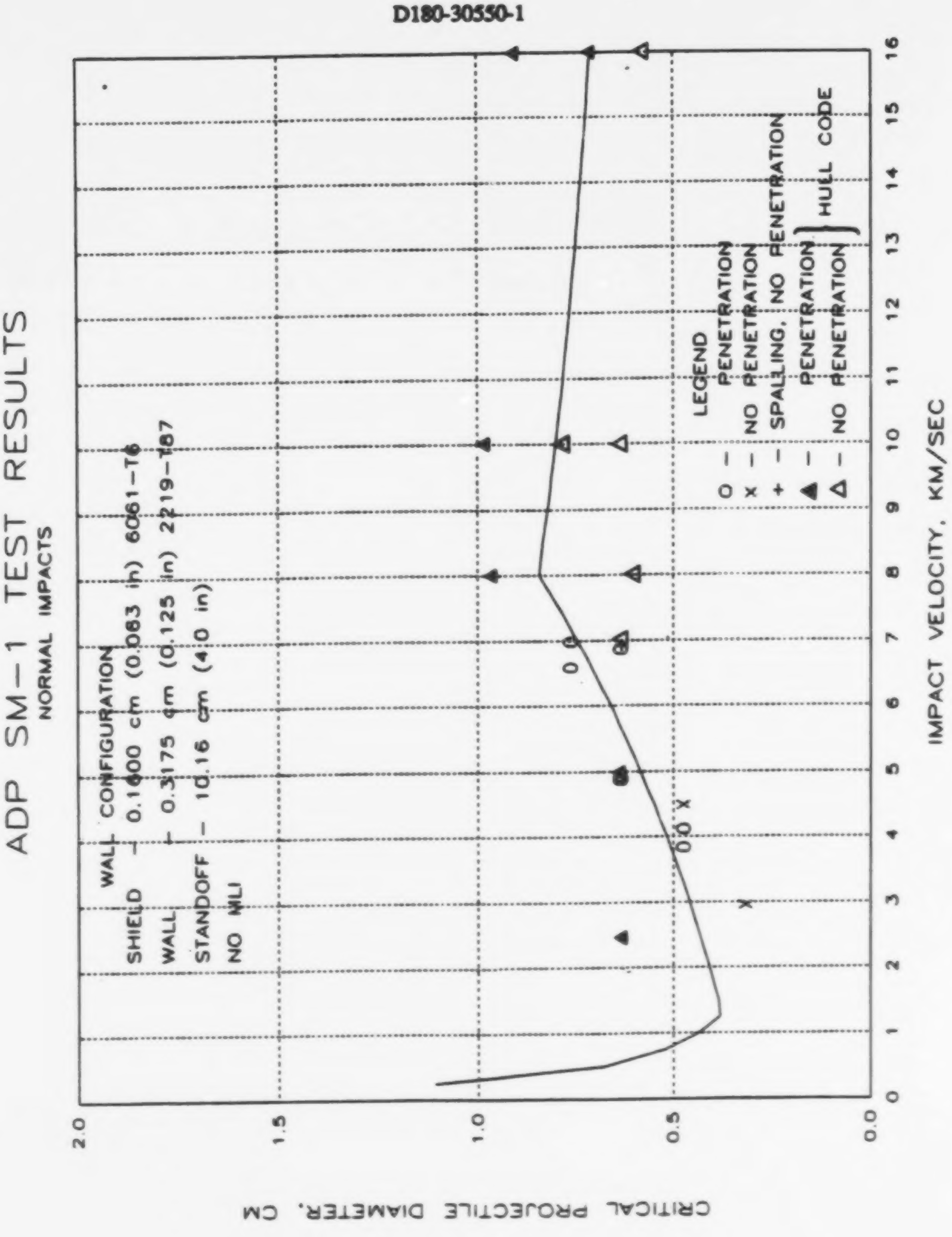

Figure 4.7-5. Normal Impact Correlation

and can therefore be applied to Space Station integrated wall designs. This function is completely described in a companion report to this contract.

Features of PEN4 not found in the other penetration functions include (1) the penetration of a plate by multiple impacts is allowed, (2) the crater depth relation was validated by hydrocode for impact velocities greater than 8 km/s, (3) the residual velocity relationship is applicable to both rigid and deformable, spherical and cubic projectiles, and (4) it accurately models the mass decrease of the largest residual fragment for impacts above 3 km/s. A comparison between PEN4 and the HULL code results is shown in figure 4.8-1. In all cases the HULL penetrations are above the PEN4 function, and in all but one case the HULL nonpenetrations are below the PEN4 function.

4.9 SINGLE PLATE PENETRATION FUNCTION

To account for the possibility of impact on a wall without a shield, a single plate penetration function, the Schmidt-Holsapple crater volume equation (ref. 4-9) is included in the BUMPER computer code; this is penetration function number 4 in figure 4.7-1. This equation was developed from many tests over a wide range of material densities and impact velocities, and applies to both debris and meteoroid impacts. A comparison of critical particle sizes for equivalent weight single and double wall structures is shown in figure 4.9-1. The 0.70 factor used to determine the critical plate thickness prevents a penetration caused from spalling. The curves illustrate the significant benefit obtained from double- over single-walled construction.

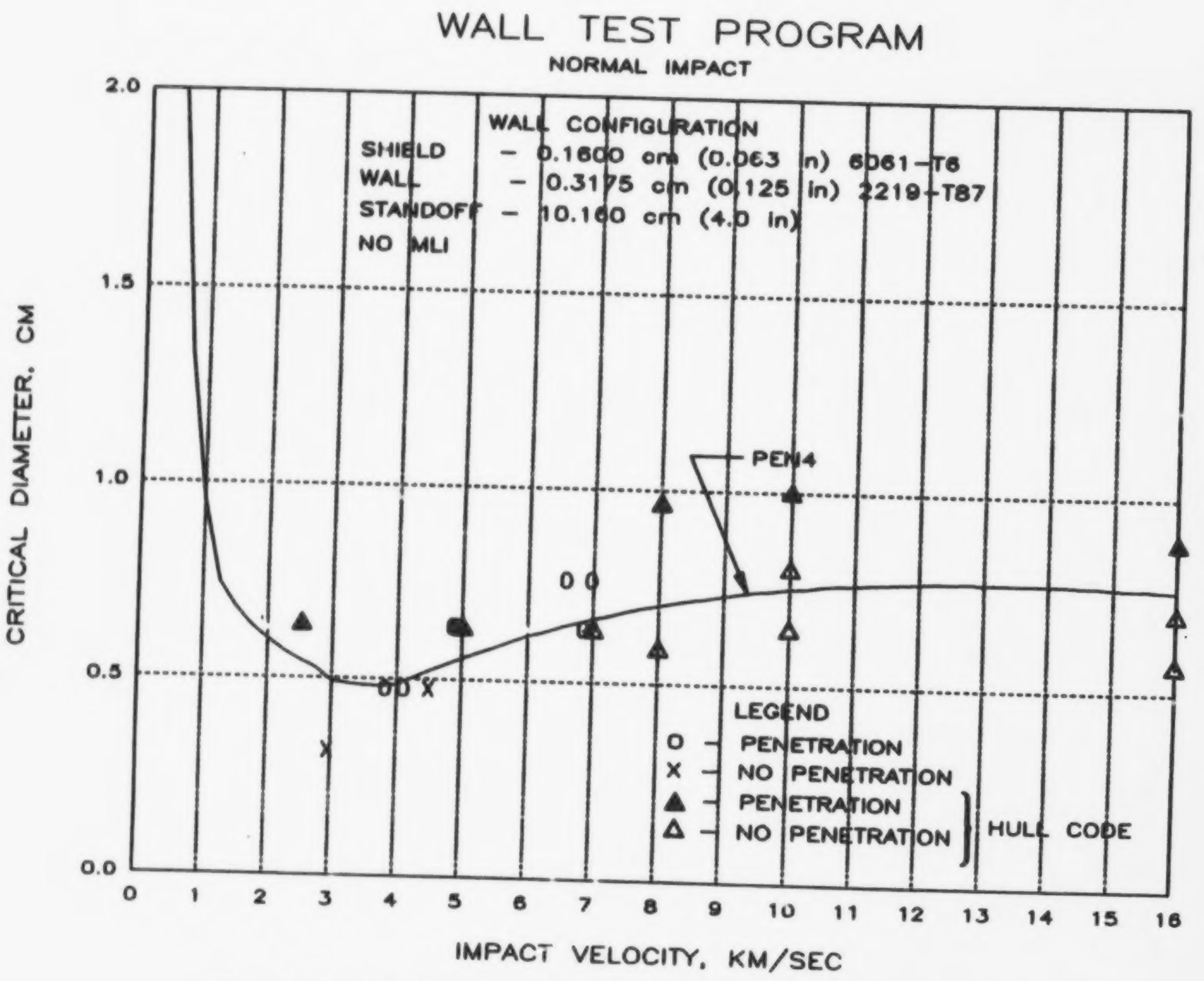

Figure 4.8-1. Analytical Hypervelocity Impact Penetration Function Prediction/Test Data Comparison

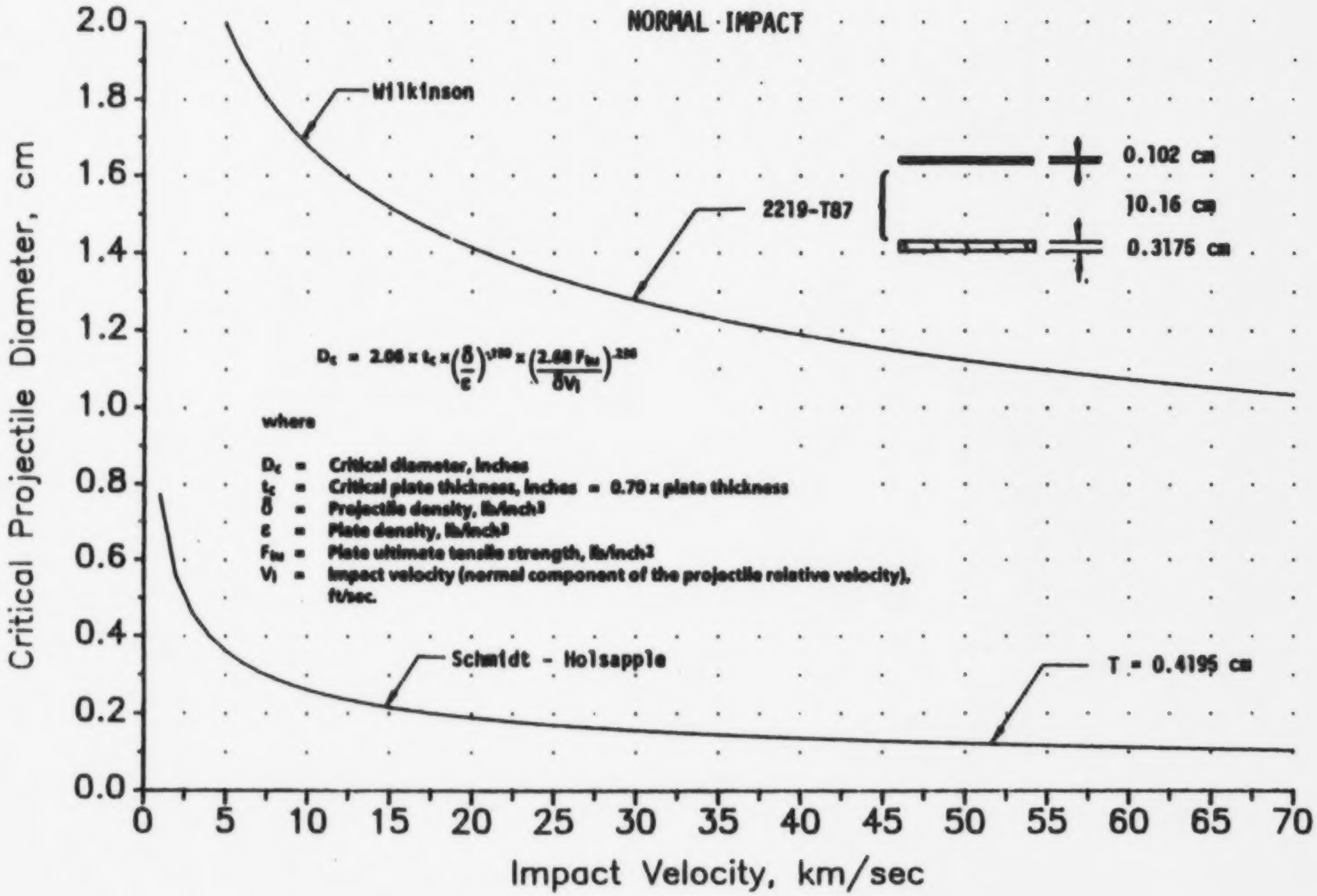

$$D_c = 2.06 \times t_c \times \left(\frac{\delta}{\varepsilon}\right)^{.159} \times \left(\frac{2.68\,F_{tu}}{\delta V_i}\right)^{-.236}$$

where

D_c = Critical diameter, inches
t_c = Critical plate thickness, inches = 0.70 x plate thickness
δ = Projectile density, lb/inch³
ε = Plate density, lb/inch³
F_{tu} = Plate ultimate tensile strength, lb/inch²
V_i = Impact velocity (normal component of the projectile relative velocity), ft/sec.

Figure 4.9-1. Comparison of Penetration Resistance to Meteoroids of Single Wall and Double Wall Structures

5.0 INTERNAL EFFECTS OF PENETRATION

5.1 TASK 2 DATA ANALYSIS - TRANSIENT EFFECTS

A survey of transient penetration effects from previous test programs is illustrated in figure 5.1-1. The following is a summary analysis of data collected under this contract's effects of penetration test program. A complete report on this evaluation is contained in appendix I.

Pressure Pulse. The pressure pulse, noise, and flash data collected during testing were evaluated by a physiologist from the Boeing Crew System/Life Support organization. A pressure impulse resulting from a pressure wall penetration probably would cause no more than a temporary threshold shift (temporary deafness) in a crew member's hearing. If the crew member was especially close to the impact site, eardrum rupture could occur. Eardrum rupture is not necessarily a serious condition if it heals without infection.

Light Flash. The photodiode data show light flash from a penetration occurs in the visible spectrum. Light intensity evaluations of these data show in most cases the measured light flashes exceed visual tolerance criteria. Flash blindness could occur if a crew member were looking directly at the flash. Internal structure should largely shield crew members from the light flash and also attenuate the effects of pressure pulse.

5.2 PHYSIOLOGICAL EFFECTS OF PRESSURE LOSS

Following the transient effects of penetration, module pressure loss will threaten the crew. In our study of repair techniques for module walls penetrated by debris particles, we assumed the module would be evacuated and repaired later by a crew member in EVA equipment. We based this assumption on the belief that inadequate time was available to locate the damage and perform the repair before the module internal pressure decayed to hazardous levels. To examine the validity of this assumption, we compared the pressure decay rate of a punctured module with capability of unprotected crew at the various atmospheric pressure levels. A summary of this investigation, performed by a physiologist from the Boeing Crew System/Life Support organization, is given in appendix E.

The results show for a 2.54-cm (1-in) diameter hole, approximately 10 min are available before supplemental 100% oxygen must be supplied to avoid the onset of hypoxia. It is reasonable to assume the availability of supplemental oxygen in a walk-around configuration as emergency equipment in each module. In the event such equipment is not available, the module should be evacuated unless it was certain the leak could be stopped in about 20 min. This is a very risky scenario because failure to perform the repair would likely result in death for the crew left in the module. Even if the repair could be performed, significant risk remains owing to the significant time required to repressurize the module and transfer the crew to a recompression facility.

With supplemental oxygen, the time of useful function can be extended to about 40 min. This approach also involves significant risk because although hypoxia can be prevented to about 4 psia, there is a high probability of decompression sickness (bends) occurring. Furthermore, several oxygen containers would be necessary owing to the extended time required to make repairs and repressurize the module. Figure 5.2-1 summarizes the physiological effects of penetration on the crew.

It appears that, for holes larger than a fraction of an inch, the crew should evacuate the module unless the damage can be located and identified within a few minutes of penetration. A remote system for estimating the hole size seems desirable because the puncture may be hidden by internal structure. For instance, the system monitoring the internal pressure could estimate the hole size and forecast the safe operation time available from pressure decay measurements made immediately after a puncture.

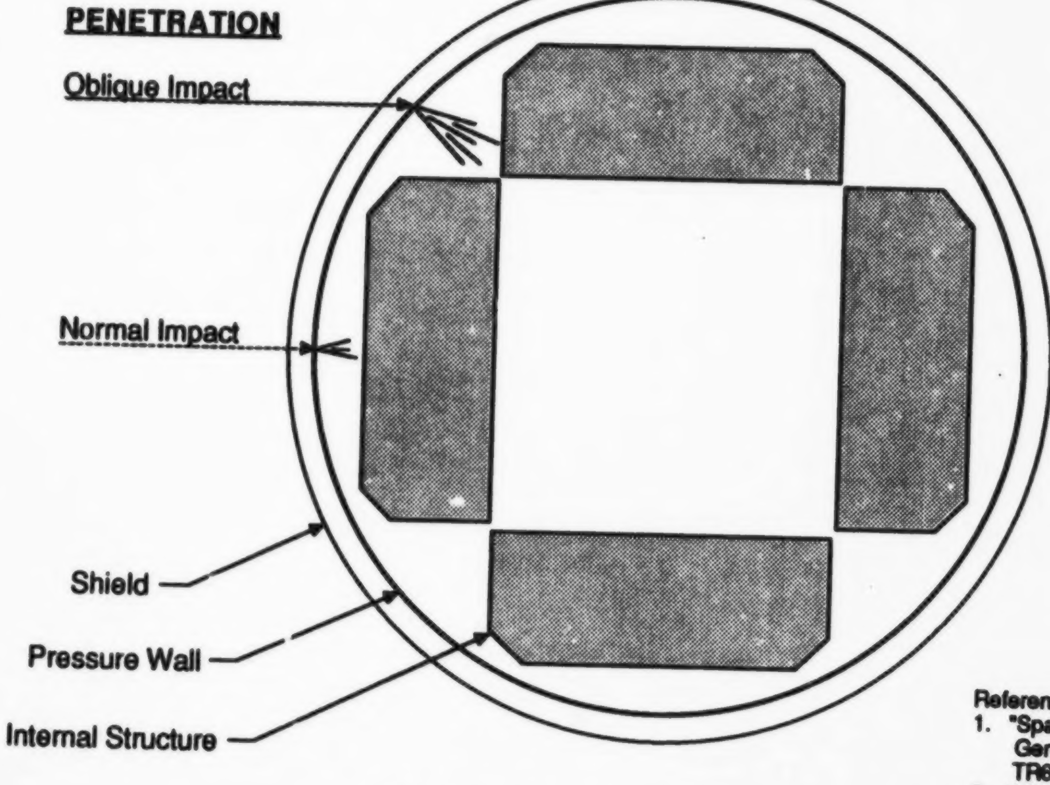

Space Station Module Cross Sectional View

RESPONSE

Fragments:
High-speed, hot, and molten debris from projectile and wall material can travel 1.2 m (4 ft) in 2 ms.

Shock:
Pressure pulse up to .48 MPa (70lb/in^2) and traveling up to 2.7 km/s (9000 ft/s) reflects from internal surfaces. (Pressure and speed decreases with distance and time.)

Flash/Temperature:
Flash of heat and light,
800 to 1200 w/ster,
up to 14.7 Mw/m^2 (1300 Btu/ft^2-s)
producing up to 177 C (350° F) temperatures in materials.

References:
1. "Spacecraft Interior Hazards from Hypervelocity Impact," General Motors Defense Research Laboratories, TR66-13, March 1966.
2. "Hypervelocity Particle Penetration Into Manned Spacecraft Atmospheres," Boeing Document D2-24149-1.

Figure 5.1-1. Transient Effects of Penetration Within a Pressurized Cabin.

Condition	Effect on Crew	Prognosis
Pressure Pulse	Temporary hearing loss, ear drum rupture.	Not a lethal threat to crew unless an individual is very close to the point of penetration. Ear drum rupture will heal over time.
Light Flash	Temporary blindness, retinal burns.	Unlikely threat to crew unless an individual is gazing directly at the point of penetration.
Pressure Decay	Decompression sickness, hypoxia, unconsciousness.	Must have supplemental oxygen available when pressure drops below 10 psia. Must evacuate the module when pressure drops below 4 psia.

Figure 5.2-1. Effects of Pressure Wall Penetration on Crew Physiology.

6.0 REPAIR TECHNIQUES

Some Space Station module components susceptible to hypervelocity impact damage are listed in figure 6.0-1 along with brief descriptions of repair concepts to treat the damage. The entries cover module structure from body-mounted radiators to internal utility lines. This contract focused on pressure wall damage repair and describes procedures, tools, and patches for performing such a repair.

Definition. Our working definition of pressure wall repair is an emergency procedure to maintain or restore design performance to a penetrated Space Station module. The scope is limited to repairs applied locally by a Space Station crew lacking specialized repair skills.

Most repair procedures are optimally applied to the pressure side of the pressure wall because the pressure differential works to hold them in place. Repairs performed from outside the module will require a blind-side technique to hold it in place.

The penetration size will directly affect crew response. Following a small penetration, the atmosphere loss rate may be low enough to permit application of a simple patch in the normal interior environment to temporarily stop the leak. The crew could then apply a permanent repair without donning special life support equipment. Following a more severe penetration (producing a larger hole), the crew may need to evacuate the damaged module, seal off the remaining modules, and then reenter the module in a pressure garment assembly (PGA) to complete the repair. The repair procedures described below assume the more rigorous requirements of a pressure-suited astronaut to account for a worst case condition.

Requirements and Assumptions. The following specifications for repair method design and testing ensure the repair methods developed will be applicable in the Space Station environment, yet focus primarily on the repair task itself:

a. All repairs can be performed under vacuum and zero-gravity conditions.

b. The damage location is known. The EVA or IVA astronaut will not be required to search extensively for the penetration.

	Damaged Components	Module Repair Location	Repair Concept	Preliminary Work	Inspect & Verify Completed Work
  1 2	Body Mounted Radiator / Debris Shield Skin Holes < 0.4" Heat Pipe - none	External	Refurbish or Replace	Remove & Replace	
3	Support Structure	External			
4	Multilayer Insulation Multiple Holes Ragged Holes 6" X 6" Surface Damage 10" X 10"	External	Patch or Replace MLI Blanket	Cut or Remove MLI to expose damage	Visual
5	Pressure Wall - Exterior Irregular Hole 1" X 0.5" Surface Craters 5" dia area Raised Lip	External	Attach additional aluminum plates over the area.	Remove MLI blanket and loose debris. Inspect	Visual
6	Pressure Wall - Interior Irregular Hole 1" X 0.5" Chipped Paint Spall	Internal	Patch	Locate & Inspect	Visual
7	Attachment Fixtures and Mechanisms	Internal	Replace Components		
8	Electric and Fluid Lines	Internal and External	Replace Segments		System Check
9	Windows	External	Replace	Apply Internal Temporary Seal	Seal Check

Figure 6.0-1. On-Orbit Repair of Integrated Common Module Wall

c. The MLI blankets are approximately as wide as the radiator panels and reside directly under each radiator panel.

d. The appropriate procedure for removing and replacing radiator panels will be developed and specified under separate efforts.

e. Repair of body-mounted radiator panels or other subsystems is not considered.

6.1 PATCH METHODS DEVELOPED AND THEIR APPLICATIONS

Pressure wall patch techniques developed during this contract are summarized in figure 6.1-1.

Layered Patch. The basic design is shown in figure 6.1-2. Each layer performs a critical function. Aluminum foil (8 to 12 mils thick) provides the pressure seal and conforms to pressure wall curvature and to any irregularities in the damaged area. The Kevlar or silicone-foam pad prevents sharp edges of the damage from puncturing the aluminum foil. The adhesive used must be space qualified and resist degradation from possible exposure to the low Earth orbit environment including atomic oxygen and high vacuum. The Teflon release ply protects the adhesive layer during patch handling. The release tabs allow an astronaut wearing pressure suit gloves to easily remove the release ply. The Velcro square attached in the center provides a temporary handle attachment point. This design cannot support the pressure differential over a hole with diameter greater than 1 in.

Long versions of this patch, as shown in figure 6.1-3, could repair long and narrow cracks. Alternative materials could be substituted for the Kevlar layer; for instance, a rubber pad, a wire mesh, or a combination of layers to optimize performance.

A simplified patch would include only the aluminum foil and adhesive and may be especially useful as an initial repair on multiple small holes or as a supplement to other repair techniques.

Rubber Ring Patch. The basic design is shown in figure 6.1-4. The stiff aluminum plate spaced 6.35 to 19.05 mm (0.25 to 0.75 in) away from the pressure wall surface gives this patch more durability than the layered patch. As an alternative to aluminum, the plate material could be a stiff composite such as graphite epoxy. The rubber spacer provides a gap between the damage and the plate, and conforms to irregularities in the surface. In addition to sealing a penetration, this

	Rubber Ring Method	Layered Patch Method
Advantages	● Simple installation. ● Durable. ● Reliable seal.	● Simple installation. ● Reliable seal. ● Conforms closely to wall. ● Various shapes can be fabricated to cover a wide range of expected damage.
Applications	● Out of plane deformations up to 13-mm (0.5-in) and within 152-mm (6-in) diameter. ● Interior surface only.	● Minor out-of-plane deformations only. ● Sharp edges must be confined to 102-mm (4-in) diameter. (Patch could be fabricated in a larger or differently shaped version.) ● Interior surface only.

Figure 6.1-1. Space Station Pressure Wall Repair Concept Summary.

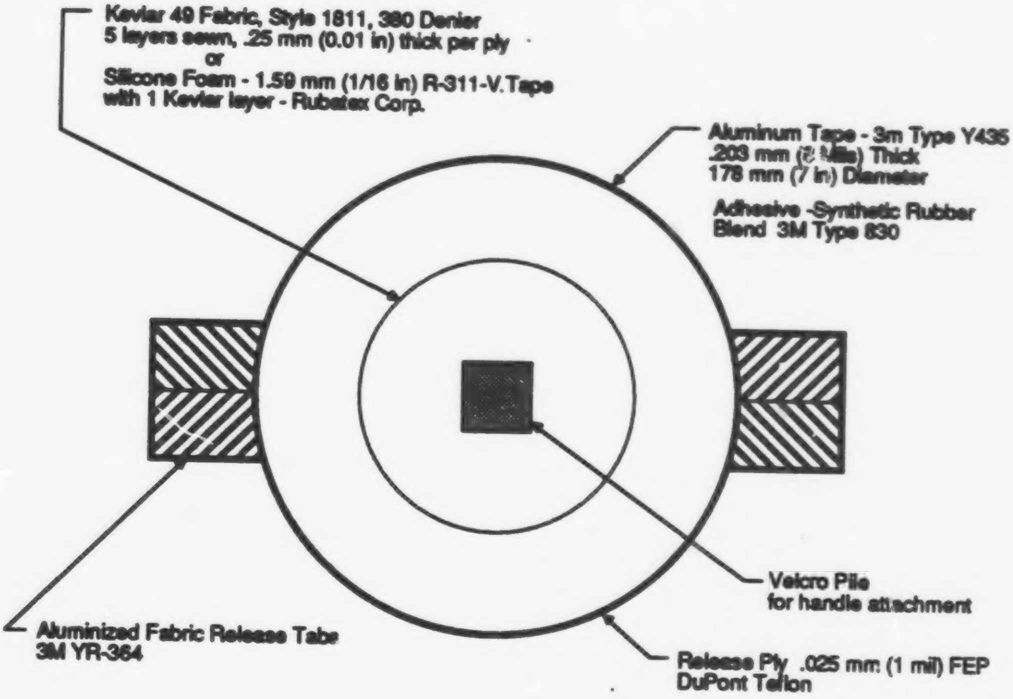
Kevlar 49 Fabric, Style 1811, 380 Denier
5 layers sewn, .25 mm (0.01 in) thick per ply
or
Silicone Foam - 1.59 mm (1/16 in) R-311-V.Tape
with 1 Kevlar layer - Rubatex Corp.
Aluminum Tape - 3m Type Y435
.203 mm (8 Mils) Thick
178 mm (7 in) Diameter
Adhesive -Synthetic Rubber
Blend 3M Type 830
Velcro Pile
for handle attachment
Aluminized Fabric Release Tabs
3M YR-364
Release Ply .025 mm (1 mil) FEP
DuPont Teflon

Figure 6.1-2. Space Station Layered Patch Repair Technique.

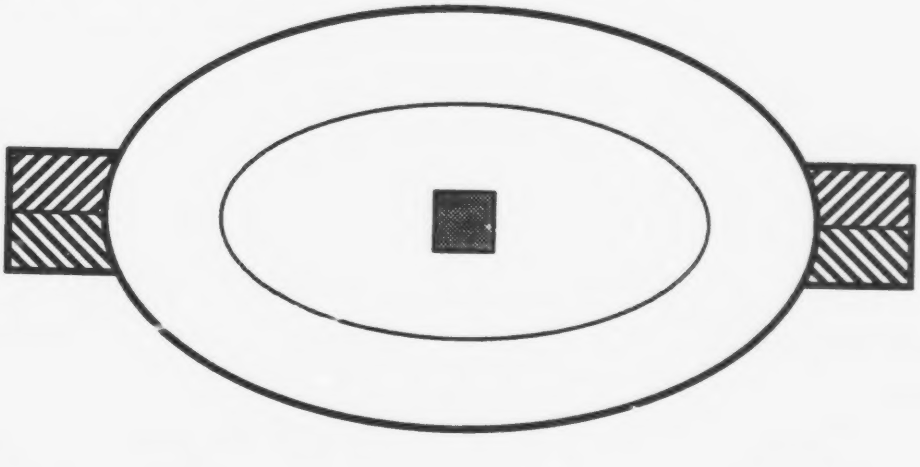

Figure 6.1-3. Alternative Concept Multilayered Patch.

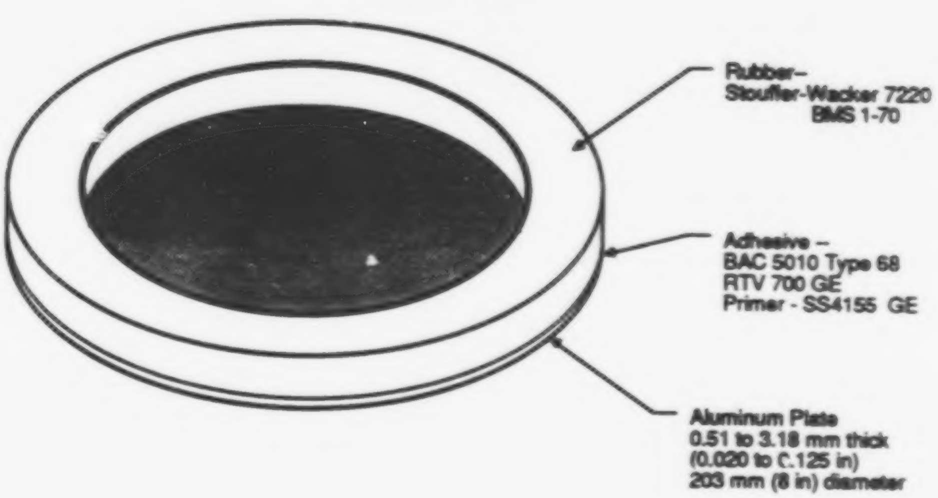
Rubber–
Stouffer-Wacker 7220
BMS 1-70
Adhesive –
BAC 5010 Type 68
RTV 700 GE
Primer - SS4155 GE
Aluminum Plate
0.51 to 3.18 mm thick
(0.020 to 0.125 in)
203 mm (8 in) diameter

Figure 6.1-4. Rubber Ring Patch Design.

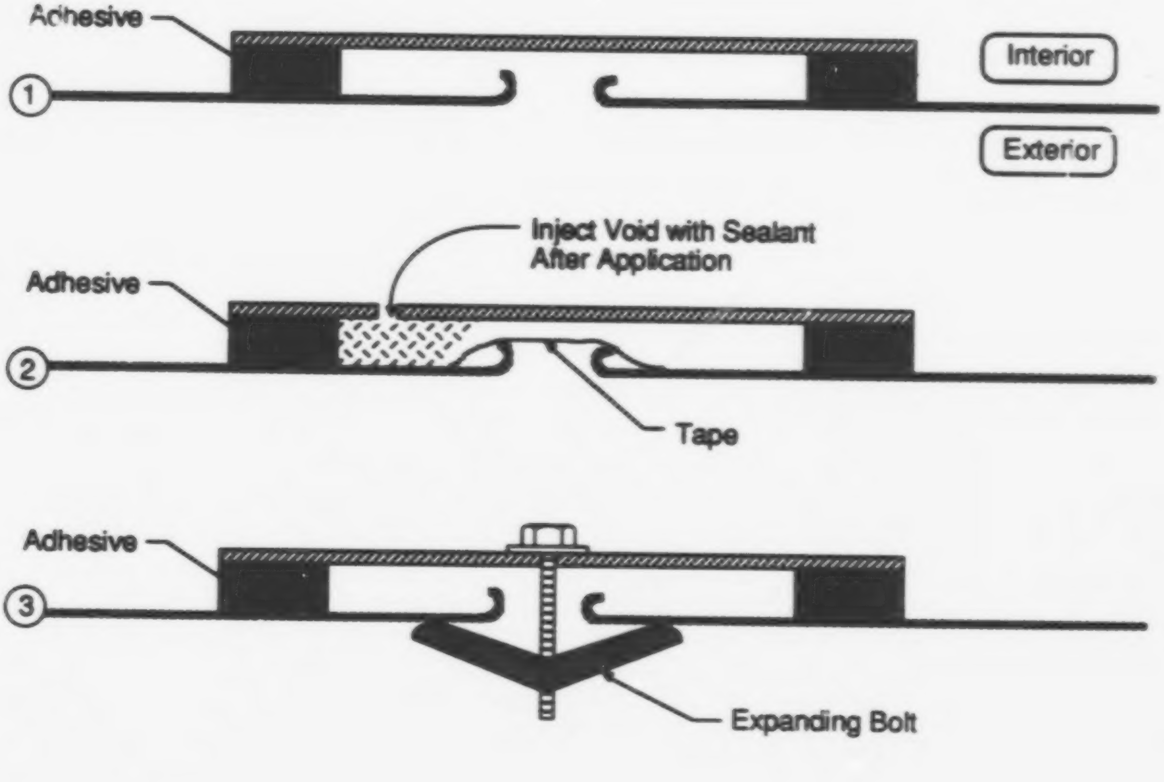
Adhesive
①
Interior
Exterior
Inject Void with Sealant After Application
Adhesive
②
Tape
Adhesive
③
Expanding Bolt

Figure 6.1-5. Rubber Ring Patch Alternative Application Methods.

technique could be used to protect a previously applied temporary or less durable patch and to provide a redundant seal.

The rubber ring method lends itself to several installation alternatives, as illustrated in figure 6.1-5. The basic installation is shown in item 1. A plate stiff enough to resist the 14.7-lb/in^2 pressure differential will require preshaping to seal against the pressure wall contour. Using a thinner, more flexible plate to conform to various pressure wall curvatures may require injecting a stiff sealant (as shown in item 2 to support the plate under the 14.7-lb/in^2 pressure differential. A tape cover would prevent the sealant escaping through the hole. Item 3 shows this patch held in place and actually formed to the cylindrical contour with a bolt and expanding nut inserted through the penetration.

6.2 REPAIR TOOLS DEVELOPED

The layered and rubber ring patches require special tools to aid a pressure-suited astronaut in their application. The following tools were developed under this contract with assistance from spacecraft crew systems specialists to ensure conformance with applicable NASA requirements; for instance, all tools incorporate a tether attachment ring and Velcro-lined handles to aid in securing them during use and storage.

Abrasion/Cleanup Tool. This tool (fig. 6.2-1(a)) is used to prepare the interior pressure wall surface for a good adhesive bond. The abrasive side is used to remove items such as loosened paint and penetration-related debris from the pressure wall area intended for patch application. The abrasive could range from Scotch Brite to a wire brush depending on the performance required. The adhesive side is used perform final cleanup and to test the surface for patch adhesion.

Alignment Template. To ensure the patch is centered over the penetration, we have developed a template (fig. 6.2-1(b)) for marking alignment lines directly on the pressure wall. The clear template is visually centered directly over the penetration. A hole in the template's center allows clearance for any out-of-plane damage. The astronaut then applies visible marks in three or four places around the template circumference.

ORIGINAL
OF POOR

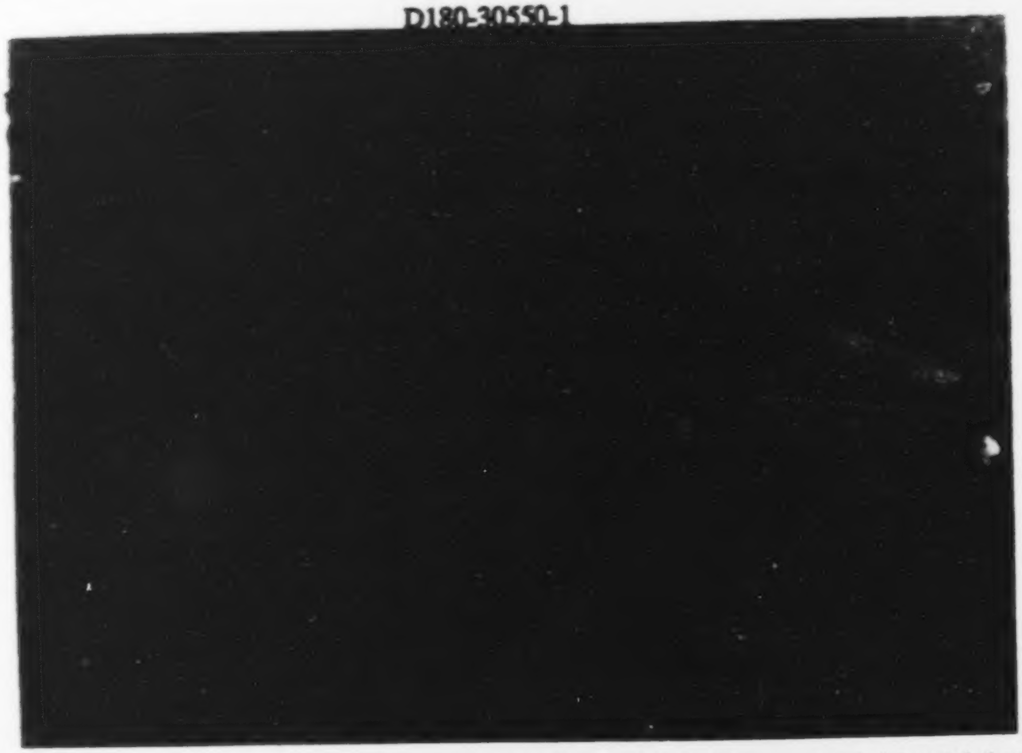

Figure 6.2-1. Repair Tools and Patches: (a) cleaning tool, (b) alignment tool, (c) patch handle, (d) layered patch, (e) rubber ring patch..

Tool	Features	Uses	Reference[1]
EVA Trash Bag	Overlapping baffle & velcro strap	Hold small items during repair activity.	P/N 101176-20157
EVA Trash Bag	Without baffle & strap	Hold large items during repair activity.	P/N 101176-20160
Mini Work Station	Holds several tool caddies	Organize repair tools.	P/N 10150-10050-05
Scissors		Cut away damaged MLI.	P/N 10159-20001-02
Tool Caddy	Velcro lined	Stow and tether repair tools.	P/N 10153-10053-03
EMU Lights and Battery		Provide general lighting.	P/N 10161-10061-04 P/N 10161-20002-01
EVA Portable Flashlight		Provide lighting in recessed locations.	P/N 10172-20561-02
Tape Caddy		Hold supplemental adhesive tape.	P/N 10159-20004-03
Portable Foot Restraint		Allow two handed repair operation.	

(1) Part numbers refer to the STS Tool Catalog

Figure 6.2-2. Required Existing Tools From the Space Transportation System Inventory.

Marker. We used a felt-tipped marker (not illustrated) in our simulations; however, we do not expect this to work well in a vacuum because the ink volatiles will quickly evaporate. Alternatives we have identified include a graphite pencil and a grease pencil.

Patch Handle and Burnisher. Poor manual dexterity and tactile sensation in space suit gloves led to designing a detachable handle (fig. 6.2-1(c)) that would make patch manipulation easier. The handle's function was extended to burnishing and smoothing out the layered patch after application. Combining tool functions in this way reduces the equipment required by the astronaut and reduces task complexity.

In addition to these tools, we have identified tools from the EVA Catalog Tools and Equipment (JSC-20466) to ease repair task performance in vacuum and zero-g conditions. These tools are listed in figure 6.2-2. In general, the selected tools help carry and organize the above tools for task efficiency. Foot restraints will be required to keep the astronauts stationary during repair work.

Equipment and Tool Configuration. Figure 6.2-3 lists the repair tools required during three types of repair activity: external repair or replacement of the MLI blankets, and patching a hole from the inside. Internal pressure wall repair is desired so the pressure differential can be used to advantage. External pressure wall repair methods will require methods for resisting the pressure for long time periods for permanent repairs.

6.3 PATCH APPLICATION DEMONSTRATED

To ensure our repair techniques were as valid as possible for Space Station, we prepared and then demonstrated patch application procedures. Demonstrations occurred in both terrestrial laboratories and the MSFC neutral buoyancy simulation facility.

Layered Patch Application Laboratory Demonstration. The most critical assumption applied to identifying repair tasks was the need to perform repair in a vacuum, which requires that the astronaut work in a pressure suit. Keeping in mind the constraints imposed by this condition, figure 6.3-1 lists all the individual tasks important to completing an effective pressure wall repair.

MLI Repair
(outside module)

- Portable Foot Restraint
- Mini Work Station
- Large Trash Bag w/ Baffle
  - MLI Blanket Patch
- Tool Caddy
  - Scissors
- Tape Caddy
  - Tape

MLI Replacement
(outside module)

- Portable Foot Restraint
- Mini Work Station
- Trash Bag w/o Baffle
  - New MLI Blanket
- Trash Bag w/ Baffle

IVA Patch
(astronaut in space suit inside unpressurized module)

- Portable Foot Restraint
- Mini Work Station
- Large Trash Bag w/ Baffle
- Tool Caddy #1
  - Abrasive Tool & Cleaning Pad
- Tool Caddy #2
  - Burnishing Tool
- Tool Caddy #3
  - Alignment Template
  - Marker
- Tool Caddy #4
  - Patch w/ Detachable Handle

Figure 6.2-3. Organization of Space Station Wall Repair Tools.

Step	Task Time, minutes	Total Time, minutes	Task Description
1	1	1	Translate to damaged area.
2	5	6	Attach portable foot restraint.
3	1	7	Inspect the hole area, and check for other holes.
4	1	8	Deploy trash bag and attach to structure or MWS.
5	1	9	Open the tool caddy.
6	1	10	Remove abrasive tool and cleaning pad combination.
7	3	13	Abrade rough edges; remove loose paint and material.
8	1	14	Remove backing from cleaning pad.
9	1	15	Discard backing in trash bag.
10	2	17	Collect loose material, dust, chips with cleaning pad.
11	3	20	Remove expended pad layers and continue cleaning as required.
12	1	21	Return tool to tool caddy.
13	1	22	Remove alignment template from tool caddy.
14	1	23	Remove backing from template face & discard backing in trash bag.
15	2	25	Center template alignment cross hair over hole center and press firmly in place. Release handle.
16	1	26	Remove marker tool from tool caddy.
17	2	28	Mark pressure wall adjacent to template guide marks at a minimum of 3 locations.
18	1	29	Return marker to tool caddy.
19	1	30	Remove alignment template and return to tool caddy.
20	1	31	Remove patch with detachable handle from tool caddy.
21	1	32	Verify fit of selected patch against wall markings.
22	1	33	Remove the backing from the patch, and discard backing in trash bag.
23	2	35	Align patch with marks on wall and press firmly into place.
24	1	36	Remove handle from patch, and return it to caddy.

Figure 6.3-1. Preliminary Task Analysis Interior(PGA)Patch Application Task Analysis

Step	Task Time, minutes	Total Time, minutes	Task Description
25	1	37	Remove burnisher from tool caddy.
26	3	40	Burnish bubbles, folds, and creased edges in the patch.
27	1	41	Return burnisher to tool caddy.
28	3	44	Visually inspect the completed patch, check for loose edges. (Reburnish if required).
29		44	Repair complete; repressurize the module.
			Monitor patch during repressurization.
			In a shirt sleeve environment, place tape over velcro on the patch.

Figure 6.3-1. Preliminary Task Analysis Interior (PGA) Patch Application Task Analysis (Continued)

The time estimates are based on judgments of crew systems analysts and reflect a ground rule that limited minimum task time to 1 min.

Repair task timeline performance using the developed tools and patch is illustrated in figures 6.3-2 through 6.3-9. Figure 6.3-2 shows the hypervelocity impact test article used to apply the patch to for a realistic demonstration. This was the backwall of an article tested at MSFC and represents a complete penetration with spalling, dimpling, and several rough edges. The test article was mounted vertically for the repair procedure.

A goal in the cleaning steps was to minimize released particles. A fine powder was formed during Scotch Brite abrading of step 7 (fig. 6.3-3). The cleaning tool adhesive surface used as shown in figure 6.3-4 was able to collect some of this powder.

Patch alignment over the hole was crucial for sealing the hole and ensuring the protective Kevlar or foam pad could protect the aluminum foil. The alignment template was clear, so the damaged area was visible through it. A hole in the center of the alignment tool ensured it could lie flat against the pressure wall, as shown in figure 6.3-5, without interference from the damage.

As a final step before applying the patch, a verification fit was made to ensure the alignment is correct as shown in figure 6.3-6. After the release plies protecting the adhesive are removed, the patch is applied over the hole as shown in figure 6.3-7. The patch handle is removed after the patch is secured in place. The final step is to ensure good adhesion by burnishing the patch surface with the patch handle as shown in figure 6.3-8. The completed patch is shown in figure 6.3-9.

6.4 RUBBER RING PATCH APPLICATION

The task timeline for the rubber ring patch application is shown in figure 6.4-1. The tasks are similar to the layered patch tasks in figure 6.3-1 and shown in the photographs. The patch is shown applied to a curved panel in figure 6.4-2. The curvature is a 82-in radius, equivalent to our reference configuration module design.

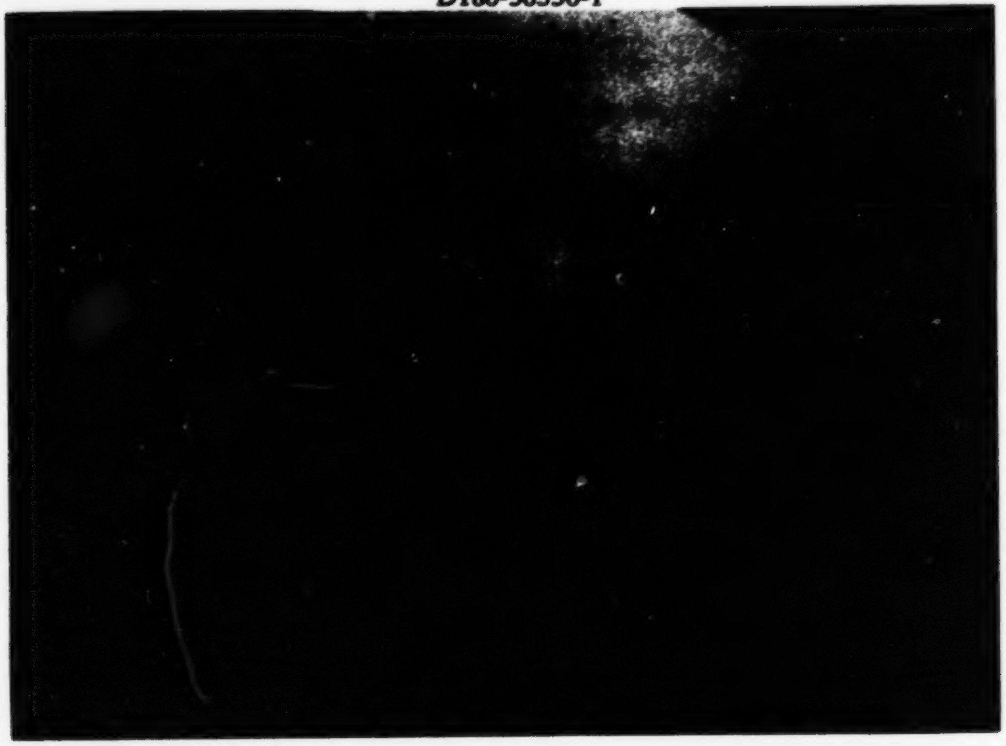

Figure 6.3-2. Hypervelocity Impact Damage for Repair Demonstration.

ORIGINAL PAGE IS
OF POOR QUALITY

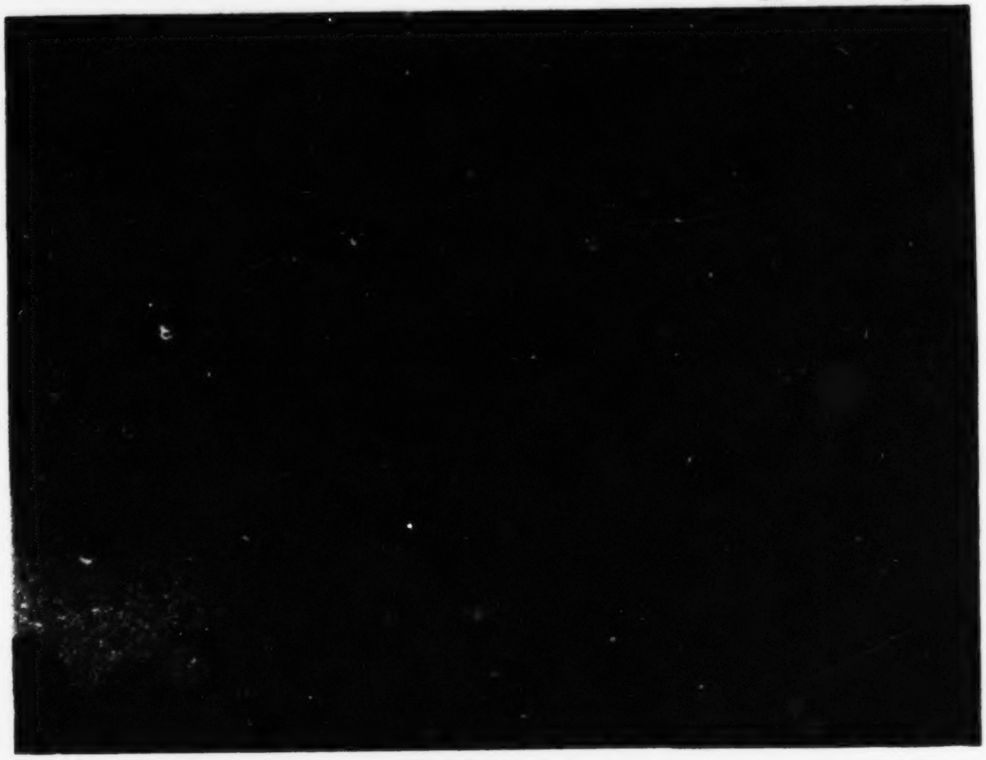

Figure 6.3-3. Abrade the Wall Surface With the Cleaning Tool to Remove Loose Material.

ORIGINAL PAGE IS

Figure 6.3-4. Collect Loose Material With Adhesive Surface On Cleaning Tool.

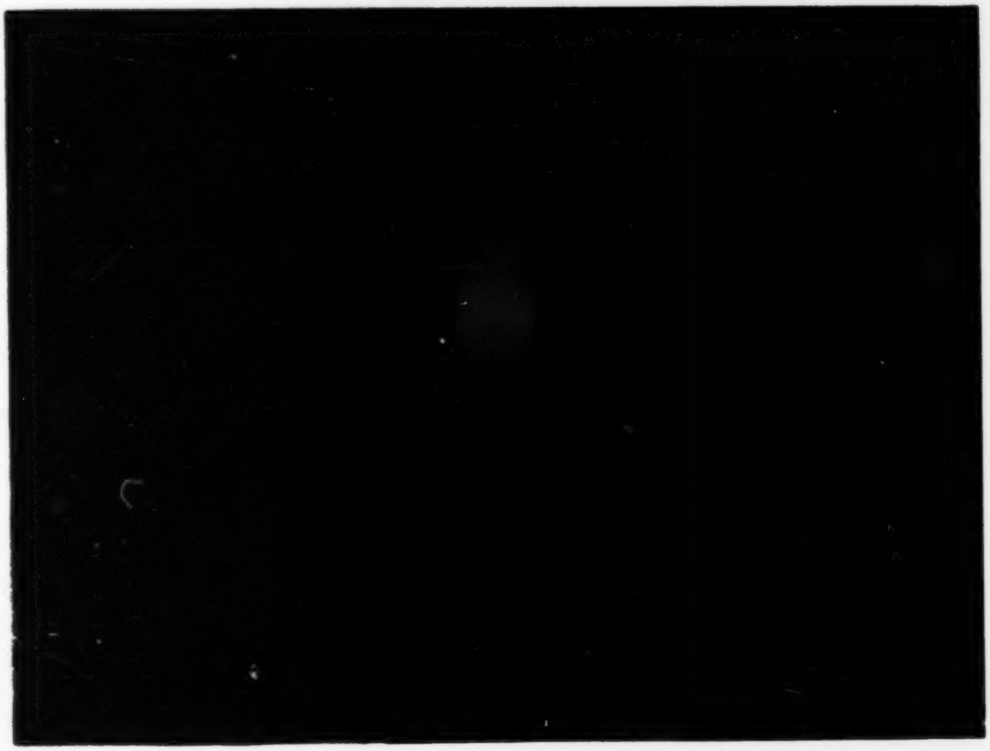

Figure 6.3-5. Center Alignment Template Over Hole.

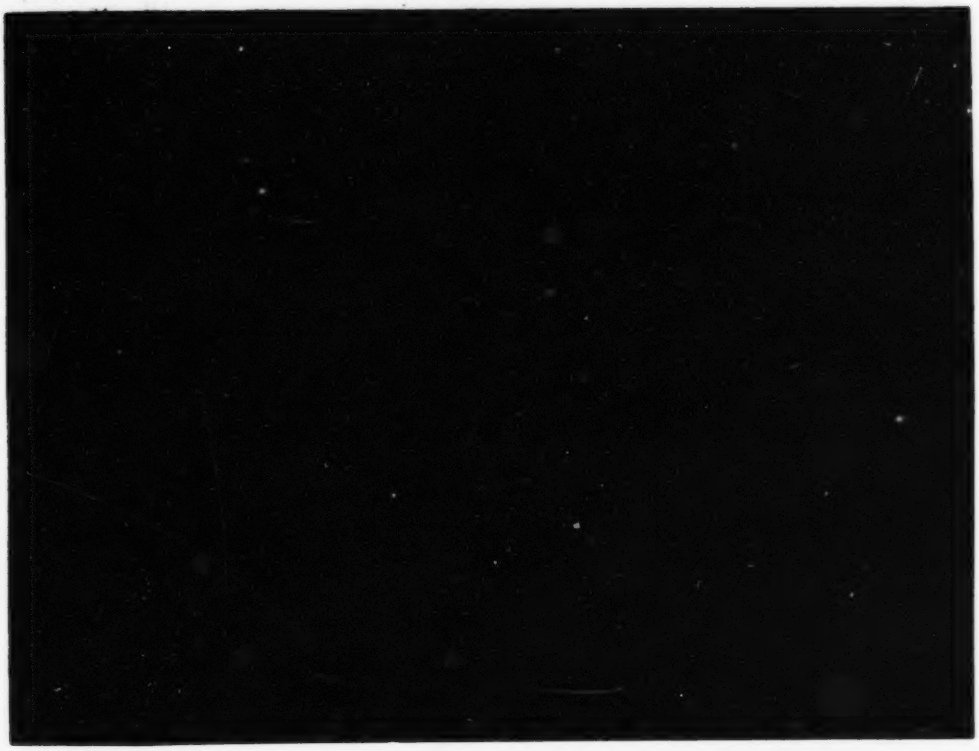

Figure 6.3-6. Verify Fit of Selected Patch Against Wall Markings.

Figure 6.3-7. Press Patch Firmly Into Place.

ORIGINAL PAGE IS
OF POOR QUALITY

ORIGINAL PAGE IS

Figure 6.3-8. Burnish Bubbles, Folds, and Creased Edges With Patch Handle.

Figure 6.3-9. The Completed Layered Patch.

Step	Task Time, min	Total Time, min	Task Description
1			Translate to damaged area, and attach portable foot restraint.
2	1	1	Inspect the damage area, and check for other holes.
3	1	2	Deploy trash bag and attach to structure or MWS.
4	1	3	Open the tool caddy and remove rag or wiping mit.
5	3	6	Clean 10 inch diameter area around damage to remove loose dirt, grease, and fluids. Replace rag or mit.
6	3	9	Remove abrasive tool and cleaning pad combination from tool caddy. Clean ring area 3 inches wide and 8 inches diameter to remove loose paint and material.
7	3	12	Remove backing from cleaning pad, discard backing in trash bag, and collect loose material with adhesive surface. Remove expended layers and discard into trash bag as required. Return tool to tool caddy.
8	1	13	Remove alignment template from tool caddy. Remove backing from template face and discard into trash bag.
9	1	14	Center alignment template over hole and press firmly in place.
10	2	16	Remove marker tool from tool caddy. Mark pressure wall at 3 locations 90-deg apart. Return marker to tool caddy.
11	1	17	Return alignment template to tool caddy.
20	1	18	Remove patch from tool caddy, and verify fit.
22	1	19	Remove the backing from the patch, and discard backing in trash bag.
23	1	20	Align patch with marks and press it into place.
24	1	21	Remove handle from patch, and return it to caddy.
28	2	23	Visually inspect the completed patch.
29	1	24	Remove tape strip from tape caddy, and place over velcro on patch.
31		24	Repair complete; repressurize the module.

Figure 6.4-1. Rubber Ring Patch Application Task Timeline.

ORIGINAL PAGE IS
OF POOR QUALITY

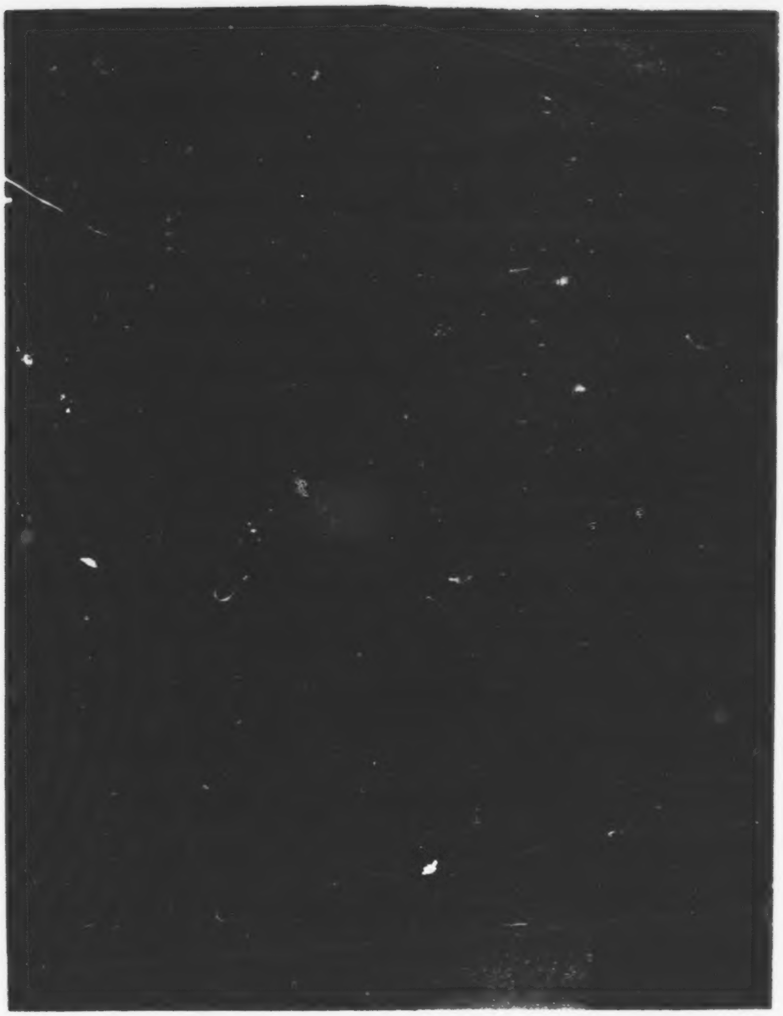

Figure 6.4-2. The Rubber Ring Patch Applied to a Curved Panel.

6.5 CONCLUSIONS OF LABORATORY PATCH DEMONSTRATIONS

The following conclusions are based on laboratory testing and conversations with NASA personnel and representatives of CAMPUS Inc.:

a. Cleaning tools and techniques must be compatible with the constraints of a suited astronaut and NASA safety requirements (ref. 2-5).

b. Tools should be well organized for astronaut efficiency.

c. Detailed station and azimuth markings on module interior and exterior walls would add to the complete description of the damage and aid in specifying its location when previously located from the opposite side.

d. Alignment marks on the patch should be applied with paint, stain, ink, or equivalent so they do not interfere with the burnishing operation.

e. The alignment template should be marked with a simple protractor and with a scale of concentric rings to aid the astronaut in describing details of the damage.

f. The burnisher handle should be approximately 10 in long to improve two-handed use when extra pressure is required. All other handles must be at least 6 in long.

g. Pending clarification of EVA requirements, all removable release plies may need to be captive to prevent accidental release.

h. Adhesive layer and release ply combinations should be selected and configured to prevent adhesive layer removal when the release ply is removed.

i. An additional task sequence is needed to describe repair tool refurbishment.

The following recommendations were made by Bill Pogue of CAMUS, Inc., a space operations consultant:

a. Tabs for removal of any adhesive release backing should contrast visually (color, pattern) with the patch or tool.

b. The color of the adhesive layers on the cleaning tool should contrast with the picked up and adhering particles. (Light and dark bands or stripes would provide contrast with a wide variety of particles.)

c. Use the alignment template to mark arcs rather than ticks on the pressure wall to align the patch. Arcs would be easier to see and would not require the patch be rotated to a precise orientation. The tick marks could also be deleted from the patch.

d. While graphite may be the best substance to use for a marker, graphite particles could be released during use, and there is the danger of breaking off the tip.

e. Develop a method to assess patch performance such as a leak indicator built into the patch, for example dust or dye. (A liquid crystal coating could reveal an area experiencing a local drop in temperature. A temperature drop could indicate an anomaly stemming from an impact or penetration.)

f. The pressurized air throttling through a penetration and expanding would cause ice to build up at the hole and tend to close the hole. Small holes would tend to close altogether (i.e., self-seal). (Nevertheless, as the pressure wall at room temperature warmed the ice it would melt and sublimate, and the hole would open again.) Such ice and moisture must be removed before the patch is applied.

g. Tabs for removing multiple adhesive layers on tools should not only be staggered, but when possible alternated from one side to the other. This would ease removal of the layers.

h. Exterior MLI blankets should be segmented into sizes easily manageable by EVA astronauts. Rolling a long MLI blanket may be a difficult and therefore unrealistic activity.

Additional Questions Raised. Several questions emerged during our repair simulations that we were unable to resolve under this contract but should be considered in future studies:

a. How can extra, nonstandard, or emergency patch material and tools be passed from the pressurized to the unpressurized module?

b. Can the pressurized nodes be used as airlocks to move from the pressurized to the unpressurized station areas?

c. Should a complete repair kit be included in each module?

d. What will be the quality and intensity of lighting behind the internal subsystem racks? Will supplemental lighting be required?

e. Can a suited astronaut reach the pressure wall through the internal rack support structure? Will subsystems such as fluid lines block access to portions of the pressure wall?

f. Can a suited astronaut successfully remove and relocate the internal equipment racks?

g. Would application of this patch be significantly different on a hole still bleeding atmosphere? How can this best be simulated?

6.6 NEUTRAL BUOYANCY SIMULATIONS

A complete description of the neutral buoyancy simulated tests is provided in appendix B. Important overall lessons learned were that (1) astronaut positioning at the repair site is a significant issue for efficient work and (2) tool handling and motions should be kept as simple as possible.

6.7 PATCH MATERIALS

The patch materials used to construct these demonstration versions are listed in the diagrams but not all have been space qualified. When possible, we used representative materials available in our laboratories that could be easily processed. Alternative, space grade materials are listed in figure 6.7-1. Two elastomers not yet space grade show promise in preliminary tests. The SWS-7220 U showed extremely low sensitivity to atomic oxygen in a laboratory plasma asher test. The polyphosphazene performs within the NASA outgassing requirements. We believe functioning models of our patch designs can be constructed with these space grade materials. Using space grade materials will facilitate qualifying the patches for space application.

Other advanced materials have potential applications in pressure wall repair; for example, adhesives that use ultraviolet (UV) radiation to induce curing are being developed. Radiation sources available include the sun, fluorescent lamps, pulsed lamps, medium pressure mercury lamps, and electrodeless mercury lamps. Advantages of such adhesives include fast room

	Features								
	Space Grade	Boeing Space Qualified	Controlled Volatility	Non-Corrosive	Electrically Conductive	Low Density	One Part	Two Part	Manufacturer
Sealants									
DC 6-1104 (3)	●	●	●	●			●		Dow Corning
DC 6-1125 (5)	●		●	●			●		Dow Corning
Sealant Adhesives									
CV-1142 (1)(3)	●		●	●			●		McGHAN NuSIL
CV-1143 (1)(3)	●		●	●			●		McGHAN NuSIL
CV-1500 (1)(4)	●		●	●	●		●		McGHAN NuSIL
CV-2564 (1)(3)	●		●			●		●	McGHAN NuSIL
CV-2566 (1)	●		●					●	McGHAN NuSIL
RTV 142 (1)	●	●	●	●			●		General Electric
Foam									
CCF1-2365	●		●					●	McGHAN NuSIL
SILASTIC S-5370	●					●		●	Dow Corning
Primer									
RTV 566	●							●	General Electric
DC 1204 (2)	●								Dow Corning
Low Durometer Elastomers									
CV1-2500 (2)	●		●					●	McGHAN NuSIL
SWS-7220 U (6)(7)							●		Stouffer-Wacker
Polyphosphazene (7)									Ethyl Corp.

(1) Silicone
(2) Clear
(3) Translucent
(4) Black
(5) White
(6) Uncatalyzed methyl vinyl silicone
(7) Potential for space qualification

Figure 6.7-1. Potential Repair Materials.

temperature cure, reduced energy requirements and fire hazard when compared with high-temperature cure, and reduced volatiles.

Electron beam (EB) curing adhesives are alternatives to UV curing adhesives. EB adhesives can be heavily pigmented because the electron beam is penetrating, whereas the UV adhesives are thickness limited. EB curing requires an inert atmosphere while UV does not. UV curable resin systems are currently available that will satisfy NASA outgassing requirements for space usage.

7.0 DESIGN EVALUATION COMPUTER CODE

Overview. Prior to this contract the method of analysis for hypervelocity impacts (> 2.0 km/s) consisted of using flux equation, time in orbit, surface area, and the required PNP to calculate a design particle. This was assumed to be the largest particle likely encountered during a spacecraft's lifetime. Candidate wall designs were then tested using projectiles of this size, fired by devices such as two-stage, light-gas guns. If the wall design could withstand this impact, it was considered adequate. This technique assumes that the resistance of the wall to such an impact follows a power function with velocity (i.e., the function describing the relation between critical diameter and velocity is continuous and varies as a power of impact velocity).

Testing conducted under a Boeing contract with NASA/Lewis in 1965 (ref. 3-2) as well as other studies reveal a different situation. These investigations showed three distinct failure mechanisms involved during hypervelocity impact of a two-plate structure similar to that first recommended by Whipple (ref. 7-1). Figure 7.0-1 shows predictions of the response function of the reference wall configuration for impact by aluminum spheres from 0.1 to 16 km/s and for impact angle ranging from 0-deg (normal) to 60-deg. The first failure mechanism (0.1 to 3.0 km/s) is characterized by ballistic penetration of both plates by a projectile remaining essentially intact and maintaining most of its mass and velocity. The second failure mechanism (3.0 to 8.0 km/s) is characterized by a fragmenting projectile causing failure of the second plate through a combination of multiple impact craters and spallation. In general, higher impact velocities produce smaller projectile fragments, resulting in less wall damage. The final failure mechanism is characterized by projectile and wall fragments vaporizing and imparting an impulse load to the second plate. Impulse failure of the backwall is easily recoganized by cracks and petaling with little or no cratering.

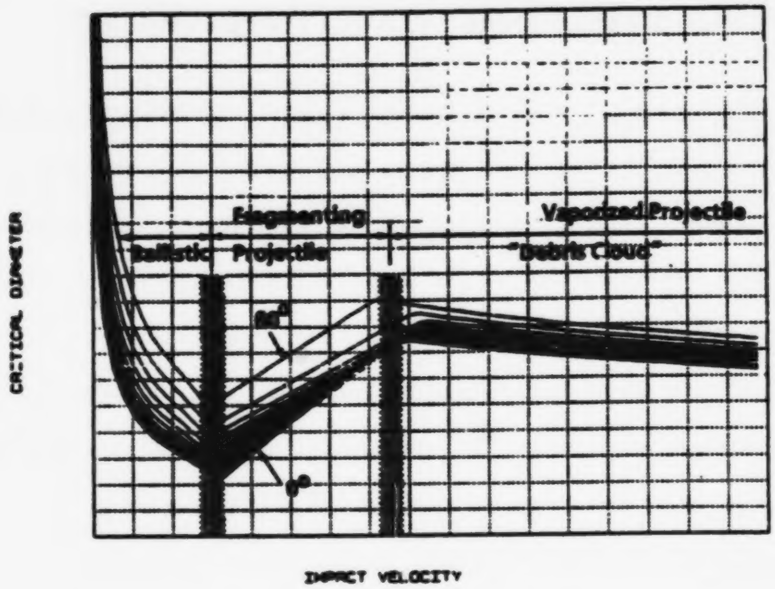

Figure 7.0-1. Wall Response Function

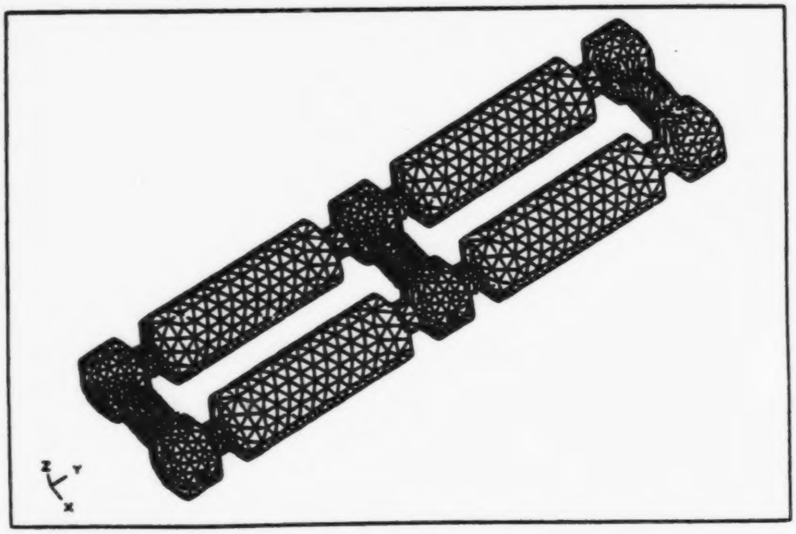

Figure 7.1-1. Space Station Geometry Model, 5000 Elements

The design evaluation computer code developed under the contract is BUMPER. This refers to both the family of codes; BUMPER, GEOMETRY, and RESPONSE, as a whole and to one of the modules within this family. The theory upon which these codes are based may be found in Appendix G of this report.

7.1 BUILDING THE SPACE STATION MODEL

Because of the nonlinear response of a typical wall configuration, the directionality of the debris environment (and the meteoroid environment when considering Earth shielding), and the rigorous PNP requirements, we take a discrete element approach in describing Space Station geometry. Space Station was modeled in a manner similar to a finite element model to take maximum advantage of mutual self-shielding and to allow the integration of the nonlinear effects of impact angle and velocity over the entire range of possibilities. A finite element model of the reference configuration is shown in figure 7.1-1. This approach allows us to analyze a specific Space Station configuration, orientation, and orbit. Using a model of this type gives us power and flexibility both in analysis and in the presentation of the results. Using a large number of elements permits modeling a Space Station design containing various aluminum single and double wall configurations. The vulnerability of specific areas can be assessed, and the Space Station can be partitioned to analyze specific subunits such as modules.

There are no provisions for modeling windows within BUMPER. A suitable penetration function for multipane windows did not exist during the time of performance of this contract, and it was beyond the scope to develop one.

7.2 HIDDEN SURFACE ALGORITHM

It was necessary to develop a hidden surface algorithm to make full use of a geometry model as previously described. In the analysis a threat direction is chosen that is in the plane of the orbit for debris or out of plane for meteoroids. The algorithm determines whether a particular element faces the threat and eliminates all those that do not. It then determines whether any element is hidden behind another and eliminates those that are. This is done by transforming the original coordinates of the nodes into a coordinate system having one axis parallel to the threat direction. The nodes are projected onto a plane perpendicular to the threat direction. The centroid of each element is calculated and then sorted in relation to the threat. An algorithm then determines whether an element's centroid is hidden by the bounding of another element. The cosine of the impact angle is output for each exposed element of each threat angle, allowing the penetrating flux to be calculated and summed over the entire environment. Figure 7.2-1 shows an example of the hidden surface algorithm for a typical meteoroid threat angle.

7.3 APPROACH TO MODELING ORBITAL DEBRIS

Figure 7.3-1 shows the seven steps used in analyzing debris impacts but assuming only normal impacts. For each unique wall configuration, it is first necessary to determine the critical projectile diameter (1). For each impact velocity increment (4), the critical projectile diameter is calculated by using the appropriate penetration equations described later in this report. This projectile diameter (2) is used to determine the number of particles of this size or larger (3). All particles larger than this will penetrate at this particular velocity and therefore must be accounted for in the probability equations. Because penetrations are rare occurrences, the correct probability function to use is the Poisson probability function (6). Our interest is in the probability of no occurrences, therefore by setting $N = 0$ the equation simplifies as shown. Because the probability of the impact velocity in question occurring is extremely small (4), the probability of small delta around this velocity is calculated. The equation that must be solved is shown in (7) and is approximated by a summation in the design analysis code.

This technique must be expanded further as shown in figure 7.3-2, when considering a single surface element in the model. A threat direction is chosen (1) that determines the impact angle relative to a vector normal to the elements surface (2). The threat direction also determines the impact velocity (3) by assuming all orbits are circular and therefore that everything at that orbital altitude has the same orbital velocity. By using the appropriate penetration function for the

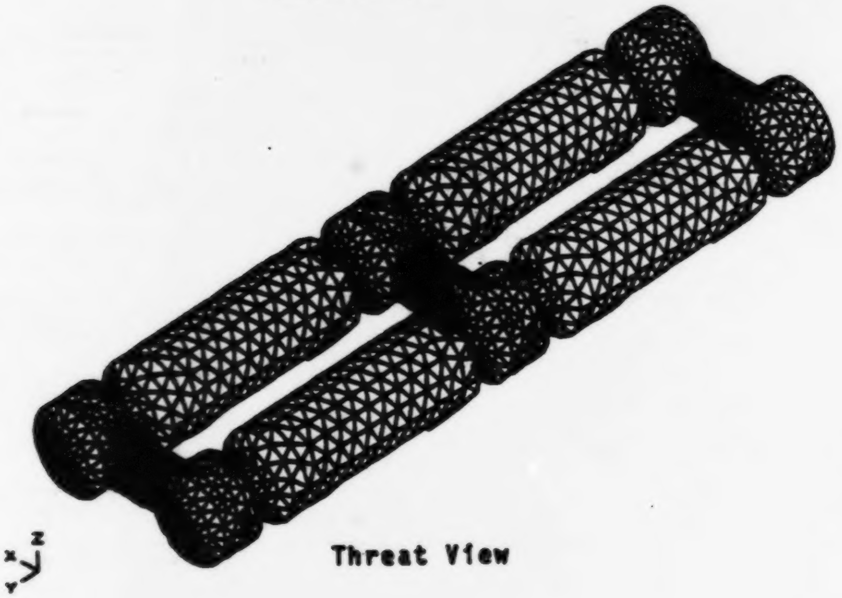

Threat View

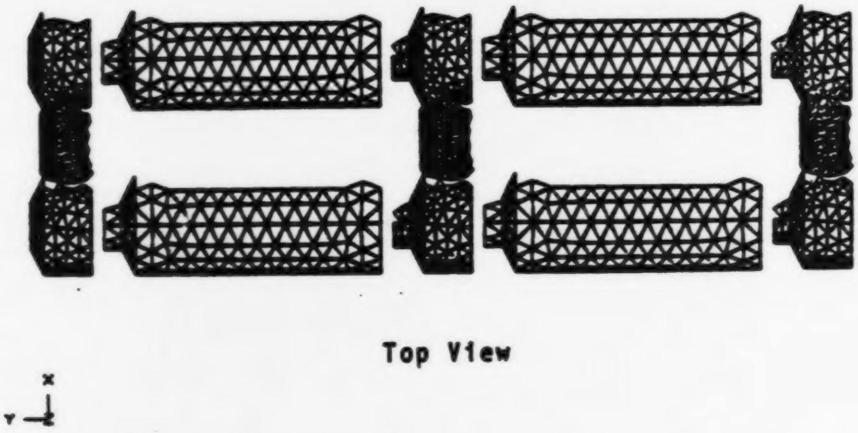

Top View

Figure 7.2-1. Output of Hidden Surface Algorithm for Meteoroid Threat Angle

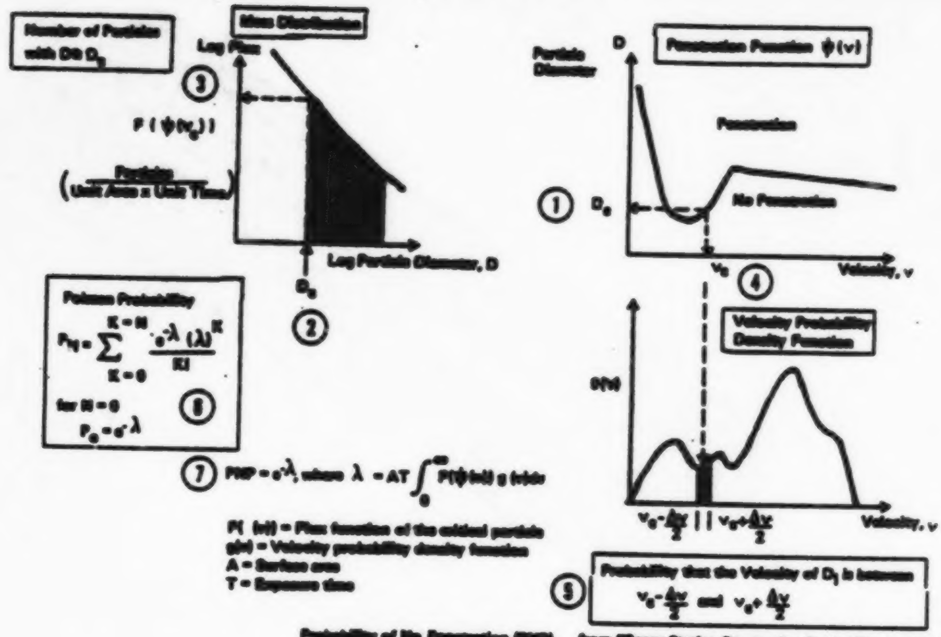
Number of Particles with D≥ Dc
Mass Distribution
Log Flux
③
F (ψ(vc))
Particles / (Unit Area x Unit Time)
Log Particle Diameter, D
Dc
②
Poisson Probability
$P_N = \sum_{K=0}^{K=N} \frac{e^{-\lambda}(\lambda)^K}{K!}$
for N = 0
$P_0 = e^{-\lambda}$
⑥
⑦ $PNP = e^{-\lambda}$, where $\lambda = AT\int_0^{\infty} F(\psi(v))\, g(v)dv$
F(ψ(v)) = Flux function of the critical particle
g(v) = Velocity probability density function
A = Surface area
T = Exposure time
Particle Diameter
D
Penetration Function ψ(v)
Penetration
No Penetration
① Dc
vc
④
Velocity, v
Velocity Probability Density Function
g(v)
$v_c - \frac{\Delta v}{2}$
$v_c + \frac{\Delta v}{2}$
Velocity, v
⑤ Probability that the Velocity of Di is between $v_c - \frac{\Delta v}{2}$ and $v_c + \frac{\Delta v}{2}$

Probability of No Penetration (PNP) from "Space Station Penetration Probability Model", Fritz Scholz, Boeing Computer Services

Figure 7.3-1. Debris Impact Analysis Approach

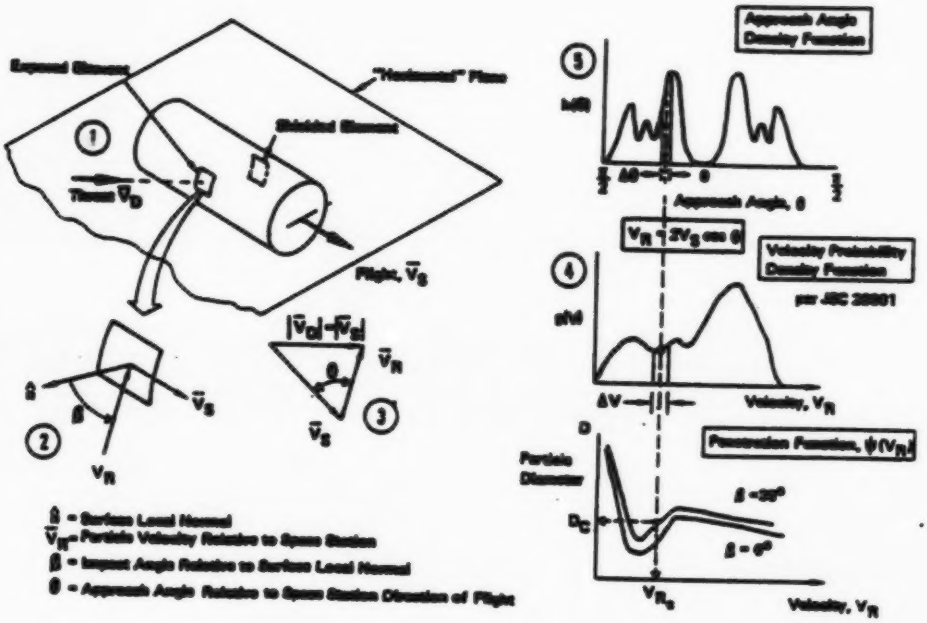
Exposed Element
"Horizontal" Plane
①
Shielded Element
Threat $\bar{V}_D$
Flight, $\bar{V}_S$
$\hat{n}$
β
$\bar{V}_S$
②
V_R
$|\bar{V}_D| - |\bar{V}_S|$
$\bar{V}_R$
θ
$\bar{V}_S$
③
$\hat{n}$ = Surface Local Normal
$\bar{V}_R$ = Particle Velocity Relative to Space Station
β = Impact Angle Relative to Surface Local Normal
θ = Approach Angle Relative to Space Station Direction of Flight
Approach Angle Density Function
⑤
h(θ)
$-\frac{\pi}{2}$
Δθ
0
$\frac{\pi}{2}$
Approach Angle, θ
$V_R = 2V_S \cos\theta$
Velocity Probability Density Function
per JSC 20001
④
g(v)
ΔV
Velocity, V_R
D
Penetration Function, $\psi(V_R)$
Particle Diameter
β = 30°
D_C
β = 0°
V_{R_c}
Velocity, V_R

Figure 7.3-2. Debris Impact Analysis of Space Station Elements

ORIGINAL PAGE IS
OF POOR QUALITY

calculated impact angle, the critical diameter can be calculated. The probability of both the impact velocity (4) and threat or approach angle (5) occurring is calculated. The summation is then expanded to include all possible approach angle and all elements. Within the code the penetrating flux for each element is stored, allowing PNP calculations for each element, for elements representing a single Space Station critical element (SSCE), or for the overall Space Station.

7.4 APPROACH TO MODELING METEOROIDS

The approach to modeling the meteoroid environment is similar to that used for debris, but expanded for out of plane angles. The meteoroid model and corrections for Earth orbit were mentioned previously in section 2.0. The flux equation shown in figure 2.2-1 comes from reference 2-2; but the best explanation of the equation is given in reference 2-6, which states, "The exact meaning of N can be confusing. It is the flux in one direction through a flat plate of one square meter area. Thus, if the directional flux were j particles/(m^2-sec-steradian) and j is isotropic, then N = 3.14159 x j."

Each element in the model is then exposed to a hemisphere (fig. 7.4-1) that has been divided into surface elements of equal area. The probability of meteoroid flux coming from a direction defined by the centroid of the surface element is the area of that surface element divided by the area of the hemisphere. The dot product of the vector from the surface element centroid and the velocity vector (X-axis) of the spacecraft defines the threat angle used to determine exposed areas. This technique was used to ensure that all combinations of possible approach angles were equally likely.

The modeling of the velocity effects for meteoroids is handled differently that for debris. The entire velocity spectrum, which is in turn defined by the approach angle, is used in evaluating a Space Station model for debris impacts. For meteoroids, the velocity distribution is independent of approach angle. The correct approach to modeling meteoroids is to select an approach angle, calculate the probability of that angle occurring, calculate the probability of the flux coming from that angle, and then calculate the critical particle diameter for velocity increments between 10 and

72 km/s. The probability of that velocity increment occuring would then have to be factored into the analysis. This would be very tedious and time-consuming even using computers.

We took an alternative approach to see if it was actually necessary to account for the entire velocity range when calculating PNP due to meteoroids. A sensitivity study was done to determine the effect of using an average meteoroid velocity of 20 km/s versus the SP-8013 (ref. 2-2) distribution on PNP for 10, 20, and 30 years of exposure time. An early version of BUMPER that did not account for geometry, but which did use the SP-8013 meteoroid velocity distribution, was used to calculate the overall PNP due to meteoroid impacts. The code was then modified to use a constant meteoroid velocity of 20 km/s. These results, presented in figure 7.4-2, show almost no difference between the two approaches to velocity. A second study was done to see if there was any difference in the analysis using an average velocity but accounting for the effects of Space Station orbital velocity of 7.5 km/s. These results, given in figure 7.4-3, again show almost no difference between the two approaches.

The conclusions reached were that (1) meteoroids were not a design driver when compared with the debris environment, (2) use of an average meteoroid velocity of 20 km/s was adequate for calculating a PNP for Space Station due to meteoroid impacts, and (3) effects of orbital velocity should be accounted for to correctly model the distribution of impacts on the upper and forward surfaces of Space Station.

7.5 PENETRATION FUNCTION

The penetration function is a series of equations that determine the diameter of a debris or meteoroid spherical projectile that just penetrates a given wall configuration at a specific impact velocity and angle. This information can then be used to determine the penetrating flux on an element and/or overall PNP. A complete description of penetration functions used is presented in section 4.0.

- **Element coordinates selected to provide elements of equal area.**
- **Threat angles θ_i and ϕ_j are measured to centroid of curved surface element.**
- **Allcombinations of θ_i and ϕ_j are equally likely.**

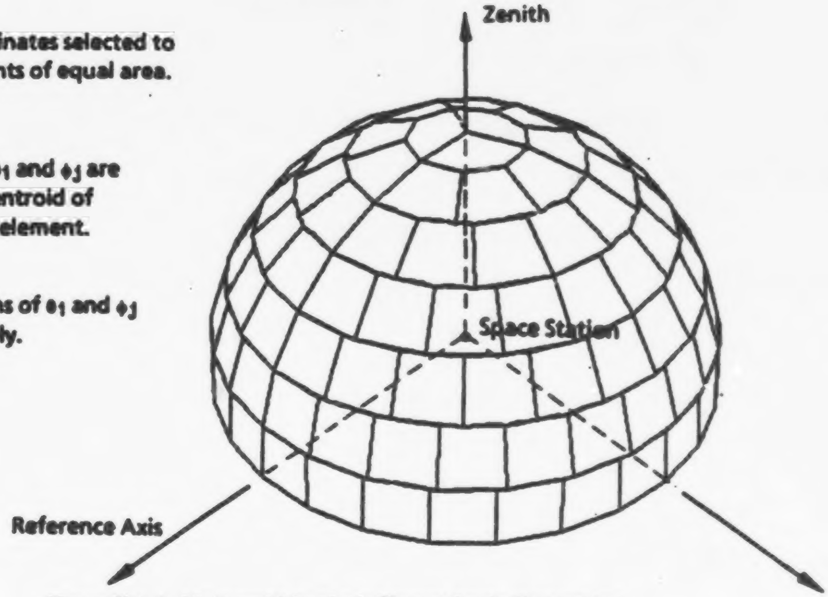

Figure 7.4-1. Meteoroid Analysis Threat Angle Generation

Condition	Probability of No Penetration, % Exposure Time, Years		
	10	20	30
Constant Velocity [1]	99.925%	99.849%	99.774%
SP 8013 Distribution [2]	99.923%	99.845%	99.768%

Note 1 $V_{meteoroid}$ = 20km/sec, reference wall design, $V_{space\ station}$ = 0
Note 2 SP 8013 velocity distribution, reference wall design, $V_{space\ station}$ = 0

Figure 7.4-2. Effect of Meteoroid Velocity on Total Space Station PNP

Condition	Probability of No Penetration, % Exposure Time, Years		
	10	20	30
No Orbital Velocity [1]	99.966%	99.932%	99.897%
With Velocity Effects [2]	99.964%	99.929%	99.893%

Note 1 $V_{meteoroid}$ = 20 km/sec, $V_{space\ station}$ = 0, Reference Configuration
Note 2 $V_{meteoroid}$ = 20 km/sec, $V_{space\ station}$ = 7.5 km/sec, Reference Configuration

Figure 7.4-3. Effect of Space Station Orbital Velocity on Total Space Station PNP

7.6 DESIGN ANALYSIS COMPUTER CODE

A highly modular computer code named BUMPER was developed to bring all of the preceding elements together. Figure 7.6-1 graphically shows the flow of data through the various modules, which will be described in more detail in the following sections.

7.7 MODEL GENERATION

SUPERTAB is a finite element preprocessor and postprocessor that was used to generate the geometry model. It was selected because of convenience and familiarity and is not critical to the analysis. SUPERTAB's Universal File Format (UFF) was selected as the means of transmitting the geometry information to the GEOMETRY module. This was again done for convenience and is not critical to the analysis. Any finite element generation system or code may be used as long as the rules stated in the users document are followed.

7.8 GEOMETRY MODULE

The GEOMETRY module reads the UFF, which contains the node and triangular element definitions of the Space Station model. The surface area of all elements is calculated and written to a file, along with the threat information and element and property identifications. For each threat angle, the cosine of the impact angle for each element, which is unique for each threat angle, is calculated. This allows the back side elements to be eliminated from further consideration. The remaining elements are sorted in relation to the threat direction to allow the shadowing subroutine to efficiently eliminate elements that are hidden behind other elements. For each threat angle, a list of exposed element points and the associated cosine are written out. This information is then used by the BUMPER module to compute the appropriate statistics. The GEOMETRY module requires a relatively large amount of computing resources, but need only be executed once for a given configuration and orientation.

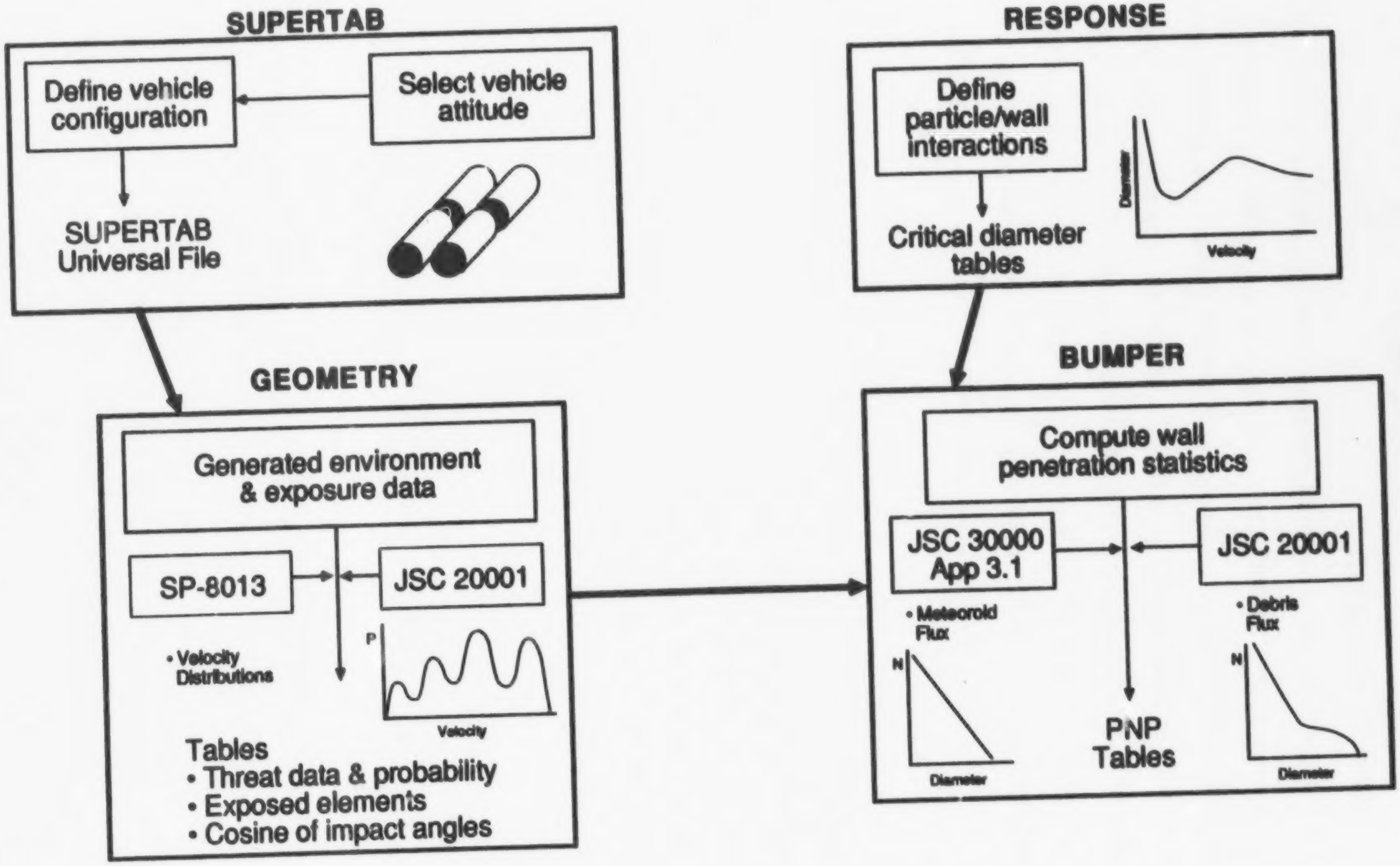
SUPERTAB
Define vehicle configuration
Select vehicle attitude
SUPERTAB Universal File
RESPONSE
Define particle/wall interactions
Critical diameter tables
Diameter
Velocity
GEOMETRY
Generated environment & exposure data
SP-8013
JSC 20001
• Velocity Distributions
P
Velocity
Tables
• Threat data & probability
• Exposed elements
• Cosine of impact angles
BUMPER
Compute wall penetration statistics
JSC 30000 App 3.1
JSC 20001
• Meteoroid Flux
N
Diameter
PNP Tables
• Debris Flux
N
Diameter

Figure 7.6-1. Design Analysis Computer Code - Data Flow.

7.9 RESPONSE MODULE

The RESPONSE module contains the penetration functions described in section 4.0. Using these functions, RESPONSE builds tables of critical projectile diameters as a function of impact velocity, impact angle, and wall configuration. These tables are read by the BUMPER module and used to calculate the penetrating flux. A great deal of flexibility is inherent in using this approach. The response function could simply be a lookup table if there was sufficient test data to fill one out, a constant to evaluate a specific threat such as a single projectile/velocity combination, or a combination of empirical and theoretical equations as we have now. The response function would have to be in a binary file compatible with FORTRAN formats used in the RESPONSE and BUMPER modules.

7.10 BUMPER MODULE

The BUMPER module reads in the tables of exposed elements and projected areas from GEOMETRY and the tables of critical diameters from RESPONSE. Using this information and the flux equations from SP-8013 and JSC 20001, it calculates the flux of the critical projectile. This flux multiplied by the projected area of the element multiplied by the probability of the threat occurring is summed up for all elements and all threats.

7.11 CONTOUR MODULE

CONTOUR produces the data base that may be used by user-supplied software to produce design contour plots. The plots show the relationship between shield and vessel wall thickness and PNP for a given shield standoff. An example of this plot is shown in figure 7.11-1. Contours of this type will be extremely useful to designers in developing optimized wall configurations.

This code is similar to BUMPER with the exception that the RESPONSE module has been incorporated as a subroutine. The range of input variables must be defined by determining a minimum, maximum, and increment for shield and wall thicknesses as well as standoff, insulation, and type of threat. CONTOUR then loops through the parameters calculating PNP for each unique

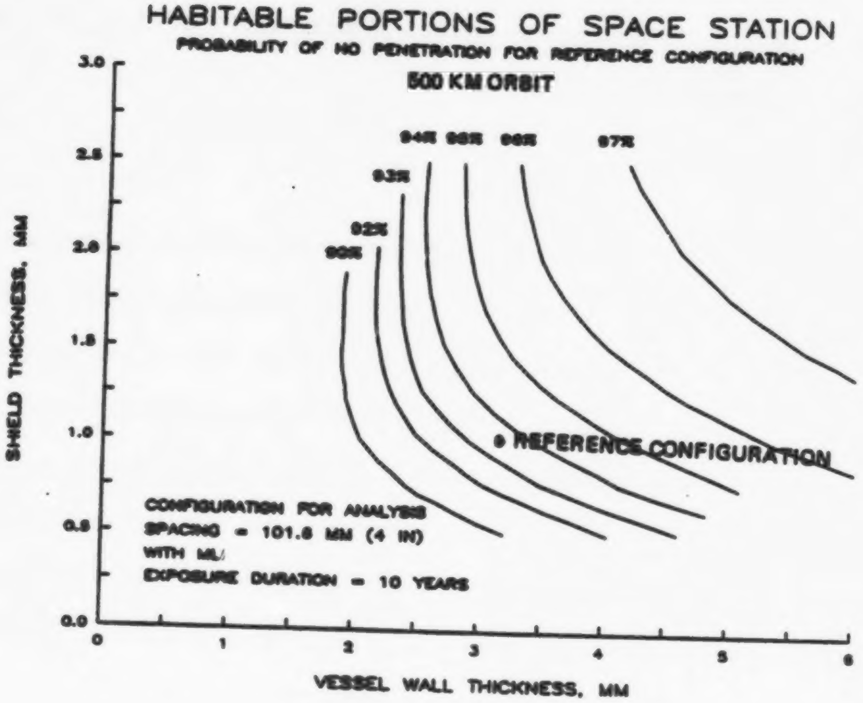

Figure 7.11-1. Design Contour

combination of wall configuration parameters. It then writes a summary file containing these parameters along with their calculated PNP.

7.12 ANALYSIS RESULTS

The output from BUMPER can be displayed in several ways. Because the probability of penetration (1.0 - PNP) is calculated and stored on an element basis it can be displayed as contours of equal threat on the Space Station model. Figure 7.12-1 shows the threat distribution for debris. The greatest threat is to the leading edges and sides of Space Station, while the inner portions that are self-shielded show almost no threat. Plots such as these can be used by designer for placement of critical and sensitive items such as pressurized tanks. Figure 7.12-2 is a similar plot of threat contours for meteoroids and shows the increased threat to the upper and forward parts of Space Station. The Earth prevents meteoroids from approaching from below the plane of orbit, resulting in very low levels of threat to surfaces that face Earth.

7.13 ORIENTATION SENSITIVITY STUDY

By a simple coordinate system transformation it is possible to determine the effects of different Space Station orientations on PNP. Figure 7.13-1 shows the results of such a sensitivity study. The reference orientation is shown at the top with a PNP of 93.4%. Rotating the model 90-deg around the Z-axis simulates the effect orbiting Space Station broadside to the velocity vector. This orientation shows a modest improvement over the reference orientation. The worst orientation is rotating the model 90-deg around the velocity vector. This exposes the most surface area to the threat and results in the lowest PNP.

The results of additional sensitivity studies are presented in section 2.0.

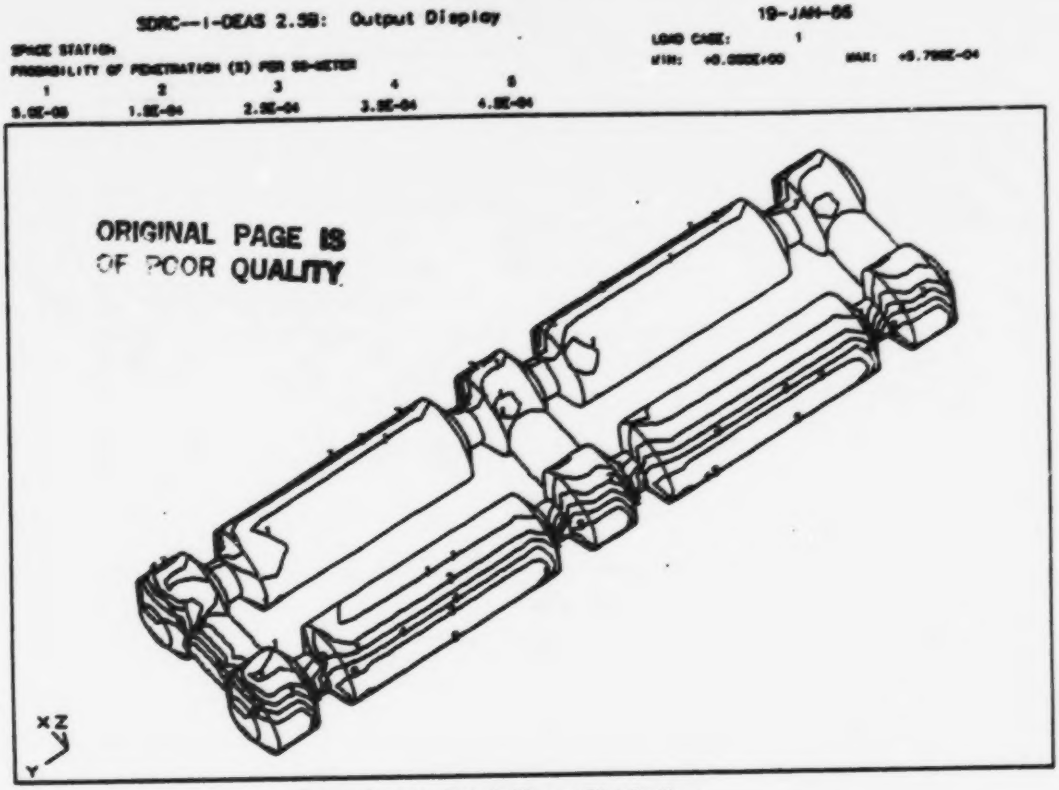
SDRC--I-DEAS 2.5B: Output Display
19-JAN-86
SPACE STATION
PROBABILITY OF PENETRATION (X) PER SQ-METER
LOAD CASE: 1
MIN: +0.000E+00
MAX: +5.796E-04
1
5.0E-05
2
1.5E-04
3
2.5E-04
4
3.5E-04
5
4.5E-04
X Z
Y

ORIGINAL PAGE IS
OF POOR QUALITY

Figure 7.12-1. Debris Threat Distribution

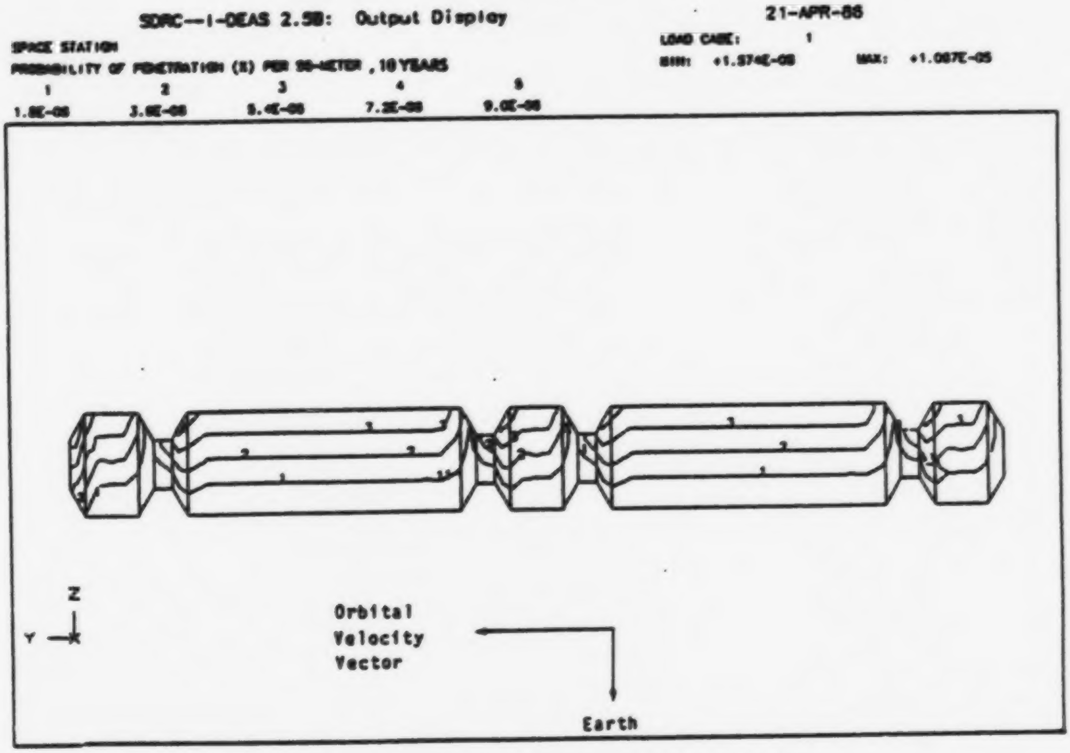
SDRC--I-DEAS 2.5B: Output Display
21-APR-86
SPACE STATION
PROBABILITY OF PENETRATION (X) PER SQ-METER , 10 YEARS
LOAD CASE: 1
MIN: +1.574E-08
MAX: +1.087E-05
1
1.8E-06
2
3.6E-06
3
5.4E-06
4
7.2E-06
5
9.0E-06
Z
Y
Orbital Velocity Vector
Earth

Figure 7-12-2. Meteoroid Threat Distribution, Side View

Orientations	Probability of No Penetration
Reference Configurations 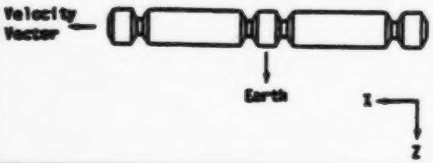 Velocity Vector Earth X Z	93.4%
Rotation 90° Around Z Axis 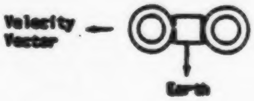 Velocity Vector Earth	95.3%
Rotation 90° Around X Axis 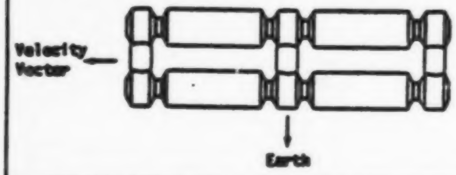 Velocity Vector Earth	87.8%

Figure 7.13-1. Results of Orientation Sensitivity Study

7.14 THEORY

The rigorous theoretical derivation upon which our analysis technique is based can be found in appendix G. This comprehensive section deals with both debris and meteoroids and how they impact a body in orbit.

8.0 DESIGN GUIDE

8.1 INTEGRATED WALL DESIGN

The Space Station will present new problems in designing for safety and reliability as described in the Space Station Systems Requirements Document 0001, Revision A, p. A-115:

> A.13.1 DESIGN APPROACH TO ORBITAL DEBRIS AND METEOROID PROTECTION
>
> The past approach to protecting spacecraft against meteoroids has been to add sufficient shielding and/or redundancy to provide a desired reliability in a known environment. This approach has worked well for the relatively short lifetime, small structures of the past; however, when this approach is applied to SSPE, its larger size, longer lifetime, and the addition of an orbital debris environment cause the following problems to emerge:
>
> - The amount of shielding required to achieve the current design reliability will add significant weight.
> - Current design does not adequately address the issue of crew safety. Consequently, a conservative approach would suggest that reliability be increased which would increase the shielding weight further.
> - The current debris environment does not include recent measurements nor debris that has been and will be generated by antisatellite tests, the possible debris from unanticipated satellite breakups, SSPE operations, or other unexpected activities in LEO.
>
> The following possible approach combines shielding and/or redundancy with engineering design and operations to provide a level of crew safety comparable to certain industrial standards. Different levels of safety could be required for noncritical hardware. Thus, in addition to a 0.95 hardware reliability against meteoroid and debris damage, the SSPE should be designed and operated in a manner such that the individual crewman would not be exposed to a risk of more than 0.0005 (1 per 2000) accidental deaths per year as a consequence of meteoroid and debris strikes.
>
> In addition to limiting the damage caused by the rupture of the pressure vessel (e.g., closed doors to confine the loss of pressure, automatic systems that decrease the net oxygen loss rate for a short time, arrangements of internal hardware to decrease the amount of shrapnel) the following could be implemented.
>
> - A damage prevention concept to include onboard detection of orbital debris
> - Collision warning
> - Possibly a collision avoidance system
> - An area with maximum shielding where the crew spends most of their time or could go in case of emergency
> - Crew activities planned so that the safety goal is maintained. This might limit the number of hours a crewmember could stay in more hazardous areas such as EVA or a lightly shielded work area.

PRECEDING PAGE BLANK NOT FILMED

The designer can approach these concerns with the analytical techniques and principles discussed here. Components of our reference configuration integrated wall are illustrated in figure 8.1-1, and their relevance to hypervelocity penetration resistance is discussed in the following paragraphs.

Shield. In addition to possible use as thermal radiators, the shield is intended to break a projectile into fragments that the backwall can successfully resist. A body of test data exists for thicknesses from 0.51 mm (0.020 in) to 2.03 mm (0.080 in.) The design thickness will depend on structural rigidity requirements, thermal performance (if it also performs as a thermal radiator), and penetration resistance requirements. Some work has indicated an optimum ratio exists between shield thickness and projectile diameter (ref. 3-1); nevertheless, this effect may not be relevant for a shield intended to protect against a range of projectile sizes and impact angles.

Theoretical work (app. F) has shown the shield material's shock impedance should be matched to the expected projectile material's shock impedance. Because aluminum is the primary component of orbital debris, aluminum should perform well as a shield and better than composite materials and many other metals. In this study, no other material was found to work better.

Another study (ref. 4-5) showed shield areal density roughly determines shield effectiveness. This implies shield effectiveness is gained only at the cost of shield weight. An important exception occurs for materials with volume densities below 2 g/cm^3, which are less effective on an areal density basis. Such materials include magnesium, magnesium-lithium, and polyethylene. Conversely, lead and cadmium perform better than the areal density rule indicates. These results reinforce the conclusion that aluminum is a good shield material because it is structurally more efficient than either lead or cadmium.

Backwall. The backwall of the integrated wall design serves as the module pressure wall. Because backwall penetration is the effect we wish to minimize, backwall thickness is one of, if not the most, important variable in the integrated wall design. Increasing backwall thickness will always increase the PNP. The module wall may require stiffness augmentation in the form of structural rings, integral isogrid or waffle grid, and/or integral ribs. In general, this additional

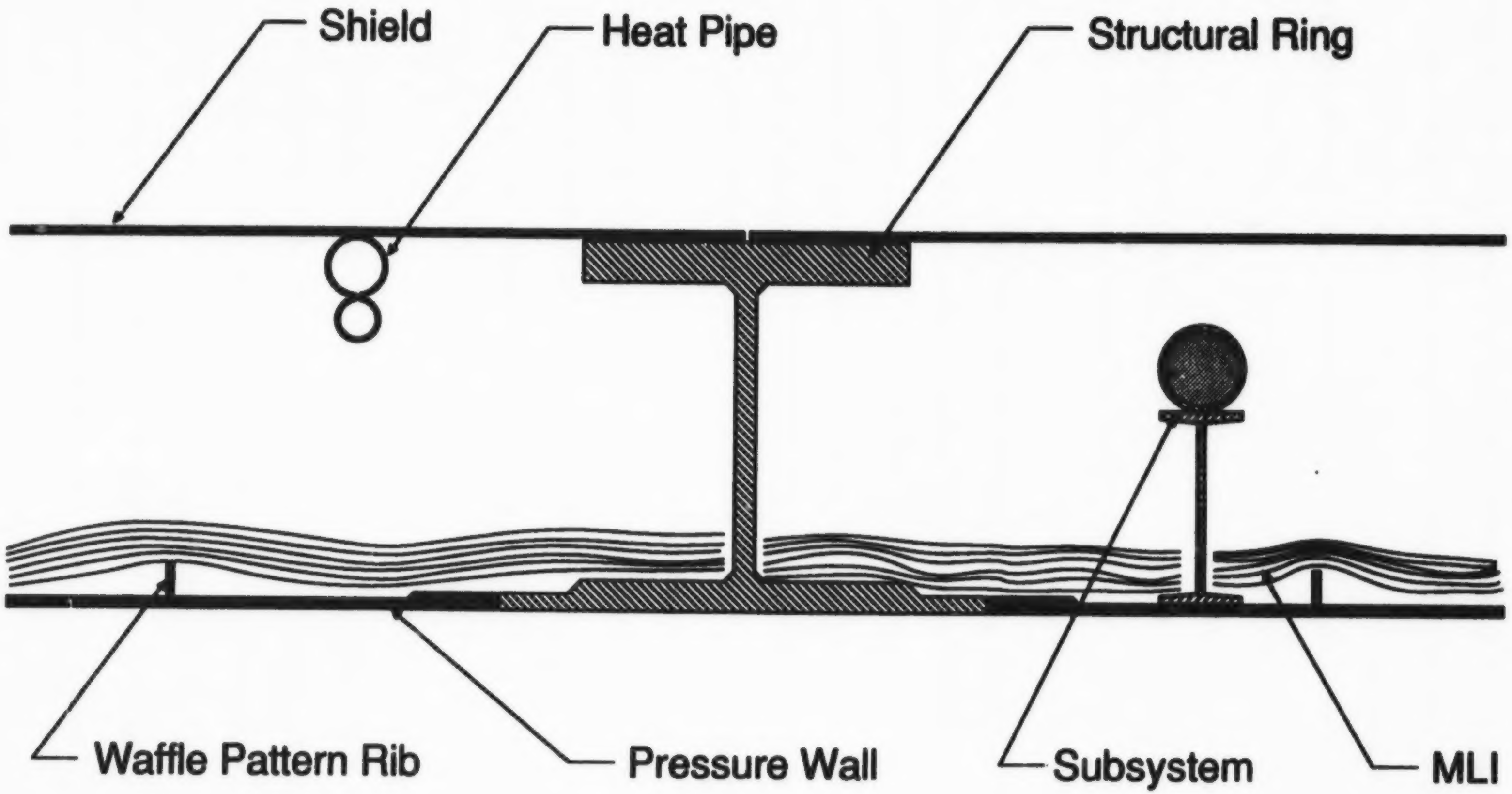
Shield
Heat Pipe
Structural Ring
Waffle Pattern Rib
Pressure Wall
Subsystem
MLI

Figure 8.1-1. Space Station Integrated Wall Structure

structure will contribute a small amount toward penetration resistance; however, we neglect the contribution in calculating overall PNP. To achieve maximum PNP, extra structure is better spread evenly over the backwall surface.

Relatively low internal module pressure (< 15 lb/in^2) means critical crack lengths in the pressure wall will be long, approximately 50 cm (20 in) The presence of a waffle stiffening pattern will improve resistance to crack growth.

Spacing. The spacing between the shield and backwall allows expansion of projectile and shield fragments and/or vapor cloud before they impact the backwall; however, the positive effects of this diminish as the spacing increases.

MLI. MLI is included in the module design to thermally isolate the modules from temperature variations outside. MLI also absorbs fragmented particles from the projectile shield interaction and hence contributes toward penetration resistance. In all testing, the MLI has been attached to the backwall. This position seems optimum, as the fragments are dispersed to the maximum extent, minimizing the chance for overlapping impacts. All MLI used in this study contained 30 layers with separator netting between each layer and beta cloth on the front surface. No conclusions on optimum MLI design are possible based on this data alone.

Structural Members. Structural stiffening members and supports may be attached to the pressure wall's exterior surface. In general, this structure should contribute to pressure wall penetration resistance; however, we do not account for it in the analysis. These members may also be damaged by impacts. This damage should be accounted for if the members are important in carrying loads during orbital operations.

Material Selection. Materials we reviewed for application to integrated wall design are listed in figure 8.1-2. The materials were assessed on advantages and disadvantages in their use and performance. Considerations included relative weight, fabrication cost, and demonstrated resistance to penetration. Resin matrix composites are susceptible to atomic oxygen (AO) erosion and will require development of durable protective coatings before use in long-life spacecraft. In addition, low thermal conductivity of resin composites will preclude their use as thermal radiators.

Material	Shield	Wall	Advantages	Disadvantages
Resin Matrix Composites	√		Low weight.	*Small impact data base, shock impedance mismatch, vulnerable to atomic oxygen.*
Metal Matrix Composites	√		Low weight.	*Development time and costs, fabrication costs, small impact data base.*
Lithium Aluminum	√	√	Low weight, good shield.	*Additional development required.*
Beryllium	√		Excellent shielding properties.	*High cost, fabrication dificulties.*
Magnesium	√		Low weight.	*High cost, fabrication dificulties.*
5000 Series Aluminum		√		*Poor fracture toughness.*
Titanuim	√	√	Good strength & stiffness.	*High weight, high fabrication cost, small impact data base.*
2219-T87	√	√	Weldable, impact test data base available	
7075-T73	√		Good strength, thermally conductive.	
6061-T6	√		Weldable, impact test data base available.	
2024-T861	√		Common aerospace aluminum.	

Figure 8.1-2. Review of Potential Space Station Integrated Wall Materials.

Metal matrix composites are less sensitive to AO, but will require further development for manufacturing feasibility and lower cost. Lithium aluminum, after some preliminary tests, appears to perform well as a shield but also will require more development. Beryllium and magnesium may incur high machining costs. Titanium, while relatively stiff and strong, may be too heavy for module construction.

The aluminum alloys listed at the bottom of figure 8.1-2 are widely used in the aerospace industry. We used the BUMPER analysis to assess the relatively small differences in performance as shield materials of these alloys. BUMPER allows us to assess performance across the expected distribution of impact angles and velocities and to make station-level comparisons with one value, PNP. Only shield materials were varied. The baseline for comparison was our reference configuration materials. Performance of all other combinations of materials was compared with this baseline as shown in figure 8.1-3. This comparison shows the baseline combination of materials performs marginally better than the other materials, but these differences are within the limits of BUMPER.

Similar comparisons of backwall materials demonstrated even less material differentiation. Within the limits of our penetration analysis technique, no aluminum alloy stands out as a superior backwall material. We therefore concluded that specific material selection for integrated wall design is determined by factors other than hypervelocity penetration resistance.

Optimum Design. Designs can be optimized (within the discussed limitations) using the BUMPER analysis code and the design plots described in section 7.11.

8.2 MODULE CONFIGURATION

Dimensions. Dimensions for the reference configuration are shown in figure 1.3-1. Adjustments to these dimensions will not significantly alter the conclusions reached.

	Shield Material	Backwall Material	Percent of Baseline PNP*
Baseline →	7075-T73	2219-T87	0%
	6061-T6	2219-T87	-0.69%
	2219-T87	2219-T87	-0.20%
	2024-T861	2219-T87	-0.29%

* Probability of No Penetration

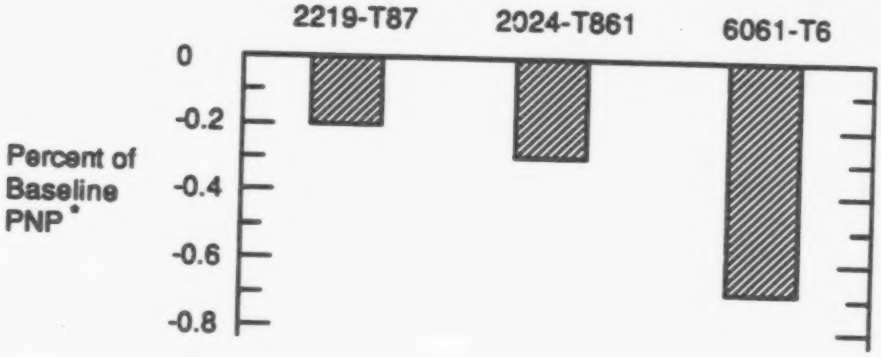

Figure 8.1-3. Shield Materials Penetration Resistance Trade Study.

End Cones/Bulkheads. Most external surfaces are subject to hypervelocity impact from meteoroids or orbital debris and will require shielding for optimum system PNP. Any subsystems (e.g., fluid tanks, lines) located against the pressure wall or end cone will serve to protect the wall in that region. On the other hand, these subsystems may in turn need shielding to achieve their own required PNP.

Internal Structure. Internal structure or subsystems will be at risk only if the pressure shell is penetrated. Internal structure arranged close to the pressure wall will absorb damage during a penetration and will limit injury to crew, but may also hinder pressure wall access. Therefore, internal structure and subsystems should provide enough clearance to permit repair of all pressure wall areas.

8.3 MODULE PATTERN

Effect of Mutual Shielding. The ability of Space Station elements to block each other from the orbital debris flux can be used to advantage when configuring the module pattern. Figure 8.3-1, created by the BUMPER code, shows how one module shields much of the surface area on another module from a specific debris threat. Only the elements shown are vulnerable to the indicated threat.

Possible Orientations. Mutual shielding affects the overall station PNP. Three orientations of the reference configuration module pattern are shown in figure 7.12-1. Each orientation exposes a different amount of surface area to the debris threat and results in different PNP by orbital debris. Because debris holds a greater threat to Space Station, the module pattern orientation chosen should minimize area exposed to the debris threat.

Relative Threat to Module Pattern Regions. The BUMPER code also reveals relative differences among regions of the module pattern in impact susceptibility. These regions occur around the module pattern perimeter as shown in figure 8.3-2. The safest areas are on the pattern interior (areas safe from debris impact) and on Earth facing sides (safe from meteoroid impact.)

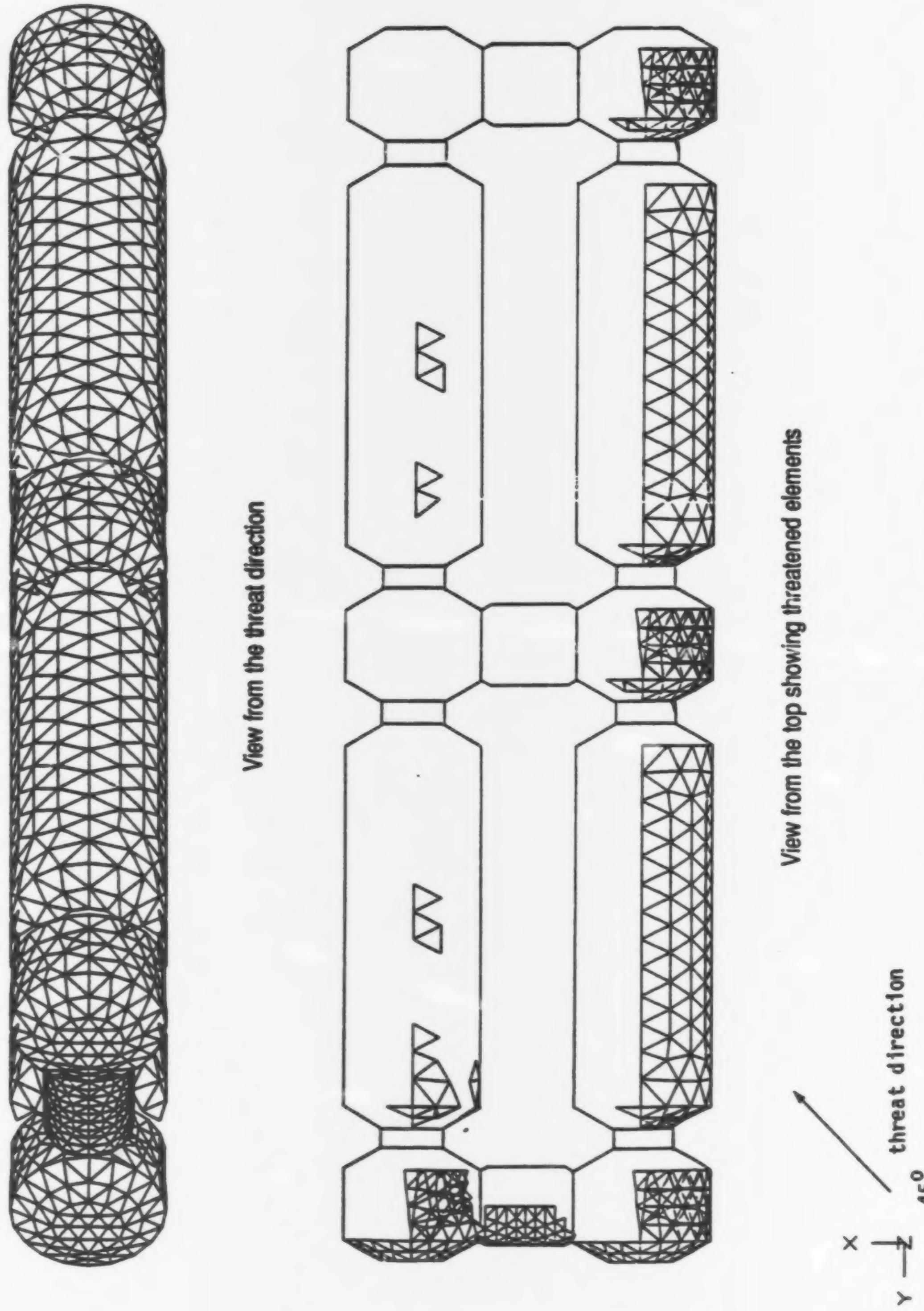

View from the threat direction

View from the top showing threatened elements

threat direction
45°
X
Y
Z

Figure 8.3-1. Self-Shielding of Space Station Module Pattern

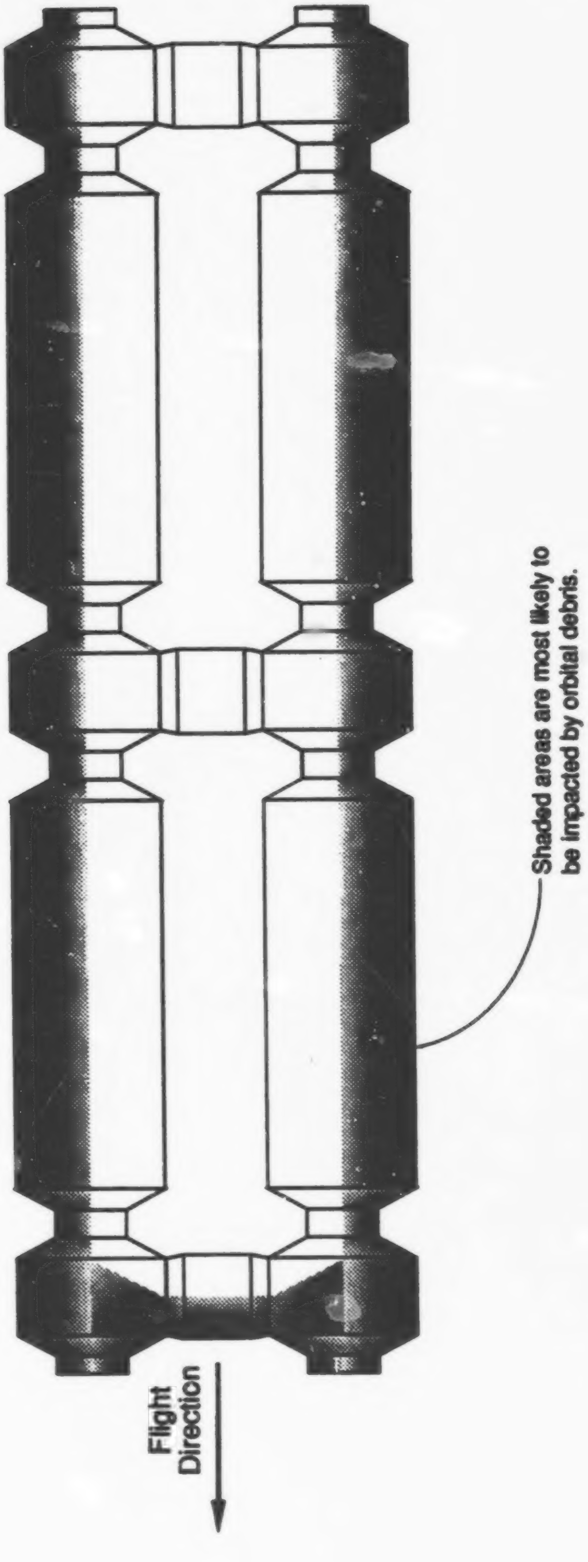

Shaded areas are most likely to be impacted by orbital debris.
Flight Direction

Figure 8.3-2. Space Station Module Pattern Vulnerable Areas.

9.0 CONCLUSIONS

This report demonstrates that we have complied with all contract objectives and requirements as directed in the contract statement of work. Compliance is shown in figure 9.0-1.

Major Results. Some of our major conclusions follow:

a. Impact incidence angles have definite effect on damage (sec. 4.1.)

b. Impact incidence angles are expected to range between 0- and 90-deg with the majority occurring above 45-deg (sec. 2.0.)

c. Optimum shield thickness depends on incidence angles. Thick shields are detrimental at angles above 65-deg (sec. 4.1.)

d. Multilayer insulation (MLI) filters out small projectile and shield fragments approaching the backwall from the shield impact, thus preventing overlapped craters and reducing backwall damage (sec. 4.1.)

e. Multiple variable linear regression can be used to uncover trends in a large test data base. Results must be used with caution, however, due to limitations in the range of test variables available (sec. 4.3.)

f. Backwall spallation is an increasing danger as velocity increases (sec. 4.4.)

g. Kevlar and dSiC/Al materials do not perform as well as aluminum in shielding the backwall (sec. 4.5.)

h. Some double shield configurations perform better than single shields (sec. 4.6.)

i. The majority of orbital debris impacts will occur at velocities above the capability of most light-gas guns (sec. 2.0.)

j. Increases in the debris flux will require test projectiles larger than currently tested.

k. Uncertainties in the debris environment translate into uncertainties in integrity of design (sec. 2.0.)

Objectives: Identify and develop an Integrated Module Wall Design and a Penetration Control Plan.
Demonstrate Technology Readiness.

Integrated Module Design - Optimum Configurations

Bumper on Standoffs - Section 4.1
Multiple Bumpers on Standoffs - Section 4.6
High Performance MLI Between Bumper and Wall - Section 4.1
Integrated Wall Design - Sections 7.0 & 8.0

Deliverable Items

Test Hardware Documentation - Appendix D
Test Hardware - provided at time of test
Test Requirements - Section 3.0
Test Reports - Section 4.0
Module Wall Design Guide - Sections 7.0 & 8.0

Penetration Control Plan

Design to Inhibit and Resist Penetration - Sections 7.0 & 8.0
Assessing the Effects of Penetration - Sections 3.0, 4.0, & 5.0
Locating and Assessing the Degree of Damage - Section 9.0
Repair Tools and Techniques - Section 6.0

Deliverable Items

Design Requirements for Penetration Control - 7.0 & 8.0
Test Hardware Documentation - Appendix D
Test Hardware - provided at time of test
Test Requirements - Section 3.0
Test Reports - Section 5.0 and Appendices E & I
Repair Procedures - Section 6.0

Figure 9.0-1. Compliance With Contract Objectives and Requirements.

l. The pressure pulse and light flash occurring upon pressure wall penetration will be harmful to crew members if they are close to and unobstructed from the impact site. Because substructure (e.g., racks, cabinets) will intervene, this threat is considered small (sec. 5.0.)

m. Rapid pressure loss following a penetration will require immediate crew evacuation of the effected module. A hole large enough to cause rapid pressure loss (of 1-in diameter and larger) has lower probability than incipient penetration upon which the PNP calculation is based (sec. 5.0.)

n. We have developed and demonstrated two viable repair techniques and associated procedures. We have also developed or identified required tools (sec. 6.0.)

o. We have developed an analysis technique to assess integrated wall designs and Space Station PNP. The analysis can also identify areas of the Space Station highly vulnerable to debris or meteoroid impact (sec. 7.0.)

p. The BUMPER code developed under this contract allows designers to optimize shield, backwall, insulation, and spacing for a given Space Station, orbit, orientation, and configuration (sec. 7.0.)

Areas for Further Study and Testing. These are areas in which we believe further testing and study are required.

a. Multiple Shields and MLI. The effectiveness of double shields and MLI has been demonstrated. Additional testing and analysis is required to quantify effectiveness as a function of thickness and standoff for multiple shields, and as a function of number of layers and standoff for MLI. Quantification is important so designs can be optimized and overall station safety assessed.

b. High Incidence Angle Impacts. Most impact data available use a 0-deg incidence angle; however, most Space Station impacts are expected to occur at angles above 45-deg, where the mechanics of multiplate impact appear to be different. The majority of future testing should use incidence angles at 45-deg and above.

c. **High Velocity Impacts.** Alternative experimental techniques or additional theoretical methods must be developed to increase confidence in impact mechanics above 8 km/s.

REFERENCES

2-1 "Orbital Debris Environment for Space Station," JSC 20001, D. J. Kessler.

2-2 "Meteoroid Environment Model 1969 [Near Earth to Lunar Surface] ," NASA SP-8013, March 1969.

2-3 "Natural Environment Design Criteria for the Space Station Program Definition Phase," NASA TM-82585, William W. Vaughan, July 1984.

2-4 "Baseline Meteoroid/Debris Damage Tolerance Probabilities," SSCBD/SSCN BB000123A, Space Station Control Board, 24 November 1986.

2-5 SPACE STATION SS-SRD-0001, Sec. 3.0, Rev. A, 12 January 1987.

2-6 "Appendix A: Natural Environment Definition for Design," JSC 30000, Sec. 3, App. A.

3-1 "Multiplate-Damage Study," AFATL-TR-67-116, G. T. Burch, The Boeing Company, September 1967.

3-2 "Meteoroid Protection for Spacecraft Structures," D2-24056, Contract NASA CR-54201, J. F. Lundeberg, P. H. Stern, and R. J. Bristow, The Boeing Company, October 1965.

3-3 "Advanced Development Program SM-1 Meteoroid - Debris Impact Shield Testing Final Report," D483-50121-1, Contract NAS8-36526, D.S. Raese, The Boeing Company, January 1987.

3-4 "A Space Debris Simulation Facility for Spacecraft Materials Evaluation," Roy A. Taylor, SAMPE Quarterly, Vol. 18, No. 2, January 1987, pp. 28-34.

4-1 "Penetrations Equations Handbook for Kinetic Energy Penetrator," 61 JTCG/ME 77-16, 1 November 1977.

4-2 BMDP Statistical Software, 1440 Sepulveda Boulevard, Los Angeles, CA 90025.

4-3 Impact Dynamics, J. A. Zukas, John Wiley & Sons, 1982, p. 221.

4-4 "Engineering Considerations in Hypervelocity Impact," J. W. Gehring Jr., High-Velocity Impact Phenomena, Chapter IX, edited by Ray Kinslow, Academic Press, 1970.

4-5 "Effects of Bumper Material Properties on the Operation of Spaced Meteoroid Shields," H. F. Swift and A. K. Hopkins, AIAA Journal of Spacecraft, Vol. 7, No. 1, January 1970.

4-6 "A Penetration Criterion for Double-Walled Structures Subject to Meteoroid Impact," J.P.D. Wilkinson, AIAA Journal, October 1969.

4-7 Results of HULL Code presented to MSFC on 29 October 1986 by Dr. Robert Becker, U.S. Army Strategic Defense Command.

4-8 "Investigation of High-Velocity Fragments Impacting Plate Arrays," NSWC TR 78-66, Naval Surface Weapons Center, Dahlgren Virginia, March 1979.

4-9 "On the Scaling of Crater Dimensions 2. Impact Processes," K. A. Holsapple and R. M. Schmidt, Journal of Geophysical Research, N87, Vol. B3, 10 March 1982.

7-1 "Meteoritic Phenomena and Meteorites," F. L. Whipple, Physics and Medicine of the Upper Atmosphere, University of New Mexico Press, 1952.

7-2 "Space Vehicle Meteoroid Shielding Design," B. G. Cour-Palais, ESA SP-153, 1979.

7-3 "PEN4 Version 7 Hypervelocity Impact Analysis," D180-29230-1, M. D. Bjorkman, J. D. Geiger, The Boeing Company, 27 February 1986.

Appendix A - Test Data Summary

The following tables contain key test data describing the hypervelocity impact testing performed for this contract. All testing was performed at the Marshall Space Flight Center hypervelocity test facility. Test program details are described in section 3.0, and results are analyzed in sections 4.0 and 5.0.

Explaination of Column Heading

Test Number - Number assigned in test matrix.
Shield Material - Material of shield.
Shield T1 (in) - Thickness of shield in inches.
Standoff (in) - Standoff between shield and backwall in inches.
MLI ? - Was 30 layers of multilayer insulation included between shield and backwall
Back Wall Matl - Material of backwall (pressure wall).
Backwall T2 (in) - Thickness of backwall in inches.
Witness. Material - Material of witness plates.
Spacing Wit. (in) - Spacing between witness sheets.
Thick Wit. (in) - Thickness of witness sheets in inches.
Proj. Matl. - Material of projectile.
Proj. Dia. (in) - Projectile diameter in inches. Cylinderical projectiles have L/D ratio of 1 to 1.
Impact Angle (deg) - Angle of impact in degrees with respect to shield.
Impact Vel. (km/sec) - Velocity of projectile at shield impact in kilometers/second.
Wall Pen.? - Was the backwall penetrated, YES or NO.
Wall Spalled? - Was the backwall spalled but not penetrated, YES, NO, or not applicable (N/A).
Crater Depth Backwall - Depth of deepest crater in backwall in inches. Equal to Back Wall T2 (in) if plate is penetrated.
Mat. Rem. Nor. (in) - Thickness of remaining backwall material in inches for normal impact component.
Mat. Rem. Flt. (in) - Thickness of remaining backwall material in inches for flight path component.
Witness Sheets Penetrated - Number of witness sheets penetrated after backwall penetration.

IMPACT TESTING DATA BASE
Specimen Configuration and Material

Test Number	Shield Material	Shield T1 (in)	Standoff (in)	MLI?	Back Wall Matl.	Back Wall T2 (in)	Witness Material	Spacing Wit. (in)	Thickness Wit. (in)
201A	6061-T6	0.040	4.00	YES	2219-T87	0.125	2024-T3	1.000	0.020
201B	6061-T6	0.040	4.00	YES	2219-T87	0.125	2024-T3	1.000	0.020
201C	6061-T6	0.040	4.00	YES	2219-T87	0.125	2024-T3	1.000	0.020
201D	6061-T6	0.040	4.00	YES	2219-T87	0.125	2024-T3	1.000	0.020
202A	6061-T6	0.040	4.00	NO	2219-T87	0.125	2024-T3	1.000	0.020
202B	6061-T6	0.040	4.00	NO	2219-T87	0.125	2024-T3	1.000	0.020
202C	6061-T6	0.040	4.00	NO	2219-T87	0.125	2024-T3	1.000	0.020
202D	6061-T6	0.040	4.00	NO	2219-T87	0.125	2024-T3	1.000	0.020
202E	6061-T6	0.040	4.00	NO	2219-T87	0.125	2024-T3	1.000	0.020
202F	6061-T6	0.040	4.00	NO	2219-T87	0.125	2024-T3	1.000	0.020
203A	6061-T6	0.040	4.00	YES	2219-T87	0.125	2024-T3	1.000	0.020
203B	6061-T6	0.040	4.00	YES	2219-T87	0.125	2024-T3	1.000	0.020
203C	6061-T6	0.040	4.00	YES	2219-T87	0.125	2024-T3	1.000	0.020
203D	6061-T6	0.040	4.00	YES	2219-T87	0.125	2024-T3	1.000	0.020
203E	6061-T6	0.040	4.00	YES	2219-T87	0.125	2024-T3	1.000	0.020
203F	6061-T6	0.040	4.00	YES	2219-T87	0.125	2024-T3	1.000	0.020
203G	6061-T6	0.040	4.00	YES	2219-T87	0.125	2024-T3	1.000	0.020
204A	6061-T6	0.040	4.00	NO	2219-T87	0.125	2024-T3	1.000	0.020
204B	6061-T6	0.040	4.00	NO	2219-T87	0.125	2024-T3	1.000	0.020
204C	6061-T6	0.040	4.00	NO	2219-T87	0.125	2024-T3	1.000	0.020
204D	6061-T6	0.040	4.00	NO	2219-T87	0.125	2024-T3	1.000	0.020
205A	6061-T6	0.063	4.00	YES	2219-T87	0.125	2024-T3	1.000	0.020
205B	6061-T6	0.063	4.00	YES	2219-T87	0.125	2024-T3	1.000	0.020
205C	6061-T6	0.063	4.00	YES	2219-T87	0.125	2024-T3	1.000	0.020
205D	6061-T6	0.063	4.00	YES	2219-T87	0.125	2024-T3	1.000	0.020
205E	6061-T6	0.063	4.00	YES	2219-T87	0.125	2024-T3	1.000	0.020
206A	6061-T6	0.063	4.00	NO	2219-T87	0.125	2024-T3	1.000	0.020
206B	6061-T6	0.063	4.00	NO	2219-T87	0.125	2024-T3	1.000	0.020
206C	6061-T6	0.063	4.00	NO	2219-T87	0.125	2024-T3	1.000	0.020
206D	6061-T6	0.063	4.00	NO	2219-T87	0.125	2024-T3	1.000	0.020
206E	6061-T6	0.063	4.00	NO	2219-T87	0.125	2024-T3	1.000	0.020
206F	6061-T6	0.063	4.00	NO	2219-T87	0.125	2024-T3	1.000	0.020
207A	6061-T6	0.063	4.00	YES	2219-T87	0.125	2024-T3	1.000	0.020
207B	6061-T6	0.063	4.00	YES	2219-T87	0.125	2024-T3	1.000	0.020
207C	6061-T6	0.063	4.00	YES	2219-T87	0.125	2024-T3	1.000	0.020
208A	6061-T6	0.063	4.00	NO	2219-T87	0.125	2024-T3	1.000	0.020
208B	6061-T6	0.063	4.00	NO	2219-T87	0.125	2024-T3	1.000	0.020
208C	6061-T6	0.063	4.00	NO	2219-T87	0.125	2024-T3	1.000	0.020
208D	6061-T6	0.063	4.00	NO	2219-T87	0.125	2024-T3	1.000	0.020
208E	6061-T6	0.063	4.00	NO	2219-T87	0.125	2024-T3	1.000	0.020

IMPACT TESTING DATA BASE
Secimen Configuration and Material

Test Number	Shield Material	Shield T1 (in)	Standoff (in)	MLI?	Back Wall Matl.	Back Wall T2 (in)	Witness Material	Spacing Wit. (in)	Thickness Wit. (in)
209A	6061-T6	0.063	4.00	YES	2219-T87	0.125	2024-T3	1.000	0.020
209B	6061-T6	0.063	4.00	YES	2219-T87	0.125	2024-T3	1.000	0.020
209D	6061-T6	0.063	4.00	YES	2219-T87	0.125	2024-T3	1.000	0.020
210B	6061-T6	0.063	4.00	YES	2219-T87	0.125	2024-T3	1.000	0.020
210D	6061-T6	0.063	4.00	YES	2219-T87	0.125	2024-T3	1.000	0.020
211B	6061-T6	0.063	4.00	YES	2219-T87	0.125	2024-T3	1.000	0.020
211D	6061-T6	0.063	4.00	YES	2219-T87	0.125	2024-T3	1.000	0.020
212B	6061-T6	0.063	4.00	YES	2219-T87	0.125	2024-T3	1.000	0.020
213A	6061-T6	0.080	4.00	NO	2219-T87	0.188	2024-T3	1.000	0.020
213B	6061-T6	0.080	4.00	NO	2219-T87	0.188	2024-T3	1.000	0.020
214A	6061-T6	0.040	8.00	NO	2219-T87	0.188	2024-T3	1.000	0.020
214B	6061-T6	0.040	8.00	NO	2219-T87	0.188	2024-T3	1.000	0.020
214C	6061-T6	0.040	8.00	NO	2219-T87	0.188	2024-T3	1.000	0.020
214D	6061-T6	0.040	8.00	NO	2219-T87	0.188	2024-T3	1.000	0.020
215A	6061-T6	0.040	8.00	YES	2219-T87	0.188	2024-T3	1.000	0.020
215B	6061-T6	0.040	8.00	YES	2219-T87	0.188	2024-T3	1.000	0.020
215C	6061-T6	0.040	8.00	YES	2219-T87	0.188	2024-T3	1.000	0.020
215D	6061-T6	0.040	8.00	YES	2219-T87	0.188	2024-T3	1.000	0.020
216A	6061-T6	0.080	4.00	NO	2219-T87	0.188	2024-T3	1.000	0.020
216B	6061-T6	0.080	4.00	NO	2219-T87	0.188	2024-T3	1.000	0.020
216C	6061-T6	0.080	4.00	NO	2219-T87	0.188	2024-T3	1.000	0.020
217A	6061-T6	0.040	8.00	NO	2219-T87	0.188	2024-T3	1.000	0.020
217B	6061-T6	0.040	8.00	NO	2219-T87	0.188	2024-T3	1.000	0.020
218A	6061-T6	0.040	8.00	YES	2219-T87	0.188	2024-T3	1.000	0.020
218B	6061-T6	0.040	8.00	YES	2219-T87	0.188	2024-T3	1.000	0.020
218C	6061-T6	0.040	8.00	YES	2219-T87	0.188	2024-T3	1.000	0.020
221A	6061-T6	0.040	4.00	YES	2219-T87	0.125	2024-T3	1.000	0.020
221B	6061-T6	0.040	4.00	YES	2219-T87	0.125	2024-T3	1.000	0.020
221C	6061-T6	0.040	4.00	YES	2219-T87	0.125	2024-T3	1.000	0.020
221D	6061-T6	0.040	4.00	YES	2219-T87	0.125	2024-T3	1.000	0.020

IMPACT TESTING DATA BASE
Specimen Configuration and Material

Test Number	Shield Material	Shield T1 (in)	Standoff (in)	MLI?	Back Wall Matl.	Back Wall T2 (in)	Witness Material	Spacing Wit. (in)	Thickness Wit. (in)
222A	6061-T6	0.040	4.00	NO	2219-T87	0.125	2024-T3	1.000	0.020
222B	6061-T6	0.040	4.00	NO	2219-T87	0.125	2024-T3	1.000	0.020
222C	6061-T6	0.040	4.00	NO	2219-T87	0.125	2024-T3	1.000	0.020
226A	6061-T6	0.032	6.00	YES	2219-T87	0.100	2024-T3	1.000	0.020
226B	6061-T6	0.032	6.00	YES	2219-T87	0.100	2024-T3	1.000	0.020
226C	6061-T6	0.032	6.00	YES	2219-T87	0.100	2024-T3	1.000	0.020
227A	6061-T6	0.032	6.00	YES	2219-T87	0.063	2024-T3	1.000	0.020
227B	6061-T6	0.032	6.00	YES	2219-T87	0.063	2024-T3	1.000	0.020
228A	6061-T6	0.032	6.00	NO	2219-T87	0.063	2024-T3	1.000	0.020
228B	6061-T6	0.032	6.00	NO	2219-T87	0.063	2024-T3	1.000	0.020
228C	6061-T6	0.032	4.00	NO	2219-T87	0.188	2024-T3	1.000	0.020
228D	6061-T6	0.032	4.00	NO	2219-T87	0.188	2024-T3	1.000	0.020
229A	6061-T6	0.080	4.00	YES	2219-T87	0.188	2024-T3	1.000	0.020
229B	6061-T6	0.080	4.00	YES	2219-T87	0.188	2024-T3	1.000	0.020
229C	6061-T6	0.080	4.00	YES	2219-T87	0.188	2024-T3	1.000	0.020
230A	6061-T6	0.063	4.00	YES	2219-T87	0.125	2024-T3	1.000	0.020
230B	6061-T6	0.063	4.00	YES	2219-T87	0.125	2024-T3	1.000	0.020
230C	6061-T6	0.063	4.00	NO	2219-T87	0.125	2024-T3	1.000	0.020
230D	6061-T6	0.063	4.00	NO	2219-T87	0.125	2024-T3	1.000	0.020
230E	6061-T6	0.063	4.00	NO	2219-T87	0.125	2024-T3	1.000	0.020
231A	6061-T6	0.063	4.000	NO	2219-T87	0.125	2024-T3	1.000	0.020
231B	6061-T6	0.063	4.000	NO	2219-T87	0.125	2024-T3	1.000	0.020
231C	6061-T6	0.063	4.000	NO	2219-T87	0.125	2024-T3	1.000	0.020
231D	6061-T6	0.063	4.000	NO	2219-T87	0.125	2024-T3	1.000	0.020

IMPACT TESTING DATA BASE
Test Parameters and Results

Test Number	Proj. Matl.	Proj. Dia. (in)	Impact Angle (deg)	Impact Vel. (km/sec)	Wall Pen. ?	Wall Spalled?	Crater Depth T2 (in)
201A	1100-AL	0.250	45.00	4.330	YES	NA	0.125
201B	1100-AL	0.250	45.00	5.510	YES	NA	0.025
201C	1100-AL	0.250	45.00	7.210	YES	NA	0.125
201D	1100-AL	0.250	45.00	7.690	YES	NA	0.006
202A	1100-AL	0.187	45.00	3.530	YES	NA	0.125
202B	1100-AL	0.187	45.00	4.300	YES	NA	0.125
202C	1100-AL	0.187	45.00	5.260	YES	NA	0.006
202D	1100-AL	0.187	45.00	6.500	YES	NA	0.125
202E	1100-AL	0.187	45.00	7.190	YES	NA	0.125
202F	1100-AL	0.187	45.00	7.510	YES	NA	0.125
203A	1100-AL	0.300	65.00	6.450	NO	NO	0.042
203B	1100-AL	0.300	65.00	3.670	NO	NO	0.049
203C	1100-AL	0.300	65.00	2.720	NO	NO	0.020
203D	1100-AL	0.300	65.00	5.590	NO	NO	0.037
203E	1100-AL	0.300	65.00	6.750	NO	NO	0.064
203F	1100-AL	0.350	65.00	3.040	NO	NO	0.090
203G	1100-AL	0.350	65.00	4.700	YES	NA	0.125
204A	1100-AL	0.250	65.00	4.810	YES	NA	0.125
204B	1100-AL	0.250	65.00	5.870	NO	NO	0.102
204C	1100-AL	0.250	65.00	4.300	NO	NO	0.052
204D	1100-AL	0.250	65.00	3.180	NO	NO	0.055
205A	1100-AL	0.250	45.00	4.200	YES	NA	0.125
205B	1100-AL	0.250	45.00	4.620	YES	NA	0.125
205C	1100-AL	0.250	45.00	5.300	YES	NA	0.125
205D	1100-AL	0.250	45.00	6.420	NO	NO	0.057
205E	1100-AL	0.250	45.00	3.150	YES	NA	0.125
206A	1100-AL	0.187	45.00	4.780	YES	NA	0.125
206B	1100-AL	0.187	45.00	5.090	NO	NO	0.120
206C	1100-AL	0.187	45.00	5.700	NO	NO	0.080
206D	1100-AL	0.187	45.00	3.690	NO	NO	0.090
206E	1100-AL	0.187	45.00	3.240	NO	NO	0.080
206F	1100-AL	0.187	45.00	6.240	NO	NO	0.070
207A	1100-AL	0.300	65.00	5.860	YES	NA	0.125
207B	1100-AL	0.300	65.00	6.470	YES	NA	0.125
207C	1100-AL	0.300	65.00	7.080	NO	NO	0.049
208A	1100-AL	0.250	65.00	5.040	NO	NO	0.058
208B	1100-AL	0.250	65.00	4.380	YES	NA	0.125
208C	1100-AL	0.250	65.00	3.420	NO	NO	0.120
208D	1100-AL	0.250	65.00	5.630	YES	NA	0.125
208E	1100-AL	0.250	65.00	6.480	YES	NA	0.125

IMPACT TESTING DATA BASE
Test Parameters and Results

Test Number	Proj. Matl.	Proj. Dia. (in)	Impact Angle (deg)	Impact Vel. (km/sec)	Wall Pen. ?	Wall Spalled?	Crater Depth T2 (in)
209A	1100-AL	0.250	65.00	4.370	NO	NO	0.061
209B	1100-AL	0.250	65.00	6.400	NO	NO	0.068
209D	1100-AL	0.250	65.00	7.400	NO	NO	0.067
210B	1100-AL	0.350	65.00	5.670	YES	NA	0.125
210D	1100-AL	0.350	65.00	7.050	YES	NA	0.125
211B	1100-AL	0.350	45.00	5.880	YES	NA	0.125
211D	1100-AL	0.350	45.00	6.840	YES	NA	0.125
212B	1100-AL	0.300	45.00	6.380	YES	NA	0.031
213A	1100-AL	0.313	0.00	4.910	YES	NA	0.188
213B	1100-AL	0.313	0.00	5.900	YES	NA	0.188
214A	1100-AL	0.250	0.00	5.650	NO	YES	0.105
214B	1100-AL	0.250	15.00	5.010	YES	NA	0.188
214C	1100-AL	0.250	0.00	4.830	YES	NA	0.188
214D	1100-AL	0.250	0.00	4.850	YES	NA	0.188
215A	1100-AL	0.350	0.00	4.660	YES	NA	0.188
215B	1100-AL	0.350	0.00	5.480	YES	NA	0.188
215C	1100-AL	0.350	0.00	6.310	NO	NO	0.084
215D	1100-AL	0.350	0.00	6.160	YES	NA	0.188
216A	1100-AL	0.350	45.00	6.100	YES	NA	0.188
216B	1100-AL	0.350	45.00	6.570	YES	NA	0.188
216C	1100-AL	0.313	45.00	6.960	YES	NA	0.188
217A	1100-AL	0.313	45.00	6.650	YES	NA	0.188
217B	1100-AL	0.313	45.00	7.100	YES	NA	0.188
218A	1100-AL	0.350	45.00	5.820	YES	NA	0.188
218B	1100-AL	0.350	45.00	6.400	YES	NA	0.188
218C	1100-AL	0.350	45.00	6.880	YES	NA	0.188
221A	1100-AL	0.187	45.00	6.670	NO	NO	0.056
221B	1100-AL	0.187	45.00	5.970	NO	NO	0.041
221C	1100-AL	0.187	45.00	4.620	NO	NO	0.054
221D	1100-AL	0.187	45.00	4.140	NO	NO	0.055

IMPACT TESTING DATA BASE
Test Parameters and Results

Test Number	Proj. Matl.	Proj. Dia. (in)	Impact Angle (deg)	Impact Vel. (km/sec)	Wall Pen. ?	Wall Spalled?	Crater Depth T2 (in)
222A	1100-AL	0.125	45.00	5.600	NO	NO	0.052
222B	1100-AL	0.125	45.00	5.030	NO	NO	0.053
222C	1100-AL	0.125	45.00	3.330	NO	NO	0.046
226A	1100-AL	0.250	45.00	4.480	YES	NA	0.100
226B	1100-AL	0.250	45.00	5.490	YES	NA	0.100
226C	1100-AL	0.250	45.00	6.800	YES	NA	0.100
227A	1100-AL	0.250	45.00	5.640	YES	NA	0.063
227B	1100-AL	0.250	45.00	7.250	YES	NA	0.063
228A	1100-AL	0.313	0.00	6.050	YES	NA	0.063
228B	1100-AL	0.313	0.00	6.750	YES	NA	0.063
228C	1100-AL	0.250	0.00	6.980	YES	NA	0.188
228D	1100-AL	0.250	0.00	6.650	YES	NA	0.188
229A	1100-AL	0.313	0.00	5.300	NO	NO	0.090
229B	1100-AL	0.313	0.00	3.070	YES	NA	0.188
229C	1100-AL	0.313	0.00	3.560	YES	NA	0.188
230A	1100-AL	0.187	45.00	4.410	NO	NO	0.047
230B	1100-AL	0.187	45.00	3.240	NO	NO	0.032
230C	1100-AL	0.250	45.00	5.160	YES	NA	0.125
230D	1100-AL	0.250	45.00	5.590	YES	NA	0.125
230E	1100-AL	0.250	45.00	6.620	YES	NA	0.125
231A	1100-AL	0.187	65.000	3.380	NO	NO	
231A	1100-AL	0.187	65.000	2.490	NO	NO	
231A	1100-AL	0.313	65.000	6.590	YES	N/A	
231A	1100-AL	0.313	65.000	7.260	YES	N/A	

IMPACT TESTING DATA BASE
Test Parameters and Results

Test Number	Mat.Rem. Nor.(in)	Mat.Rem. Flt.(in)	Witness Sheets Penetrated
201A	0.096	0.000	2.50
201B	0.100	0.125	4.00
201C	0.000	0.000	0.25
201D	0.119	0.125	2.75
202A			0.00
202B			1.50
202C	0.072	0.000	2.50
202D	0.066	0.000	2.00
202E	0.094	0.000	0.00
202F	0.098	0.000	0.75
203A	0.086	0.083	0.00
203B	0.076	0.085	0.00
203C	0.105	0.115	0.00
203D	0.088	0.092	0.00
203E	0.061	0.070	0.00
203F	0.081	0.035	0.00
203G	0.078	0.000	0.25
204A	0.064	0.000	1.00
204B	0.023	0.064	0.00
204C	0.073	0.075	0.00
204D	0.070	0.101	0.00
205A	0.079	0.000	0.25
205B	0.079	0.000	0.50
205C	0.080	0.000	1.25
205D	0.099	0.068	0.00
205E	0.081	0.000	2.00
206A			1.00
206B			0.00
206C			0.00
206D			0.00
206E			0.00
206F	0.055	0.064	0.00
207A	0.058	0.000	0.25
207B	0.000	0.082	0.10
207C	0.076	0.078	0.00
208A	0.067	0.075	0.00
208B	0.000	0.078	0.50
208C			0.00
208D			0.00
208E	0.000	0.051	1.00

IMPACT TESTING DATA BASE
Test Parameters and Results

Test Number	Mat.Rem. Nor.(in)	Mat.Rem. Flt.(in)	Witness Sheets Penetrated
209A	0.064	0.110	0.00
209B	0.057	0.125	0.00
209D	0.058	0.104	0.00
210B	0.000	0.074	0.25
210D	0.000	0.125	0.50
211B	0.108	0.000	4.00
211D			4.00
212B	0.094	0.125	2.75
213A	0.000	0.000	3.25
213B	0.000	0.000	0.25
214A	0.083	0.083	0.00
214B	0.000	0.000	1.00
214C			0.00
214D			0.25
215A			3.25
215B			1.25
215C	0.104	0.104	0.00
215D	0.000	0.000	1.00
216A	0.090	0.000	5.00
216B	0.092	0.000	5.00
216C	0.102	0.000	1.80
217A	0.127	0.000	4.00
217B	0.125	0.000	4.00
218A	0.125	0.000	4.00
218B	0.125	0.000	4.00
218C	0.125	0.000	4.00
221A	0.105	0.069	0.00
221B	0.125	0.084	0.00
221C	0.094	0.071	0.00
221D	0.108	0.070	0.00

IMPACT TESTING DATA BASE
Test Parameters and Results

Test Number	Mat.Rem. Nor.(in)	Mat.Rem. Flt.(in)	Witness Sheets Penetrated
222A	0.083	0.073	0.00
222B	0.072	0.083	0.00
222C	0.107	0.079	0.00
226A			4.50
226B			4.25
226C			2.00
227A			3.25
227B			2.00
228A			4.50
228B			4.50
228C	0.000	0.000	2.00
228D	0.000	0.000	1.00
229A			0.00
229B			2.25
229C			0.25
230A	0.111	0.078	0.00
230B	0.116	0.093	0.00
230C	0.049	0.000	3.00
230D	0.000	0.000	2.50
230E	0.000	0.000	1.50
			0.000
			0.000
			0.250
			0.250

Appendix B - Test Report - Neutral Buoyancy Simulation of Pressure Wall Repair

The following report contains observations on simulated repair procedures performed in the Marshall Space Flight Center neutral buoyancy simulation facility. These repair simulations were based on the procedures described in section 6.0.

OBSERVER'S REPORT - NEUTRAL BUOYANCY REPAIR TEST
MARSHALL SPACE FLIGHT CENTER 3/27/86

This test demonstrated the tasks required for astronauts to perform a non structural repair inside a space station module while wearing pressure suits. The repair consisted of applying a patch on the internal module surface to restore the module's pressure containment ability. The test was performed in the MSFC Neutral Buoyancy Simulator (NBS) with tools and simulated space station module structure provided by Boeing and fabricated by Essex under a subcontract. Simulation astronauts were Brand Griffin and Gerald Carr. The primary tasks were 1) removing intervening subsystem racks, 2) preparing the wall surface, and 3) applying the patch. Two repairs were demonstrated, one for round hole and damage, and another for a gash.

Subsystem Rack Removal

To gain access to the pressure wall, the astronauts had to disconnect and remove racks representing subsystems, storage, or experimental equipment. The astronauts reported that there was no particular problem completing this task. However, in the pressure suits it was necessary to remove at least two 21 inch wide racks to gain useful access to the wall.

Restraining the Astronauts

Some sort of restraint is required whenever the astronauts need to apply a force. Proper restraint is important for efficient and accurate work and to reduce fatigue. Two methods of restraint were demonstrated: foot restraints and hand holds.

Foot restraints in general provide better restraint than hand holds, however they can be difficult to adjust and can restrict motion. One-foot and two-foot restraints were tried. In general, two-foot restraints provide more security and were preferred by the astronauts over one-foot restraints. However, Griffin surmised that with training and experience the one-foot restraint would be useful in circumstances where extra mobility is required.

In Carr's opinion, with adequate hand holds the repair tasks could be performed without foot restraints. This implies the need for hand holds at frequent intervals on the pressure wall (behind the racks.) During one test run, a tool caddy was attached to a hand hold which decreased the hand hold length available to the astronauts.

Repair Tools

Cleaning / Abrading Tool - The NBS version of this tool requires improvement for effective use. The angles on the work surfaces were too shallow to allow complete contact with the wall surface or to allow application of sufficient pressure during manual abrading. Carr suggested a rounded tool surface (such as a half cylinder shape) would be easier to use. Alternatively, an adjustable angle would also permit more flexibility.

In general, abrading has been judged by the simulator astronauts to be a potentially tiring activity. Carr recommended that a hand held power tool be developed to do this job. This could be an attachment for the STS hand held rotary power tool.

Alignment Template - Several problems appeared during use of the template. The self rewinding tether connecting the template to the tool caddy tended to inadvertently pull the template off the wall after it was attached. Attachment was with velcro to simulate adhesive. The template was designed for application on two patch sizes, and this introduced extra complexity. In one instance Griffin seemed to be confused by the template, and began applying marks in locations inappropriate for the patch being applied until reminded by the test director. In previous tests, the JSC astronauts did not like the template at all, and preferred to eyeball the mark locations or merely use a hand spread over the hole as the template.

Patch Handle - The patch handle designed for the NBS test could be adjusted to various angles with the patch, however it could not be adequately attached to the patch. Apparently the velcro surface area was not large enough, though high strength velcro was used. The water viscosity probably contributed to the problem. Griffin and Carr suggested using a patch handle that would not be removed after patch application, or could be cut from the patch if necessary.

The Patch - Two patches were used: a 7 inch diameter disk to cover damage with a round pattern, and an oblong patch to cover gashes. Both were fabricated from aluminum foil (approximately 6 mils thick) and used velcro rather than adhesive as the attachment method. No adhesive could be identified permitting under water application. The lack of adhesive meant that the burnishing action could only be simulated, and the astronaut could not perceive the effectiveness of the burnishing tool or the burnishing activity.

Burnisher - In this test the forward edge of the abrading / cleaning tool was used as the burnisher. This approach seemed adequate for the simulated patch using velcro in place of an adhesive. However, dry demonstrations of this patch application indicated that the burnishing pressure needed to ensure good adhesion required two hands. Two handed operation can only be done in a foot restraint. A more effective procedure to burnishing may be to use a roller or brayer.

Hammer - The hammer was apparently a good general repair tool with several potential applications. It was intended to beat down the sharp edges around the penetration before applying the patch. Although the test occurred on simulated damage, all the astronauts concluded that this concept was sound. Other uses for a hammer of the design used here are: 1) as a probe to feel the texture, sharp points, and edges of the damage near the hole, 2) as a burnisher; the curvature of the head might be just the design needed, 3) as a patch handle by attaching a velcro section to the end of the hammer handle.

Overall Conclusions

Astronaut positioning at the repair site is a more significant problem than defining the repair procedure. Most of the test time was spent removing racks and securing the astronauts in a workable position.

Another problem is tool handling. This may have been aggravated by the negative buoyancy of most tools. Attachment clips on tethers between the tools and the tool caddies cannot be removed by the suited astronauts. This should be kept in mind when planning work activity and time lines.

Griffin did not like dealing with the trash bag. Trouble may be caused by the water viscosity and because the bag was a simulation, not the actual item. However, he suggested that we not use a trash bag, but leave a small adhesive section on all release plies so they can be attached to a convenient surface. Final clean up would occur in shirt sleeves after repressurization.

Experience seems to be an important factor in working efficiency. In the opinion of some test personnel, experienced JSC astronauts could complete tasks in half the time of inexperienced test subjects. Carr said he had to relearn neutral buoyancy skills, and found himself "torquing" in incorrect directions.

Carr also suggested that designers tour the skylab mockup at MSFC to gain insight into design for weightless activity.

Martin Gibbins

Martin Gibbins

Appendix C - Data Base for Linear Regression

In addition to the test data collected under this contract, four other sources of test data were used to develop the linear regression penetration function described in section 4.0. These additional sources included other testing performed at MSFC (for the SM-1 advanced development program, and for Martin Marietta Aerospace), and programs conducted at Boeing laboratories on previous study programs (ref. 3-1 and 3-2.)

Explaination of Column Heading

Source of Data	-	ADP SM1 - Reference 3-3. BOEING - Boeing IR&D performed at NASA/MSFC. Bristow - Reference 3-2. BURCH - Reference 3-1. IWALL - Testing performed under this contract. MARTIN - Martin Marietta IR&D performed at MSFC.
Test Number	-	Number assigned in test matrix.
Shield Material	-	Material of shield.
Shield T1 (in)	-	Thickness of shield in inches.
Standoff (in)	-	Standoff between shield and backwall in inches.
MLI ?	-	Was 30 layers of multilayer insulation included between shield and backwall
Back Wall Matl	-	Material of backwall (pressure wall).
Backwall T2 (in)	-	Thickness of backwall in inches.
Proj. Matl.	-	Material of projectile.
Proj. Dia. (in)	-	Projectile diameter in inches. Cylinderical
Impact Angle (deg)	-	Angle of impact in degrees with respect to shield.
Impact Vel. (km/s)	-	Velocity of projectile at shield impact in kilometers/second.
Wall Pen.?	-	Was the backwall penetrated, YES or NO.
Wall Spalled?	-	Was the backwall spalled but not penetrated, YES, NO, or not applicable (N/A).
Crater Depth Backwall	-	Depth of deepest crater in backwall in inches. Equal to Back Wall T2 (in) if plate is penetrated.
Witness. Material	-	Material of witness plates.
Spacing Wit. (in)	-	Spacing between witness sheets.
Thick Wit. (in)	-	Thickness of witness sheets in inches. projectiles have L/D ratio of 1 to 1.
Mat. Rem. Nor. (in)	-	Thickness of remaining backwall material in inches for normal impact component.
Mat. Rem. Flt. (in)	-	Thickness of remaining backwall material in inches for flight path component.
Nn (normal)	-	Number of witness sheets penetrated by normal component after backwall penetration.
Nf (flight)	-	Number of witness sheets penetrated by flight path component after backwall penetration.
N' (largest)	-	Largest of Nn or Nf. To be used in regression.
MLI	-	1.0 if specimen has MLI, otherwise 0.0.
N(ang)	-	Number of equivalent backwalls penetrated, see Sec. 2.0. Dependent variable in regression.
T1^1/3	-	Shield thickness, inches, raised to (1/3) power.
T2	-	Backwall thickness, inches.
Log(S)/D	-	Log (base 10) of spacing in inches divided by projectile diameter in inches.
MLI*T1	-	MLI (1.0 or 0.0) times shield thickness.
Dia^1/3	-	Projectile diameter raised to (1/3) power.

V*Cos^2 - Velocity (km/sec) times square of Cosine of impact angle.

Tan - Tangent of impact angle.

N' - Number of calculated equivalent backwall plates penetrated, using regression coefficients.

Residual - Difference between N(ang) and N'.

IMPACT TESTING REGRESSION DATA BASE

Specimen Configuration and Material

Source of Data	Test Number	Shield Material	Shield T1 (in)	Standoff (in)	MLI?	Back Wall Matl.	Back Wall T2 (in)	Proj. Matl. .	Proj. Dia. (in)	Impact Angle (deg)	Impact Vel. (km/sec)
ADP SM1	12C	6061-T6	0.063	4.00	YES	2219-T87	0.125	1100-AL	0.250	0.00	4.330
ADP SM1	12D	6061-T6	0.063	4.00	YES	2219-T87	0.125	1100-AL	0.250	0.00	3.960
ADP SM1	13	6061-T6	0.063	6.00	NO	2219-T87	0.125	1100-AL	0.250	0.00	4.770
ADP SM1	13B	6061-T6	0.063	6.00	NO	2219-T87	0.125	1100-AL	0.250	0.00	6.150
ADP SM1	13C	6061-T6	0.063	6.00	NO	2219-T87	0.125	1100-AL	0.250	0.00	5.790
ADP SM1	13D	6061-T6	0.063	6.00	YES	2219-T87	0.125	1100-AL	0.250	0.00	5.980
ADP SM1	13E	6061-T6	0.063	6.00	YES	2219-T87	0.125	1100-AL	0.250	0.00	3.940
ADP SM1	14B	6061-T6	0.063	6.00	NO	2219-T87	0.125	1100-Al	0.187	0.00	3.710
ADP SM1	14C	6061-T6	0.063	6.00	YES	2219-T87	0.125	1100-Al	0.187	0.00	3.740
ADP SM1	14D	6061-T6	0.063	6.00	NO	2219-T87	0.125	1100-AL	0.187	0.00	3.260
ADP SM1	14E	6061-T6	0.063	6.00	YES	2219-T87	0.125	1100-AL	0.188	0.00	2.770
ADP SM1	14F	6061-T6	0.063	6.00	YES	2219-T87	0.125	1100-AL	0.188	0.00	2.950
ADP SM1	15	6061-T6	0.063	6.00	NO	2219-T87	0.125	1100-Al	0.125	0.00	2.850
ADP SM1	15B	6061-T6	0.063	6.00	YES	2219-T87	0.125	1100-AL	0.125	0.00	2.110
ADP SM1	15C	6061-T6	0.063	6.00	NO	2219-T87	0.125	1100-Al	0.125	0.00	3.010
ADP SM1	16	6061-T6	0.063	6.00	NO	2219-T87	0.125	6061-T6	0.300	0.00	5.140
ADP SM1	16A	6061-T6	0.063	6.00	NO	2219-T87	0.125	6061-T6	0.300	0.00	6.040
ADP SM1	16B	6061-T6	0.063	6.00	NO	2219-T87	0.125	6061-T6	0.300	0.00	6.330
ADP SM1	16C	6061-T6	0.063	6.00	NO	2219-T87	0.125	6061-T6	0.300	0.00	6.630
ADP SM1	16E	6061-T6	0.063	6.00	NO	2219-T87	0.125	6061-T6	0.300	0.00	6.780
ADP SM1	16G	6061-T6	0.063	6.00	NO	2219-T87	0.125	6061-T6	0.300	0.00	7.180
ADP SM1	16H	6061-T6	0.063	6.00	YES	2219-T87	0.125	6061-T6	0.300	0.00	7.130
ADP SM1	16J	6061-T6	0.063	6.00	YES	2219-T87	0.125	6061-T6	0.300	0.00	6.930
ADP SM1	16K	6061-T6	0.063	6.00	YES	2219-T87	0.125	6061-T6	0.300	0.00	6.730
ADP SM1	16L	6061-T6	0.063	6.00	YES	2219-T87	0.125	6061-T6	0.300	0.00	4.820
ADP SM1	16M	6061-T6	0.063	6.00	YES	2219-T87	0.125	6061-T6	0.300	0.00	3.370
ADP SM1	16N	6061-T6	0.063	6.00	YES	2219-T87	0.125	6061-T6	0.300	0.00	3.760
ADP SM1	16P	6061-T6	0.063	6.00	YES	2219-T87	0.125	6061-T6	0.300	0.00	4.230
ADP SM1	17	6061-T6	0.063	4.00	NO	2219-T87	0.125	6061-T6	0.300	0.00	7.013
ADP SM1	20C	6061-T6	0.063	6.00	NO	2219-T87	0.125	1100-AL	0.300	0.00	6.630
ADP SM1	20F	6061-T6	0.063	6.00	YES	2219-T87	0.125	1100-AL	0.300	0.00	4.960
ADP SM1	20H	6061-T6	0.063	6.00	YES	2219-T87	0.125	1100-AL	0.300	0.00	4.680
ADP SM1	21	6061-T6	0.063	4.00	NO	2219-T87	0.125	1100-AL	0.300	0.00	6.630
ADP SM1	21B	6061-T6	0.063	4.00	YES	2219-T87	0.125	1100-AL	0.300	0.00	6.890
ADP SM1	21C	6061-T6	0.063	4.00	YES	2219-T87	0.125	1100-AL	0.300	0.00	6.600
ADP SM1	21D	6061-T6	0.063	4.00	YES	2219-T87	0.125	1100-AL	0.300	0.00	5.850
ADP SM1	24C	6061-T6	0.063	6.00	NO	2219-T87	0.125	6061-T6	0.250	0.00	5.800
ADP SM1	24F	6061-T6	0.063	6.00	NO	2219-T87	0.125	6061-T6	0.250	0.00	5.880
ADP SM1	24G	6061-T6	0.063	6.00	YES	2219-T87	0.125	6061-T6	0.250	0.00	4.310
ADP SM1	25	6061-T6	0.063	6.00	NO	2219-T87	0.125	6061-T6	0.187	0.00	3.710
ADP SM1	25A	6061-T6	0.063	6.00	NO	2219-T87	0.125	6061-T6	0.187	0.00	3.270
ADP SM1	25B	6061-T6	0.063	6.00	NO	2219-T87	0.125	6061-T6	0.187	0.00	2.250
ADP SM1	25C	6061-T6	0.063	6.00	NO	2219-T87	0.125	6061-T6	0.187	0.00	2.590
ADP SM1	25D	6061-T6	0.063	6.00	YES	2219-T87	0.125	6061-T6	0.187	0.00	1.620
ADP SM1	27	6061-T6	0.063	4.00	NO	2219-T87	0.125	1100-AL	0.187	0.00	4.530
ADP SM1	27A	6061-T6	0.063	4.00	NO	2219-T87	0.125	1100-AL	0.187	0.00	3.870
ADP SM1	27B	6061-T6	0.063	4.00	NO	2219-T87	0.125	1100-AL	0.187	0.00	4.150
ADP SM1	27C	6061-T6	0.063	4.00	YES	2219-T87	0.125	1100-AL	0.187	0.00	3.680
ADP SM1	27D	6061-T6	0.063	4.00	YES	2219-T87	0.125	1100-AL	0.187	0.00	3.080
ADP SM1	27E	6061-T6	0.063	4.00	YES	2219-T87	0.125	1100-AL	0.187	0.00	2.830
ADP SM1	27F	6061-T6	0.063	4.00	YES	2219-T87	0.125	1100-AL	0.187	0.00	2.540
ADP SM1	28	6061-T6	0.063	4.00	NO	2219-T87	0.125	1100-AL	0.125	0.00	3.000
ADP SM1	33	6061-T6	0.040	4.00	NO	2219-T87	0.125	1100-AL	0.250	0.00	7.210
ADP SM1	33B	6061-T6	0.040	4.00	NO	2219-T87	0.125	1100-AL	0.250	0.00	4.850
ADP SM1	33B1	6061-T6	0.040	4.00	NO	2219-T87	0.125	1100-AL	0.250	0.00	5.260
ADP SM1	33C	6061-T6	0.040	4.00	NO	2219-T87	0.125	1100-AL	0.250	0.00	5.530
ADP SM1	34C	6061-T6	0.040	4.00	YES	2219-T87	0.100	1100-AL	0.250	0.00	5.490
ADP SM1	34C1	6061-T6	0.040	4.00	YES	2219-T87	0.100	1100-AL	0.250	0.00	4.410
ADP SM1	34C2	6061-T6	0.063	4.00	YES	2219-T87	0.100	1100-AL	0.250	0.00	5.170
ADP SM1	35	6061-T6	0.063	6.00	NO	2219-T87	0.125	1100-AL	0.350	0.00	6.690
ADP SM1	35B	6061-T6	0.063	6.00	YES	2219-T87	0.125	1100-AL	0.350	0.00	6.300
ADP SM1	35C	6061-T6	0.080	6.00	YES	2219-T87	0.125	1100-AL	0.350	0.00	5.720
BOEING	001A	6061-T6	0.080	4.00	NO	2219-T87	0.125	1100-AL	0.313	45.00	6.640
BOEING	001B	6061-T6	0.080	4.00	YES	2219-T87	0.125	1100-AL	0.313	45.00	6.560
BOEING	002A	6061-T6	0.063	4.00	NO	2219-T87	0.125	1100-AL	0.313	45.00	6.550
BOEING	002B	6061-T6	0.063	4.00	YES	2219-T87	0.125	1100-AL	0.313	45.00	6.510

IMPACT TESTING REGRESSION DATA BASE
Specimen Configuration and Material

Source of Data	Test Number	Shield Material	Shield T1 (in)	Standoff (in)	MLI?	Back Wall Matl.	Back Wall T2 (in)	Proj. Matl.	Proj. Dia. (in)	Impact Angle (deg)	Impact Vel. (km/sec)
Bristow	36	2024-T3	0.020	2.50	NO	2024-T3	0.020	Al	0.125	0.00	7.440
Bristow	37	2024-T3	0.040	2.50	NO	2024-T3	0.020	Al	0.125	0.00	7.560
Bristow	40	2024-T3	0.020	2.50	NO	2024-T3	0.020	Al	0.125	0.00	6.550
Bristow	46	2024-T3	0.020	2.50	NO	2024-T3	0.020	Al	0.250	0.00	6.000
Bristow	55	2024-T3	0.020	5.00	NO	2024-T3	0.020	Al	0.250	0.00	5.760
Bristow	56	2024-T3	0.020	5.00	NO	2024-T3	0.020	Al	0.125	0.00	7.590
Bristow	59	2024-T3	0.020	2.50	NO	2024-T3	0.020	Al	0.250	0.00	6.250
Bristow	81	2024-T3	0.020	5.00	NO	2024-T3	0.020	Al	0.125	0.00	7.590
Bristow	82	2024-T3	0.020	5.00	NO	2024-T3	0.020	Al	0.125	0.00	7.800
Bristow	83	2024-T3	0.020	2.50	NO	2024-T3	0.020	Al	0.125	0.00	7.830
Bristow	91	2024-T3	0.020	2.50	NO	2024-T3	0.020	Al	0.125	0.00	1.400
Bristow	92	2024-T3	0.020	2.50	NO	2024-T3	0.020	Al	0.125	0.00	3.140
Bristow	109	2024-T3	0.020	2.50	NO	2024-T3	0.020	Al	0.125	0.00	7.710
Bristow	110	2024-T3	0.020	7.00	NO	2024-T3	0.020	Al	0.125	0.00	7.770
Bristow	117	2024-T3	0.020	1.25	NO	2024-T3	0.010	Al	0.063	0.00	5.030
Bristow	118	2024-T3	0.020	1.25	NO	2024-T3	0.010	Al	0.063	0.00	6.160
BURCH	1675	2024-T3	0.040	3.00	NO	2024-T3	0.020	2017 AL	0.250	0.00	4.970
BURCH	1676	2024-T3	0.040	3.00	NO	2024-T3	0.020	2017 AL	0.250	0.00	5.790
BURCH	1677	2024-T3	0.040	3.00	NO	2024-T3	0.020	2017 AL	0.250	30.00	5.330
BURCH	1678	2024-T3	0.040	3.00	NO	2024-T3	0.020	2017 AL	0.250	45.00	5.090
BURCH	1679	2024-T3	0.080	3.00	NO	2024-T3	0.020	2017 AL	0.250	30.00	5.240
BURCH	1680	2024-T3	0.080	3.00	NO	2024-T3	0.020	2017 AL	0.250	45.00	5.270
BURCH	1681	2024-T3	0.160	3.00	NO	2024-T3	0.020	2017 AL	0.250	30.00	5.090
BURCH	1682	2024-T3	0.160	3.00	NO	2024-T3	0.020	2017 AL	0.250	45.00	5.360
BURCH	1684	2024-T3	0.080	3.00	NO	2024-T3	0.020	2017 AL	0.250	60.00	5.240
BURCH	1686	2024-T3	0.040	6.00	NO	2024-T3	0.020	2017 AL	0.250	30.00	5.360
BURCH	1687	2024-T3	0.040	6.00	NO	2024-T3	0.020	2017 AL	0.250	45.00	5.120
BURCH	1688	2024-T3	0.040	6.00	NO	2024-T3	0.020	2017 AL	0.250	60.00	4.630
BURCH	1689	2024-T3	0.040	9.00	NO	2024-T3	0.020	2017 AL	0.250	45.00	5.090
BURCH	1690	2024-T3	0.040	9.00	NO	2024-T3	0.020	2017 AL	0.250	60.00	4.970
BURCH	1691	2024-T3	0.040	3.00	NO	2024-T3	0.020	2017 AL	0.250	70.00	4.570
BURCH	1693	2024-T3	0.040	3.00	NO	2024-T3	0.010	2017 AL	0.125	45.00	4.480
BURCH	1694	2024-T3	0.040	3.00	NO	2024-T3	0.020	2017 AL	0.125	45.00	5.820
BURCH	1695	2024-T3	0.040	3.00	NO	2024-T3	0.040	2017 AL	0.250	45.00	5.360
BURCH	1696	2024-T3	0.040	3.00	NO	2024-T3	0.040	2017 AL	0.250	45.00	5.330
BURCH	1699	2024-T3	0.020	3.00	NO	2024-T3	0.020	2017 AL	0.250	60.00	4.050
BURCH	1702	2024-T3	0.040	3.00	NO	2024-T3	0.020	2017 AL	0.125	60.00	3.960
BURCH	1703	2024-T3	0.040	3.00	NO	2024-T3	0.010	2017 AL	0.125	60.00	4.180
BURCH	1705	2024-T3	0.020	3.00	NO	2024-T3	0.020	2017 AL	0.250	45.00	4.540
BURCH	1706	2024-T3	0.020	3.00	NO	2024-T3	0.020	2017 AL	0.250	60.00	5.490
BURCH	1707	2024-T3	0.040	3.00	NO	2024-T3	0.020	2017 AL	0.250	60.00	5.300
BURCH	1708	2024-T3	0.040	3.00	NO	2024-T3	0.020	2017 AL	0.250	45.00	5.520
BURCH	1709	2024-T3	0.040	3.00	NO	2024-T3	0.020	2017 AL	0.250	60.00	5.210
BURCH	1710	2024-T3	0.080	3.00	NO	2024-T3	0.020	2017 AL	0.250	30.00	5.120
BURCH	1711	2024-T3	0.080	3.00	NO	2024-T3	0.020	2017 AL	0.250	45.00	5.210
BURCH	1712	2024-T3	0.080	3.00	NO	2024-T3	0.020	2017 AL	0.250	60.00	5.300
BURCH	1713	2024-T3	0.160	3.00	NO	2024-T3	0.020	2017 AL	0.250	30.00	5.240
BURCH	1714	2024-T3	0.160	3.00	NO	2024-T3	0.020	2017 AL	0.250	45.00	5.360
BURCH	1716	2024-T3	0.020	2.00	NO	2024-T3	0.020	2017 AL	0.250	30.00	5.210
BURCH	1717	2024-T3	0.020	2.00	NO	2024-T3	0.020	2017 AL	0.250	45.00	5.000
BURCH	1719	2024-T3	0.020	5.00	NO	2024-T3	0.020	2017 AL	0.250	30.00	5.120
BURCH	1721	2024-T3	0.020	5.00	NO	2024-T3	0.020	2017 AL	0.250	60.00	5.460
BURCH	1725	2024-T3	0.020	1.00	NO	2024-T3	0.020	2017 AL	0.125	30.00	5.300
BURCH	1726	2024-T3	0.040	3.00	NO	2024-T3	0.040	2017 AL	0.250	30.00	5.270
BURCH	1727	2024-T3	0.040	3.00	NO	2024-T3	0.040	2017 AL	0.250	45.00	5.150
BURCH	1728	2024-T3	0.040	3.00	NO	2024-T3	0.040	2017 AL	0.250	60.00	5.300

IMPACT TESTING REGRESSION DATA BASE
Specimen Configuration and Material

Source of Data	Test Number	Shield Material	Shield T1 (in)	Standoff (in)	MLI?	Back Wall Matl.	Back Wall T2 (in)	Proj. Matl.	Proj. Dia. (in)	Impact Angle (deg)	Impact Vel. (km/sec)
IWALL	201A	6061-T6	0.040	4.00	YES	2219-T87	0.125	1100-AL	0.250	45.00	4.330
IWALL	201B	6061-T6	0.040	4.00	YES	2219-T87	0.125	1100-AL	0.250	45.00	5.510
IWALL	201C	6061-T6	0.040	4.00	YES	2219-T87	0.125	1100-AL	0.250	45.00	7.210
IWALL	201D	6061-T6	0.040	4.00	YES	2219-T87	0.125	1100-AL	0.250	45.00	7.690
IWALL	202A	6061-T6	0.040	4.00	NO	2219-T87	0.125	1100-AL	0.187	45.00	3.530
IWALL	202B	6061-T6	0.040	4.00	NO	2219-T87	0.125	1100-AL	0.187	45.00	4.300
IWALL	202C	6061-T6	0.040	4.00	NO	2219-T87	0.125	1100-AL	0.187	45.00	5.260
IWALL	202D	6061-T6	0.040	4.00	NO	2219-T87	0.125	1100-AL	0.187	45.00	6.500
IWALL	202E	6061-T6	0.040	4.00	NO	2219-T87	0.125	1100-AL	0.187	45.00	7.190
IWALL	202F	6061-T6	0.040	4.00	NO	2219-T87	0.125	1100-AL	0.187	45.00	7.510
IWALL	203A	6061-T6	0.040	4.00	YES	2219-T87	0.125	1100-AL	0.300	65.00	6.450
IWALL	203B	6061-T6	0.040	4.00	YES	2219-T87	0.125	1100-AL	0.300	65.00	3.670
IWALL	203C	6061-T6	0.040	4.00	YES	2219-T87	0.125	1100-AL	0.300	65.00	2.720
IWALL	203D	6061-T6	0.040	4.00	YES	2219-T87	0.125	1100-AL	0.300	65.00	5.590
IWALL	203E	6061-T6	0.040	4.00	YES	2219-T87	0.125	1100-AL	0.300	65.00	6.750
IWALL	203F	6061-T6	0.040	4.00	YES	2219-T87	0.125	1100-AL	0.350	65.00	3.040
IWALL	203G	6061-T6	0.040	4.00	YES	2219-T87	0.125	1100-AL	0.350	65.00	4.700
IWALL	204A	6061-T6	0.040	4.00	NO	2219-T87	0.125	1100-AL	0.250	65.00	4.810
IWALL	204B	6061-T6	0.040	4.00	NO	2219-T87	0.125	1100-AL	0.250	65.00	5.870
IWALL	204C	6061-T6	0.040	4.00	NO	2219-T87	0.125	1100-AL	0.250	65.00	4.300
IWALL	204D	6061-T6	0.040	4.00	NO	2219-T87	0.125	1100-AL	0.250	65.00	3.180
IWALL	205A	6061-T6	0.063	4.00	YES	2219-T87	0.125	1100-AL	0.250	45.00	4.200
IWALL	205B	6061-T6	0.063	4.00	YES	2219-T87	0.125	1100-AL	0.250	45.00	4.620
IWALL	205C	6061-T6	0.063	4.00	YES	2219-T87	0.125	1100-AL	0.250	45.00	5.300
IWALL	205D	6061-T6	0.063	4.00	YES	2219-T87	0.125	1100-AL	0.250	45.00	6.420
IWALL	205E	6061-T6	0.063	4.00	YES	2219-T87	0.125	1100-AL	0.250	45.00	3.150
IWALL	206A	6061-T6	0.063	4.00	NO	2219-T87	0.125	1100-AL	0.187	45.00	4.780
IWALL	206B	6061-T6	0.063	4.00	NO	2219-T87	0.125	1100-AL	0.187	45.00	5.090
IWALL	206C	6061-T6	0.063	4.00	NO	2219-T87	0.125	1100-AL	0.187	45.00	5.400
IWALL	206D	6061-T6	0.063	4.00	NO	2219-T87	0.125	1100-AL	0.187	45.00	3.690
IWALL	206E	6061-T6	0.063	4.00	NO	2219-T87	0.125	1100-AL	0.187	45.00	3.240
IWALL	206F	6061-T6	0.063	4.00	NO	2219-T87	0.125	1100-AL	0.187	45.00	6.240
IWALL	207A	6061-T6	0.063	4.00	YES	2219-T87	0.125	1100-AL	0.300	65.00	5.860
IWALL	207B	6061-T6	0.063	4.00	YES	2219-T87	0.125	1100-AL	0.300	65.00	6.470
IWALL	207C	6061-T6	0.063	4.00	YES	2219-T87	0.125	1100-AL	0.300	65.00	7.080
IWALL	208A	6061-T6	0.063	4.00	NO	2219-T87	0.125	1100-AL	0.250	65.00	5.040
IWALL	208B	6061-T6	0.063	4.00	NO	2219-T87	0.125	1100-AL	0.250	65.00	4.380
IWALL	208C	6061-T6	0.063	4.00	NO	2219-T87	0.125	1100-AL	0.250	65.00	3.420
IWALL	208D	6061-T6	0.063	4.00	NO	2219-T87	0.125	1100-AL	0.250	65.00	5.630
IWALL	208E	6061-T6	0.063	4.00	NO	2219-T87	0.125	1100-AL	0.250	65.00	6.480
IWALL	209A	6061-T6	0.063	4.00	YES	2219-T87	0.125	1100-AL	0.250	65.00	4.370
IWALL	209B	6061-T6	0.063	4.00	YES	2219-T87	0.125	1100-AL	0.250	65.00	6.400
IWALL	209D	6061-T6	0.063	4.00	YES	2219-T87	0.125	1100-AL	0.250	65.00	7.400
IWALL	210B	6061-T6	0.063	4.00	YES	2219-T87	0.125	1100-AL	0.350	65.00	5.670
IWALL	210D	6061-T6	0.063	4.00	YES	2219-T87	0.125	1100-AL	0.350	65.00	7.050
IWALL	211B	6061-T6	0.063	4.00	YES	2219-T87	0.125	1100-AL	0.350	45.00	5.880
IWALL	211D	6061-T6	0.063	4.00	YES	2219-T87	0.125	1100-AL	0.350	45.00	6.840
IWALL	212B	6061-T6	0.063	4.00	YES	2219-T87	0.125	1100-AL	0.300	45.00	6.380
IWALL	213A	6061-T6	0.080	4.00	NO	2219-T87	0.188	1100-AL	0.313	0.00	4.910
IWALL	213B	6061-T6	0.080	4.00	NO	2219-T87	0.188	1100-AL	0.313	0.00	5.900
IWALL	214A	6061-T6	0.040	8.00	NO	2219-T87	0.188	1100-AL	0.250	0.00	5.650
IWALL	214B	6061-T6	0.040	8.00	NO	2219-T87	0.188	1100-AL	0.250	15.00	5.010
IWALL	214C	6061-T6	0.040	8.00	NO	2219-T87	0.188	1100-AL	0.250	0.00	4.830
IWALL	214D	6061-T6	0.040	8.00	NO	2219-T87	0.188	1100-AL	0.250	0.00	4.850
IWALL	215A	6061-T6	0.040	8.00	YES	2219-T87	0.188	1100-AL	0.350	0.00	4.660
IWALL	215B	6061-T6	0.040	8.00	YES	2219-T87	0.188	1100-AL	0.350	0.00	5.480
IWALL	215C	6061-T6	0.040	8.00	YES	2219-T87	0.188	1100-AL	0.350	0.00	6.310
IWALL	215D	6061-T6	0.040	8.00	YES	2219-T87	0.188	1100-AL	0.350	0.00	6.160
IWALL	216A	6061-T6	0.080	4.00	NO	2219-T87	0.188	1100-AL	0.350	45.00	6.100
IWALL	216B	6061-T6	0.080	4.00	NO	2219-T87	0.188	1100-AL	0.350	45.00	6.570
IWALL	216C	6061-T6	0.080	4.00	NO	2219-T87	0.188	1100-AL	0.313	45.00	6.960
IWALL	217A	6061-T6	0.040	8.00	NO	2219-T87	0.188	1100-AL	0.313	45.00	6.650
IWALL	217B	6061-T6	0.040	8.00	NO	2219-T87	0.188	1100-AL	0.313	45.00	7.100
IWALL	218A	6061-T6	0.040	8.00	YES	2219-T87	0.188	1100-AL	0.350	45.00	5.820
IWALL	218B	6061-T6	0.040	8.00	YES	2219-T87	0.188	1100-AL	0.350	45.00	6.400

IMPACT TESTING REGRESSION DATA BASE
Specimen Configuration and Material

Source of Data	Test Number	Shield Material	Shield T1 (in)	Standoff (in)	MLI?	Back Wall Matl.	Back Wall T2 (in)	Proj. Matl.	Proj. Dia. (in)	Impact Angle (deg)	Impact Vel. (km/sec)
IWALL	218C	6061-T6	0.040	8.00	YES	2219-T87	0.188	1100-AL	0.350	45.00	6.880
IWALL	221A	6061-T6	0.040	4.00	YES	2219-T87	0.125	1100-AL	0.187	45.00	6.670
IWALL	221B	6061-T6	0.040	4.00	YES	2219-T87	0.125	1100-AL	0.187	45.00	5.970
IWALL	221C	6061-T6	0.040	4.00	YES	2219-T87	0.125	1100-AL	0.187	45.00	4.620
IWALL	221D	6061-T6	0.040	4.00	YES	2219-T87	0.125	1100-AL	0.187	45.00	4.140
IWALL	222A	6061-T6	0.040	4.00	NO	2219-T87	0.125	1100-AL	0.125	45.00	5.600
IWALL	222B	6061-T6	0.040	4.00	NO	2219-T87	0.125	1100-AL	0.125	45.00	5.030
IWALL	222C	6061-T6	0.040	4.00	NO	2219-T87	0.125	1100-AL	0.125	45.00	3.330
IWALL	226A	6061-T6	0.032	6.00	YES	2219-T87	0.100	1100-AL	0.250	45.00	4.480
IWALL	226B	6061-T6	0.032	6.00	YES	2219-T87	0.100	1100-AL	0.250	45.00	5.490
IWALL	226C	6061-T6	0.032	6.00	YES	2219-T87	0.100	1100-AL	0.250	45.00	6.800
IWALL	227A	6061-T6	0.032	6.00	YES	2219-T87	0.063	1100-AL	0.250	45.00	5.640
IWALL	227B	6061-T6	0.032	6.00	YES	2219-T87	0.063	1100-AL	0.250	45.00	7.250
IWALL	228A	6061-T6	0.032	6.00	NO	2219-T87	0.063	1100-AL	0.313	0.00	6.050
IWALL	228B	6061-T6	0.032	6.00	NO	2219-T87	0.063	1100-AL	0.313	0.00	6.750
IWALL	228C	6061-T6	0.032	4.00	NO	2219-T87	0.188	1100-AL	0.250	0.00	6.980
IWALL	228D	6061-T6	0.032	4.00	NO	2219-T87	0.188	1100-AL	0.250	0.00	6.650
IWALL	229A	6061-T6	0.080	4.00	YES	2219-T87	0.188	1100-AL	0.313	0.00	5.300
IWALL	229B	6061-T6	0.080	4.00	YES	2219-T87	0.188	1100-AL	0.313	0.00	3.070
IWALL	229C	6061-T6	0.080	4.00	YES	2219-T87	0.188	1100-AL	0.313	0.00	3.560
IWALL	230A	6061-T6	0.063	4.00	YES	2219-T87	0.125	1100-AL	0.187	45.00	4.410
IWALL	230B	6061-T6	0.063	4.00	YES	2219-T87	0.125	1100-AL	0.187	45.00	3.290
IWALL	230C	6061-T6	0.063	4.00	NO	2219-T87	0.125	1100-AL	0.250	45.00	5.160
IWALL	230D	6061-T6	0.063	4.00	NO	2219-T87	0.125	1100-AL	0.250	45.00	5.590
IWALL	230E	6061-T6	0.063	4.00	NO	2219-T87	0.125	1100-AL	0.250	45.00	6.620
MARTIN	101	6061-T6	0.080	4.00	NO	2219-T87	0.125	1100-AL	0.187	0.00	3.094
MARTIN	101A	6061-T6	0.080	4.00	NO	2219-T87	0.125	1100-AL	0.187	0.00	3.696
MARTIN	101B	6061-T6	0.080	4.00	NO	2219-T87	0.125	1100-AL	0.187	0.00	4.270
MARTIN	102	6061-T6	0.080	4.00	NO	2219-T87	0.125	1100-AL	0.300	0.00	7.200
MARTIN	102A	6061-T6	0.080	4.00	YES	2219-T87	0.125	1100-AL	0.300	0.00	5.350
MARTIN	102B	6061-T6	0.080	4.00	YES	2219-T87	0.125	1100-AL	0.300	0.00	5.960
MARTIN	102C	6061-T6	0.080	4.00	YES	2219-T87	0.125	1100-AL	0.300	0.00	4.740
MARTIN	102D	6061-T6	0.080	4.00	YES	2219-T87	0.125	1100-AL	0.300	0.00	3.830
MARTIN	105	6061-T6	0.080	4.00	NO	2219-T87	0.125	1100-AL	0.350	45.00	3.510
MARTIN	105A	6061-T6	0.080	4.00	NO	2219-T87	0.125	1100-AL	0.350	60.00	4.050
MARTIN	105B	6061-T6	0.080	4.00	NO	2219-T87	0.125	1100-AL	0.350	75.00	3.890
MARTIN	106	6061-T6	0.080	4.00	NO	2219-T87	0.125	1100-AL	0.350	45.00	6.840
MARTIN	106A	6061-T6	0.080	4.00	NO	2219-T87	0.125	1100-AL	0.375	60.00	6.660
MARTIN	106B	6061-T6	0.080	4.00	NO	2219-T87	0.125	1100-AL	0.375	75.00	6.730
MARTIN	106-1	6061-T6	0.080	4.00	NO	2219-T87	0.125	1100-AL	0.350	60.00	6.800
MARTIN	106-2	6061-T6	0.080	4.00	NO	2219-T87	0.125	1100-AL	0.350	75.00	6.650
MARTIN	107	6061-T6	0.080	4.00	NO	2219-T87	0.175	1100-AL	0.350	0.00	6.800
MARTIN	107A	6061-T6	0.080	4.00	NO	2219-T87	0.200	1100-AL	0.350	0.00	6.740
MARTIN	107B	6061-T6	0.080	4.00	NO	2219-T87	0.225	1100-AL	0.350	0.00	6.820
MARTIN	108	6061-T6	0.080	12.00	NO	2219-T87	0.125	1100-AL	0.350	0.00	6.850
MARTIN	109	6061-T6	0.080	4.00	NO	2219-T87	0.125	1100-AL	0.187	0.00	7.390
MARTIN	109A	6061-T6	0.080	4.00	NO	2219-T87	0.125	1100-AL	0.187	0.00	4.060
MARTIN	109B	6061-T6	0.080	4.00	NO	2219-T87	0.125	1100-AL	0.187	0.00	3.610
MARTIN	109C	6061-T6	0.080	4.00	NO	2219-T87	0.125	1100-AL	0.187	0.00	2.560
MARTIN	109D	6061-T6	0.080	4.00	NO	2219-T87	0.125	1100-AL	0.187	0.00	2.000
MARTIN	110	6061-T6	0.080	4.00	NO	2219-T87	0.125	6061-T6	0.300	0.00	7.130
MARTIN	113	6061-T6	0.063	4.00	NO	2219-T87	0.125	6061-T6	0.250	60.00	3.180
MARTIN	113A	6061-T6	0.063	4.00	NO	2219-T87	0.125	6061-T6	0.250	45.00	3.200
MARTIN	114	6061-T6	0.063	4.00	NO	2219-T87	0.125	6061-T6	0.300	60.00	3.340
MARTIN	114A	6061-T6	0.063	4.00	NO	2219-T87	0.125	6061-T6	0.300	45.00	3.510
MARTIN	121-1	6061-T6	0.080	6.00	NO	2219-T87	0.125	1100-AL	0.300	0.00	6.730
MARTIN	121-2	6061-T6	0.080	6.00	NO	2219-T87	0.125	1100-AL	0.300	0.00	6.390
MARTIN	135A	6061-T6	0.063	4.00	NO	2219-T87	0.125	1100-AL	0.250	30.00	5.930
MARTIN	135B	6061-T6	0.063	4.00	NO	2219-T87	0.125	1100-AL	0.250	30.00	7.240
MARTIN	135C	6061-T6	0.063	4.00	NO	2219-T87	0.125	1100-AL	0.250	30.00	6.760
MARTIN	135D	6061-T6	0.063	4.00	NO	2219-T87	0.125	1100-AL	0.250	30.00	6.930
MARTIN	135E	6061-T6	0.063	4.00	NO	2219-T87	0.125	1100-AL	0.250	30.00	7.310
MARTIN	136A	6061-T6	0.063	4.00	NO	2219-T87	0.125	1100-AL	0.250	55.00	6.250
MARTIN	136B	6061-T6	0.063	4.00	NO	2219-T87	0.125	1100-AL	0.250	55.00	7.300

IMPACT TESTING REGRESSION DATA BASE
Test Results

		Wall Pen. ?	Wall Spalled?	Crater Depth Backwall	Witness Material	Spacing Wit. (in)	Thick Wit. (in)	Mat.Rem. Nor.(in)	Mat.Rem. Flt.(in)	Nn (normal)	Nf (flight)	N' (largest)	MLI
ADP SM1	12C	NO	NO	0.100	2024-T3	0.500	0.020			0.000	0.000	0.000	1.000
ADP SM1	12D	NO	NO	0.120	2024-T3	0.500	0.020			0.000	0.000	0.000	1.000
ADP SM1	13	YES	NA	0.125	2024-T3	0.500	0.020			1.500	0.000	1.500	0.000
ADP SM1	13B	NO	YES	0.020	2024-T3	0.500	0.020			0.250	0.000	0.250	0.000
ADP SM1	13C	YES	NA	0.125	2024-T3	0.500	0.020			2.000	0.000	2.000	0.000
ADP SM1	13D	NO	NO	0.010	2024-T3	0.500	0.020			0.000	0.000	0.000	1.000
ADP SM1	13E	NO	NO	0.070	2024-T3	0.500	0.020			0.000	0.000	0.000	1.000
ADP SM1	14B	NO	YES	0.060	2024-T3	0.500	0.020			0.500	0.000	0.500	0.000
ADP SM1	14C	NO	NO	0.020	2024-T3	0.500	0.020			0.000	0.000	0.000	1.000
ADP SM1	14D	YES	NA	0.125	2024-T3	0.500	0.020			0.750	0.000	0.750	0.000
ADP SM1	14E	YES	NA	0.125	2024-T3	0.500	0.020			0.500	0.000	0.500	1.000
ADP SM1	14F	NO	NO	0.060	2024-T3	0.500	0.020			0.000	0.000	0.000	1.000
ADP SM1	15	NO	NO	0.020	2024-T3	0.500	0.020			0.000	0.000	0.000	0.000
ADP SM1	15B	NO	NO	0.040	2024-T3	0.500	0.020			0.000	0.000	0.000	1.000
ADP SM1	15C	NO	NO	0.020	2024-T3	0.500	0.020			0.000	0.000	0.000	0.000
ADP SM1	16	YES	NA	0.125	2024-T3	0.500	0.020			2.500	0.000	2.500	0.000
ADP SM1	16A	YES	NA	0.125	2024-T3	0.500	0.020			2.000	0.000	2.000	0.000
ADP SM1	16B	YES	NA	0.125	2024-T3	0.500	0.020			1.500	0.000	1.500	0.000
ADP SM1	16C	YES	NA	0.125	2024-T3	0.500	0.020			1.500	0.000	1.500	0.000
ADP SM1	16E	YES	NA	0.125	2024-T3	0.500	0.020			0.500	0.000	0.500	0.000
ADP SM1	16G	NO	YES	0.120	2024-T3	0.500	0.020			0.500	0.000	0.500	0.000
ADP SM1	16H	NO	NO	0.010	2024-T3	0.500	0.020			0.000	0.000	0.000	1.000
ADP SM1	16J	NO	NO	0.010	2024-T3	0.500	0.020			0.000	0.000	0.000	1.000
ADP SM1	16K	NO	NO	0.010	2024-T3	0.500	0.020			0.000	0.000	0.000	1.000
ADP SM1	16L	NO	NO	0.070	2024-T3	0.500	0.020			0.000	0.000	0.000	1.000
ADP SM1	16M	YES	NA	0.125	2024-T3	0.500	0.020			2.000	0.000	2.000	1.000
ADP SM1	16N	YES	NA	0.125	2024-T3	0.500	0.020			3.500	0.000	3.500	1.000
ADP SM1	16P	YES	NA	0.125	2024-T3	0.500	0.020			1.500	0.000	1.500	1.000
ADP SM1	17	YES	NA	0.125	2024-T3	0.500	0.020			2.000	0.000	2.000	0.000
ADP SM1	20C	YES	NA	0.125	2024-T3	0.500	0.020			1.250	0.000	1.250	0.000
ADP SM1	20F	NO	NO	0.090	2024-T3	0.500	0.020			0.000	0.000	0.000	1.000
ADP SM1	20H	YES	NA	0.125	2024-T3	0.500	0.020			0.250	0.000	0.250	1.000
ADP SM1	21	YES	NA	0.125	2024-T3	0.500	0.020			2.250	0.000	2.250	0.000
ADP SM1	21B	NO	NO	0.010	2024-T3	0.500	0.020			0.000	0.000	0.000	1.000
ADP SM1	21C	NO	NO	0.010	2024-T3	0.500	0.020			0.000	0.000	0.000	1.000
ADP SM1	21D	YES	NA	0.125	2024-T3	0.500	0.020			1.000	0.000	1.000	1.000
ADP SM1	24C	YES	NA	0.125	2024-T3	0.500	0.020			0.250	0.000	0.250	0.000
ADP SM1	24F	YES	NA	0.125	2024-T3	0.500	0.020			0.500	0.000	0.500	0.000
ADP SM1	24G	NO	YES	0.120	2024-T3	0.500	0.020			0.000	0.000	0.000	1.000
ADP SM1	25	NO	NO	0.080	2024-T3	0.500	0.020			0.000	0.000	0.000	0.000
ADP SM1	25A	NO	NO	0.030	2024-T3	0.500	0.020			0.000	0.000	0.000	0.000
ADP SM1	25B	YES	NA	0.125	2024-T3	0.500	0.020			2.500	0.000	2.500	0.000
ADP SM1	25C	NO	NO	0.070	2024-T3	0.500	0.020			0.000	0.000	0.000	0.000
ADP SM1	25D	NO	NO	0.120	2024-T3	0.500	0.020			0.000	0.000	0.000	1.000
ADP SM1	27	NO	NO	0.020	2024-T3	0.500	0.020			0.000	0.000	0.000	0.000
ADP SM1	27A	YES	NA	0.125	2024-T3	0.500	0.020			0.500	0.000	0.500	0.000
ADP SM1	27B	YES	NA	0.125	2024-T3	0.500	0.020			0.500	0.000	0.500	0.000
ADP SM1	27C	NO	NO	0.060	2024-T3	0.500	0.020			0.000	0.000	0.000	1.000
ADP SM1	27D	NO	NO	0.030	2024-T3	0.500	0.020			0.000	0.000	0.000	1.000
ADP SM1	27E	NO	NO	0.050	2024-T3	0.500	0.020			0.000	0.000	0.000	1.000
ADP SM1	27F	NO	NO	0.120	2024-T3	0.500	0.020			0.000	0.000	0.000	1.000
ADP SM1	28	NO	NO	0.010	2024-T3	0.500	0.020			0.000	0.000	0.000	0.000
ADP SM1	33	YES	NA	0.125	2024-T3	0.500	0.020			2.100	0.000	2.100	0.000
ADP SM1	33B	YES	NA	0.125	2024-T3	0.500	0.020			1.250	0.000	1.250	0.000
ADP SM1	33B1	YES	NA	0.125	2024-T3	0.500	0.020			1.200	0.000	1.200	0.000
ADP SM1	33C	NO	NO	0.100	2024-T3	0.500	0.020			0.000	0.000	0.000	0.000
ADP SM1	34C	NO	NO	0.067	2024-T3	0.500	0.020			0.000	0.000	0.000	1.000
ADP SM1	34C1	YES	NA	0.100	2024-T3	0.500	0.020			0.250	0.000	0.250	1.000
ADP SM1	34C2	NO	NO	0.050	2024-T3	0.500	0.020			0.000	0.000	0.000	1.000
ADP SM1	35	YES	NA	0.125	2024-T3	0.500	0.020			1.000	0.000	1.000	0.000
ADP SM1	35B	NO	NO	0.050	2024-T3	0.500	0.020			0.000	0.000	0.000	1.000
ADP SM1	35C	YES	NA	0.125	2024-T3	0.500	0.020			2.000	0.000	2.000	1.000
BOEING	001A	YES	NA	0.125	2024-T3	1.000	0.020	0.000	0.000	0.000	2.300	2.300	0.000
BOEING	001B	YES	NA	0.125	2024-T3	1.000	0.020	0.079	0.000	0.000	0.300	0.300	1.000
BOEING	002A	YES	NA	0.125	2024-T3	1.000	0.020	0.062	0.000	0.000	4.500	4.500	0.000
BOEING	002B	YES	NA	0.125	2024-T3	1.000	0.020	0.113	0.000	0.000	0.300	0.300	1.000

IMPACT TESTING REGRESSION DATA BASE
Test Results

		Wall Pen. ?	Wall Spalled?	Crater Depth Backwall	Witness Material	Spacing Wit. (in)	Thick Wit. (in)	Mat.Rem. Nor.(in)	Mat.Rem. Flt.(in)	Nn (normal)	Nf (flight)	N' (largest)	MLI
Bristow	36	YES	NA	0.020	2024-T3	1.000	0.020			1.700	0.000	1.700	0.000
Bristow	37	YES	NA	0.020	2024-T3	1.000	0.020			1.100	0.000	1.100	0.000
Bristow	40	YES	NA	0.020	2024-T3	1.000	0.020			1.900	0.000	1.900	0.000
Bristow	46	YES	NA	0.020	2024-T3	1.000	0.020			4.000	0.000	4.000	0.000
Bristow	55	YES	NA	0.020	2024-T3	1.000	0.020			5.000	0.000	5.000	0.000
Bristow	56	YES	NA	0.020	2024-T3	1.000	0.020			1.100	0.000	1.100	0.000
Bristow	59	YES	NA	0.020	2024-T3	1.000	0.020			4.000	0.000	4.000	0.000
Bristow	81	YES	NA	0.020	2024-T3	1.000	0.020			2.000	0.000	2.000	0.000
Bristow	82	YES	NA	0.020	2024-T3	1.000	0.020			2.000	0.000	2.000	0.000
Bristow	83	YES	NA	0.020	2024-T3	1.000	0.020			2.000	0.000	2.000	0.000
Bristow	91	YES	NA	0.020	2024-T3	1.000	0.020			4.000	0.000	4.000	0.000
Bristow	92	YES	NA	0.020	2024-T3	1.000	0.020			3.000	0.000	3.000	0.000
Bristow	109	YES	NA	0.020	2024-T3	1.000	0.020			3.000	0.000	3.000	0.000
Bristow	110	YES	NA	0.020	2024-T3	1.000	0.020			1.000	0.000	1.000	0.000
Bristow	117	YES	NA	0.010	2024-T3	1.000	0.010			1.900	0.000	1.900	0.000
Bristow	118	YES	NA	0.010	2024-T3	1.000	0.010			2.400	0.000	2.400	0.000
BURCH	1675	YES	NA	0.020	2024-T3	1.000	0.020			4.000	4.000	4.000	0.000
BURCH	1676	YES	NA	0.020	2024-T3	1.000	0.020			3.300	3.300	3.300	0.000
BURCH	1677	YES	NA	0.020	2024-T3	1.000	0.020			3.000	4.300	4.300	0.000
BURCH	1678	YES	NA	0.020	2024-T3	1.000	0.020			2.000	4.100	4.100	0.000
BURCH	1679	YES	NA	0.020	2024-T3	1.000	0.020			2.000	3.300	3.300	0.000
BURCH	1680	YES	NA	0.020	2024-T3	1.000	0.020			3.000	3.300	3.300	0.000
BURCH	1681	YES	NA	0.020	2024-T3	1.000	0.020			3.400	3.000	3.400	0.000
BURCH	1682	YES	NA	0.020	2024-T3	1.000	0.020			4.000	3.000	4.000	0.000
BURCH	1684	YES	NA	0.020	2024-T3	1.000	0.020			4.000	3.200	4.000	0.000
BURCH	1686	YES	NA	0.020	2024-T3	1.000	0.020			2.000	3.300	3.300	0.000
BURCH	1687	YES	NA	0.020	2024-T3	1.000	0.020			2.000	4.700	4.700	0.000
BURCH	1688	YES	NA	0.020	2024-T3	1.000	0.020			3.300	4.000	4.000	0.000
BURCH	1689	YES	NA	0.020	2024-T3	1.000	0.020			2.000	5.000	5.000	0.000
BURCH	1690	YES	NA	0.020	2024-T3	1.000	0.020			2.000	4.000	4.000	0.000
BURCH	1691	YES	NA	0.020	2024-T3	1.000	0.020			3.300	3.800	3.800	0.000
BURCH	1693	YES	NA	0.010	2024-T3	1.000	0.010			3.000	4.000	4.000	0.000
BURCH	1694	YES	NA	0.020	2024-T3	1.000	0.020			1.000	3.000	3.000	0.000
BURCH	1695	YES	NA	0.040	2024-T3	1.000	0.040			1.000	3.000	3.000	0.000
BURCH	1696	YES	NA	0.040	2024-T3	1.000	0.040			1.000	3.000	3.000	0.000
BURCH	1699	YES	NA	0.020	2024-T3	1.000	0.020			2.000	5.100	5.100	0.000
BURCH	1702	YES	NA	0.020	2024-T3	1.000	0.020			2.000	2.000	2.000	0.000
BURCH	1703	YES	NA	0.010	2024-T3	1.000	0.010			3.500	3.500	3.500	0.000
BURCH	1705	YES	NA	0.020	2024-T3	1.000	0.020			1.500	5.500	5.500	0.000
BURCH	1706	YES	NA	0.020	2024-T3	1.000	0.020			2.100	3.500	3.500	0.000
BURCH	1707	YES	NA	0.020	2024-T3	1.000	0.020			1.200	3.500	3.500	0.000
BURCH	1708	YES	NA	0.020	2024-T3	1.000	0.020			2.100	4.300	4.300	0.000
BURCH	1709	YES	NA	0.020	2024-T3	1.000	0.020			2.900	3.500	3.500	0.000
BURCH	1710	YES	NA	0.020	2024-T3	1.000	0.020			2.300	3.300	3.300	0.000
BURCH	1711	YES	NA	0.020	2024-T3	1.000	0.020			2.500	3.100	3.100	0.000
BURCH	1712	YES	NA	0.020	2024-T3	1.000	0.020			3.600	3.600	3.600	0.000
BURCH	1713	YES	NA	0.020	2024-T3	1.000	0.020			3.300	3.000	3.300	0.000
BURCH	1714	YES	NA	0.020	2024-T3	1.000	0.020			3.600	2.700	3.600	0.000
BURCH	1716	YES	NA	0.020	2024-T3	1.000	0.020			4.100	5.100	5.100	0.000
BURCH	1717	YES	NA	0.020	2024-T3	1.000	0.020			1.300	6.100	6.100	0.000
BURCH	1719	YES	NA	0.020	2024-T3	1.000	0.020			1.100	4.300	4.300	0.000
BURCH	1721	YES	NA	0.020	2024-T3	1.000	0.020			2.100	3.800	3.800	0.000
BURCH	1725	YES	NA	0.020	2024-T3	1.000	0.020			1.200	3.300	3.300	0.000
BURCH	1726	YES	NA	0.040	2024-T3	1.000	0.040			1.000	4.500	4.500	0.000
BURCH	1727	YES	NA	0.040	2024-T3	1.000	0.040			1.000	4.900	4.900	0.000
BURCH	1728	YES	NA	0.040	2024-T3	1.000	0.040			2.200	3.600	3.600	0.000

IMPACT TESTING REGRESSION DATA BASE
Test Results

		Wall Pen. ?	Wall Spalled?	Crater Depth Backwall	Witness Material	Spacing Wit. (in)	Thick Wit. (in)	Mat.Rem. Nor.(in)	Mat.Rem. Flt.(in)	Nn (normal)	Nf (flight)	N' (largest)	MLI
IWALL	201A	YES	NA	0.125	2024-T3	1.000	0.020	0.096	0.000	2.500	0.000	2.500	1.000
IWALL	201B	YES	NA	0.025	2024-T3	1.000	0.020	0.100	0.125	4.000	0.000	4.000	1.000
IWALL	201C	YES	NA	0.125	2024-T3	1.000	0.020	0.000	0.000	0.250	0.000	0.250	1.000
IWALL	201D	YES	NA	0.006	2024-T3	1.000	0.020	0.119	0.125	2.750	0.000	2.750	1.000
IWALL	202A	YES	NA	0.125	2024-T3	1.000	0.020			0.000	0.000	0.000	0.000
IWALL	202B	YES	NA	0.125	2024-T3	1.000	0.020			1.500	0.000	1.500	0.000
IWALL	202C	YES	NA	0.006	2024-T3	1.000	0.020	0.072	0.000	2.500	0.000	2.500	0.000
IWALL	202D	YES	NA	0.125	2024-T3	1.000	0.020	0.066	0.000	2.000	0.000	2.000	0.000
IWALL	202E	YES	NA	0.125	2024-T3	1.000	0.020	0.094	0.000	0.000	0.000	0.000	0.000
IWALL	202F	YES	NA	0.125	2024-T3	1.000	0.020	0.098	0.000	0.750	0.000	0.750	0.000
IWALL	203A	NO	NO	0.042	2024-T3	1.000	0.020	0.086	0.083	0.000	0.000	0.000	1.000
IWALL	203B	NO	NO	0.049	2024-T3	1.000	0.020	0.076	0.085	0.000	0.000	0.000	1.000
IWALL	203C	NO	NO	0.020	2024-T3	1.000	0.020	0.105	0.115	0.000	0.000	0.000	1.000
IWALL	203D	NO	NO	0.037	2024-T3	1.000	0.020	0.088	0.092	0.000	0.000	0.000	1.000
IWALL	203E	NO	NO	0.064	2024-T3	1.000	0.020	0.061	0.070	0.000	0.000	0.000	1.000
IWALL	203F	NO	NO	0.090	2024-T3	1.000	0.020	0.081	0.035	0.000	0.000	0.000	1.000
IWALL	203G	YES	NA	0.125	2024-T3	1.000	0.020	0.078	0.000	0.250	0.000	0.250	1.000
IWALL	204A	YES	NA	0.125	2024-T3	1.000	0.020	0.064	0.000	0.000	1.000	1.000	0.000
IWALL	204B	NO	NO	0.102	2024-T3	1.000	0.020	0.023	0.064	0.000	0.000	0.000	0.000
IWALL	204C	NO	NO	0.052	2024-T3	1.000	0.020	0.073	0.075	0.000	0.000	0.000	0.000
IWALL	204D	NO	NO	0.055	2024-T3	1.000	0.020	0.070	0.101	0.000	0.000	0.000	0.000
IWALL	205A	YES	NA	0.125	2024-T3	1.000	0.020	0.079	0.000	0.250	0.000	0.250	1.000
IWALL	205B	YES	NA	0.125	2024-T3	1.000	0.020	0.079	0.000	0.500	0.000	0.500	1.000
IWALL	205C	YES	NA	0.125	2024-T3	1.000	0.020	0.080	0.000	1.250	0.000	1.250	1.000
IWALL	205D	NO	NO	0.057	2024-T3	1.000	0.020	0.099	0.068	0.000	0.000	0.000	1.000
IWALL	205E	YES	NA	0.125	2024-T3	1.000	0.020	0.081	0.000	2.000	0.000	2.000	1.000
IWALL	206A	YES	NA	0.125	2024-T3	1.000	0.020			1.000	0.000	1.000	0.000
IWALL	206B	NO	NO	0.120	2024-T3	1.000	0.020			0.000	0.000	0.000	0.000
IWALL	206C	NO	NO	0.080	2024-T3	1.000	0.020			0.000	0.000	0.000	0.000
IWALL	206D	NO	NO	0.090	2024-T3	1.000	0.020			0.000	0.000	0.000	0.000
IWALL	206E	NO	NO	0.080	2024-T3	1.000	0.020			0.000	0.000	0.000	0.000
IWALL	206F	NO	NO	0.070	2024-T3	1.000	0.020	0.055	0.064	0.000	0.000	0.000	0.000
IWALL	207A	YES	NA	0.125	2024-T3	1.000	0.020	0.058	0.000	0.250	0.000	0.250	1.000
IWALL	207B	YES	NA	0.125	2024-T3	1.000	0.020	0.000	0.082	0.100	0.000	0.100	1.000
IWALL	207C	NO	NO	0.049	2024-T3	1.000	0.020	0.076	0.078	0.000	0.000	0.000	1.000
IWALL	208A	NO	NO	0.058	2024-T3	1.000	0.020	0.067	0.075	0.000	0.000	0.000	0.000
IWALL	208B	YES	NA	0.125	2024-T3	1.000	0.020	0.000	0.078	0.500	0.000	0.500	0.000
IWALL	208C	NO	NO	0.120	2024-T3	1.000	0.020			0.000	0.000	0.000	0.000
IWALL	208D	YES	NA	0.125	2024-T3	1.000	0.020			0.000	0.000	0.000	0.000
IWALL	208E	YES	NA	0.125	2024-T3	1.000	0.020	0.000	0.051	1.000	0.000	1.000	0.000
IWALL	209A	NO	NO	0.061	2024-T3	1.000	0.020	0.064	0.110	0.000	0.000	0.000	1.000
IWALL	209B	NO	NO	0.068	2024-T3	1.000	0.020	0.057	0.125	0.000	0.000	0.000	1.000
IWALL	209D	NO	NO	0.067	2024-T3	1.000	0.020	0.058	0.104	0.000	0.000	0.000	1.000
IWALL	210B	YES	NA	0.125	2024-T3	1.000	0.020	0.000	0.074	0.250	0.000	0.250	1.000
IWALL	210D	YES	NA	0.125	2024-T3	1.000	0.020	0.000	0.125	0.500	0.000	0.500	1.000
IWALL	211B	YES	NA	0.125	2024-T3	1.000	0.020	0.108	0.000	4.000	0.000	4.000	1.000
IWALL	211D	YES	NA	0.125	2024-T3	1.000	0.020			4.000	0.000	4.000	1.000
IWALL	212B	YES	NA	0.031	2024-T3	1.000	0.020	0.094	0.125	2.750	0.000	2.750	1.000
IWALL	213A	YES	NA	0.188	2024-T3	1.000	0.020	0.000	0.000	0.000	3.250	3.250	0.000
IWALL	213B	YES	NA	0.188	2024-T3	1.000	0.020	0.000	0.000	0.000	0.250	0.250	0.000
IWALL	214A	NO	YES	0.105	2024-T3	1.000	0.020	0.083	0.083	0.000	0.000	0.000	0.000
IWALL	214B	YES	NA	0.188	2024-T3	1.000	0.020	0.000	0.000	0.000	1.000	1.000	0.000
IWALL	214C	YES	NA	0.188	2024-T3	1.000	0.020			0.000	0.000	0.000	0.000
IWALL	214D	YES	NA	0.188	2024-T3	1.000	0.020			0.000	0.250	0.250	0.000
IWALL	215A	YES	NA	0.188	2024-T3	1.000	0.020			0.000	3.250	3.250	1.000
IWALL	215B	YES	NA	0.188	2024-T3	1.000	0.020			0.000	1.250	1.250	1.000
IWALL	215C	NO	NO	0.084	2024-T3	1.000	0.020	0.104	0.104	0.000	0.000	0.000	1.000
IWALL	215D	YES	NA	0.188	2024-T3	1.000	0.020	0.000	0.000	0.000	1.000	1.000	1.000
IWALL	216A	YES	NA	0.188	2024-T3	1.000	0.020	0.090	0.000	0.000	5.000	5.000	0.000
IWALL	216B	YES	NA	0.188	2024-T3	1.000	0.020	0.092	0.000	0.000	5.000	5.000	0.000
IWALL	216C	YES	NA	0.188	2024-T3	1.000	0.020	0.102	0.000	0.000	1.800	1.800	0.000
IWALL	217A	YES	NA	0.188	2024-T3	1.000	0.020	0.127	0.000	0.000	4.000	4.000	0.000
IWALL	217B	YES	NA	0.188	2024-T3	1.000	0.020	0.125	0.000	0.000	4.000	4.000	0.000
IWALL	218A	YES	NA	0.188	2024-T3	1.000	0.020	0.125	0.000	0.000	4.000	4.000	1.000
IWALL	218B	YES	NA	0.188	2024-T3	1.000	0.020	0.125	0.000	0.000	4.000	4.000	1.000

IMPACT TESTING REGRESSION DATA BASE
Test Results

		Wall Pen. ?	Wall Spalled?	Crater Depth Backwall	Witness Material	Spacing Wit. (in)	Thick Wit. (in)	Mat.Rem. Nor.(in)	Mat.Rem. Flt.(in)	Nn (normal)	Nf (flight)	N' (largest)	MLI
IWALL	218C	YES	NA	0.188	2024-T3	1.000	0.020	0.125	0.000	0.000	4.000	4.000	1.000
IWALL	221A	NO	NO	0.056	2024-T3	1.000	0.020	0.105	0.069	0.000	0.000	0.000	1.000
IWALL	221B	NO	NO	0.041	2024-T3	1.000	0.020	0.125	0.084	0.000	0.000	0.000	1.000
IWALL	221C	NO	NO	0.054	2024-T3	1.000	0.020	0.094	0.071	0.000	0.000	0.000	1.000
IWALL	221D	NO	NO	0.055	2024-T3	1.000	0.020	0.108	0.070	0.000	0.000	0.000	1.000
IWALL	222A	NO	NO	0.052	2024-T3	1.000	0.020	0.083	0.073	0.000	0.000	0.000	0.000
IWALL	222B	NO	NO	0.053	2024-T3	1.000	0.020	0.072	0.083	0.000	0.000	0.000	0.000
IWALL	222C	NO	NO	0.046	2024-T3	1.000	0.020	0.107	0.079	0.000	0.000	0.000	0.000
IWALL	226A	YES	NA	0.100	2024-T3	1.000	0.020			0.000	4.500	4.500	1.000
IWALL	226B	YES	NA	0.100	2024-T3	1.000	0.020			0.000	4.250	4.250	1.000
IWALL	226C	YES	NA	0.100	2024-T3	1.000	0.020			0.000	2.000	2.000	1.000
IWALL	227A	YES	NA	0.063	2024-T3	1.000	0.020			0.000	3.250	3.250	1.000
IWALL	227B	YES	NA	0.063	2024-T3	1.000	0.020			0.000	2.000	2.000	1.000
IWALL	228A	YES	NA	0.063	2024-T3	1.000	0.020			4.500	0.000	4.500	0.000
IWALL	228B	YES	NA	0.063	2024-T3	1.000	0.020			4.500	0.000	4.500	0.000
IWALL	228C	YES	NA	0.188	2024-T3	1.000	0.020	0.000	0.000	2.000	0.000	2.000	0.000
IWALL	228D	YES	NA	0.188	2024-T3	1.000	0.020	0.000	0.000	1.000	0.000	1.000	0.000
IWALL	229A	NO	NO	0.090	2024-T3	1.000	0.020			0.000	0.000	0.000	1.000
IWALL	229B	YES	NA	0.188	2024-T3	1.000	0.020			2.250	0.000	2.250	1.000
IWALL	229C	YES	NA	0.188	2024-T3	1.000	0.020			0.250	0.000	0.250	1.000
IWALL	230A	NO	NO	0.047	2024-T3	1.000	0.020	0.111	0.078	0.000	0.000	0.000	1.000
IWALL	230B	NG	NO	0.032	2024-T3	1.000	0.020	0.116	0.093	0.000	0.000	0.000	1.000
IWALL	230C	YES	NA	0.125	2024-T3	1.000	0.020	0.049	0.000	0.000	3.000	3.000	0.000
IWALL	230D	YES	NA	0.125	2024-T3	1.000	0.020	0.000	0.000	0.000	2.500	2.500	0.000
IWALL	230E	YES	NA	0.125	2024-T3	1.000	0.020	0.000	0.000	0.000	1.500	1.500	0.000
MARTIN	101	YES	NA	0.125	2024-T3	0.500	0.020			2.000	0.000	2.000	0.000
MARTIN	101A	YES	NA	0.125	7075-T73	0.500	0.032			0.750	0.000	0.750	0.000
MARTIN	101B	NO	YES	0.110	7075-T73	0.500	0.032			0.000	0.000	0.000	0.000
MARTIN	102	NO	YES	0.110	7075-T73	0.500	0.032			0.500	0.000	0.500	0.000
MARTIN	102A	NO	NO	0.020	2024-T3	0.500	0.032			0.000	0.000	0.000	1.000
MARTIN	102B	NO	NO	0.010	2024-T3	0.500	0.032			0.000	0.000	0.000	1.000
MARTIN	102C	NO	NO	0.060	2024-T3	0.500	0.032			0.000	0.000	0.000	1.000
MARTIN	102D	YES	NA	0.125	2024-T3	0.500	0.032			0.000	0.000	0.000	1.000
MARTIN	105	YES	NA	0.125	2024-T3	0.500	0.020			1.000	0.000	1.000	0.000
MARTIN	105A	YES	NA	0.125	2024-T3	0.500	0.020			1.000	0.000	1.000	0.000
MARTIN	105B	YES	NA	0.125	2024-T3	0.500	0.020			1.000	0.000	1.000	0.000
MARTIN	106	YES	NA	0.125	2024-T3	0.500	0.020			3.000	0.000	3.000	0.000
MARTIN	106A	YES	NA	0.125	2024-T3	0.500	0.020			3.250	0.000	3.250	0.000
MARTIN	106B	YES	NA	0.125	2024-T3	0.500	0.020			2.000	0.000	2.000	0.000
MARTIN	106-1	YES	NA	0.125	2024-T3	0.500	0.020			0.000	1.500	1.500	0.000
MARTIN	106-2	YES	NA	0.125	2024-T3	0.500	0.020			0.000	0.000	0.000	0.000
MARTIN	107	YES	NA	0.175	2024-T3	0.500	0.020			4.000	0.000	4.000	0.000
MARTIN	107A	YES	NA	0.200	2024-T3	0.500	0.020			2.500	0.000	2.500	0.000
MARTIN	107B	YES	NA	0.225	2024-T3	0.500	0.020			0.750	0.000	0.750	0.000
MARTIN	108	YES	NA	0.125	2024-T3	0.500	0.020			0.000	0.000	0.000	0.000
MARTIN	109	NO	NO	0.050	2024-T3	0.500	0.020			0.000	0.000	0.000	0.000
MARTIN	109A	NO	NO	0.050	2024-T3	0.500	0.020			0.000	0.000	0.000	0.000
MARTIN	109B	NO	NO	0.090	2024-T3	0.500	0.020			0.000	0.000	0.000	0.000
MARTIN	109C	NO	YES	0.100	2024-T3	0.500	0.020			0.000	0.000	0.000	0.000
MARTIN	109D	NO	NO	0.080	2024-T3	0.500	0.020			0.000	0.000	0.000	0.000
MARTIN	110	YES	NA	0.125	2024-T3	0.500	0.020			1.500	0.000	1.500	0.000
MARTIN	113	NO	NO	0.040	2024-T3	0.500	0.020			0.000	0.000	0.000	0.000
MARTIN	113A	YES	NA	0.125	2024-T3	0.500	0.020			2.000	0.000	2.000	0.000
MARTIN	114	NO	NO	0.110	2024-T3	0.500	0.020			0.000	0.000	0.000	0.000
MARTIN	114A	YES	NA	0.125	2024-T3	0.500	0.020			2.000	0.000	2.000	0.000
MARTIN	121-1	YES	NA	0.125	7075-T6	1.000	0.020			0.000	0.000	0.000	0.000
MARTIN	121-2	YES	NA	0.125	7075-T6	1.000	0.020			2.100	0.000	2.100	0.000
MARTIN	135A	YES	NA	0.125	7075-T6	1.000	0.020			0.000	2.000	2.000	0.000
MARTIN	135B	YES	NA	0.125	7075-T6	1.000	0.020			0.000	0.250	0.250	0.000
MARTIN	135C	YES	NA	0.125	7075-T6	1.000	0.020			0.000	1.750	1.750	0.000
MARTIN	135D	YES	NA	0.125	7075-T6	1.000	0.020			0.000	2.250	2.250	0.000
MARTIN	135E	YES	NA	0.125	7075-T6	1.000	0.020			0.000	0.250	0.250	0.000
MARTIN	136A	YES	NA	0.125	2024-T3	1.000	0.020			0.000	1.000	1.000	0.000
MARTIN	136B	NO	YES	0.120	2024-T3	1.000	0.020			0.000	0.250	0.250	0.000

IMPACT TESTING REGRESSION DATA BASE
Regression Analysis and Results

		N(ang)	T1^1/3	T2	LOG(S)/D	MLI*T1	Dia^1/3	V*Cos^2	Tan	N'	Residual
ADP SM1	12C	0.904	0.398	0.125	2.408	0.063	0.6300	4.330	0.000	1.135	0.231
ADP SM1	12D	0.982	0.398	0.125	2.408	0.063	0.6300	3.960	0.000	1.238	0.257
ADP SM1	13	1.515	0.398	0.125	3.113	0.000	0.6300	4.770	0.000	1.724	0.209
ADP SM1	13B	0.435	0.398	0.125	3.113	0.000	0.6300	6.150	0.000	1.338	0.904
ADP SM1	13C	1.687	0.398	0.125	3.113	0.000	0.6300	5.790	0.000	1.439	-0.248
ADP SM1	13D	0.317	0.398	0.125	3.113	0.063	0.6300	5.980	0.000	0.550	0.233
ADP SM1	13E	0.768	0.398	0.125	3.113	0.063	0.6300	3.940	0.000	1.120	0.352
ADP SM1	14B	0.716	0.398	0.125	4.161	0.000	0.5718	3.710	0.000	1.241	0.525
ADP SM1	14C	0.435	0.398	0.125	4.161	0.063	0.5718	3.740	0.000	0.397	-0.037
ADP SM1	14D	1.258	0.398	0.125	4.161	0.000	0.5718	3.260	0.000	1.367	0.110
ADP SM1	14E	1.172	0.398	0.125	4.139	0.063	0.5729	2.770	0.000	0.683	-0.489
ADP SM1	14F	0.716	0.398	0.125	4.139	0.063	0.5729	2.950	0.000	0.632	-0.084
ADP SM1	15	0.435	0.398	0.125	6.225	0.000	0.5000	2.850	0.000	0.384	-0.051
ADP SM1	15B	0.596	0.398	0.125	6.225	0.063	0.5000	2.110	0.000	-0.245	-0.840
ADP SM1	15C	0.435	0.398	0.125	6.225	0.000	0.5000	3.010	0.000	0.340	-0.095
ADP SM1	16	1.858	0.398	0.125	2.594	0.000	0.6694	5.140	0.000	2.116	0.257
ADP SM1	16A	1.687	0.398	0.125	2.594	0.000	0.6694	6.040	0.000	1.864	0.178
ADP SM1	16B	1.515	0.398	0.125	2.594	0.000	0.6694	6.330	0.000	1.783	0.268
ADP SM1	16C	1.515	0.398	0.125	2.594	0.000	0.6694	6.630	0.000	1.699	0.184
ADP SM1	16E	1.172	0.398	0.125	2.594	0.000	0.6694	6.780	0.000	1.657	0.486
ADP SM1	16G	0.982	0.398	0.125	2.594	0.000	0.6694	7.180	0.000	1.546	0.564
ADP SM1	16H	0.317	0.398	0.125	2.594	0.063	0.6694	7.130	0.000	0.724	0.407
ADP SM1	16J	0.317	0.398	0.125	2.594	0.063	0.6694	6.930	0.000	0.780	0.463
ADP SM1	16K	0.317	0.398	0.125	2.594	0.063	0.6694	6.730	0.000	0.836	0.519
ADP SM1	16L	0.768	0.398	0.125	2.594	0.063	0.6694	4.820	0.000	1.370	0.601
ADP SM1	16M	1.687	0.398	0.125	2.594	0.063	0.6694	3.370	0.000	1.775	0.088
ADP SM1	16N	2.202	0.398	0.125	2.594	0.063	0.6694	3.760	0.000	1.666	-0.536
ADP SM1	16P	1.515	0.398	0.125	2.594	0.063	0.6694	4.230	0.000	1.534	0.019
ADP SM1	17	1.687	0.398	0.125	2.007	0.000	0.6694	7.013	0.000	1.695	0.008
ADP SM1	20C	1.429	0.398	0.125	2.594	0.000	0.6694	6.630	0.000	1.699	0.270
ADP SM1	20F	0.861	0.398	0.125	2.594	0.063	0.6694	4.960	0.000	1.331	0.469
ADP SM1	20H	1.086	0.398	0.125	2.594	0.063	0.6694	4.680	0.000	1.409	0.323
ADP SM1	21	1.773	0.398	0.125	2.007	0.000	0.6694	6.630	0.000	1.802	0.030
ADP SM1	21B	0.317	0.398	0.125	2.007	0.063	0.6694	6.890	0.000	0.894	0.577
ADP SM1	21C	0.317	0.398	0.125	2.007	0.063	0.6694	6.600	0.000	0.975	0.658
ADP SM1	21D	1.343	0.398	0.125	2.007	0.063	0.6694	5.850	0.000	1.185	-0.159
ADP SM1	24C	1.086	0.398	0.125	3.113	0.000	0.6300	5.800	0.000	1.436	0.350
ADP SM1	24F	1.172	0.398	0.125	3.113	0.000	0.6300	5.880	0.000	1.414	0.242
ADP SM1	24G	0.982	0.398	0.125	3.113	0.063	0.6300	4.310	0.000	1.017	0.035
ADP SM1	25	0.816	0.398	0.125	4.161	0.000	0.5718	3.710	0.000	1.241	0.425
ADP SM1	25A	0.523	0.398	0.125	4.161	0.000	0.5718	3.270	0.000	1.364	0.841
ADP SM1	25B	1.858	0.398	0.125	4.161	0.000	0.5718	2.250	0.000	1.649	-0.209
ADP SM1	25C	0.768	0.398	0.125	4.161	0.000	0.5718	2.590	0.000	1.554	0.786
ADP SM1	25D	0.982	0.398	0.125	4.161	0.063	0.5718	1.620	0.000	0.990	0.008
ADP SM1	27	0.435	0.398	0.125	3.220	0.000	0.5718	4.530	0.000	1.177	0.742
ADP SM1	27A	1.172	0.398	0.125	3.220	0.000	0.5718	3.870	0.000	1.361	0.190
ADP SM1	27B	1.172	0.398	0.125	3.220	0.000	0.5718	4.150	0.000	1.283	0.112
ADP SM1	27C	0.716	0.398	0.125	3.220	0.063	0.5718	3.680	0.000	0.579	-0.137
ADP SM1	27D	0.523	0.398	0.125	3.220	0.063	0.5718	3.080	0.000	0.747	0.224
ADP SM1	27E	0.659	0.398	0.125	3.220	0.063	0.5718	2.830	0.000	0.817	0.157
ADP SM1	27F	0.982	0.398	0.125	3.220	0.063	0.5718	2.540	0.000	0.898	-0.084
ADP SM1	28	0.317	0.398	0.125	4.816	0.000	0.5000	3.000	0.000	0.589	0.272
ADP SM1	33	1.721	0.342	0.125	2.408	0.000	0.6300	7.210	0.000	1.493	-0.228
ADP SM1	33B	1.429	0.342	0.125	2.408	0.000	0.6300	4.850	0.000	2.153	0.724
ADP SM1	33B1	1.412	0.342	0.125	2.408	0.000	0.6300	5.260	0.000	2.038	0.626
ADP SM1	33C	0.904	0.342	0.125	2.408	0.000	0.6300	5.530	0.000	1.963	1.059
ADP SM1	34C	0.834	0.342	0.100	2.408	0.040	0.6300	5.490	0.000	1.884	1.050
ADP SM1	34C1	1.098	0.342	0.100	2.408	0.040	0.6300	4.410	0.000	2.185	1.088
ADP SM1	34C2	0.730	0.398	0.100	2.408	0.063	0.6300	5.170	0.000	1.340	0.610
ADP SM1	35	1.343	0.398	0.125	2.223	0.000	0.7047	6.690	0.000	2.109	0.766
ADP SM1	35B	0.659	0.398	0.125	2.223	0.063	0.7047	6.300	0.000	1.383	0.723
ADP SM1	35C	1.687	0.431	0.125	2.223	0.080	0.7047	5.720	0.000	1.126	-0.561
BOEING	001A	1.790	0.431	0.125	1.924	0.000	0.6790	3.320	1.000	1.910	0.121
BOEING	001B	1.103	0.431	0.125	1.924	0.080	0.6790	3.280	1.000	0.860	-0.243
BOEING	002A	2.545	0.398	0.125	1.924	0.000	0.6790	3.275	1.000	2.116	-0.429
BOEING	002B	1.103	0.398	0.125	1.924	0.063	0.6790	3.255	1.000	1.286	0.183

IMPACT TESTING REGRESSION DATA BASE
Regression Analysis and Results

		N(ang)	T1^1/3	T2	LOG(S)/D	NLI*T1	Dia^1/3	V*Cos^2	Tan	N'	Residual
Bristow	36	1.700	0.271	0.020	3.184	0.000	0.5000	7.440	0.000	2.224	0.524
Bristow	37	1.100	0.342	0.020	3.184	0.000	0.5000	7.560	0.000	1.776	0.676
Bristow	40	1.900	0.271	0.020	3.184	0.000	0.5000	6.550	0.000	2.472	0.572
Bristow	46	4.000	0.271	0.020	1.592	0.000	0.6300	6.000	0.000	4.236	0.236
Bristow	55	5.000	0.271	0.020	2.796	0.000	0.6300	5.760	0.000	4.092	-0.908
Bristow	56	1.100	0.271	0.020	5.592	0.000	0.5000	7.590	0.000	1.760	0.660
Bristow	59	4.000	0.271	0.020	1.592	0.000	0.6300	6.250	0.000	4.166	0.166
Bristow	81	2.000	0.271	0.020	5.592	0.000	0.5000	7.590	0.000	1.760	-0.240
Bristow	82	2.000	0.271	0.020	5.592	0.000	0.5000	7.800	0.000	1.701	-0.299
Bristow	83	2.000	0.271	0.020	3.184	0.000	0.5000	7.830	0.000	2.115	0.115
Bristow	91	4.000	0.271	0.020	3.184	0.000	0.5000	1.400	0.000	3.911	-0.089
Bristow	92	3.000	0.271	0.020	3.184	0.000	0.5000	3.140	0.000	3.425	0.425
Bristow	109	3.000	0.271	0.020	3.184	0.000	0.5000	7.710	0.000	2.148	-0.852
Bristow	110	1.000	0.271	0.020	6.761	0.000	0.5000	7.770	0.000	1.505	0.505
Bristow	117	1.900	0.271	0.010	1.538	0.000	0.3979	5.030	0.000	2.315	0.415
Bristow	118	2.400	0.271	0.010	1.538	0.000	0.3979	6.160	0.000	2.000	-0.400
BURCH	1675	4.000	0.342	0.020	1.908	0.000	0.6300	4.970	0.000	4.054	0.054
BURCH	1676	3.300	0.342	0.020	1.908	0.000	0.6300	5.790	0.000	3.825	0.525
BURCH	1677	4.300	0.342	0.020	1.908	0.000	0.6300	3.998	0.577	3.901	-0.399
BURCH	1678	4.100	0.342	0.020	1.908	0.000	0.6300	2.545	1.000	3.996	-0.104
BURCH	1679	3.300	0.431	0.020	1.908	0.000	0.6300	3.930	0.577	3.399	0.099
BURCH	1680	3.300	0.431	0.020	1.908	0.000	0.6300	2.635	1.000	3.450	0.150
BURCH	1681	3.400	0.543	0.020	1.908	0.000	0.6300	3.818	0.577	2.773	-0.627
BURCH	1682	4.000	0.543	0.020	1.908	0.000	0.6300	2.680	1.000	2.780	-1.220
BURCH	1684	4.000	0.431	0.020	1.908	0.000	0.6300	1.310	1.732	3.282	-0.718
BURCH	1686	3.300	0.342	0.020	3.113	0.000	0.6300	4.020	0.577	3.684	0.384
BURCH	1687	4.700	0.342	0.020	3.113	0.000	0.6300	2.560	1.000	3.781	-0.919
BURCH	1688	4.000	0.342	0.020	3.113	0.000	0.6300	1.158	1.732	3.635	-0.365
BURCH	1689	5.000	0.342	0.020	3.817	0.000	0.6300	2.545	1.000	3.662	-1.338
BURCH	1690	4.000	0.342	0.020	3.817	0.000	0.6300	1.243	1.732	3.488	-0.512
BURCH	1691	3.800	0.342	0.020	1.908	0.000	0.6300	0.535	2.747	3.273	-0.527
BURCH	1693	4.000	0.342	0.010	3.817	0.000	0.5000	2.240	1.000	2.592	-1.408
BURCH	1694	3.000	0.342	0.020	3.817	0.000	0.5000	2.910	1.000	2.229	-0.771
BURCH	1695	3.000	0.342	0.040	1.908	0.000	0.6300	2.680	1.000	3.607	0.607
BURCH	1696	3.000	0.342	0.040	1.908	0.000	0.6300	2.665	1.000	3.611	0.611
BURCH	1699	5.100	0.271	0.020	1.908	0.000	0.6300	1.013	1.732	4.300	-0.800
BURCH	1702	2.000	0.342	0.020	3.817	0.000	0.5000	0.990	1.732	2.227	0.227
BURCH	1703	3.500	0.342	0.010	3.817	0.000	0.5000	1.045	1.732	2.388	-1.112
BURCH	1705	5.500	0.271	0.020	1.908	0.000	0.6300	2.270	1.000	4.487	-1.013
BURCH	1706	3.500	0.271	0.020	1.908	0.000	0.6300	1.373	1.732	4.200	0.700
BURCH	1707	3.500	0.342	0.020	1.908	0.000	0.6300	1.325	1.732	3.799	0.299
BURCH	1708	4.300	0.342	0.020	1.908	0.000	0.6300	2.760	1.000	3.936	-0.364
BURCH	1709	3.500	0.342	0.020	1.908	0.000	0.6300	1.303	1.732	3.805	0.305
BURCH	1710	3.300	0.431	0.020	1.908	0.000	0.6300	3.840	0.577	3.424	0.124
BURCH	1711	3.100	0.431	0.020	1.908	0.000	0.6300	2.605	1.000	3.458	0.358
BURCH	1712	3.600	0.431	0.020	1.908	0.000	0.6300	1.325	1.732	3.277	-0.323
BURCH	1713	3.300	0.543	0.020	1.908	0.000	0.6300	3.930	0.577	2.742	-0.558
BURCH	1714	3.600	0.543	0.020	1.908	0.000	0.6300	2.680	1.000	2.780	-0.820
BURCH	1716	5.100	0.271	0.020	1.204	0.000	0.6300	3.908	0.577	4.464	-0.636
BURCH	1717	6.100	0.271	0.020	1.204	0.000	0.6300	2.500	1.000	4.546	-1.554
BURCH	1719	4.300	0.271	0.020	2.796	0.000	0.6300	3.840	0.577	4.204	-0.096
BURCH	1721	3.800	0.271	0.020	2.796	0.000	0.6300	1.365	1.732	4.046	0.246
BURCH	1725	3.300	0.271	0.020	0.000	0.000	0.5000	3.975	0.577	3.325	0.025
BURCH	1726	4.500	0.342	0.040	1.908	0.000	0.6300	3.953	0.577	3.562	-0.938
BURCH	1727	4.900	0.342	0.040	1.908	0.000	0.6300	2.575	1.000	3.636	-1.264
BURCH	1728	3.600	0.342	0.040	1.908	0.000	0.6300	1.325	1.732	3.447	-0.153

IMPACT TESTING REGRESSION DATA BASE
Regression Analysis and Results

		N(ang)	T1^1/3	T2	LOG(S)/D	MLI*T1	Dia^1/3	V*Cos^2	Tan	N'	Residual
IWALL	201A	1.858	0.342	0.125	2.408	0.040	0.6300	2.165	1.000	1.637	-0.221
IWALL	201B	2.373	0.342	0.125	2.408	0.040	0.6300	2.755	1.000	1.472	-0.901
IWALL	201C	1.086	0.342	0.125	2.408	0.040	0.6300	3.605	1.000	1.235	0.149
IWALL	201D	1.944	0.342	0.125	2.408	0.040	0.6300	3.845	1.000	1.168	-0.776
IWALL	202A	1.000	0.342	0.125	3.220	0.000	0.5718	1.765	1.000	1.542	0.542
IWALL	202B	1.515	0.342	0.125	3.220	0.000	0.5718	2.150	1.000	1.435	-0.080
IWALL	202C	1.858	0.342	0.125	3.220	0.000	0.5718	2.630	1.000	1.300	-0.558
IWALL	202D	1.687	0.342	0.125	3.220	0.000	0.5718	3.250	1.000	1.127	-0.560
IWALL	202E	1.000	0.342	0.125	3.220	0.000	0.5718	3.595	1.000	1.031	0.031
IWALL	202F	1.258	0.342	0.125	3.220	0.000	0.5718	3.755	1.000	0.986	-0.271
IWALL	203A	0.609	0.342	0.125	2.007	0.040	0.6694	1.152	2.145	1.553	0.944
IWALL	203B	0.653	0.342	0.125	2.007	0.040	0.6694	0.655	2.145	1.692	1.038
IWALL	203C	0.435	0.342	0.125	2.007	0.040	0.6694	0.486	2.145	1.739	1.304
IWALL	203D	0.575	0.342	0.125	2.007	0.040	0.6694	0.998	2.145	1.596	1.021
IWALL	203E	0.738	0.342	0.125	2.007	0.040	0.6694	1.206	2.145	1.538	0.800
IWALL	203F	0.861	0.342	0.125	1.720	0.040	0.7047	0.543	2.145	2.135	1.274
IWALL	203G	1.086	0.342	0.125	1.720	0.040	0.7047	0.839	2.145	2.052	0.966
IWALL	204A	1.343	0.342	0.125	2.408	0.000	0.6300	0.859	2.145	1.691	0.347
IWALL	204B	0.912	0.342	0.125	2.408	0.000	0.6300	1.048	2.145	1.638	0.726
IWALL	204C	0.671	0.342	0.125	2.408	0.000	0.6300	0.768	2.145	1.716	1.045
IWALL	204D	0.689	0.342	0.125	2.408	0.000	0.6300	0.568	2.145	1.772	1.084
IWALL	205A	1.086	0.398	0.125	2.408	0.063	0.6300	2.100	1.000	1.022	-0.064
IWALL	205B	1.172	0.398	0.125	2.408	0.063	0.6300	2.310	1.000	0.964	-0.208
IWALL	205C	1.429	0.398	0.125	2.408	0.063	0.6300	2.650	1.000	0.869	-0.561
IWALL	205D	0.700	0.398	0.125	2.408	0.063	0.6300	3.210	1.000	0.712	0.012
IWALL	205E	1.687	0.398	0.125	2.408	0.063	0.6300	1.575	1.000	1.169	-0.518
IWALL	206A	1.343	0.398	0.125	3.220	0.000	0.5718	2.390	1.000	1.039	-0.304
IWALL	206B	0.982	0.398	0.125	3.220	0.000	0.5718	2.545	1.000	0.996	0.015
IWALL	206C	0.816	0.398	0.125	3.220	0.000	0.5718	2.700	1.000	0.953	0.136
IWALL	206D	0.861	0.398	0.125	3.220	0.000	0.5718	1.845	1.000	1.192	0.330
IWALL	206E	0.816	0.398	0.125	3.220	0.000	0.5718	1.620	1.000	1.255	0.438
IWALL	206F	0.768	0.398	0.125	3.220	0.000	0.5718	3.120	1.000	0.835	0.067
IWALL	207A	1.086	0.398	0.125	2.007	0.063	0.6694	1.047	2.145	0.949	-0.136
IWALL	207B	1.034	0.398	0.125	2.007	0.063	0.6694	1.156	2.145	0.919	-0.115
IWALL	207C	0.653	0.398	0.125	2.007	0.063	0.6694	1.265	2.145	0.888	0.235
IWALL	208A	0.705	0.398	0.125	2.408	0.000	0.6300	0.900	2.145	1.351	0.646
IWALL	208B	1.172	0.398	0.125	2.408	0.000	0.6300	0.782	2.145	1.384	0.212
IWALL	208C	0.982	0.398	0.125	2.408	0.000	0.6300	0.611	2.145	1.432	0.450
IWALL	208D	1.000	0.398	0.125	2.408	0.000	0.6300	1.006	2.145	1.322	0.322
IWALL	208E	1.343	0.398	0.125	2.408	0.000	0.6300	1.157	2.145	1.279	-0.064
IWALL	209A	0.722	0.398	0.125	2.408	0.063	0.6300	0.781	2.145	0.549	-0.173
IWALL	209B	0.758	0.398	0.125	2.408	0.063	0.6300	1.143	2.145	0.448	-0.310
IWALL	209D	0.753	0.398	0.125	2.408	0.063	0.6300	1.322	2.145	0.398	-0.355
IWALL	210B	1.086	0.398	0.125	1.720	0.063	0.7047	1.013	2.145	1.371	0.285
IWALL	210D	1.172	0.398	0.125	1.720	0.063	0.7047	1.259	2.145	1.302	0.130
IWALL	211B	2.373	0.398	0.125	1.720	0.063	0.7047	2.940	1.000	1.674	-0.699
IWALL	211D	2.373	0.398	0.125	1.720	0.063	0.7047	3.420	1.000	1.540	-0.834
IWALL	212B	1.944	0.398	0.125	2.007	0.063	0.6694	3.190	1.000	1.192	-0.752
IWALL	213A	1.879	0.431	0.188	1.924	0.000	0.6790	4.910	0.000	1.093	-0.786
IWALL	213B	1.068	0.431	0.188	1.924	0.000	0.6790	5.900	0.000	0.816	-0.251
IWALL	214A	0.767	0.342	0.188	3.612	0.000	0.6300	5.650	0.000	0.610	-0.157
IWALL	214B	1.271	0.342	0.188	3.612	0.000	0.6300	4.674	0.268	0.686	-0.585
IWALL	214C	1.000	0.342	0.188	3.612	0.000	0.6300	4.830	0.000	0.839	-0.161
IWALL	214D	1.068	0.342	0.188	3.612	0.000	0.6300	4.850	0.000	0.834	-0.234
IWALL	215A	1.879	0.342	0.188	2.580	0.040	0.7047	4.660	0.000	1.303	-0.577
IWALL	215B	1.338	0.342	0.188	2.580	0.040	0.7047	5.480	0.000	1.074	-0.265
IWALL	215C	0.693	0.342	0.188	2.580	0.040	0.7047	6.310	0.000	0.842	0.148
IWALL	215D	1.271	0.342	0.188	2.580	0.040	0.7047	6.160	0.000	0.884	-0.387
IWALL	216A	2.353	0.431	0.188	1.720	0.000	0.7047	3.050	1.000	1.177	-1.176
IWALL	216B	2.353	0.431	0.188	1.720	0.000	0.7047	3.285	1.000	1.111	-1.242
IWALL	216C	1.487	0.431	0.188	1.924	0.000	0.6790	3.480	1.000	0.757	-0.730
IWALL	217A	2.082	0.342	0.188	2.885	0.000	0.6790	3.325	1.000	1.153	-0.929
IWALL	217B	2.082	0.342	0.188	2.885	0.000	0.6790	3.550	1.000	1.091	-0.992
IWALL	218A	2.082	0.342	0.188	2.580	0.040	0.7047	2.910	1.000	1.056	-1.026
IWALL	218B	2.082	0.342	0.188	2.580	0.040	0.7047	3.200	1.000	0.975	-1.107

IMPACT TESTING REGRESSION DATA BASE
Regression Analysis and Results

		N(ang)	T1^1/3	T2	LOG(S)/D	MLI*T1	Dia^1/3	V*Cos^2	Tan	N'	Residual
IWALL	218C	2.082	0.342	0.188	2.580	0.040	0.7047	3.440	1.000	0.908	-1.174
IWALL	221A	0.694	0.342	0.125	3.220	0.040	0.5718	3.335	1.000	0.573	-0.121
IWALL	221B	0.602	0.342	0.125	3.220	0.040	0.5718	2.985	1.000	0.671	0.068
IWALL	221C	0.683	0.342	0.125	3.220	0.040	0.5718	2.310	1.000	0.859	0.177
IWALL	221D	0.689	0.342	0.125	3.220	0.040	0.5718	2.070	1.000	0.926	0.238
IWALL	222A	0.671	0.342	0.125	4.816	0.000	0.5000	2.800	1.000	0.237	-0.434
IWALL	222B	0.677	0.342	0.125	4.816	0.000	0.5000	2.515	1.000	0.317	-0.360
IWALL	222C	0.635	0.342	0.125	4.816	0.000	0.5000	1.665	1.000	0.554	-0.080
IWALL	226A	2.760	0.317	0.100	3.113	0.032	0.6300	2.240	1.000	2.183	-0.577
IWALL	226B	2.662	0.317	0.100	3.113	0.032	0.6300	2.745	1.000	2.042	-0.621
IWALL	226C	1.782	0.317	0.100	3.113	0.032	0.6300	3.400	1.000	1.859	0.076
IWALL	227A	2.664	0.317	0.063	3.113	0.032	0.6300	2.820	1.000	2.672	0.007
IWALL	227B	2.024	0.317	0.063	3.113	0.032	0.6300	3.625	1.000	2.447	0.423
IWALL	228A	3.304	0.317	0.063	2.486	0.000	0.6790	6.050	0.000	3.541	0.236
IWALL	228B	3.304	0.317	0.063	2.486	0.000	0.6790	6.750	0.000	3.345	0.041
IWALL	228C	1.541	0.317	0.188	2.408	0.000	0.6300	6.980	0.000	0.593	-0.948
IWALL	228D	1.271	0.317	0.188	2.408	0.000	0.6300	6.650	0.000	0.685	-0.585
IWALL	229A	0.715	0.431	0.188	1.924	0.080	0.6790	5.300	0.000	-0.077	-0.792
IWALL	229B	1.609	0.431	0.188	1.924	0.080	0.6790	3.070	0.000	0.546	-1.063
IWALL	229C	1.068	0.431	0.188	1.924	0.080	0.6790	3.560	0.000	0.409	-0.658
IWALL	230A	0.641	0.398	0.125	3.220	0.063	0.5718	2.205	1.000	0.256	-0.385
IWALL	230B	0.538	0.398	0.125	3.220	0.063	0.5718	1.620	1.000	0.419	-0.119
IWALL	230C	2.030	0.398	0.125	2.408	0.000	0.6300	2.580	1.000	1.724	-0.306
IWALL	230D	1.858	0.398	0.125	2.408	0.000	0.6300	2.795	1.000	1.664	-0.195
IWALL	230E	1.515	0.398	0.125	2.408	0.000	0.6300	3.310	1.000	1.520	0.005
MARTIN	101	1.687	0.431	0.125	3.220	0.000	0.5718	3.094	0.000	1.385	-0.302
MARTIN	101A	1.339	0.431	0.125	3.220	0.000	0.5718	3.696	0.000	1.217	-0.122
MARTIN	101B	0.944	0.431	0.125	3.220	0.000	0.5718	4.270	0.000	1.056	0.113
MARTIN	102	0.944	0.431	0.125	2.007	0.000	0.6694	7.200	0.000	1.449	0.506
MARTIN	102A	0.435	0.431	0.125	2.007	0.080	0.6694	5.350	0.000	0.905	0.471
MARTIN	102B	0.317	0.431	0.125	2.007	0.080	0.6694	5.960	0.000	0.735	0.418
MARTIN	102C	0.716	0.431	0.125	2.007	0.080	0.6694	4.740	0.000	1.076	0.360
MARTIN	102D	1.000	0.431	0.125	2.007	0.080	0.6694	3.630	0.000	1.330	0.330
MARTIN	105	1.343	0.431	0.125	1.720	0.000	0.7047	1.755	1.000	2.647	1.304
MARTIN	105A	1.343	0.431	0.125	1.720	0.000	0.7047	1.013	1.732	2.316	0.973
MARTIN	105B	1.343	0.431	0.125	1.720	0.000	0.7047	0.261	3.732	1.055	-0.288
MARTIN	106	2.030	0.431	0.125	1.720	0.000	0.7047	3.420	1.000	2.182	0.152
MARTIN	106A	2.116	0.431	0.125	1.605	0.000	0.7211	1.665	1.732	2.322	0.206
MARTIN	106B	1.687	0.431	0.125	1.605	0.000	0.7211	0.451	3.732	1.190	-0.497
MARTIN	106-1	1.515	0.431	0.125	1.720	0.000	0.7047	1.700	1.732	2.124	0.609
MARTIN	106-2	1.000	0.431	0.125	1.720	0.000	0.7047	0.445	3.732	1.003	0.003
MARTIN	107	2.129	0.431	0.175	1.720	0.000	0.7047	6.800	0.000	1.093	-1.035
MARTIN	107A	1.653	0.431	0.200	1.720	0.000	0.7047	6.740	0.000	0.670	-0.982
MARTIN	107B	1.183	0.431	0.225	1.720	0.000	0.7047	6.820	0.000	0.208	-0.975
MARTIN	108	1.000	0.431	0.125	3.083	0.000	0.7047	6.850	0.000	1.720	0.720
MARTIN	109	0.659	0.431	0.125	3.220	0.000	0.5718	7.390	0.000	0.184	-0.475
MARTIN	109A	0.659	0.431	0.125	3.220	0.000	0.5718	4.060	0.000	1.115	0.456
MARTIN	109B	0.861	0.431	0.125	3.220	0.000	0.5718	3.610	0.000	1.241	0.379
MARTIN	109C	0.904	0.431	0.125	3.220	0.000	0.5718	2.560	0.000	1.534	0.630
MARTIN	109D	0.816	0.431	0.125	3.220	0.000	0.5718	2.000	0.000	1.691	0.874
MARTIN	110	1.515	0.431	0.125	2.007	0.000	0.6694	7.130	0.000	1.469	-0.046
MARTIN	113	0.596	0.398	0.125	2.408	0.000	0.6300	0.795	1.732	1.684	1.088
MARTIN	113A	1.687	0.398	0.125	2.408	0.000	0.6300	1.600	1.000	1.998	0.311
MARTIN	114	0.944	0.398	0.125	2.007	0.000	0.6694	0.835	1.732	2.147	1.204
MARTIN	114A	1.687	0.398	0.125	2.007	0.000	0.6694	1.755	1.000	2.429	0.742
MARTIN	121-1	1.000	0.431	0.125	2.594	0.000	0.6694	6.730	0.000	1.478	0.478
MARTIN	121-2	1.721	0.431	0.125	2.594	0.000	0.6694	6.390	0.000	1.573	-0.148
MARTIN	135A	1.687	0.398	0.125	2.408	0.000	0.6300	4.448	0.577	1.513	-0.174
MARTIN	135B	1.086	0.398	0.125	2.408	0.000	0.6300	5.430	0.577	1.238	0.152
MARTIN	135C	1.601	0.398	0.125	2.408	0.000	0.6300	5.070	0.577	1.339	-0.262
MARTIN	135D	1.773	0.398	0.125	2.408	0.000	0.6300	5.198	0.577	1.303	-0.469
MARTIN	135E	1.086	0.398	0.125	2.408	0.000	0.6300	5.483	0.577	1.224	0.138
MARTIN	136A	1.343	0.398	0.125	2.408	0.000	0.6300	2.056	1.428	1.555	0.212
MARTIN	136B	0.982	0.398	0.125	2.408	0.000	0.6300	2.402	1.428	1.459	0.477

Appendix D - Test Specimen Hardware Drawings

The following drawings show the dimensions and configuration for test panels used in the task 1 and task 2 test programs. Some task 1 panels are longer to permit impact at high incidence angles. The task 2 panels were designed specifically for the mounting flange inside the large test chamber used for effects of penetration testing.

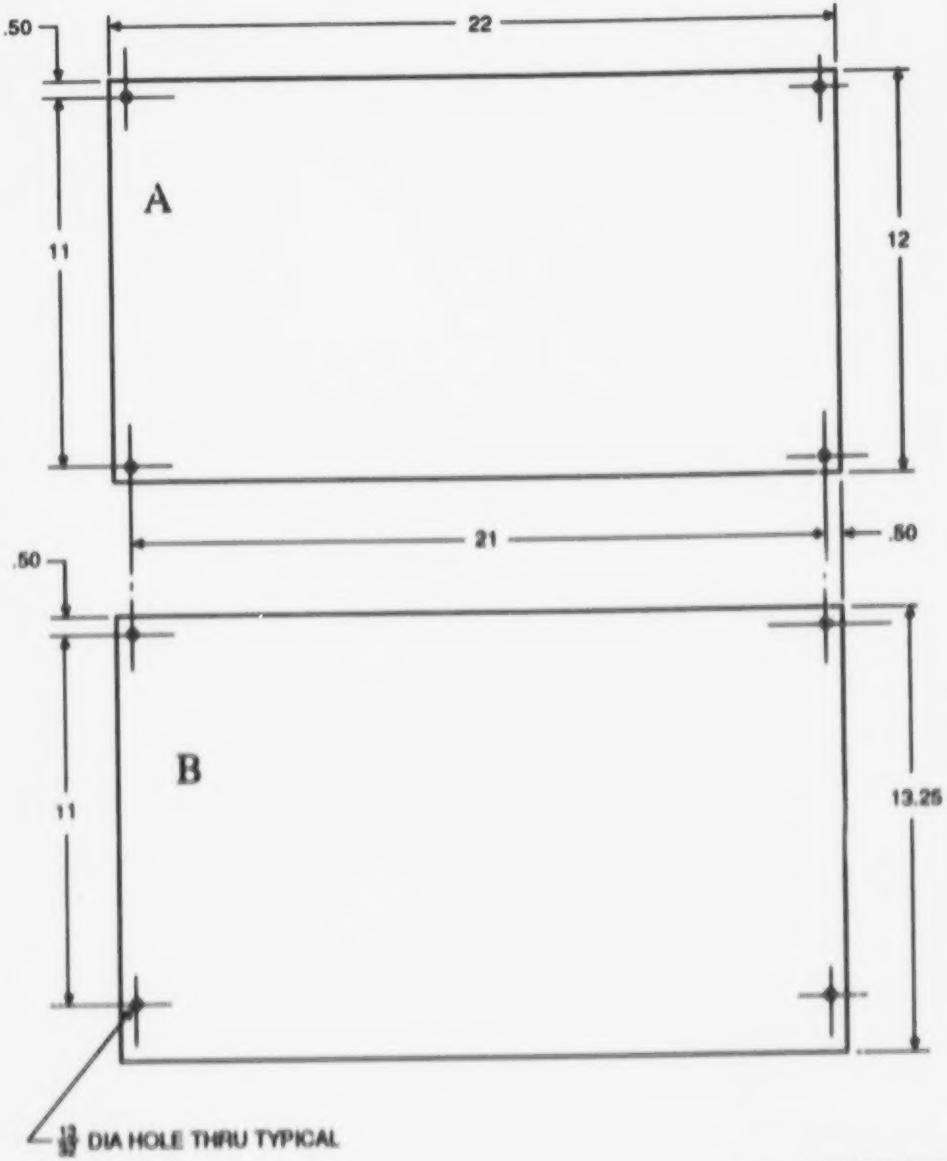
.50
22
A
11
12
21
.50
.50
B
11
13.25
13/32 DIA HOLE THRU TYPICAL

No.	Item		Thick. in.	Material	Qty.
1	Shield	A	0.040	6061-T6	
2	Shield	A	0.063	6061-T6	
3	Backwall	B	0.125	2219-T87	
4	Witness Plate	A	0.020	2024-T3	

DEBURR ALL EDGES

DIMENSIONS IN INCHES,
ALL DIMENSIONS EXCEPT
THICKNESSES ▲ .05 INCH

**Hypervelocity Impact
Test Panels - Task I**

BOEING	**NAS8-36426**
Tests 201 - 212	

C-3

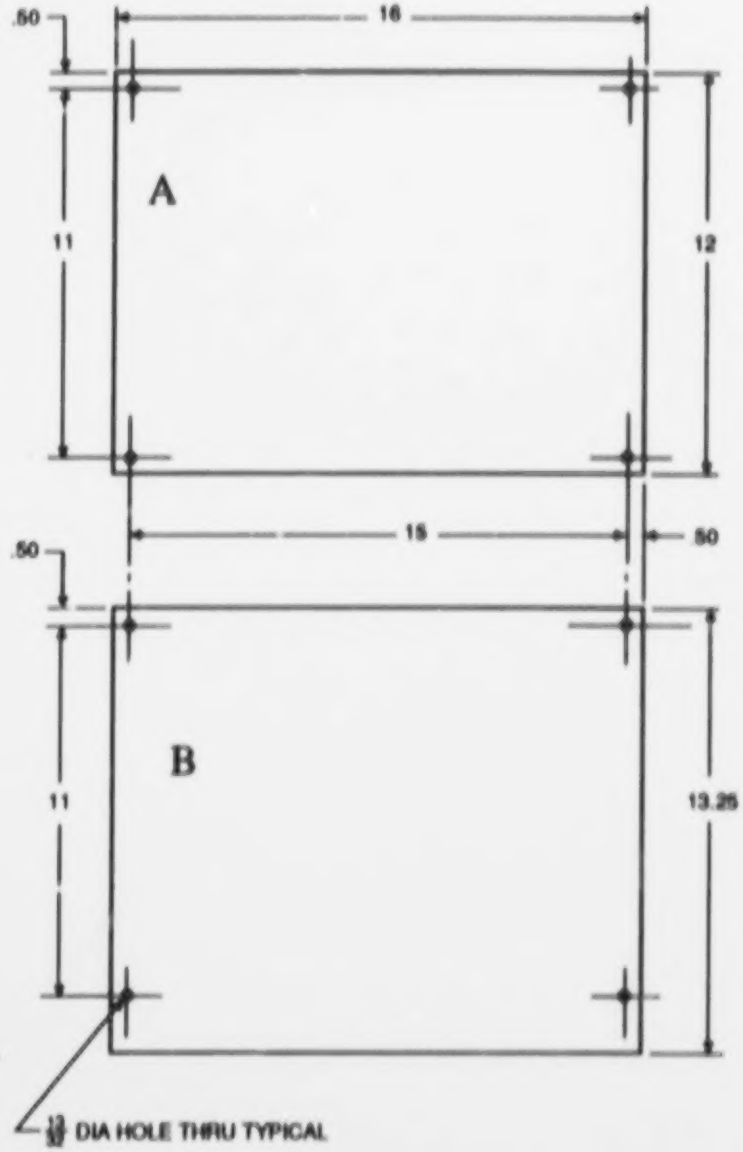
.50
16
A
11
12
.50
15
.50
B
11
13.25
$\frac{13}{32}$ DIA HOLE THRU TYPICAL

No.	Item		Thick. in.	Material	Qty.
1	Shield	A	0.032	6061-T6	14
2	Shield	A	0.040	6061-T6	18
3	Shield	A	0.063	6061-T6	4
4	Shield	A	0.080	6061-T6	4
5	Backwall	B	0.063	2219-T87	5
6	Backwall	B	0.100	2219-T87	6
7	Backwall	B	0.125	2219-T87	14
8	Backwall	B	0.188	2219-T87	10
9	Witness Plate	A	0.020	2024-T3	90

DEBURR ALL EDGES

DIMENSIONS IN INCHES.
ALL DIMENSIONS EXCEPT
THICKNESSES ± .05 INCH

Hypervelocity Impact Test Panels - Task I

BOEING	NAS8-36426

No.	Item		Thick. in.	Material	Qty.
1	Shield	A	.040	6061-T6	6
2	Shield	A	.063	ARAL	3
3	Shield	A	.063	6061-T6	3
4	Shield	B	.040	6061-T6	4
5	Shield	B	.040	dSiC	4
6	Backwall	A	.150	Li / Al	6
7	Backwall	A	.125	ARAL	3
8	Backwall	B	.125	dSiC	4
9	Backwall	A	.125	2219-T87	3
10	Backwall	B	.125	2219-T87	4
11	Witness Plate	A	.020	2024-T3	48
12	Witness Plate	B	.020	2024-T3	32

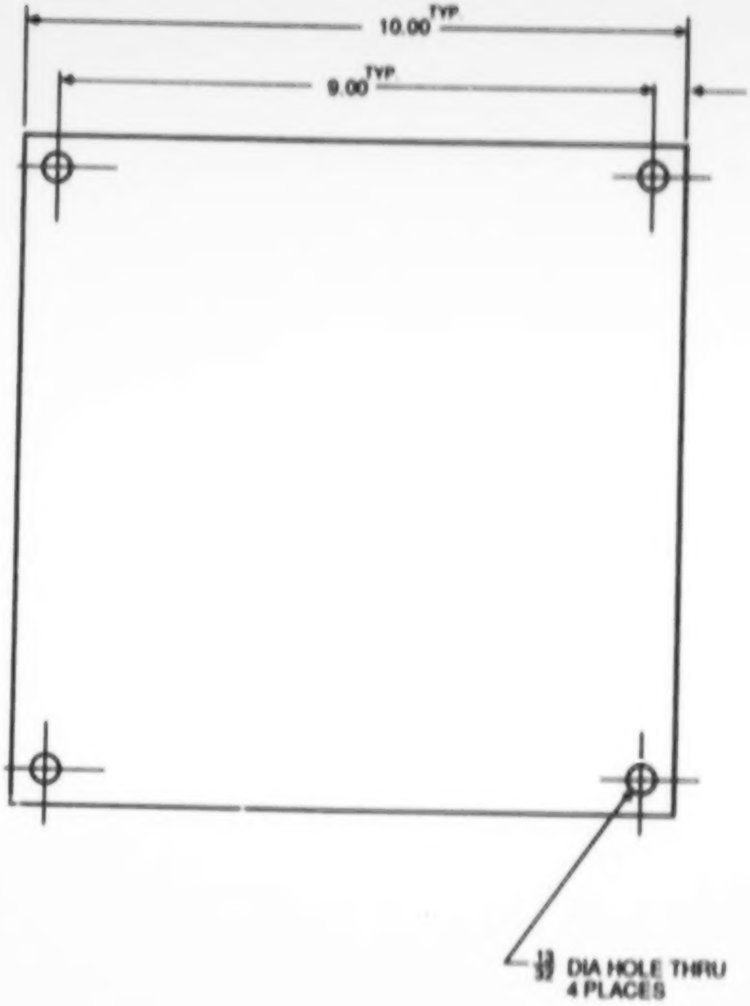
10.00 TYP.
9.00 TYP.
.50 TYP.
$\frac{13}{32}$ DIA HOLE THRU
4 PLACES

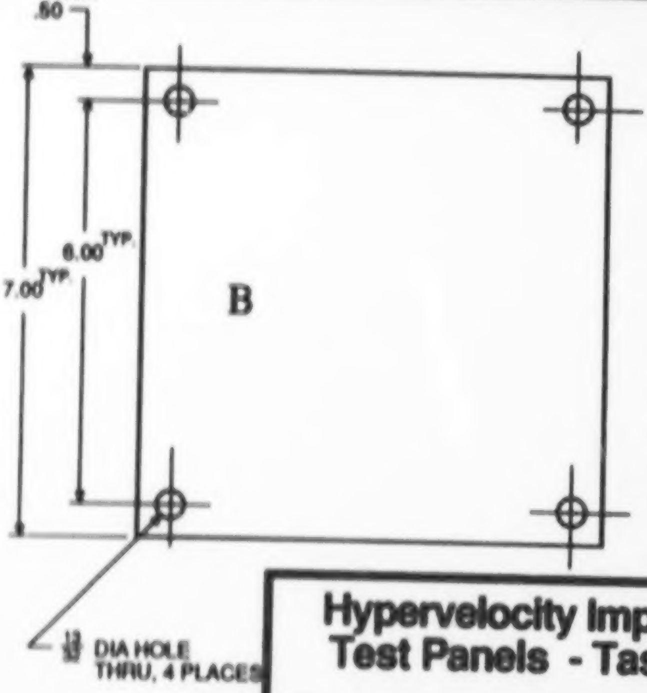
.50 TYP.
6.00 TYP.
7.00 TYP.
B
$\frac{13}{32}$ DIA HOLE
THRU, 4 PLACES

DEBURR ALL EDGES

DIMENSIONS IN INCHES.
ALL DIMENSIONS EXCEPT
THICKNESSES ± .05 INCH

Hypervelocity Impact
Test Panels - Task I

Boeing	NAS8-36426

No.	Item		Thick. in.	Material	Qty.
1	Shield	B	.063	6061-T6	12
2	Shield	B	.040	6061-T6	11
3	Backwall	A	.125	2219-T87	28

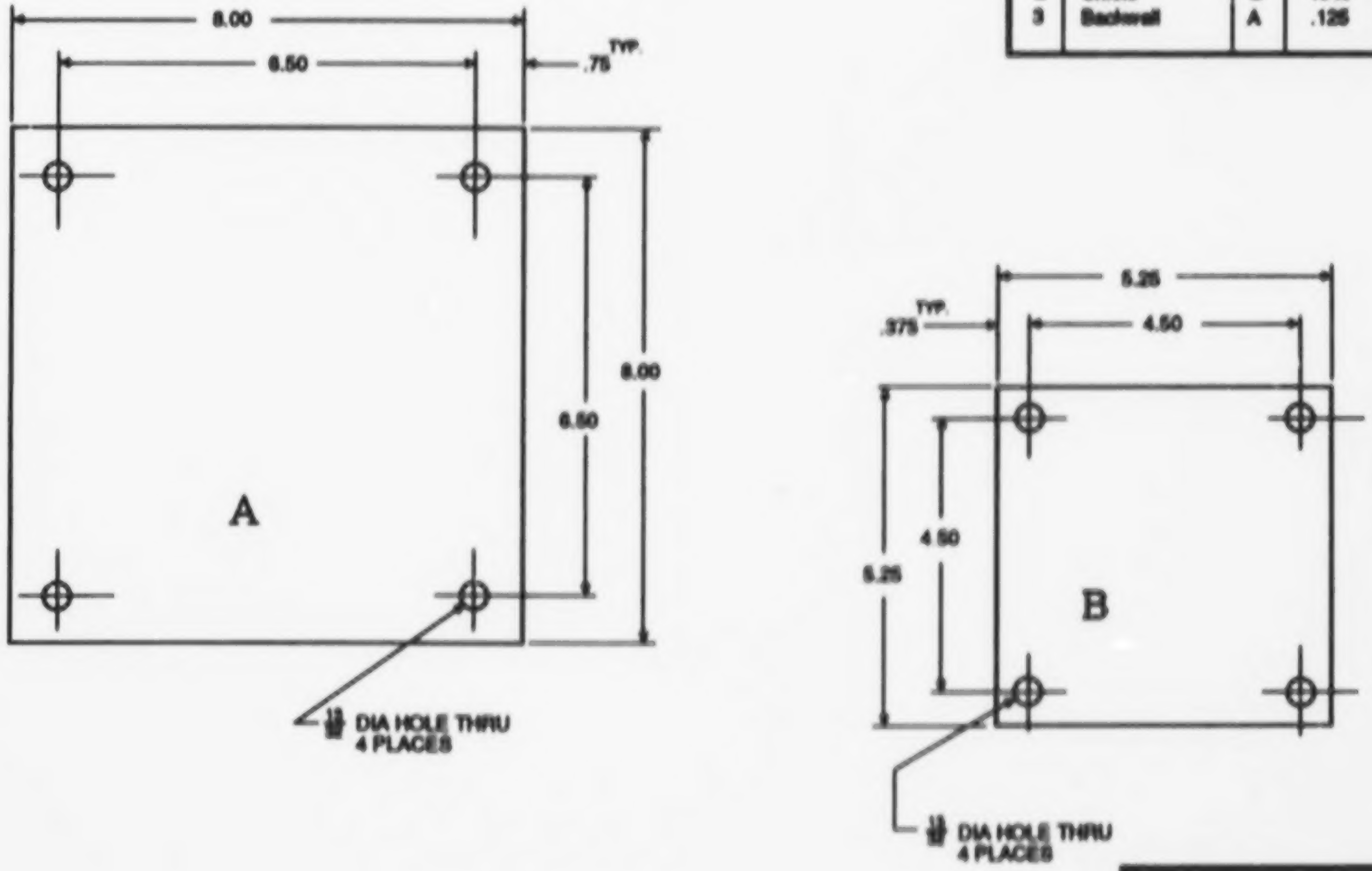
8.00
6.50
.75 TYP.
8.00
6.50
A
$\frac{13}{32}$ DIA HOLE THRU
4 PLACES
5.25
4.50
.375 TYP.
5.25
4.50
B
$\frac{13}{32}$ DIA HOLE THRU
4 PLACES

Hypervelocity Impact Test Panels - Task Ii

BOEING	NAS8-36426-10

DIMENSIONS IN INCHES.
ALL DIMENSIONS EXCEPT
THICKNESSES ± .05 INCH

DEBURR ALL EDGES

Appendix E - Physiological Effects of Decompression

In our studies of module wall repair techniques, we have assumed in the worst case the module would be evacuated and repaired later by a crew member in EVA equipment. We based this assumption on the belief that inadequate time was available to locate the damage and perform the repair before the module internal pressure decayed to hazardous levels. To examine the validity of this assumption, we compared the pressure decay rate of a punctured module with capability of unprotected crew at the various atmospheric pressure levels. This appendix is a summary of this investigation, which was performed by a physiologist from the Boeing Crew System/Life Support organization.

PHYSIOLOGIC EFFECTS OF RAPID LOSS OF SPACE STATION MODULE PRESSURE

Donald H. Reid
Boeing Aerospace Company

In the event that Space Station is impacted by space debris or micrometeoroids which actually penetrate the pressure-retaining hull, there are a number of immediate consequences and concerns regarding safety of flight. Those of a physiological nature are the subject of this paper.

If the "skin" of Space Station is punctured there will be an immediate outboard rush of air from a pressure of approximately 14.7 psia (1 ATA/ atmospheres, absolute), toward the near-vacuum of space. This phenomenon will result in a "rapid" or "explosive" decompression with the pressure decay dependent, in this case, upon the size of the opening and, of course, the ability of makeup gases to maintain a habitable pressure environment for human occupants, at least long enough to effect a repair. To the biomedical scientist, "explosive decompressions" are those occurring in 1 second or less and are extremely unlikely to occur in Space Station except in the case of complete loss of a viewing window of approximately 20" diameter.

Rapid decompressions will have physical and physiological effects. The primary physical events following perforation of the pressure vessel will be:

Noise, ranging from a swish to an explosive sound;
Flying debris, caused by the extremely rapid movement of air toward the point of penetration, and
Fogging, due to a rapid decrease in both temperature and pressure.

Not all of these phenomena may occur, especially in the case of a situation where the penetration is not over an inch in diameter and the decompression is therefore relatively slow. These physical events can both help and hinder the crew's ability to locate and repair the point of failure. The noise, flying debris and fogging will be most pronounced in the immediate vicinity of the puncture. On the other hand these consequences can obviously result in impaired vision, temporary hearing shift (deafness), and injury from flying objects. All of these effects depend upon the size of the opening and the protection afforded by hardware within the module surrounding the orifice.

In discussing the physiological effects of decompression we will assume a pressure differential of 14.7 psi (14.7 psia in module; vacuum outside Space Station). The effects of primary concern are:

- o Gas expansion (mechanical damage);
- o Acute hypoxia (lack of oxygen to the tissues of the body);
- o Decompression sickness ("bends"), and
- o Hypothermia (reduced body temperature).

GAS EXPANSION. During a rapid decompression gases within the body cavities will immediately expand in accordance with the laws of physics and if the escape of this gas from the body is impeded or blocked, excessively high internal pressures can develop depending on the volume of the contained gas and the elastic properties of the surrounding tissues and organs. This "trapped gas expansion" can occur primarily in body cavities such as the middle ears, sinuses, gastrointestinal tract and lungs. The lungs are the most vulnerable part of the body during a rapid decompression and many animal studies have shown that, following rapid decompression, there have been hemorrhages and evidence of mechanical damage to the lobes of the lungs. Rarely, however, even in extremely rapid decompressions, have these lesions been associated with detectable disability of the animals. All studies conducted indicate that the healthy human can tolerate relatively severe decompressions without apparent difficulty, providing the pulmonary airways are open.

The human body contains water vapor and carbon dioxide in much higher concentration than the surrounding environment. Since the body is approximately 80% water, at an internal temperature of 37°C the water vapor tension is 47 torr. Carbon dioxide is a waste product of metabolism which normally exerts a pressure of around 40 torr. Carbon dioxide is the primary chemical regulator of respiration. As the metabolic rate increases and more CO_2 is produced the organism compensates by breathing faster and deeper (hyperventilation). When metabolism slows and CO_2 production decreases, so does respiration. Therefore, at sea level where the total pressure is 760 torr (14.7 psia), 87 torr is due to the presence of water vapor and CO_2. Exposure of the human body to pressures below 47 torr (1 psia; 63,000 feet altitude equivalent), leads rapidly to vaporization of body fluids, a process known as ebullisn. This phenomenon is rapidly fatal, since long before the blood "boils" the body has suffered from a serious lack of oxygen (hypoxia).

The worst Space Station penetration case envisioned, an "explosive decompression" [occurring in less than one second] due to a very large opening in the module (20 inch diameter or greater), would be likely to have dire consequences. The pressure delta of 14.7 psig would expose personnel to gases expanding so rapidly that mechanical damage would occur (ebullisn). Fulminating hypoxia provides no more than 20 seconds or less of "useful conscious time" (effective performance time). Survival would only occur if personnel could be evacuated within 2-3 minutes and immediately placed in a recompression facility (hyperbaric airlock) for pressure/oxygen therapy.

HYPOXIA. Hypoxia is defined as a lack of oxygen to the tissues of the body. Without going into great detail we know that for acute exposure, people adapted to sea level require supplemental oxygen in their breathing medium at pressures below approximately 10 psia (552 torr; 10,000 feet altitude equivalent). The most dangerous aspect of hypoxia is that its symptoms are insidious, not painful and may in fact induce euphoria (a false sense of well-being). Therefore, hypoxia is not likely to be recognized by one suffering from it, especially if they are extremely busy. Between 10-8 psia symptoms will take a considerable time to develop and will affect primarily higher mental functions. People may fatigue easily, feel tired, have lapses of attention and may feel irritable, or conversely, euphoric. At pressures below 8 psia symptoms develop more rapidly and in addition to mental aberrations there may be motor effects such as tremor and twitching of muscles and possibly inability to do reasonably simple tasks. The time when a person retains consciousness at these pressures may be indefinite but his "useful consciousness" is on the order of one-half hour at around 8 psia. At a pressure of around 4 psia (200 torr; 30,000 feet altitude equivalent), "useful conscious time" is about one minute breathing ambient air. At pressures lower than 3 psia 100% oxygen alone will not prevent hypoxia and oxygen delivered under pressure is required. Below 2 psia (87 torr; 50,000 feet), all of the lung is occupied by water vapor (47 torr) and carbon dioxide (40 torr) and the individual has less than 30 seconds to take action, since, in this case, oxygen will actually be diffusing from the venous (deoxygenated) blood into the ambient environment.

In the event of a space debris puncture, then, the crew identified to locate and repair the hole will be equipped with supplemental oxygen which must be utilized below 10 psia. Because of the likelihood of mental symptoms oxygen should be utilized before the Station pressure has decayed to 10 psia. The rate of decompression is important since during a slow decompression the body can mobilize acute cardiorespiratory adaptations.

DECOMPRESSION SICKNESS. Another physiological disorder caused directly by reduced barometric pressure is decompression sickness (DCS) or "bends". This condition is an "evolved" gas problem caused by nitrogen moving from solution as the pressure in body tissues to the gaseous state in an attempt to reestablish equilibrium changes. Normally DCS does not occur at pressures greater than 8 psia but recent NASA research indicates that nitrogen bubbles can be detected in people decompressed from 14.7 to 9.5 psia. Therefore, we must consider a risk, albeit small, from DCS at pressures as high as 9.5 psia with the probability of these symptoms (joint pain; chokes; paresthesias) increasing at lower pressures. Factors known to increase the incidence of DCS in addition to absolute pressure include:

- o Rate of decompression
- o Duration of exposure to reduced pressures
- o Exercise (more exercise, more bends)
- o Amount of body fat (obese people more susceptible)
- o Ambient temperature (cold more bends), etc.

The symptoms of DCS can be virtually eliminated by "denitrogenating" (breathing 100% oxygen), which if continued long enough will eliminate over 50% of the nitrogen dissolved in body fluids and tissues. Space Station crews habituated to the normal 14.7 psia module will have no opportunity to denitrogenate in the event of a rapid decompression due to any cause. Therefore, the possibility of DCS must be dealt with operationally, that is, when the DCS risk gets high repair personnel should evacuate the damaged module. The "at risk" pressure range exists between 9.5 and 4.4 psia and the "greatly at risk" area at pressures below 4.4 psia.

The risk of bends to one or two crew members must be considered against the seriousness of consequnces of not locating and repairing punctures to the module hull. In other words, if not locating the failure would put the entire Space Station in extreme danger, procedures more risky to individual health might be employed. Even in this situation, however, there would be nothing gained by exposing personnel to environmental stresses which would overwhelm adaptive mechanisms and make normal performance impossible. In the situation where Space Station contains a hyperbaric airlock capable of generating overpressures to at least 2.8 ATA, pain only decompression sickness is potentially treatable and in this treatise we have therefore allowed the pressure to decay to as low as 4 psia before mandating crew removal. If, however, there is no hyperbaric treatment capability, crew personnel should be removed from the damaged module earlier, probably at 7.35 psia.

HYPOTHERMIA. Reduced body temperature due to extremely cold ambient temperatures, although not likely to be a serious consequence of rapid decompressions in Space Station, is an event which should be considered. The reduction in module temperature depends on many factors but for small diameter penetrations (2 inch hole or less), donning warm clothing should protect against hypothermia becoming a major medical threat.

SUMMARY

A precise physiological scenario cannot be described for a rapid decompression event in Space Station. Figure 1 shows likely physiological threats to crew health plotted against time for a one-inch diameter penetration. However, a module pressure slowly decaying to approximately 7 psia in 10 minutes or more should pose no serious medical threat, if supplemental oxygen is available to the crew personnel who will remain to locate and repair the damage and who will don the emergency oxygen system as soon as the threat is recognized. Between 9.5 and 7.4 psia decompression sickness (DCS) is possible but not probable. At pressures between 7.4 and 4.4 psia the "possible" becomes "probable" as the length of exposure increases and with other precipitating factors operable. Below 4.4 psia the probability of DCS becomes so great that, coupled with incipient hypoxia, personal safety considerations dictate removal of the crew from the damaged module. Even with 100% supplemental oxygen the repair crew should not remain in the module at pressures below 4 psia since even transient disruption of the oxygen supply could lead to rapidly occurring hypoxia. Therefore, in a situation where module pressure will decay from 14.7 to 7 psia the crew can be protected from hypoxia by breathing supplemental oxygen via approved oxygen delivery systems and the risk of DCS should not preclude attempting to locate and repair the puncture. The decreasing pressures and temperatures, per se, should be easily tolerated by healthy, experienced Astronauts. The risk of the two major physiological threats, (hypoxia and decompression sickness), increase significantly at pressures between 7-4 psia and to unacceptable levels below 4 psia.

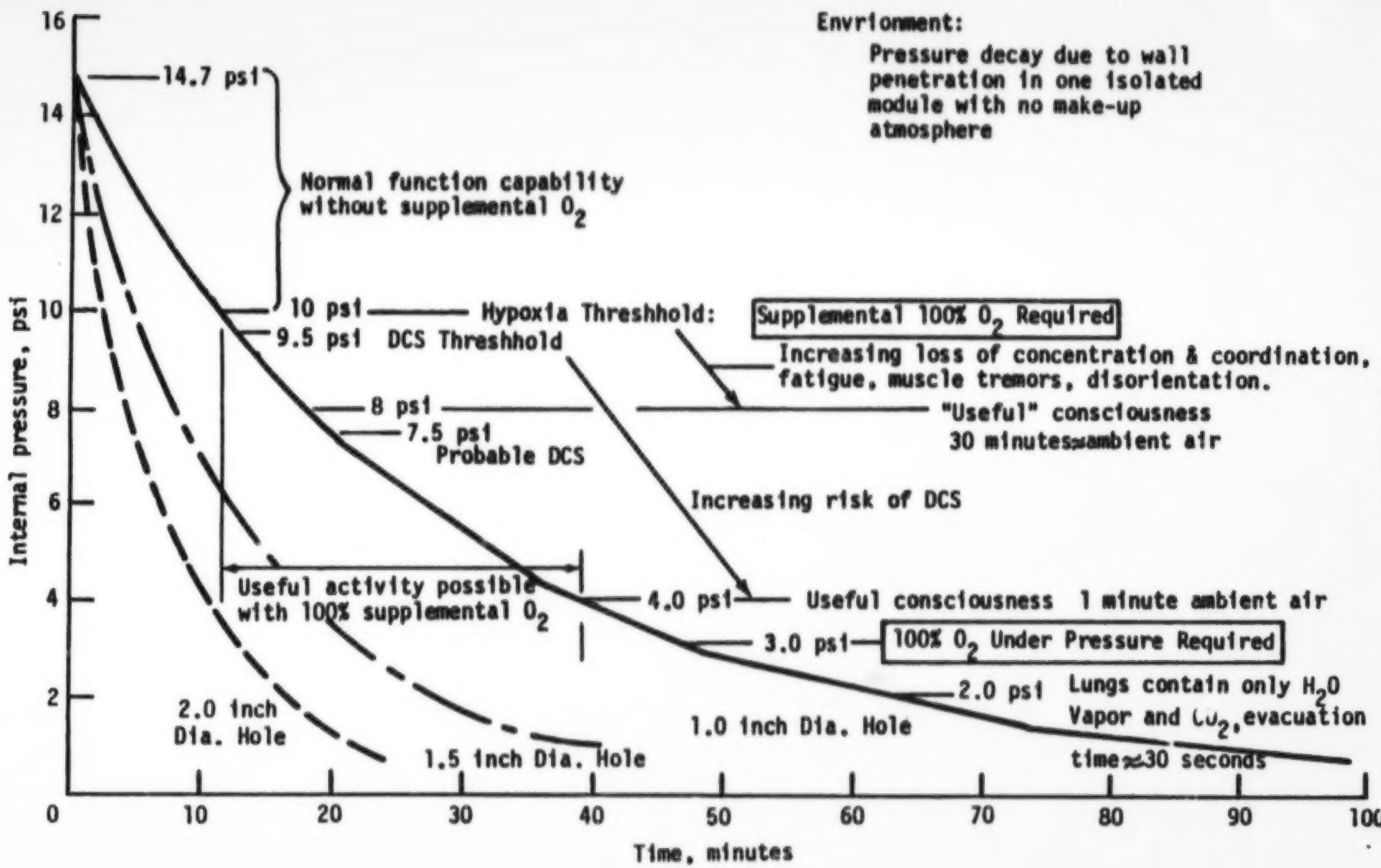

Figure 1. Physiological Threat From Rapid Loss of Space Station Module Pressure

LEGEND FOR FIGURE 1.

PHYSIOLOGICAL THREAT FROM SPACE DEBRIS PENETRATION

The assumption is that one Space Station module is penetrated by a 1 inch diameter hole caused by space debris or a micrometeoroid. With no make-up gas to maintain a 14.7 psia pressure the pressure will decay from 1 ATA to 4 psia in approximately 40 minutes. If operational considerations require location and repair of the puncture via IVA the following points are relevant to the physiological safety of the crewpersonnel. (Safety requires that at least two experienced personnel should remain together):

- If supplemental oxygen in "walk-around" configuration is available with duration of at least 1 hour, crew can work IVA until pressure decays to 4 psia, IF:
  - Symptoms of decompression sickness (DCS) do not occur. DCS will not occur at pressures above 9.5 psia but become more likely as the pressure goes below approximately 7 psia. Therefore, the most hazardous zone for DCS symptoms is any pressure below 7 psia. Time of exposure, increasing physical activity, decreasing temperature and various individual characteristics will affect probability of DCS symptoms.
- Expanding gas trapped within the body may cause discomfort but will not pose serious medical/operational threats if proper clothing is available.
- Decreasing temperatures due to reducing pressure and/or loss of ECLSS heating probably will not pose serious medical/operational threats if proper clothing is available.
- VACATE MODULE AT 4 PSIA OR ABOVE! -- Personnel should vacate isolated, damaged module by the time an absolute pressure of 4 psia is attained because even 100% oxygen cannot prevent symptoms of hypoxia.
- Serious DCS symptoms will dictate immediate evacuation of module, regardless of pressure level, to the normal Space Station pressure and may require hyperbaric therapy for treatment of bends.

This is a high risk scenario physiologically because of the possibility of DCS which increases dramatically from 9.5 psia to 4.0 psia and the certainty of hypoxia in the event of oxygen system malfunction or even transient disruption of the oxygen supply.

Conservative policy would be to immediately clear a damaged, isolatable module of personnel as soon as the risk is identified.

Appendix F - Effectiveness of Composites as Meteoroid/Debris Shields

Composite materials are emerging as viable spacecraft constituents because of their high strength and low weight. The amount of test data available on composite plates is scarce, though interest in using composites continues. The following is a theoretical assessment of composite materials as hypervelocity impact shields.

THE EFFECTIVENESS OF COMPOSITES AS METEOROID/DEBRIS SHIELDS

Michael D. Bjorkman
Boeing Aerospace Company

The effectiveness of a meteoroid/debris shield is dependent on the degree to which it fragments and spreads the meteor or orbital debris particle. A quick approach to ranking the effectiveness of shield materials uses the following simple qualitative argument.

The degree of meteor/debris (hereafter referred to as projectile) fragmentation is dependent on the magnitude of the stress and motions induced in the projectile by the impact with the shield. This in turn is dependent on the compressibility of the target material. If the target material is rigid then the projectile will stagnate at the target plate producing large stresses and radial motions in the projectile. If the target plate is very compressible then the target plate will deform around the projectile producing little stress and radial motion within the projectile.

The curve describing the shock compressibility of the target material under uniaxial strain shock waves is called the Rankine-Hugoniot curve (or R-H curve). Several collections of R-H curves have been published. The R-H curves for the shock pressure amplitude and the shock particle velocity amplitude (called p-u R-H curves) for several materials are shown in the figure and have been abstracted from reference 1 and 2. Also shown in the figure is the p-u R-H curve for an aluminum projectile traveling at 8 km/s. The intersection of the projectile and target p-u R-H curves gives the stress and particle velocity amplitude of the shock wave driven into the target and the projectile by the impact.

One notes from the figure that the shock compressibility of graphite-epoxy[3] is less than that of aluminum and thus graphite-epoxy is expected to be a less effective shield than aluminum. This conclusion is born out by recent ADP gas gun tests which show graphite-epoxy shields do not spread out the projectile fragments.

The same conclusion on the relationship between shield effectiveness and shock compressibility was made in reference 4, a study of projectile materials properties important to defeating a shielded targets by hypervelocity impact. The material properties studied in reference 4 were density, melting temperature, toughness, liquid metal surface tension, and shock compressibility. In reference 4 it was concluded that out of the five material parameters studied shock compressibility had the strongest correlation with effectiveness.

The authors of reference 4 further concluded that the optimum shield material would combine small shock compressibility (for fragmenting the projectile) with small density (to minimize perforation of the shielded plate). Even though graphite-epoxy satisfies the second condition for small density, the recent ADP tests indicate graphite-epoxy is too compressible under shock loading to meet the first condition required for spreading the projectile fragments.

Even though the whole story on shield effectiveness is not given by the figure, the shock compressibility has been shown to rank the effectiveness of shield materials. Therefore, on the basis of this criterion it is concluded that aluminum is a more effective shield material than graphite-epoxy composites.

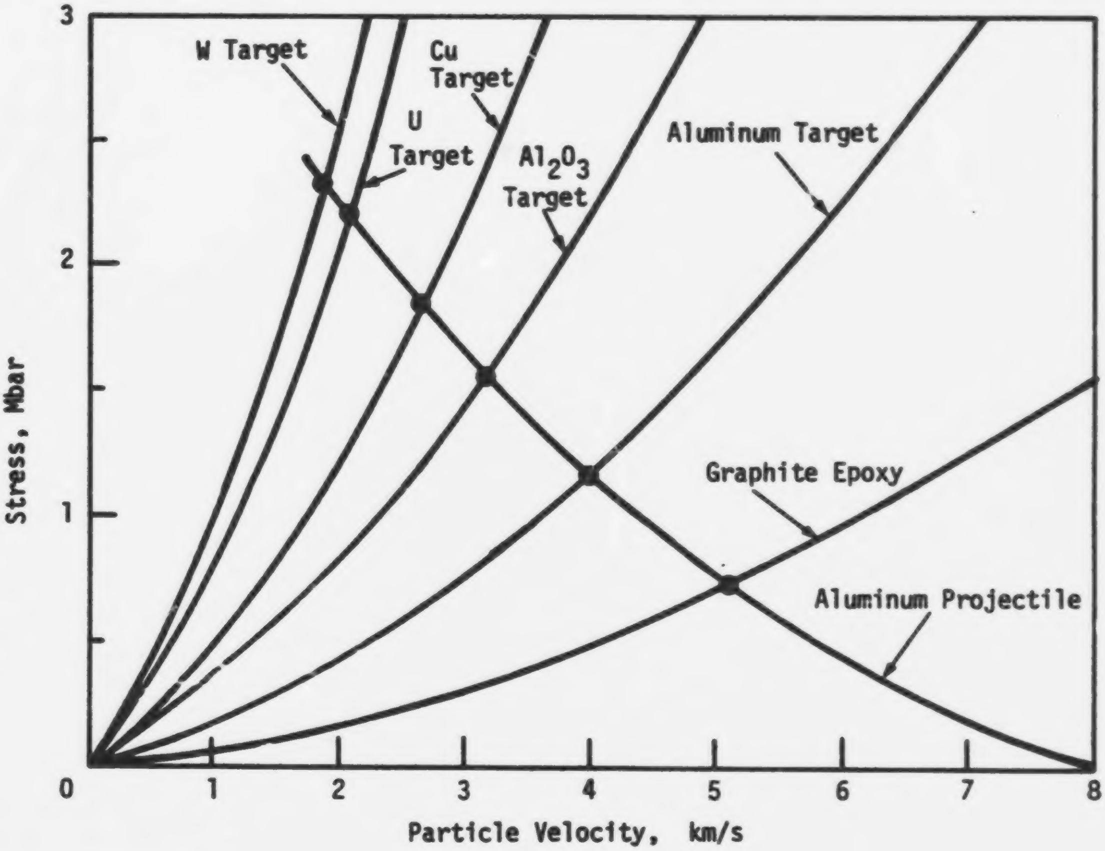

Figure 1. Material Shock Compressibility

REFERENCES AND FOOTNOTES

1. LASL Shock Hugoniot Data. ed. by Stanley Marsh. University of California Press. Berkeley, CA, 1980.
2. AFWL-TR-80-21. PUFF74 E.O.S. Compilation. Air Force Weapons Laboratory. Kirtland AFB, NM. August 1980.
3. It should be noted that it was only necessary to measure the shock compressibility of graphite-epoxy to a few kbars stress for the application made in reference 2. Thus a considerable amount of extrapolation was necessary to plot the curve on the figure.
4. AFATL-TR-67-228. Projectile Physical Properties Investigation. Air Force Armament Laboratory. Eglin AFB, FL, December 1967.

Appendix G - Mathematical Derivations of Analysis Method

The following derivations provide rigorous mathematical support for our approach to analyzing Space Station structure as implemented in the BUMPER computer code. The BUMPER implementation is described in section 7.0.

Space Station Penetration Probability Model

Revised Version: April 15, 1987

Fritz Scholz

Boeing Computer Services

Introduction

To protect a space station from penetration by debris particles orbiting the earth and from penetration by meteoroids various designs for the outer hull of this space station are under consideration. It is desired to choose a design that will keep weight requirements low and will give effective protection against such penetration. The purpose of the following analysis is to develop a measure of effectiveness for a given design. This measure is the probability that the exposed surface hull area of the space station will not be penetrated by any debris particle or meteoroid during a mission time of duration T.

The reason for making a probabilistic assessment of effectiveness is a consequence of the fact that the arrival time, velocity, striking angle and diameter (mass) of any given particle or meteoroid is variable and unknown and can at best be described only statistically.

Due to the difference in character of meteoroids and orbital space debris separate models are developed for each, although some similarities lead to repetition in the exposition. The vulnerable surface area of the space station is decomposed into manageable flat surface elements and the probabilities of no penetration are developed separately for each such surface element. In the final section all these probabilities are integrated over all the surface elements and over the two risk factors (debris and meteoroids).

Before going into the two respective probability models it appears justified to clarify certain notions of flux as they pertain to the isotropic nature of meteoroid flux and the highly directional flux of space debris.

Isotropic Flux

One way of defining isotropic flux is by the average number $F_{sp-Met}(m)$ of meteoroids of mass $\geq m$ that will pass through a sphere with cross section area $\pi r^2 = 1$ in unit time where the direction vectors of the meteoroids are equally distributed over all orientations in 3–dimensional space. Using the sphere ensures that the exposed area perpendicular to any incident meteoroid will always be a unit area.

To make this more precise and to relate it to another flux notion consider a fixed coordinate system with y–axis pointing in the space station flight direction, z–axis pointing radially away from earth and x–axis perpendicular to the previous two in the usual orientation so that the (x, y)–plane forms the tangential plane of the space station. Consider this coordinate system fixed at some point in the space station orbit. In this coordinate system describe the direction of an incoming meteoroid by the unit vector $\mathbf{k} = (\sin(\theta)\sin(\alpha),\ \cos(\theta)\sin(\alpha),\ \cos(\alpha))$ with polar angles $\alpha \in [0, \pi]$ and $\theta \in [0, 2\pi)$. At this point any earth shadowing effects are ignored. Describing the density of (α, θ) by

$$p(\alpha, \theta) = \frac{\sin(\alpha)}{2}\, I_{[0,\pi]}(\alpha)\ \frac{1}{2\pi}\, I_{[0,2\pi)}(\theta)$$

(using $I_B(x) = 1$ if $x \in B$ and $I_B(x) = 0$ otherwise) entails that the corresponding directions of $\mathbf{k} = \mathbf{k}(\alpha, \theta)$ will be equally distributed over the unit sphere centered at the origin of the coordinate system. Here "equally distributed" means that the relative frequency with which $\mathbf{k}$ points in the direction outlined by the patch $(\alpha, \alpha + d\alpha)$ and $(\theta, \theta + d\theta)$ on the unit sphere is just the area of that patch over the total surface area 4π of that unit sphere. Note that the area of that patch is $d\theta\ d\alpha\ \sin(\alpha)$ and dividing this by 4π yields $p(\alpha, \theta)\ d\alpha\ d\theta$.

The above flux isotropy is then interpreted to mean that the flux intensity in direction (α, θ) is $p(\alpha, \theta) F_{sp-Met}(m)$ or the expected number of meteoroids of mass $\geq m$ passing perpendicularly through a unit area in a unit time from direction $(\alpha, \alpha + d\alpha)$ and $(\theta, \theta + d\theta)$ is $F_{sp-Met}(m) p(\alpha, \theta)\ d\alpha\ d\theta$. The total flux $F_{sp-Met}(m)$ is recovered by integrating this infinitesimal directional flux over all possible directions.

In this context a related but different notion of flux should be mentioned. This flux, the flat plate flux and denoted by $F_{fp-Met}(m)$, is the average number of meteoroids of mass $\geq m$ that hit the upside of a flat plate of area 1 in unit time from any direction. It turns out that the relationship between these two fluxes is

$$F_{sp-Met}(m) = 4\ F_{fp-Met}(m)\ .$$

This is seen by considering the unit flat plate lying in the (x,y)–plane with the upside facing in the z–direction and integrating the infinitesimal directional flux over all directions and accounting for the fact that the directional aspect of that unit flat plate is $[\cos\alpha]^+$. Here $[x]^+ = x$ if $x \geq 0$ and $[x]^+ = 0$ otherwise, so that $[\cos(\alpha)]^+ = 0$ if $\alpha \in (\pi/2, \pi]$. Hence

$$F_{fp-Met}(m) = \int_0^{2\pi} \int_0^{\pi} [\cos(\alpha)]^+ \, F_{sp-Met}(m) p(\alpha, \theta) \, d\alpha \, d\theta$$

$$= \int_0^{2\pi} \int_0^{\pi/2} \cos(\alpha) \, F_{sp-Met}(m) \, \frac{1}{2\pi} \frac{\sin(\alpha)}{2} \, d\alpha \, d\theta \; = \; \frac{1}{4} \, F_{sp-Met}(m) \; .$$

Another way of seeing the factor 4 in the above flux relationship is by again considering the sphere with cross section $\pi r^2 = 1$, i.e. with surface area $4\pi r^2 = 4$, and decompose that surface area into many disjoint infinitesimal flat plates with area dS, so that

$$F_{sp-Met}(m) = \int_{sphere} F_{fp-Met}(m) \, dS = 4 F_{fp-Met}(m) \; .$$

It is worth pointing out that for isotropic flux and in the absence of any shielding the orientation of the flat plate makes no difference. Hence the flat plate can also be considered as a randomly tumbling plate and $F_{fp-Met}(m)$ thus also represents the average number of meteoroids of mass $\geq m$ that hit the designated upside of such a tumbling flat plate of area 1 in unit time with any incidence direction.

Relating this to [1] the following identifications can be made. The "integral flux N" given on page 74 of [1] is the same as the above fixed plate flux $F_{fp-Met}(m)$ and the "directional flux" j given on the same page of [1] is equivalent to $F_{sp-Met}(m)/(4\pi)$, i.e. the above defined "isotropic flux" per steradian.

Orbital Space Debris Flux

Orbital debris particles pose a threat to the space station only if they orbit at the same distance from earth as the space station. Such particles and the space station therefore share the same absolute velocity v_0. If $\mathbf{v}_S$ and $\mathbf{v}_D$ denote respectively the space station velocity vector and the velocity vector of some orbital debris particle then the relative velocity vector of the debris particle (relative to the space station) $\mathbf{v}_{DS} = \mathbf{v}_D - \mathbf{v}_S$

forms the angle θ with the space station flight direction. The magnitude of the relative velocity $\mathbf{v}_{DS}$ is $|\mathbf{v}_{DS}| = 2v_0 \cos\theta$. This is the effective absolute velocity with which such a debris particle will hit any exposed area of the space station. The angle θ that the incident debris particle can form with the space station flight direction can vary from $-\pi/2$ to $\pi/2$ and the frequency with which those angles occur is not uniform or isotropic over this range.

To describe and define the debris flux consider the following space station based (x, y, z) coordinate system with the positive y–direction pointing in the direction of flight of the space station, the positive z–direction pointing radially away from earth and the x–axis forming the other axis in the orbital tangential plane. Consider now a cylinder with base radius $r = 1/2$ and height $h = 1$ with its base standing on the (x, y)–plane. Then any debris particle flying in or parallel to the (x, y)–plane will view this cylinder as a square with area 1. The definition for the debris flux $F_{Deb}(d)$ parallels that of $F_{sp-Met}(m)$ as follows. $F_{Deb}(d)$ is the average number of debris particles of diameter $\geq d$ that will pass through that cylinder with cross section area $2r\, h = 1$ in unit time. The angles of the incoming debris particles are distributed over the interval $[-\pi/2, \pi/2]$ according to some density $w(\theta)$, so that $F_{Deb}(d)w(\theta)\, d\theta$ represents the average or expected number of debris particles of diameter $\geq d$, with direction angle $[\theta, \theta + d\theta]$ which pass perpendicularly through a unit area in a unit time.

As in the case of meteoroid flux there is a corresponding notion of flat plate debris flux. Here it will matter whether that flat plate is fixed, rotating or randomly tumbling. The following makes these various debris flux relationships explicit.

Fixed Plate Flux: Consider a fixed flat plate in the above (x, y, z)–coordinate system. Assume that this flat surface element, denoted by A, has area $|A|$ and unit normal vector $\mathbf{n}_A$ pointing to the designated outside of that flat plate. The angle that the relative velocity vector $\mathbf{v}_{DS}$ of the incoming debris particle forms with $\mathbf{n}_A$ is denoted by $\beta = \beta(\theta)$. The functional form of $\beta(\theta)$ is described by

$$\cos(\beta(\theta)) = \sin(\psi)\ \cos(\theta - \phi)\ .$$

where ψ and ϕ are the angles of the polar coordinate representation of

$\mathbf{n}_A$, i.e. the normal vector $\mathbf{n}_A$ forms the angle ψ with the z-axis and the projection of this normal vector onto the (x, y)-plane forms angle ϕ with the y-axis.

The area A has an exposed projection $|A|[\cos(\beta(\theta))]^+$ onto the plane perpendicular to the direction of the incoming debris particle. The $[\quad]^+$ accounts for the fact that particles can only hit the outside of A. Hence the expected number of particles, with diameter $\geq d$, hitting A from a direction $[\theta, \theta + d\theta]$ during a unit time interval is

$$|A| \; [\cos(\beta(\theta))]^+ F_{Deb}(d) \; w(\theta) d\theta$$

and summing this over all possible angles θ one obtains

$$\begin{aligned} & |A| \; F_{Deb}(d) \int_{-\pi/2}^{\pi/2} [\cos(\beta(\theta))]^+ w(\theta) d\theta \\ &= |A| \; F_{Deb}(d) \int_{-\pi/2}^{\pi/2} [\sin(\psi) \; \cos(\theta - \phi)]^+ w(\theta) d\theta \\ &= |A| \; F_{Deb}(d) \; \sin(\psi) \int_{-\pi/2}^{\pi/2} [\cos(\theta - \phi)]^+ w(\theta) d\theta \end{aligned}$$

as the average number of particles of diameter $\geq d$ which hit the outside of A from any direction during a unit time interval. Note that this fixed plate flux is highly dependent on $w(\theta)$ and on the orientation (ψ, ϕ) of the fixed plate.

To further illuminate the relation between fixed plate flux and $F_{Deb}(d)$ consider again the cylinder in the definition of $F_{Deb}(d)$. Decomposing the outside mantle of this cylinder into vertical flat plate strips of height 1 and width $d\phi/2$ (note $r = 1/2$), i.e. with area $|A| = d\phi/2$, then the integrated flux over all these flat plate strips is (using $\psi = \pi/2$, i.e. $\sin(\psi) = 1$)

$$\begin{aligned} & \int_0^{2\pi} \frac{1}{2} F_{Deb}(d) \int_{-\pi/2}^{\pi/2} [\cos(\theta - \phi)]^+ w(\theta) \; d\theta \; d\phi \\ &= \frac{1}{2} F_{Deb}(d) \int_{-\pi/2}^{\pi/2} \int_0^{2\pi} [\cos(\theta - \phi)]^+ \; d\phi \; w(\theta) \; d\theta \\ &= \frac{1}{2} F_{Deb}(d) \int_{-\pi/2}^{\pi/2} 2 \; w(\theta) \; d\theta = F_{Deb}(d) \end{aligned}$$

which coincides with the definition of the debris flux. This should not be surprising since what goes through the cylinder has to pass through its mantle and vice versa.

Rotated Plate Flux: If the above plate A is rotated around the z-axis then the average number of particles hitting this area A is further averaged over the polar angle ϕ of the normal vector $\mathbf{n}_A$ and one obtains

$$|A|\, F_{Deb}(d)\ \sin(\psi) \int_{-\pi/2}^{\pi/2} \int_0^{2\pi} \frac{1}{2\pi} [\cos(\theta - \phi)]^+ \, d\phi \, w(\theta) d\theta$$

$$= |A|\, F_{Deb}(d)\ \sin(\psi) \int_{-\pi/2}^{\pi/2} \frac{1}{\pi} w(\theta) d\theta = |A|\, F_{Deb}(d)\ \sin(\psi)\ \frac{1}{\pi}$$

which represents the average number of particles of diameter $\geq d$ hitting the area A during a unit time interval while it rotates around the z-axis. Note that the rotated plate flux is independent of $w(\theta)$.

Tumbling Plate Flux: If the above fixed plate tumbles so that it exposes its outside surface toward any direction with equal frequency then the fixed plate count should be averaged uniformly over all spherical directions, i.e. over all polar angles (ψ, ϕ) with joint density:

$$g(\psi, \phi) = \frac{1}{2} \sin(\psi) I_{[0,\pi]}(\psi)\ \frac{1}{2\pi} I_{[0,2\pi)}(\phi)\,.$$

Hence this average tumbling plate count is

$$|A|\, F_{Deb}(d) \int_0^{\pi} \frac{1}{2} \sin^2(\psi) \int_{-\pi/2}^{\pi/2} \int_0^{2\pi} \frac{1}{2\pi} [\cos(\theta - \phi)]^+ \, d\phi \, w(\theta) d\theta \, d\psi$$

$$= |A|\, F_{Deb}(d) \int_0^{\pi} \frac{1}{2} \sin^2(\psi)\ \frac{1}{\pi}\, d\psi = |A|\, F_{Deb}(d)\ \frac{1}{4}$$

Again note the tumbling flux no longer depends on the angle density $w(\theta)$. Because of this angle independence it is convenient to report the debris flux in terms of the tumbling plate flux. However, it should be realized that there is a factor 4 difference between the flux of a tumbling plate of area 1 and the original definition involving a cylinder of cross section area 1.

Probability Model for Penetration by Meteoroids

Consider a specific (approximating) flat surface element A^* that is exposed to being hit by a meteoroid. Denote its area by $|A^*|$. It seems reasonable to model the succession of meteoroids that will hit A^* as a random process. In fact, it is appropriate to model the arrival process (of the meteoroids at A^*) as a homogeneous Poisson process with some intensity λ.

Depending on its velocity, mass and impact angles such a meteoroid may also penetrate the surface element A^*. Since the objective is to derive a formula for the probability of no penetration, it is necessary to model the velocity, impact angles and mass of each incident meteoroid. This leads to a so called marked Poisson process as the appropriate vehicle for analysis, see [2], [3].

Before going into the probabilistic description of such a process let us discuss the characteristics of the incident meteoroids. The i^{th} incident meteoroid arrives at time W_i and has absolute velocity V_i, mass M_i and polar coordinate incidence angles (α_i, θ_i) as introduced in the section on isotropic meteoroid flux. Here it is assumed that the (x, y, z) coordinate system is fixed on the moving space station. The effect that this motion has on the meteoroid isotropy assumption is ignored.

The meteoroid characteristics $(V_i, M_i, \alpha_i, \theta_i)$ may be considered as independent and identically distributed random vectors. Within each such vector it is further reasonable to assume that all four components are independently distributed (ignoring any shadow effects at this point and also neglecting the fact that the space station is a moving target). Thus let V_i have density $q(v)$, let M_i have density $h(m)$, θ_i be uniformly distributed over $[0, 2\pi)$ and α_i may have density $\sin(\alpha)/2$ on the interval $[0, \pi]$. The joint density of (α, θ) is designed to assure that all meteoroid incidence directions $\mathbf{k} = \mathbf{k}(\alpha, \theta)$ relative to the space station are equally likely. (This joint distribution of (α, θ) would be somewhat distorted from the given one if the moving target effect were accounted for.) Of the two densities q and h only q can be assumed as given directly. Information about h is given only indirectly through the flux quantity $F_{sp-Met}(m)$.

Thus $(\Delta_1 \sin(\alpha_0)/2)$ $(\Delta_2/2\pi)$ $F_{sp-Met}(m)$ represents the (time) average number of meteoroids of mass $\geq m$ which, in a unit time, pass perpendicularly through a unit area whose normal vector points in the direction (α, θ), with $\alpha \in [\alpha_0, \alpha_0 + \Delta_1]$, $\theta \in [\theta_0, \theta_0 + \Delta_2]$.

Although (α, θ) describes the direction of the meteoroid relative to the space station coordinate system it is essential to introduce the plate specific incidence angle $\beta = \beta(\alpha, \theta) = \beta(\alpha, \theta, \psi, \phi)$ which is the angle formed by the direction vector $\mathbf{k} = \mathbf{k}(\alpha, \theta) = (\sin(\theta)\sin(\alpha),\ \cos(\theta)\sin(\alpha),\ \cos(\alpha))$ of the meteoroid and the normal unit vector $\mathbf{n}_{A^*} = (\sin(\phi)\sin(\psi),\ \cos(\phi)\sin(\psi),\ \cos(\psi))$ of the plate. The inner product of these two vectors yields the cosine of β as

$$\cos(\beta) = \sin(\psi)\sin(\alpha)(\cos(\phi - \theta) - 1) + \cos(\psi - \alpha)\ .$$

Using the above plate specific incidence angle β a critical penetration mass as a function of β and v is given as follows

$$M_{crit} = \psi^*(\beta, v),$$

so that the i^{th} incident meteoroid penetrates A^* if and only if $M_i \geq \psi^*(\beta_i, V_i)$.

The probabilistic structure of the marked Poisson process is specified through an intensity function λ. Here λ is a function defined on a subset S of R^5 with values in $[0, \infty)$. For the application at hand the following specification is appropriate:

$$\lambda(t, \alpha, \theta, v, m) = \lambda_0(\beta)\ I_{[0,\infty)}(t)\ \frac{1}{2\pi}\ I_{[0,2\pi)}(\theta)\ \frac{\sin(\alpha)}{2}\ I_{[0,\pi]}(\alpha)\ q(v)\ h(m)\ .$$

Here $S = [0, \infty) \times [0, \pi] \times [0, 2\pi) \times [0, \infty) \times [0, \infty)$ and t is the time variable referring to the arrival times of meteoroids. Note that in the above specification of the intensity λ the variables α, θ, v, m appear individually factored which reflects the previously discussed independence of these characteristics. However, the time intensity $\lambda_0(\beta)$ of the Poisson process does depend on $(\alpha, \theta, \psi, \phi)$ through $\beta = \beta(\alpha, \theta, \psi, \phi)$. This reflects the fact that at different angles β different amounts of the surface area A^* are (perpendicularly) exposed to the direction of the flux as given by (α, θ).

The marked Poisson process with intensity λ is a point process $\{N(C) : C \subset S\}$ such that:

- $N(C)$ has a Poisson distribution with mean or expected value

  $$\mu(C) = \int_C \lambda(t, \alpha, \theta, v, m) d(t, \alpha, \theta, v, m)$$

and

- for any k and for disjoint $C_1, \ldots, C_k \subset S$ the random variables $N(C_1), \ldots, N(C_k)$ are independent.

Here $N(C)$ represents the random number of points (incident meteoroids) with characteristics $(t, \alpha, \theta, v, m)$ in C.

In order to establish the relationship between $h(m)$ and $F_{sp-Met}(m)$ consider the following set C_0 of characteristics:

$$C_0 = \{(t, \alpha, \theta, v, m) \in S : t \leq T,\ \alpha \in [\alpha_0, \alpha_0 + \Delta_1],\ \theta \in [\theta_0, \theta_0 + \Delta_2],\ m \geq m_0\}$$

then $N(C_0)$ represents the random number of incident meteoroids which are counted during time span T, which are of mass $\geq m_0$ and which have incidence angles $\alpha \in [\alpha_0, \alpha_0 + \Delta_1]$ and $\theta \in [\theta_0, \theta_0 + \Delta_2]$.

Then the expected or average value of $N(C_0)$ is

$$E(N(C_0)) = \mu(C_0) = \int_{m_0}^{\infty} h(m)\, dm\, T \int_{\alpha_0}^{\alpha_0+\Delta_1} \int_{\theta_0}^{\theta_0+\Delta_2} \lambda_0(\beta) \frac{1}{2\pi} \frac{\sin(\alpha)}{2} d\theta\, d\alpha$$

$$\approx \overline{H}(m_0)\, T\, \lambda_0(\beta_0) \Delta_1 \Delta_2 \frac{\sin(\alpha_0)}{2} \frac{1}{2\pi}$$

where $H(m) = 1 - \overline{H}(m)$ is the cumulative distribution function of h and $\beta_0 = \beta(\alpha_0, \theta_0, \psi, \phi)$.

On the other hand the average number of meteoroids of diameter $\geq m_0$ that hit A^* from direction (α, θ) with $\alpha \in [\alpha_0, \alpha_0 + \Delta_1]$ and $\theta \in [\theta_0, \theta_0 + \Delta_2]$ during time span T is approximately

$$\Delta_1 \Delta_2 \frac{\sin(\alpha_0)}{2} \frac{1}{2\pi} F_{sp-Met}(m_0)\, T\, |A^*|\, [\cos(\beta_0)]^+ ,$$

where $|A^*|\, [\cos(\beta_0)]^+$ is the projection of the outside area of A^* onto the plane perpendicular to the direction β_0. That projection is the effective area that the meteoroids will pass perpendicularly when they hit A^* at angle β_0.

Combining the two previous flux equations yields

$$\overline{H}(m_0)\, \lambda_0(\beta_0) = F_{sp-Met}(m_0)\, |A^*|\, [\cos(\beta_0)]^+ .$$

Differentiating this with respect to m_0 would yield a corresponding relationship for h.

It is of interest to compute the quantity $E(N(C(m_0))) = \mu(C(m_0))$, where $C(m_0) = \{(t, \alpha, \theta, v, m) \in S : t \leq T, m \geq m_0\}$. Then

$$\begin{aligned}
\mu(C(m_0)) &= \overline{H}(m_0) T \int_0^{\pi} \int_0^{2\pi} \lambda_0(\beta) \frac{\sin(\alpha)}{2} \frac{1}{2\pi} \, d\theta \, d\alpha \\
&= T \, F_{sp-Met}(m_0) \, |A^*| \int_0^{\pi} \int_0^{2\pi} [\cos(\beta(\alpha, \theta))]^+ \frac{\sin(\alpha)}{2} \frac{1}{2\pi} \, d\theta \, d\alpha \\
&= T \, F_{sp-Met}(m_0) \, |A^*| \int_0^{\pi} \int_0^{2\pi} [\cos(\alpha)]^+ \frac{\sin(\alpha)}{2} \frac{1}{2\pi} \, d\theta \, d\alpha \\
&= \frac{1}{4} T \, |A^*| \, F_{sp-Met}(m_0) \, ,
\end{aligned}$$

where the above change of variable from $\beta(\alpha, \theta)$ to α utilizes the rotational symmetry of the uniform distribution over the sphere. The above equation thus reiterates the earlier relation between the isotropic flux $F_{sp-Met}(m)$ and the flat plate flux $F_{fp-Met}(m)$.

With the above marked Poisson process in place the following filtered marked Poisson process is the natural vehicle for finding the probability of no penetration. Let B be a subset of $B_0 = [0, 2\pi) \times [0, \pi]$. B defines the set of incidence angles (α, θ) which are at all possible, i.e. are not shaded out by the earth or the space station. Define the following derived or filtered intensity:

$$\lambda^*(t, \alpha, \theta, v, m) = \lambda(t, \alpha, \theta, v, m) I_B(\alpha, \theta) I_Q(m, \beta(\alpha, \theta), v),$$

where $Q = \{(m, \beta, v) : m \geq \psi^*(\beta, v)\}$.

Let $\{N^*(C), C \subset S\}$ be the corresponding point process with intensity λ^*. $N^*(C)$ counts the number of meteoroids with characteristics in C which are feasible (no blocking) and which penetrate the surface A^*. Let $C^* = \{(t, \alpha, \theta, v, m) \in S : t \leq T\}$ then $N^*(C^*)$ counts the number of penetrations of A^* during time span T and the probability of no such penetrations is

$$P(N^*(C^*) = 0) = \exp(-\mu(C^*)),$$

where

$$\mu(C^*) = \int_{C^*} \lambda^*(t, \alpha, \theta, v, m) d(t, \alpha, \theta, v, m)$$

$$= T \int\int_{B} \int_0^\infty \frac{1}{2\pi} \frac{\sin(\alpha)}{2} q(v) \overline{H}(\psi^*(\beta, v)) \lambda_0(\beta) \, dv \, d\alpha \, d\theta$$

$$= T \, |A^*| \int\int_{B} \int_0^\infty \frac{\sin(\alpha)}{4\pi} [\cos(\beta)]^+ F_{sp-Met}(\psi^*(\beta, v)) q(v) dv d\alpha d\theta =: \lambda^* T$$

which reduces to

$$\mu(C^*) = T|A^*| \int_0^\pi \int_0^\infty \frac{1}{2} \sin(\alpha) \, [\cos(\alpha)]^+ F_{sp-Met}(\psi^*(\alpha, v)) q(v) dv d\alpha$$

when $B = B_0$, i.e. when there is no shadow effect. Here again use was made of the isotropy when changing from β to α in the above integration. Hence $\exp(-\lambda^* T)$ represents the probability of no penetration of A^* by meteoroids during the time span T.

Probability Model for Penetration by Orbital Debris

Consider a specific surface element A of the space station that may be hit by orbiting debris (i.e. is not in the shadow of other parts of the space station). Using the notation introduced in the section on orbital debris flux recall that the relative velocity vector $\mathbf{v}_{DS}$ of a debris particle forms an angle θ with the space station flight direction and has relative impact velocity $v(\theta) = |\mathbf{v}_{DS}| = 2v_0 \cos(\theta)$. Further, the angle $\beta(\theta)$ that the incident debris particle forms with the normal vector of the surface element has cosine

$$\cos(\beta(\theta)) = \sin(\psi) \, \cos(\theta - \phi) \, .$$

As in the previous section it seems reasonable to model the succession of debris particles that will hit A as a random process. Again it is appropriate to model the arrival process of the particles as a homogeneous Poisson process with some intensity λ.

Depending on the velocity $v(\theta)$, impact angle $\beta(\theta)$ and size (diameter) of the particle it may also penetrate the surface element A. Since the objective is to derive a formula for the probability of no penetration it is necessary to model not only the arrival process of the particles but also their concomitant impact angles $\beta(\theta)$, velocity $v(\theta)$ and diameter D. Equivalently one may track the angle θ and diameter D for each arriving particle. This leads again to a so called marked Poisson process as the appropriate vehicle for analysis.

Before going into the probabilistic description of this process let us discuss the characteristics of the incident particles. The i^{th} incident particle arrives at time W_i, has diameter D_i and its relative velocity vector forms angle θ_i with the flight direction of the space station. Here the characteristics (D_i, θ_i) may reasonably be considered as independent and identically distributed random vectors. Within each such vector it is further reasonable to assume that D_i and θ_i are statistically independent of each other with respective densities $h(d)$ and $w(\theta)$. The density $w(\theta)$ can be assumed as given explicitly whereas the density $h(d)$ is given only indirectly through the flux quantity $F_{Deb}(d)$.

Also given is the critical penetration diameter as a function of $v = v(\theta)$ and $\beta = \beta(\theta)$, i.e.

$$D_{crit} = \psi(v, \beta),$$

so that the i^{th} incident particle penetrates A if and only if $D_i \geq \psi(v(\theta_i), \beta(\theta_i))$ and $0 \leq \beta(\theta_i) \leq \pi/2$. The latter inequality expresses the fact that the particle must hit the outside of the surface.

The probabilistic structure of the marked Poisson process is specified through an intensity function λ. Here λ is a function defined on a subset S of R^3 with values in $[0, \infty)$. For the application at hand the following specification is appropriate:

$$\lambda(t, \theta, d) = \lambda_0(\theta) I_{[0,\infty)}(t) w(\theta) h(d) \ .$$

Here $S = [0, \infty) \times [-\pi/2, \pi/2] \times [0, \infty)$ and t is the time variable referring to the arrival times of the particles. Note that $w(\theta)$ and $h(d)$ appear individually factored which reflects the previously discussed independence of the characteristics θ and D. The factor $\lambda_0(\theta)$ models the arrival time intensity of the Poisson process as a function of θ. This takes into account the fact that the surface element A only exposes a fraction of its outside surface perpendicularly to the stream of particles coming in at angle θ.

The marked Poisson process with intensity λ is a point process $\{N(C) : C \subset S\}$ such that

- $N(C)$ has a Poisson distribution with mean

  $$\mu(C) = \int_C \lambda(t, \theta, d) d(t, \theta, d)$$

  and

- for any k and for disjoint $C_1, \ldots, C_k \subset S$ the random variables $N(C_1), \ldots, N(C_k)$ are independent.

Here $N(C)$ represents the random number of incident debris particles with characteristics (t, θ, d) in C.

In order to establish the relationship between $h(d)$ and $F_{D_{eb}}(d)$ consider the following set C_0 of characteristics:

$$C_0 = \{(t, \theta, d) \in S : t \leq T, \theta \in [\theta_0, \theta_0 + \Delta], d \geq d_0\},$$

then $N(C_0)$ represents the random number of incident debris particles which are counted during time span T, which have diameter $\geq d_0$ and which have angle $\theta \in [\theta_0, \theta_0 + \Delta]$. Then the expected or average value of $N(C_0)$ is

$$E(N(C_0)) = \mu(C_0) = T \int_{d_0}^{\infty} h(x)\, dx \int_{\theta_0}^{\theta_0+\Delta} \lambda_0(\theta)\, w(\theta)\, d\theta$$

$$\approx T\, \overline{H}(d_0)\, \lambda_0(\theta_0)\, w(\theta_0)\, \Delta$$

where $H(d) = 1 - \overline{H}(d)$ is the cumulative distribution function of h.

On the other hand the average number of debris particles of diameter $\geq d_0$ that hit A with incidence angle $\theta \in [\theta_0, \theta_0 + \Delta]$ during time span T is

$$\Delta\, w(\theta_0) F_{D_{eb}}(d_0)\, T\, |A|\, [\cos\beta(\theta_0)]^+,$$

where $|A|\, [\cos\beta(\theta_0)]^+$ is the projection of the area A onto the plane perpendicular to the direction $\beta(\theta_0)$. That projection is the effective area that the debris particles will pass perpendicularly when they hit A at angle $\beta(\theta_0)$. The factor $\Delta\, w(\theta_0)$ indicates that only that part of the flux is operative at the angles $\theta \in [\theta_0, \theta_0 + \Delta]$.

Combining the two previous equations yields

$$\overline{H}(d_0)\, \lambda_0(\theta_0) = F_{D_{eb}}(d_0)\, |A|\, [\cos\beta(\theta_0)]^+.$$

Differentiating this with respect to d_0 would yield a corresponding relationship for h.

With the above marked Poisson process in place the following filtered marked Poisson process is the natural vehicle for finding the probability of no penetration. For this purpose define the derived or filtered intensity:

$$\lambda^*(t, \theta, d) = \lambda(t, \theta, d) I_Q(d, \theta)\, I_B(\theta)\,,$$

where $Q = \{(d,\theta) : d \geq \psi(v(\theta),\beta(\theta))\}$ and B is some subset of $[-\pi/2,\pi/2]$ indicating those directions θ against which the surface element A is not shielded.

Let $\{N^*(C), C \subset S\}$ be the corresponding point process with intensity λ^*. $N^*(C)$ counts the number of debris particles with characteristics in C which penetrate the surface element A. Let $C^* = \{(t,\theta,d) \in S : t \leq T\}$ then $N^*(C^*)$ counts the number of penetrations of A during time span T and the probability of no such penetrations is

$$P(N^*(C^*) = 0) = \exp(-\mu(C^*)),$$

where

$$\begin{aligned}\mu(C^*) &= \int_{C^*} \lambda^*(t,\theta,d)d(t,\theta,d)\\ &= \int_0^T \int_0^\infty \int_B \lambda_0(\theta)w(\theta)h(x)I_Q(x,\theta)d\theta dx dt\\ &= T\int_B \overline{H}(\psi(v(\theta),\beta(\theta)))\lambda_0(\theta)w(\theta)d\theta\\ &= T|A|\int_B F_{Deb}(\psi(v(\theta),\beta(\theta)))[\cos\beta(\theta)]^+ w(\theta)d\theta =: \lambda T.\end{aligned}$$

Hence $\exp(-\lambda T)$ represents the probability of no penetration of A by debris particles during time span T.

Combined Probability of no Penetration

Suppose the vulnerable surface area of the space station (SS) can be decomposed into surface elements $A_1, \ldots, A_m$ when dealing with the threat of orbital debris and into surface elements $A_1^*, \ldots, A_k^*$ when dealing with the threat of meteoroids.

The probability of no penetration of area A_i (A_i^*) by orbital debris (meteoroids) during time span T was given by $\exp(-\lambda_i T)$ ($\exp(-\lambda_i^* T)$). Computational formulae for the factors λ_i and λ_i^* were given in the previous two sections.

It is reasonable to assume that the random arrival processes of debris particles and meteoroids are independent of each other and that in addition the arrival processes corresponding to the different surface elements are independent of each other.

These independence assumptions then yield the following combined probability of no penetration for the entire space station by either orbital debris or meteoroids during the time span T:

$$
\begin{aligned}
&P(\text{no penetration of space station}) \\
&= P(\text{no penetration of SS by orbital debris}) \\
&\qquad \times P(\text{no penetration of SS by meteoroids}) \\
&= \prod_{i=1}^{m} P(\text{no penetration of } A_i \text{ by orbital debris}) \\
&\qquad \times \prod_{j=1}^{k} P(\text{no penetration of } A_j^* \text{ by meteoroids}) \\
&= \prod_{i=1}^{m} \exp(-\lambda_i T) \prod_{j=1}^{k} \exp(-\lambda_j^* T) = \exp(-T(\sum_{i=1}^{m} \lambda_i + \sum_{j=1}^{k} \lambda_j^*)).
\end{aligned}
$$

References

[1] "Space Station Program Definition and Requirements, Section 3 – Space Station Systems Requirements, Appendix 3.1: Natural Environment Definition for Design," JSC 30000, 1986.

[2] H.M. Taylor and S. Karlin (1981), *A Second Course in Stochastic Processes*, Academic Press, New York.

[3] H.M. Taylor and S. Karlin (1984), *An Introduction to Stochastic Modeling*, Academic Press, Orlando, Florida.

Appendix H - Sensitivity Analyses From Linear Regression Penetration Function

The following figures demonstrate how the critical projectile diameter line (the graphical penetration function representation) varies with variation in shield and backwall thickness. The approach to linear regression to develop a penetration function is described in section 4.0. Cases *with* and *without* MLI are included for 0-deg, 45-deg, and 65-deg incidence angles. The penetration function slope is correlated with incidence angle: 0-deg angles producing positive slopes, 45-deg angles producing nearly zero slopes, and 65-deg angles producing negative slopes. In general thicker shields and backwalls raise the penetration function.

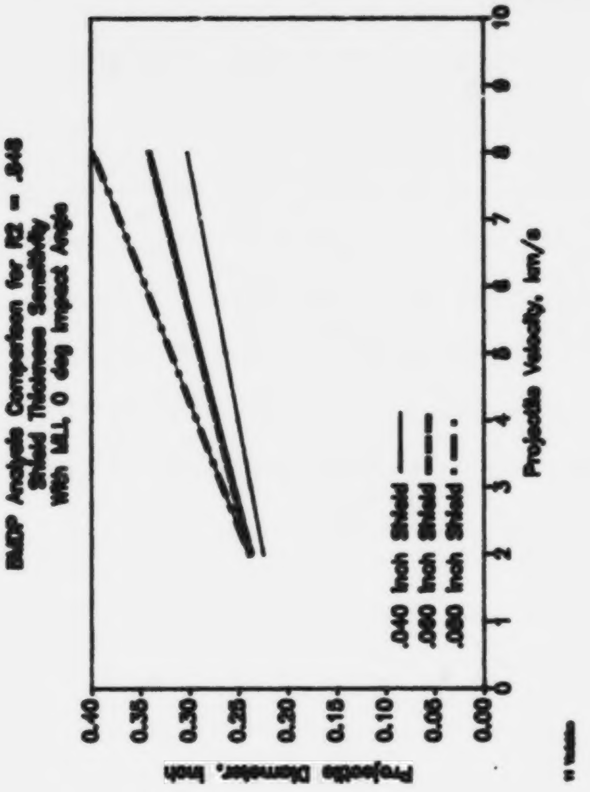
BMDP Analysis Comparison for R2 = .848
Shield Thickness Sensitivity
With MLI, 0 deg Impact Angle
.040 Inch Shield
.060 Inch Shield
.080 Inch Shield
Projectile Diameter, inch
Projectile Velocity, km/s
0.00
0.05
0.10
0.15
0.20
0.25
0.30
0.35
0.40
0
1
2
3
4
5
6
7
8
9
10

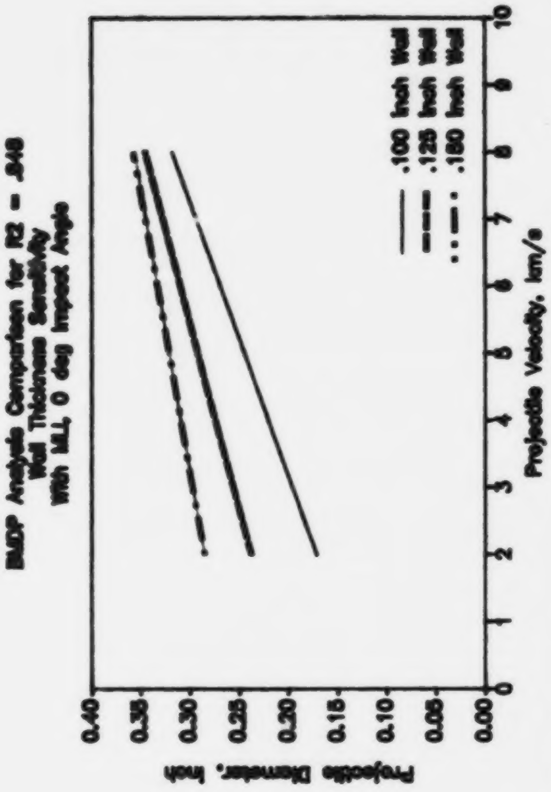
BMDP Analysis Comparison for R2 = .848
Wall Thickness Sensitivity
With MLI, 0 deg Impact Angle
.100 Inch Wall
.125 Inch Wall
.150 Inch Wall
Projectile Diameter, inch
Projectile Velocity, km/s
0.00
0.05
0.10
0.15
0.20
0.25
0.30
0.35
0.40
0
1
2
3
4
5
6
7
8
9
10

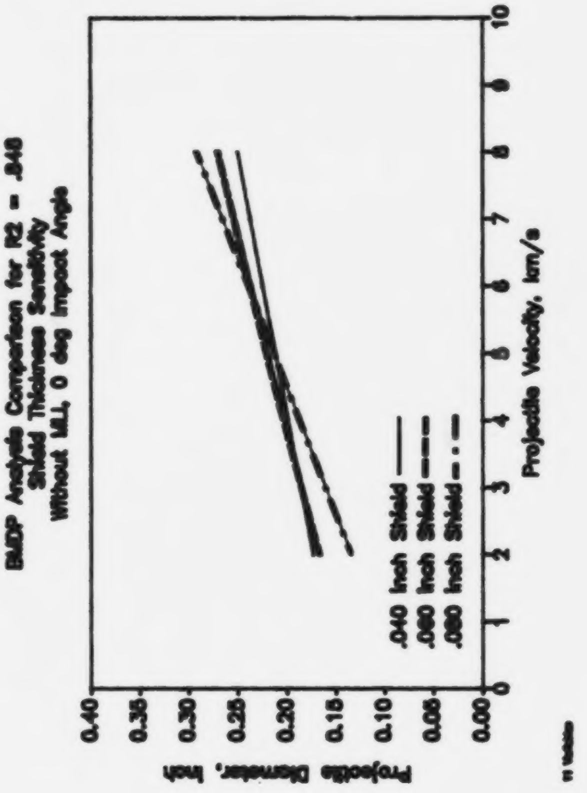
BMDP Analysis Comparison for R2 = .848
Shield Thickness Sensitivity
Without MLI, 0 deg Impact Angle
.040 Inch Shield
.060 Inch Shield
.080 Inch Shield
Projectile Diameter, inch
Projectile Velocity, km/s
0.00
0.05
0.10
0.15
0.20
0.25
0.30
0.35
0.40
0
1
2
3
4
5
6
7
8
9
10

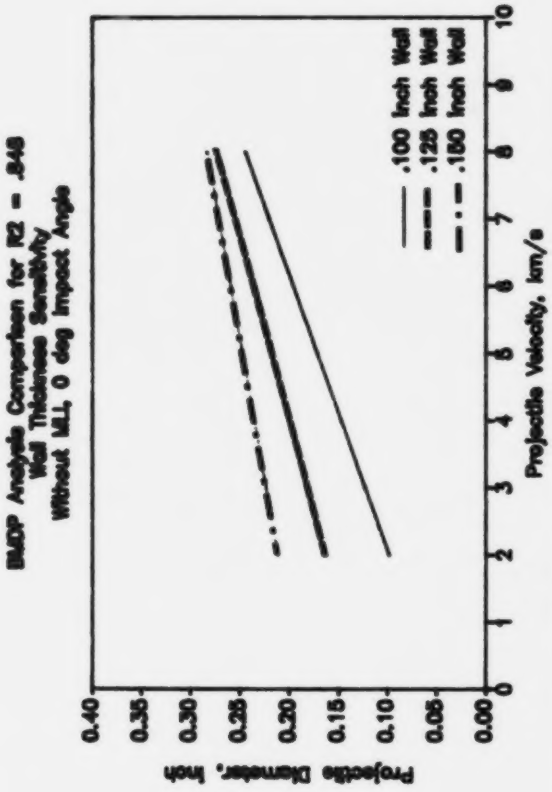
BMDP Analysis Comparison for R2 = .848
Wall Thickness Sensitivity
Without MLI, 0 deg Impact Angle
.100 Inch Wall
.125 Inch Wall
.150 Inch Wall
Projectile Diameter, inch
Projectile Velocity, km/s
0.00
0.05
0.10
0.15
0.20
0.25
0.30
0.35
0.40
0
1
2
3
4
5
6
7
8
9
10

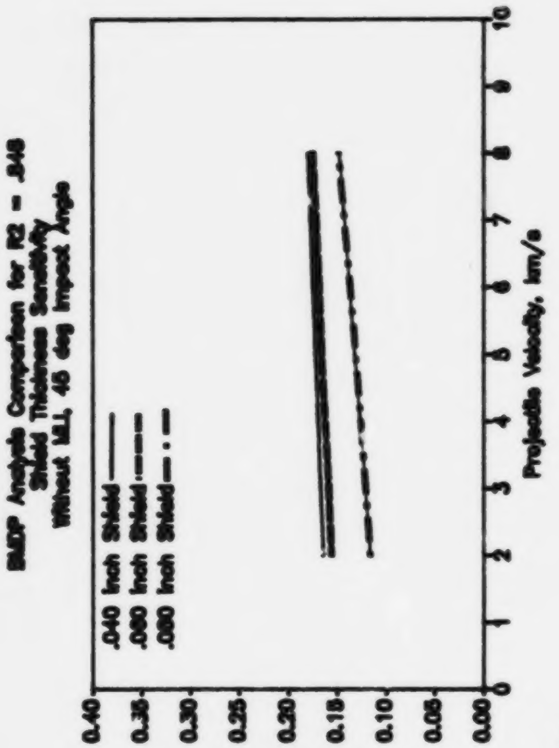

BMDP Analysis Comparison for R2 = .848
Shield Thickness Sensitivity
Without MLI, 45 deg Impact Angle
.040 Inch Shield
.060 Inch Shield
.080 Inch Shield
Projectile Diameter, inch
0.00
0.05
0.10
0.15
0.20
0.25
0.30
0.35
0.40
Projectile Velocity, km/s
0
1
2
3
4
5
6
7
8
9
10

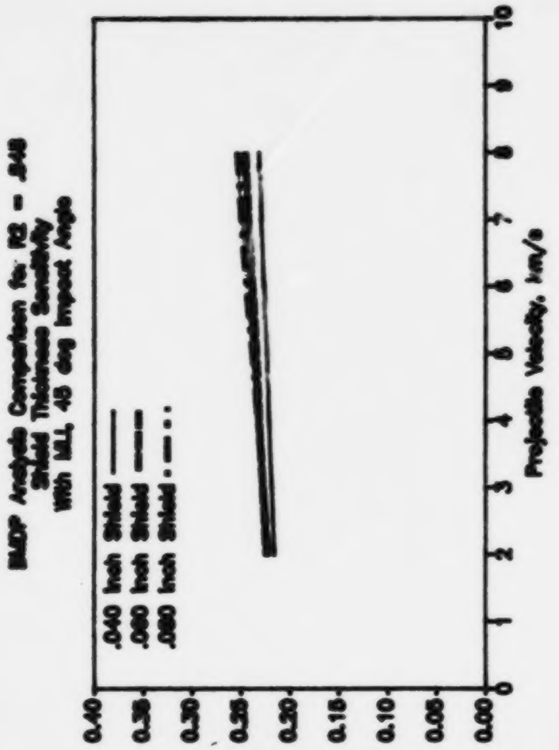

BMDP Analysis Comparison for R2 = .848
Shield Thickness Sensitivity
With MLI, 45 deg Impact Angle
.040 Inch Shield
.060 Inch Shield
.080 Inch Shield
Projectile Diameter, inch
0.00
0.05
0.10
0.15
0.20
0.25
0.30
0.35
0.40
Projectile Velocity, km/s
0
1
2
3
4
5
6
7
8
9
10

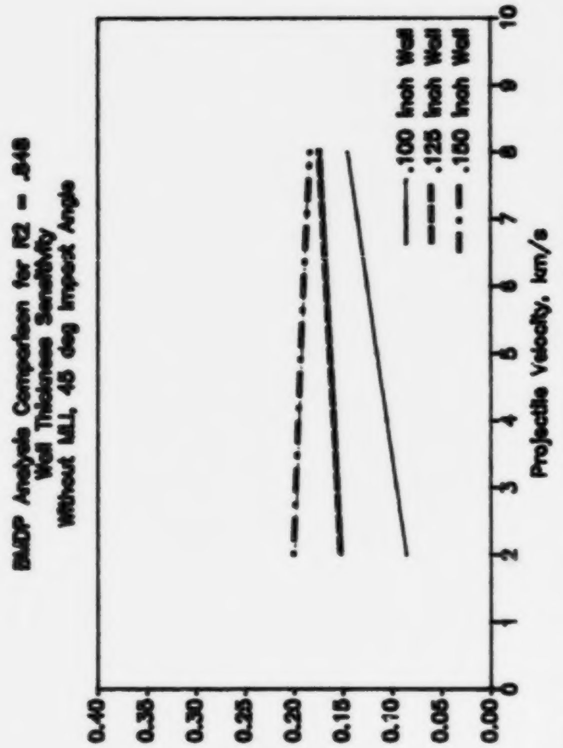

BMDP Analysis Comparison for R2 = .848
Wall Thickness Sensitivity
Without MLI, 45 deg Impact Angle
.100 Inch Wall
.125 Inch Wall
.150 Inch Wall
Projectile Diameter, inch
0.00
0.05
0.10
0.15
0.20
0.25
0.30
0.35
0.40
Projectile Velocity, km/s
0
1
2
3
4
5
6
7
8
9
10

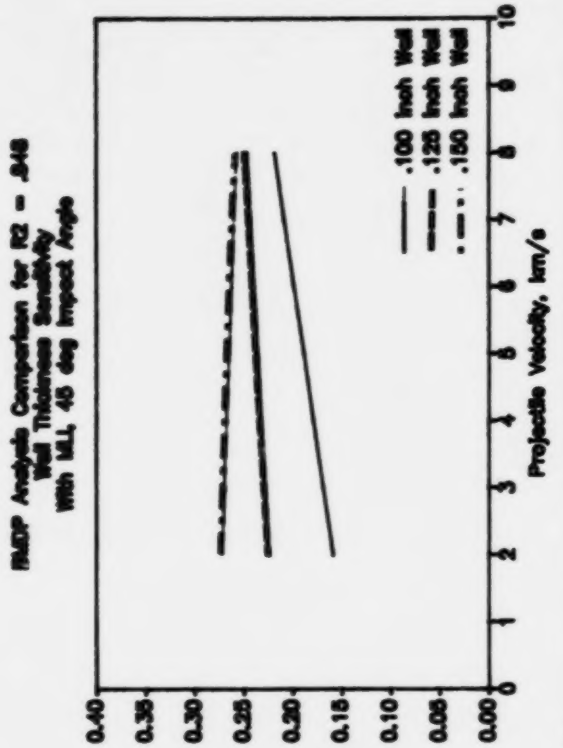

BMDP Analysis Comparison for R2 = .848
Wall Thickness Sensitivity
With MLI, 45 deg Impact Angle
.100 Inch Wall
.125 Inch Wall
.150 Inch Wall
Projectile Diameter, inch
0.00
0.05
0.10
0.15
0.20
0.25
0.30
0.35
0.40
Projectile Velocity, km/s
0
1
2
3
4
5
6
7
8
9
10

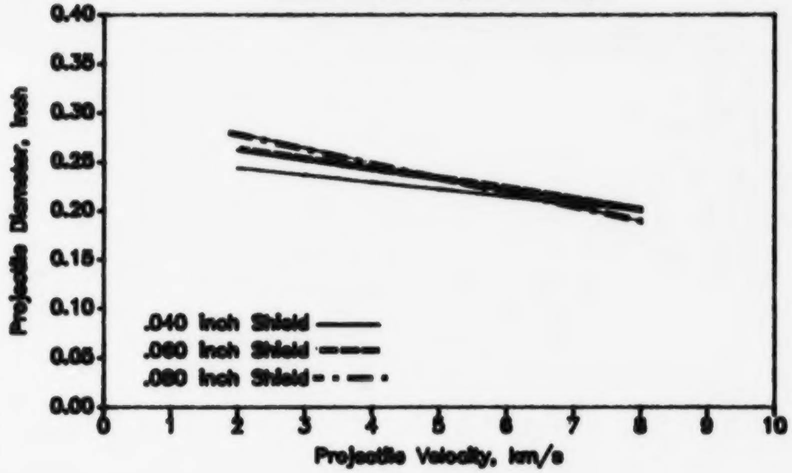

BMDP Analysis Comparison for R2 = .848
Shield Thickness Sensitivity
Without MLI, 65 deg Impact Angle

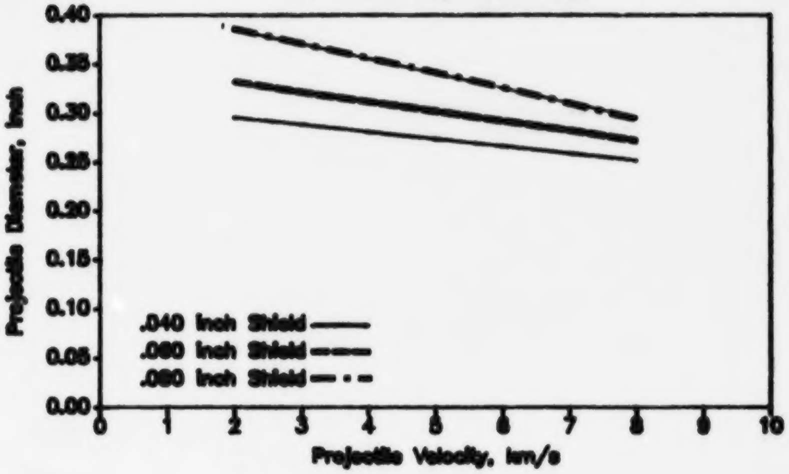

BMDP Analysis Comparison for R2 = .848
Shield Thickness Sensitivity
With MLI, 65 deg Impact Angle

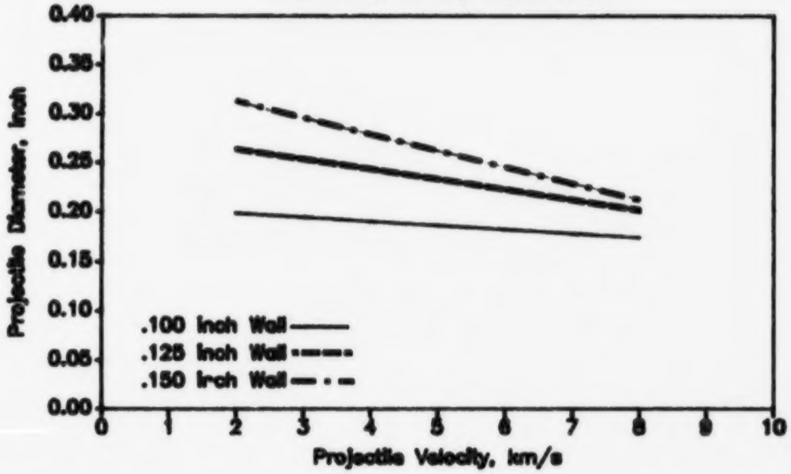

BMDP Analysis Comparison for R2 = .848
Wall Thickness Sensitivity
Without MLI, 65 deg Impact Angle

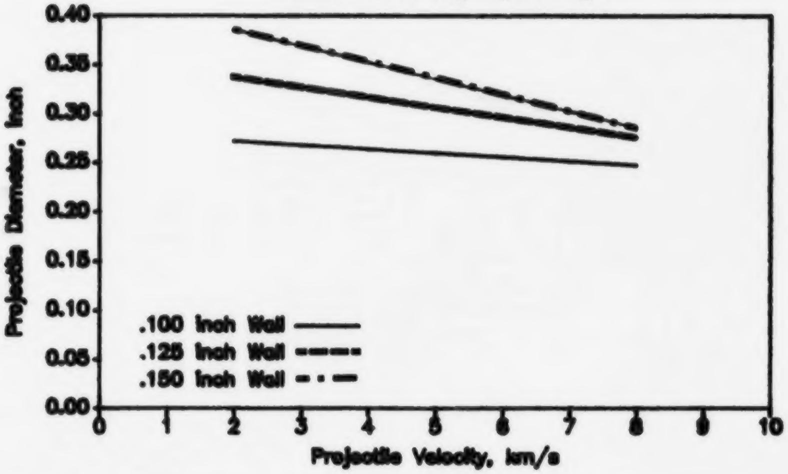

BMDP Analysis Comparison for R2 = .848
Wall Thickness Sensitivity
Without MLI, 65 deg Impact Angle

Appendix I - Physiological Significance of Sound and Noise Data

The following report represents the primary analysis for the Task 2 Effects of Penetration test program.

6 April 1987
2-3755-DHR

To:	Paul Stern	2-3600	8C-72
cc:	Alex Coronado	2-3614	82-97
	R. L. Olson	2-3755	8K-03

Subj: Physiological Significance of Sound and Noise Data from MSFC/Boeing Space Station Penetration Tests

References:
[1] "The Physiological Basis for Spacecraft Environmental Limits", NASA-RP-1045, 1979.
[2] "Bioastronautics Data Book", NASA-SP-3006, 2nd ed., 1973.
[3] "Fundamentals of Aerospace Medicine", ed. by R. L. DeHart, Lea & Febiger, Philadelphia, 1985.
[4] "Aerospace Medicine", ed. by H. G. Armstrong, Williams & Wilkins, Baltimore, 1961.
[5] "Space Physiology and Medicine", NASA-SP-447, 1982.
[6] "Life Sciences Considerations for Long Duration Manned Space Missions", vol. 1, NASA-TM-83093, 1984.
[7] Data from Subject MSFC Tests received from A. Coronado

Enclosures:
[a] Damage Risk Criterion (DRC) for Impulse Noise
[b] Luminance under varying conditions of illumination
[c] Range of luminance for visual performance
[d] The electromagnetic spectrum

SUMMARY:

NOISE -- Impulse noises on the order of 170 dB can be expected to cause a Temporary Threshold Shift (TTS) on the order of 20-25 dB in exposed individuals. This is an "auditory effect". Non-auditory physiological effects may also occur (gagging; respiratory cycle changes; visual disturbanceds; psychological effects). If the noise waveform were to persist for over 1 second and exceed 5 psig ("blast"), eardrum rupture with TTS could occur. It is expected that the fully outfitted Space Station will afford considerable sound attentuation to the penetrating object producing impulse noise.

LIGHT FLASH -- The light flash raw data appear to exceed the upper limit of visual tolerance for luminance (10^4 to 10^5 millilamberts), since most of these data were in that range. However, this physiologist feels that the attenuation afforded by the Space Station environment and the probability of such a phenomenon being directly viewed by a Space Station occupant reduces the significance of the quantitative flash intensities recorded during some of the penetration tests [7].

NOISE DATA INTERPRETATION:

Of the 24 "shot total #s" in sequence from 471-496, 15 reported data in decibels (dB) from microphones 1 and/or 2 [7]. The dB readings ranged from 160 to 195 for mic2 with a mean of 174.69 dB. For mic1 the readings ranged from 154 to 179, mean 169.50 dB. Specific data are:

Shot Total	Mic 1	Mic 2	Duration, msec
471	162 dB	182 dB	
472	171	182	
474	165	165	
475	174	195 high value	
476	---	168	
477	154 low	185	
478	154 value	163	
479	168	160	
484	175	168	
487	177	173	
489	173	163	
491	179	---	
494	175	193	
495	171	174	
496	175	---	
15 Tests	169.50	174.69 dB	

Although the specific risetime-peaks for noise were not analyzed, all were in the milli- or micro-second range which would classify the sounds as "impulse" noise. Impulse noise is dangerous to the human auditory system when it exceeds 140 dB at a distance of less than 20 cm [2]. The mechanism of action of impulse noise is that it produces mechanical disturbance of the hair cells on the organ of Corti (respnsible for "transducing" sound waves), which can result in a Temporary Threshold Shift (TTS), or if persistent, Permanent Threshold Shift (PTS). Threshold shift means simply that the threshold of hearing is re-set to a higher level -- zero keeps moving up. For example, a 180 dB peak impulse results in approximately a 25 dB TTS; a 190 dB impulse in a 50 dB TTS. Threshold shifts due to impulse noises are auditory effects, meaning the effect is to the hearing apparatus. No useful NASA requirements data were found in NASA-STD-3000 (Man-Systems Integration Standards).

There may also be non-auditory effects of noise. Over 150 dB there may be reduced visual acuity; gag sensations and respiratory rhythm changes in addition to TTS.

"Damage Risk Criteria" (DRC) for impulse noise according to CHABA (Committee on Hearing and Bio-acoustics of NRC-NAS) is given in enclosure [a]. Some typical values of peak sound pressue levels for impulse noise from reference [2] are given below. (In most of these situations the impulse sound would be repeated many times rather than just once):

dB	Example
190+	Within blast zone of exploding bomb
160-180	Within crew area of heavy artillery piece
140-170	At shooter's ear when firing handgun
125-160	At child's ear when detonating toy cap
110-130	Construction site during pile-driving

In these tests we appear to be dealing with "impulse" rather than "blast" noise. The latter differs from the former in time duration -- blasts last longer than 1 second peak and may have more than one waveform peak. CHABA DRC states the blast exposure limit as:

5 psi (unprotected ear) to prevent eardrum rupture;
10 psi (protected ear) to prevent lung damage.

If the impulse noise reaching a Space Station crewperson's ear were to be on the order of 170 dB, there would definitely be a Temporary Threshold Shift (TTS) in the person's hearing, that is, temporary deafness for normal speech-level sound. There is also the possibility, depending upon the individual's proximity to the sound, of eardum rupture. (Eardum rupture is not necessarily a serious problem if it heals without inner ear infection developing. The eardrum rupture actually prevents more serious damage to the auditory apparatus of the inner ear).

Unlike these tests, it is expected that in operational Space Station there would be considerable (? dB) attenuation of any noise-producing penetrant from the equipment racks, etc. which will occupy the inside of the modules.

I conclude that even single impulse noises on the order of 170 dB will have definite audiological effects which, however, will not cause permanent deafness nor be life threatening.

LIGHT FLASH DATA INTERPRETATION:

Interpretation of the light intensity data of subject tests has proven less straightforward than for the noise data because of the difficulty converting mW/cm^2 to physiologically meaningful units and because of the great disparity in data recorded by the photodiodes within the test chamber ("L1 through L7"). The raw flash intensity data are:

Test #	Transducer #	mW/cm^2	mL*
471	L2	4.5	3,060
472	L3	190	129,200
	L6	217	147,560
473	No light flash data		
474	L3	54	36,720
	L5	21	14,280
475	L2	52+	35,360
	L6	200	136,000
476	L3	255	173,400

	L6	534	363,120
477	L2	31	21,080
	L5	27	18,360
478	L2	51+	34,680
	L4	44	29,920
	L5	53+	36,040
479	No light flash data		
480	L2	60+	40,800
481	No light flash data		
482	Page missing		
483	L1	25	17,000
	L2	52+	35,360
	L3	30	20,400
484	No light flash data		
485	"No penetration"		
487	L2	51+	34,680
	L4	141	95,880
	L6	98	66,640
488	L3	125	85,000
	L6	205	139,400
489	No light flash data		
490	L3	105	71,400
	L4	83	56,440
	L6	58	39,440
491	L3	320	217,600
	L6	650	442,000
492	No light flash data		
493	No light flash data		
494	L3	525	357,000
	L6	770	523,600
495	L3	375	255,000
	L6	970	659,600
496	L3	157	106,760
	L6	270	183,600

---

* mL = millilamberts, a unit of luminance -- these values were calculated by multiplying the mW/cm^2 data by 680. "Luminance is the photometric term corresponding to radiance and refers to the amount of visible light coming from an external surface which is illuminated or is self-luminous. Luminance is the product of the illumination falling on a surface and the luminous reflectance of the surface" [2].

Literature Review. The available literature were reviewed for information about flash light or "flashblindness". No absolute quantities were given at which reversible or permanent chorioretinal eye damage would be done so this determination was made by inference. No useful specifications/requirements data were found in NASA-STD-3000.

Regarding Flashblindness: Reference [2] states that "Momentary exposure to a very intense flash of light results in a loss of visual sensitivity which may take some time to be restored. Such exposures are likely to be accidental... Recovery time depends upon the intensity and duration of the flash... For any given task, recovery time can be shortened by increasing the task luminance in the period immediately following the flash."

Reference [3], in discussing nuclear flash protection, states that the "...potential dnager of flashblindness and chorioretinal burns resulting from viewing nuclear fireballs has now become a concern to aircrew members... During daylight, with a high ambient illumination and through a small pupillary diameter, the retinal burn and flashblindness problem is greatly diminished. At night, with a large pupil, protection is a must..."

Regarding tolerance to extremely bright light flashes: Reference [4] states that "At 10,000 feet, the intensity of light is 12,000 foot-candles and in space is about 13,600 ft-c. At these levels light is too intense for comfort." Reference [3] says that "the rays that concern us on earth are from 300-2100 nm in wavelength, with an intensity varying between 10,000 ft-c at ground level to about 13,000 ft-c at presently attainable altitudes." [1 foot-candle/ft-c is about 0.9 millilamberts].

The most helpful information in interpreting the subject data come from reference [3]: "The upper limit of tolerance for normal vision is between 10^4 and 10^5 log mL of luminance. This would be equivalent to staring at the sun or at the detonation of a nuclear weapon". [See enclosures b and c]

Significance of the light flash data: These data were reported to be within a wavelength range of 300-1100 nanometers (nm) which encompasses the visible light spectrum [enclosure d] and takes in some of the UV and IR wavelengths. With the exception of the value for L2 in shot #471, all of the light flashes tabulated above exceed the visual tolerance criteria just discussed and illustrated graphically in enclosure [b].

As with the impulse noises, I assume that in operational Space Station there will be significant attenuation of light flashes due to the equipment racks, etc., which will line the inside of the modules. It is probable that personnel would not be exposed to any light flash at all. However, IF an individual were exposed to such light intensities directly (looking in the direction of the penetrating object) and IF the ambient light level were low, it is probable that temporary "blindness" would occur and it is possible that retinal burns could occur. Given the expected environment within Space Station and the low probability (subjective) of a person gazing directly at such a flash causes me to conclude that such flashes would not permanently damage the visual apparatus of an individual and would not otherwise jeopardize "safety of flight".

Donald H. Reid

DONALD H. REID, Ph.D.
M/S 8K-03 773-0028

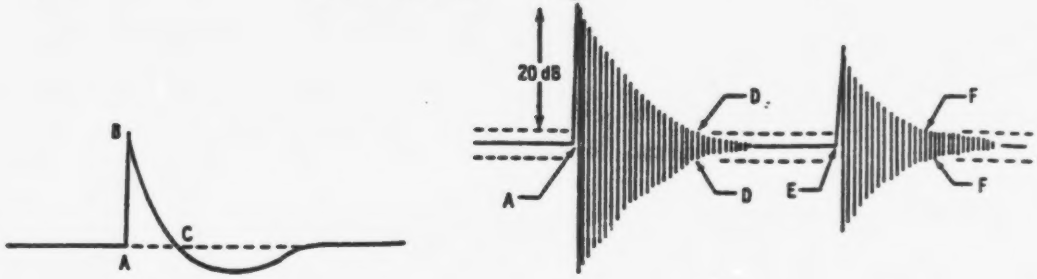

(a) Type A–duration.

(b) Type B–duration.

Impulse waveforms. See text for explanation.

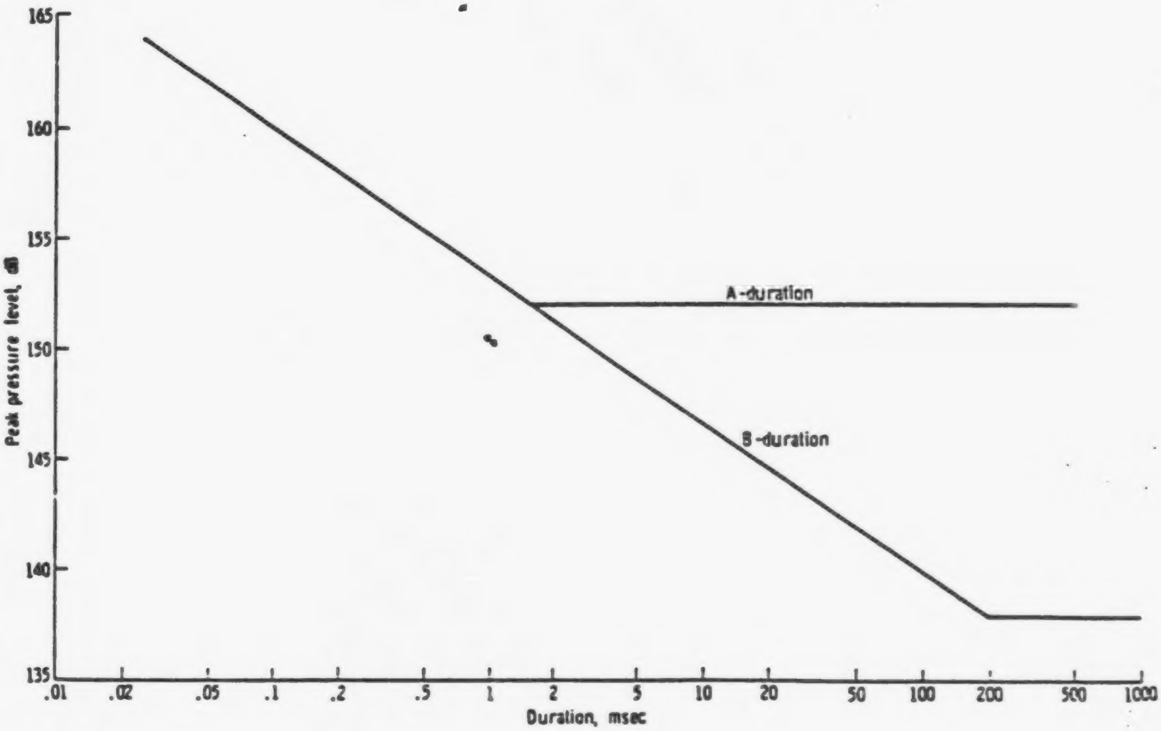

Damage risk criterion for impulse noise (gunfire); reference pressure is 2 × 10^{-5} N/m^2. See text for discussion.

Enclosure (a)

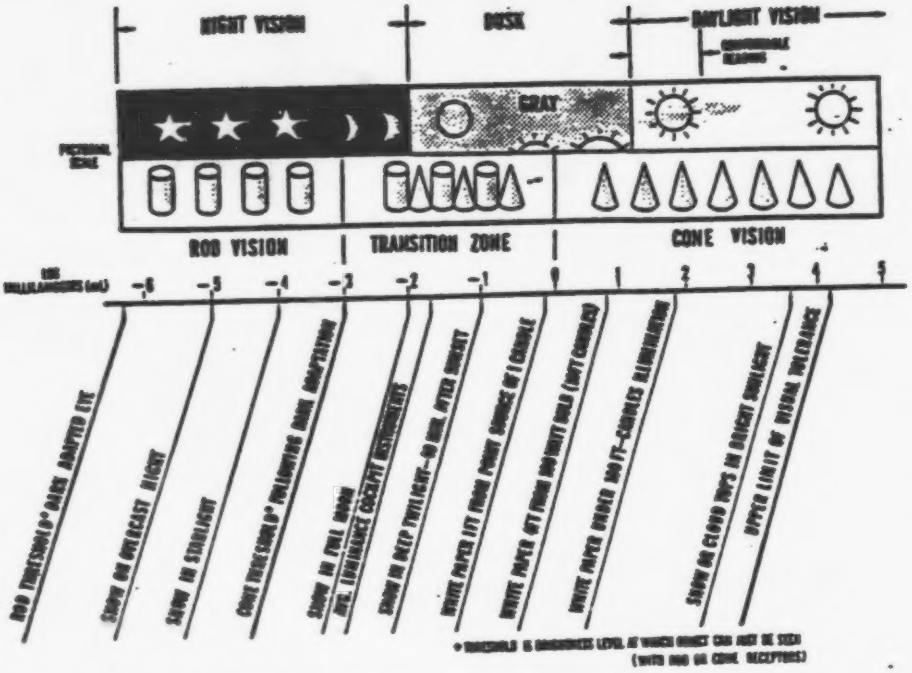
NIGHT VISION
DUSK
DAYLIGHT VISION
COMFORTABLE READING
PICTORIAL SCALE
GRAY
ROD VISION
TRANSITION ZONE
CONE VISION
LOG MILLILAMBERTS (mL)
−6
−5
−4
−3
−2
−1
0
1
2
3
4
5
ROD THRESHOLD* DARK ADAPTED EYE
SNOW ON OVERCAST NIGHT
SNOW IN STARLIGHT
CONE THRESHOLD* FOLLOWING DARK ADAPTATION
SNOW IN FULL MOON
AVE. LUMINANCE COCKPIT INSTRUMENTS
SNOW IN DEEP TWILIGHT—40 MIN. AFTER SUNSET
WHITE PAPER 1FT FROM POINT SOURCE OF 1 CANDLE
WHITE PAPER 1FT FROM 100 WATT BULB (100T CANDLES)
WHITE PAPER UNDER 500 FT-CANDLES ILLUMINATION
SNOW OR CLOUD TOPS IN BRIGHT SUNLIGHT
UPPER LIMIT OF VISUAL TOLERANCE
* THRESHOLD IS BRIGHTNESS LEVEL AT WHICH OBJECT CAN JUST BE SEEN
(WITH ROD OR CONE RECEPTORS)

Luminance under varying conditions of illumination.

Enclosure (b)

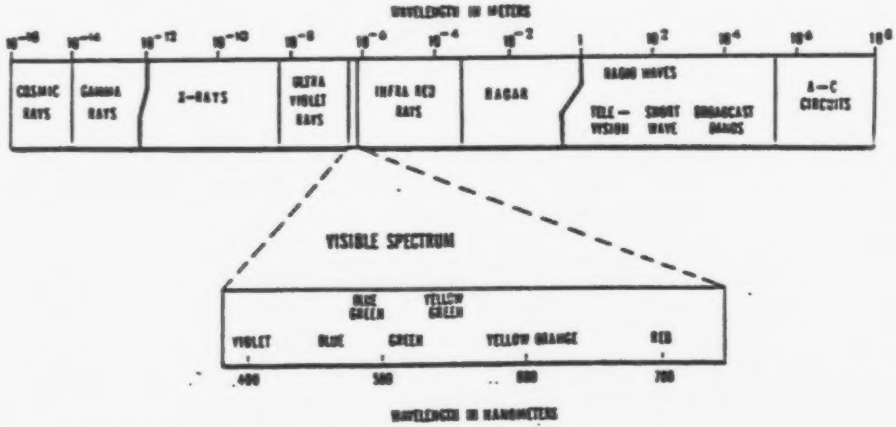
WAVELENGTH IN METERS
10^{-16}
10^{-14}
10^{-12}
10^{-10}
10^{-8}
10^{-6}
10^{-4}
10^{-2}
1
10^{2}
10^{4}
10^{6}
10^{8}
COSMIC RAYS
GAMMA RAYS
X-RAYS
ULTRA VIOLET RAYS
INFRA RED RAYS
RADAR
RADIO WAVES
TELE-VISION
SHORT WAVE
BROADCAST BANDS
A-C CIRCUITS
VISIBLE SPECTRUM
BLUE GREEN
YELLOW GREEN
VIOLET
BLUE
GREEN
YELLOW ORANGE
RED
400
500
600
700
WAVELENGTH IN NANOMETERS

The electromagnetic spectrum.

Enclosure (d)

ORIGINAL PAGE IS
OF POOR QUALITY

Range of Luminance for Visual Performance

	Luminance in mL	Object	Notes
1 x 10^9			
	7×10^8	Sun	Viewed from outside earth's atmosphere
	4.4×10^8	Sun	Viewed from the earth
1 x 10^8	8×10^7	A-Bomb	Fireball 4 miles from point of detonation of an 800 KT weapon.
1 x 10^7			
1 x 10^6			
1 x 10^5			
	1.38×10^4	Venus	Assume albedo (r) of 0.59 viewed from outside atmosphere
	9.4×10^3	Earth	Viewed from space with cloud cover ($r = 0.8$)
1 x 10^4	6.4×10^3	Mercury	Viewed from outside atmosphere ($r = 0.069$)
	4.3×10^3	Earth	Viewed in January from outside atmosphere, no clouds ($r = 0.39$)
	2.9×10^3	Jupiter	Viewed from outside atmosphere ($r = 0.56$)
	2×10^3	Sky	Average sky on clear day
	1.2×10^3	Moon	Full moon viewed from outside of atmosphere ($r = 0.073$)
1 x 10^3	9.6×10^2	Saturn	Viewed from outside atmosphere ($r = 0.63$)
	9×10^2	Mars	Viewed from outside atmosphere ($r = 0.15$)
	8×10^2	Moon	Full moon viewed from earth
	5×10^2	Sky	Average sky on cloudy day
	2.4×10^2	Uranus	Viewed from outside the earth ($r = 0.63$)
1 x 10^2	1.1×10^2	Neptune	Viewed from outside atmosphere ($r = 0.73$)
	2×10^1	White paper in good reading light	
	1.6×10^1	Movie screen (indoors)	
1 x 10	1×10^1	TV screen	
	7×10^0	Pluto	Viewed from outside the atmosphere
1 x 10^0	9×10^{-1}	Snow in light of full moon	
1 x 10^{-1}			
	2×10^{-2}	Lower limit for useful color vision	
1 x 10^{-2}	7.5×10^{-3}	Earth	Viewed from outside atmosphere with full moon
	1×10^{-3}	Upper limit for night vision	
1 x 10^{-3}			

mL = millilamberts

Enclosure (c)

Appendix J - Test Data Compared With Regression Function

Test data obtained under task 1 testing for aluminum sphere on aluminum plate impact is presented here plotted as projectile diameter versus projectile velocity. Also included in the plots is the regression derived penetration function (described in sec. 4.3) corresponding to the data points.

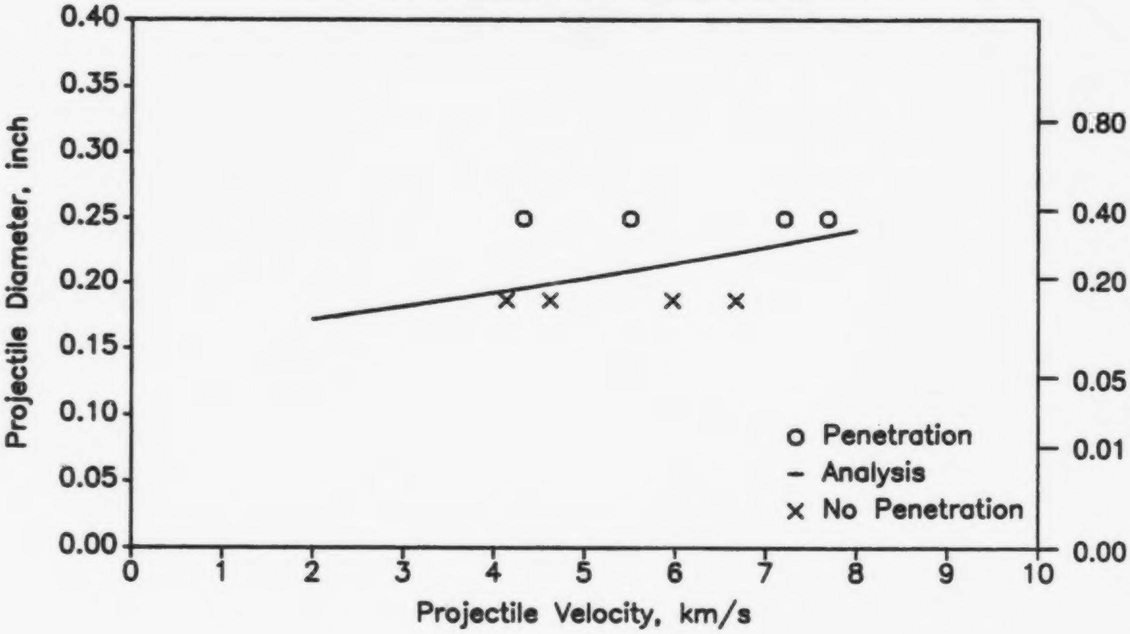

NAS8–36426 Task I Test Series 201
.040 inch Shield, .125 inch Wall
4 inch Spacing, MLI, 45 deg Angle

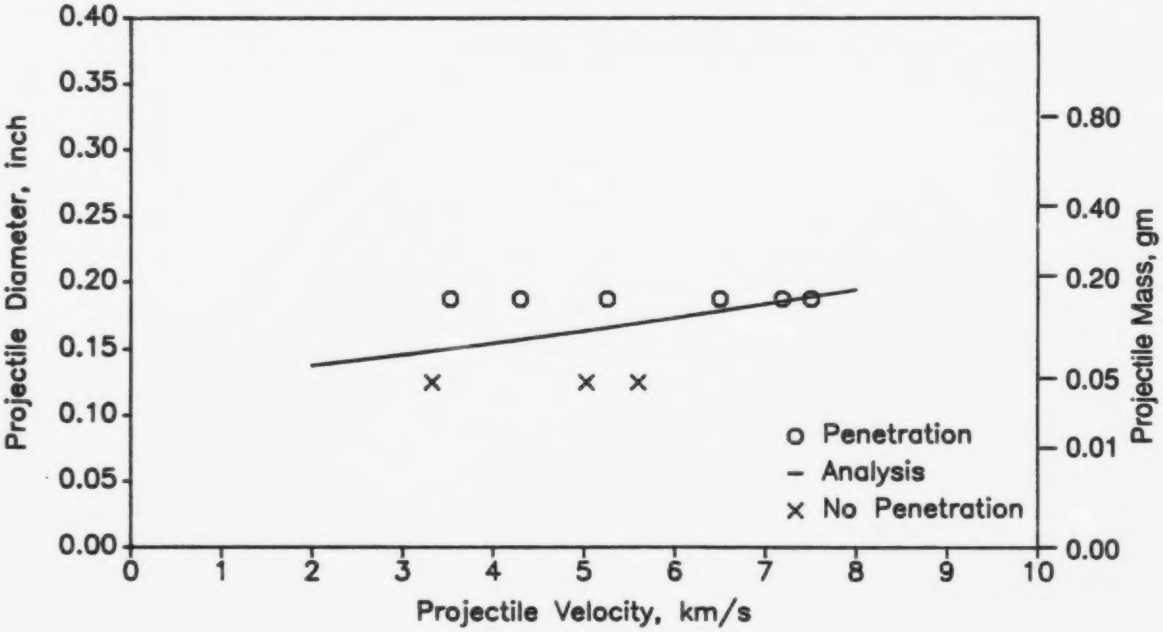

NAS8–36426 Task I Test Series 202
.040 inch Shield, .125 inch Wall
4 inch Spacing, No MLI, 45 deg Angle

1/28/87

NAS8−36426 Task I Test Series 203
.040 inch Shield, .125 inch Wall
4 inch Spacing, MLI, 65 deg Angle

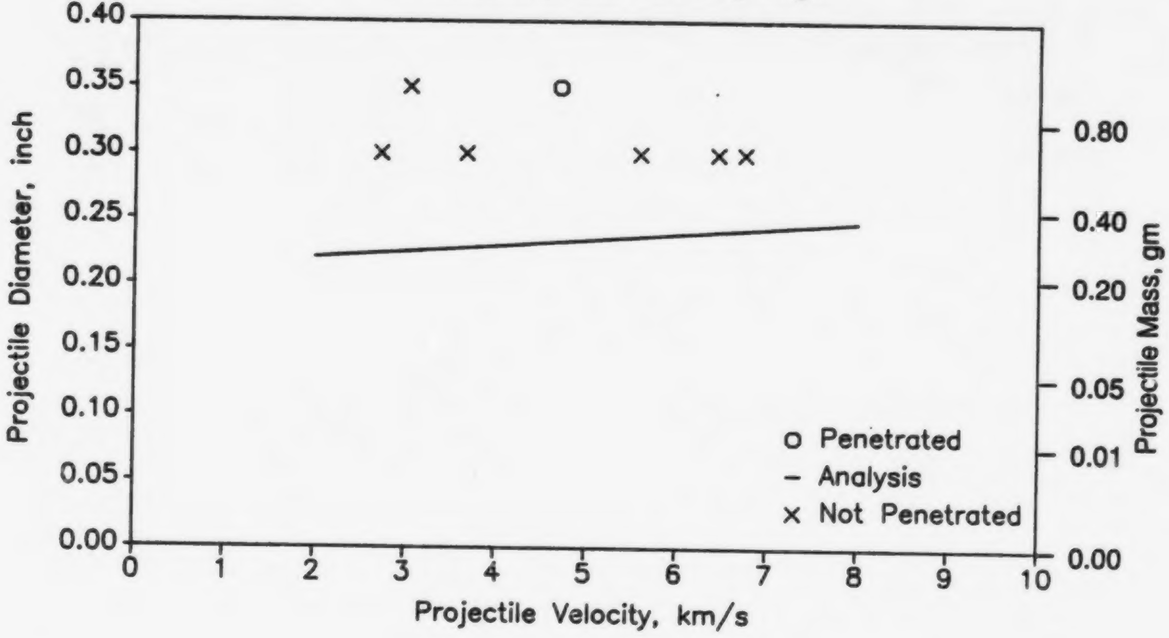

NAS8−36426 Task I Test Series 204
.040 inch Shield, .125 inch Wall
4 inch Spacing, No MLI, 65 deg Angle

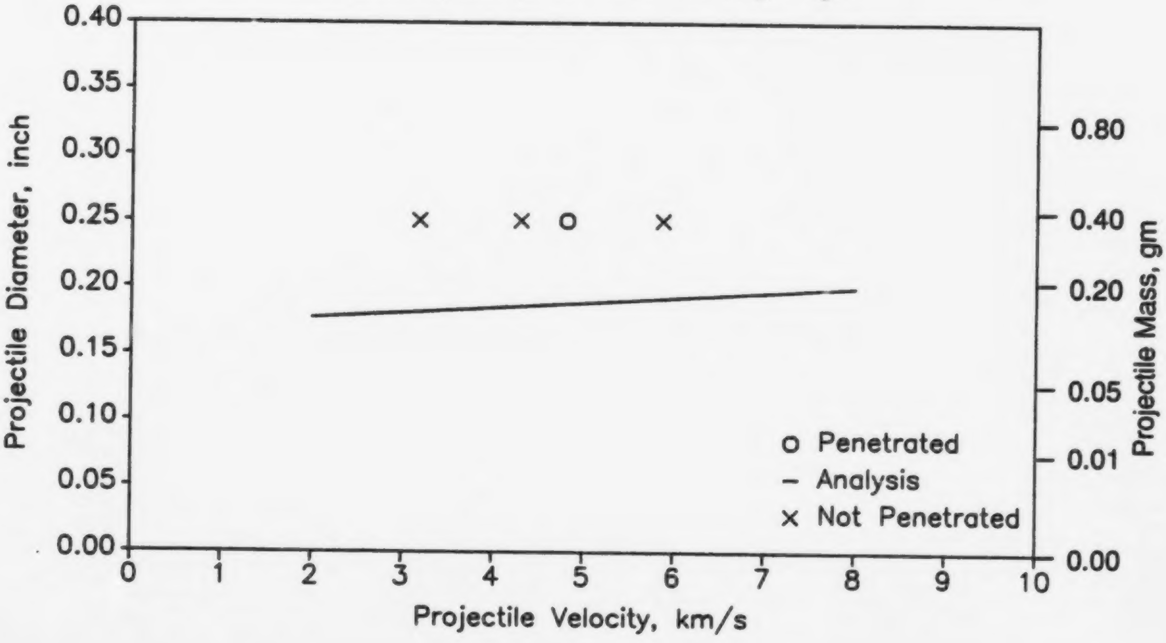

NAS8-36426 Task I Series 205
.063 inch Shield, .125 inch Wall
4 inch Spacing, MLI, 45 deg Angle

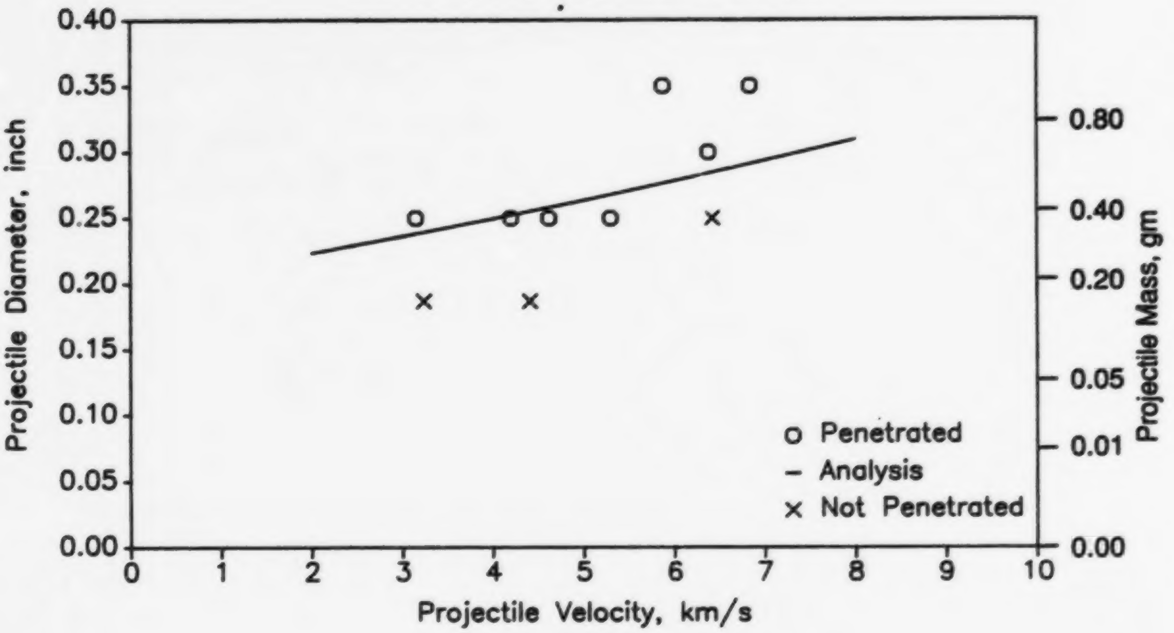

NAS8-36426 Task I Test Series 206
.063 inch Shield, .125 inch Wall
4 inch Spacing, No MLI, 45 deg Angle

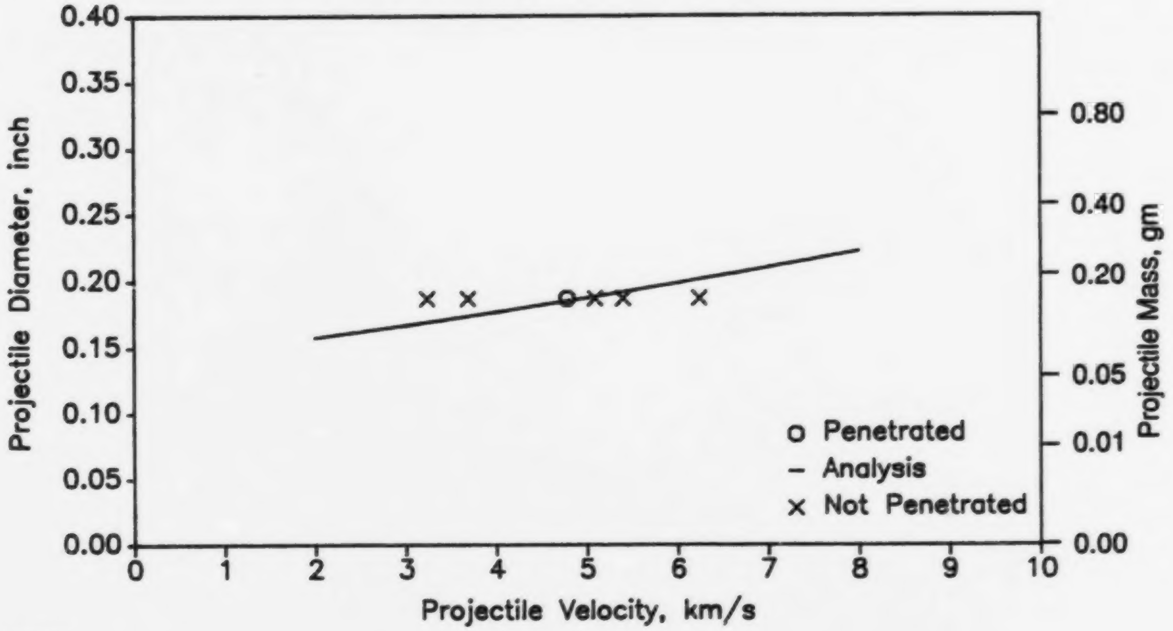

1/29/87

NAS8-36426 Task I Test Series 207
.063 inch Shield, .125 inch Wall
4 inch Spacing, MLI, 65 deg Angle

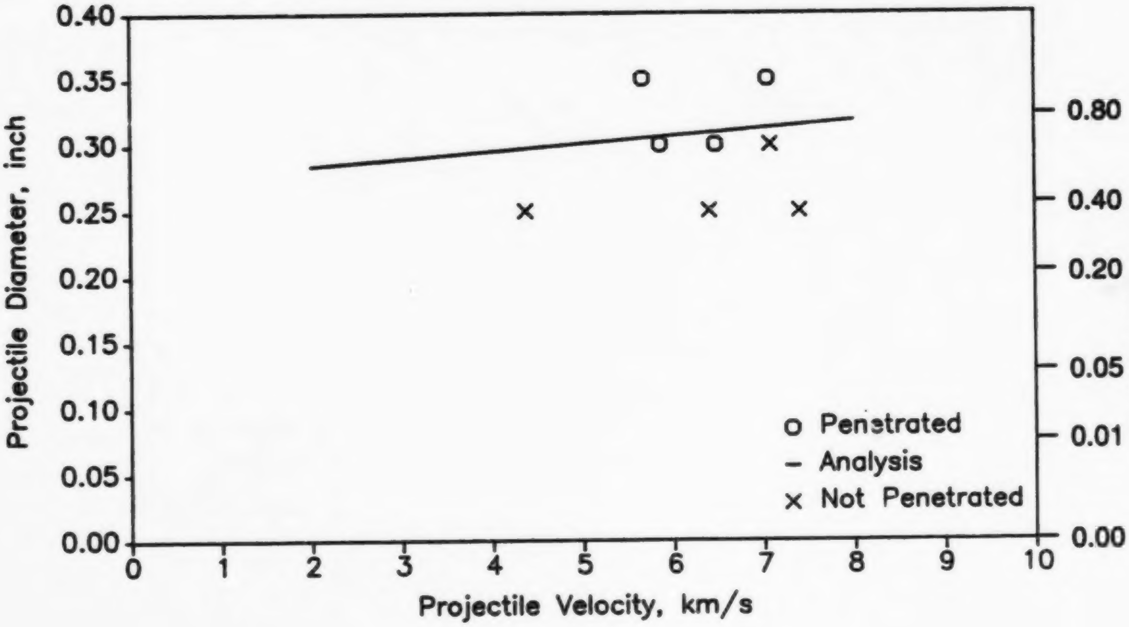

NAS8-36426 Task I Test Series 208
.063 inch Shield, .125 inch Wall
4 inch Spacing, No MLI, 65 deg Angle

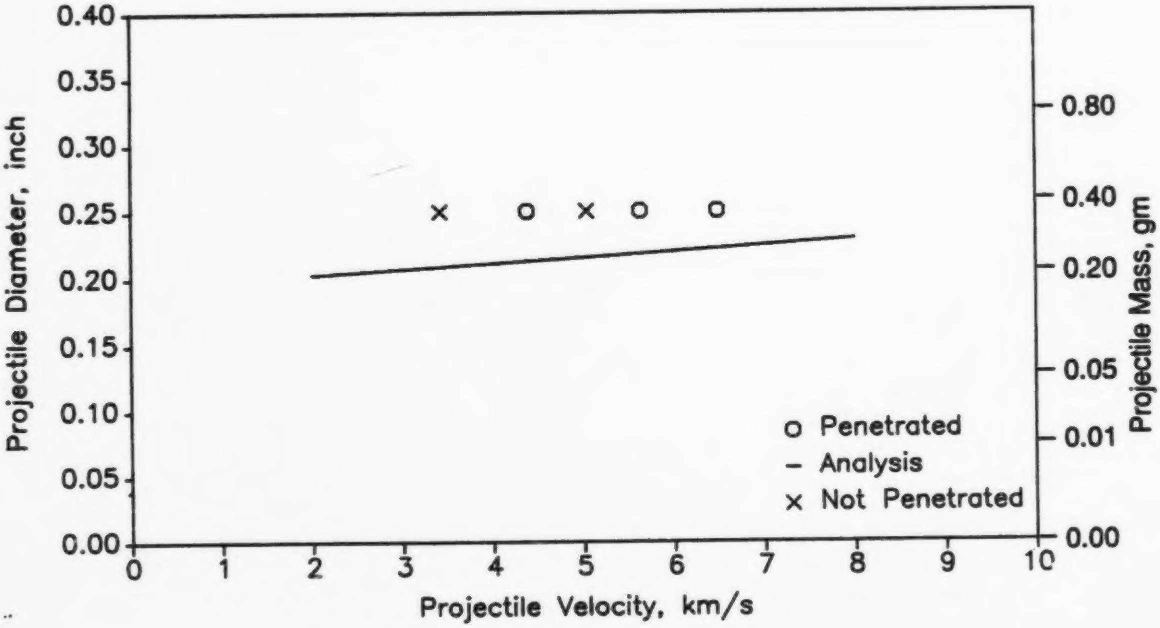

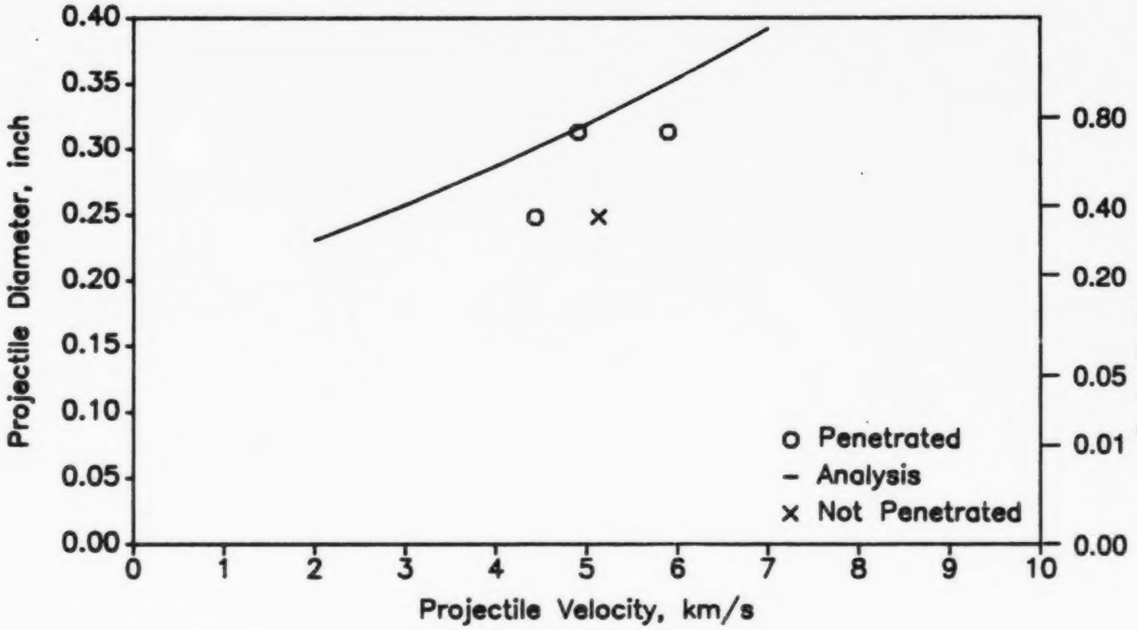

NAS8-36426 Task I Test Series 213
.080 inch Shield, .188 inch Wall
4 inch Spacing, No MLI, 0 deg Angle

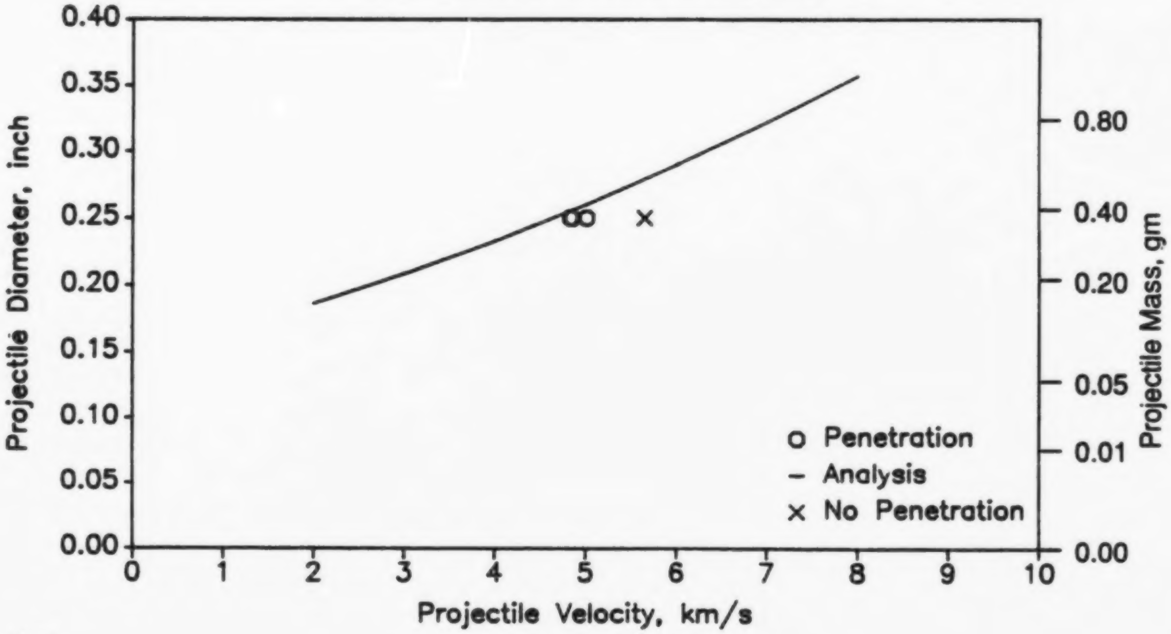

NAS8-36426 Task I Test Series 214
.040 inch Shield, .188 inch Wall
8 inch Spacing, No MLI, 0 deg Angle

NASB-36426 Task I Test Series 215
.040 inch Shield, .188 inch Wall
8 inch Spacing, MLI, 0 deg Angle

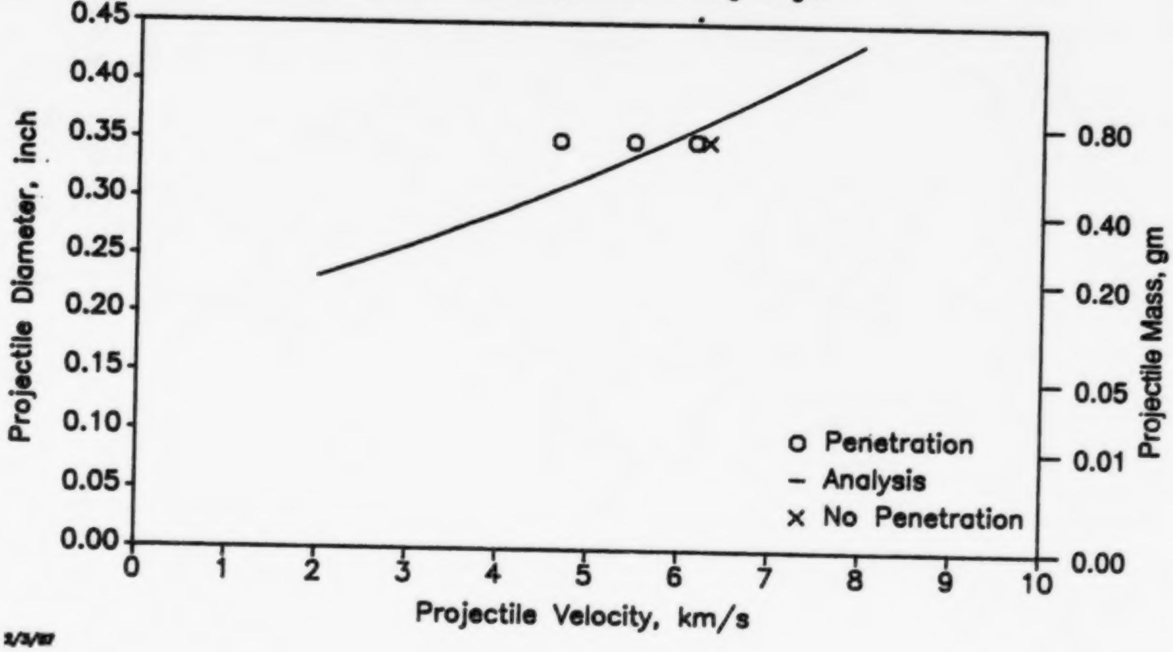

2/3/87

NASB-36426 Task I Test Series 216
.080 inch Shield, .188 inch Wall
4 inch Spacing, No MLI, 45 deg Angle

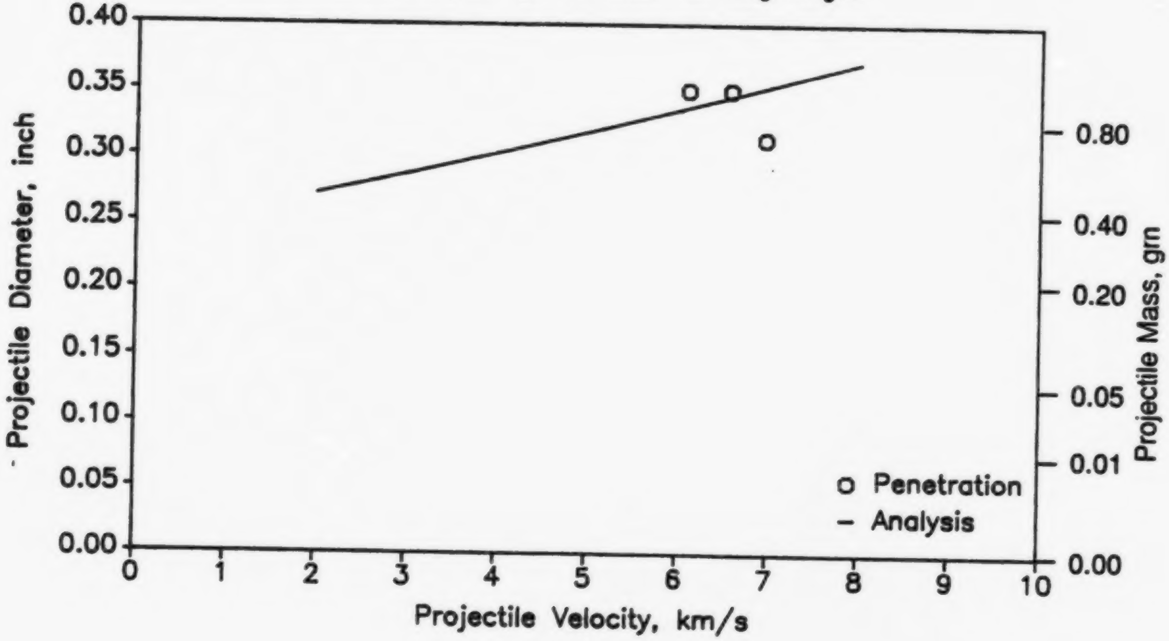

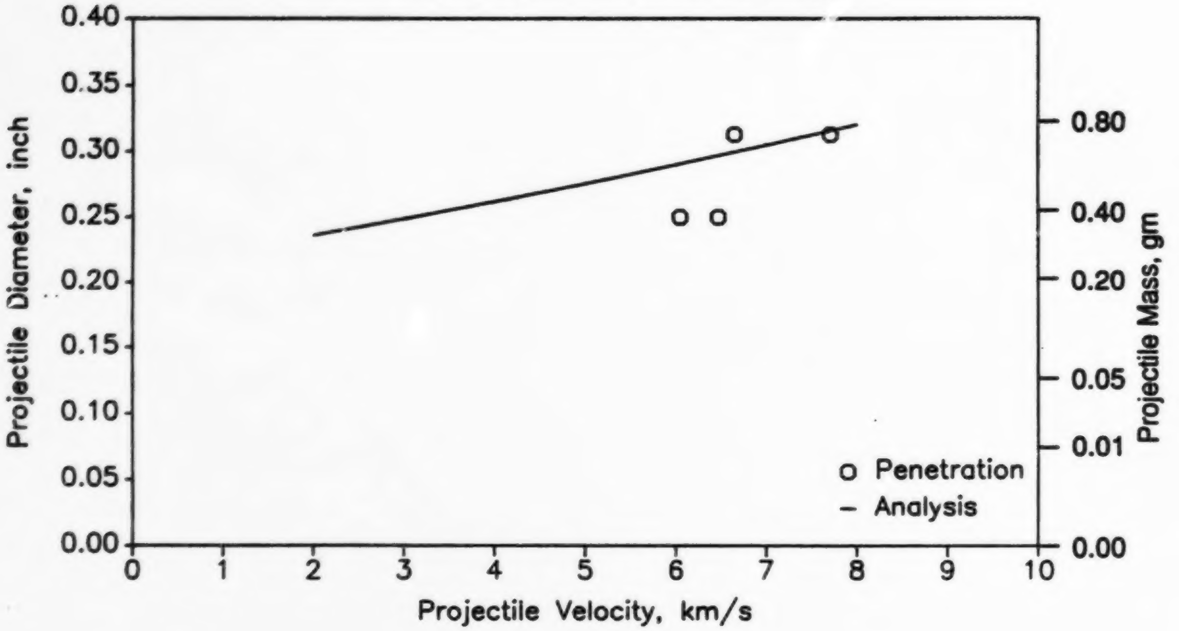

NAS8–36426 Task I Test Series 217
.040 inch Shield, .188 inch Wall
8 inch Spacing, No MLI, 45 deg Angle

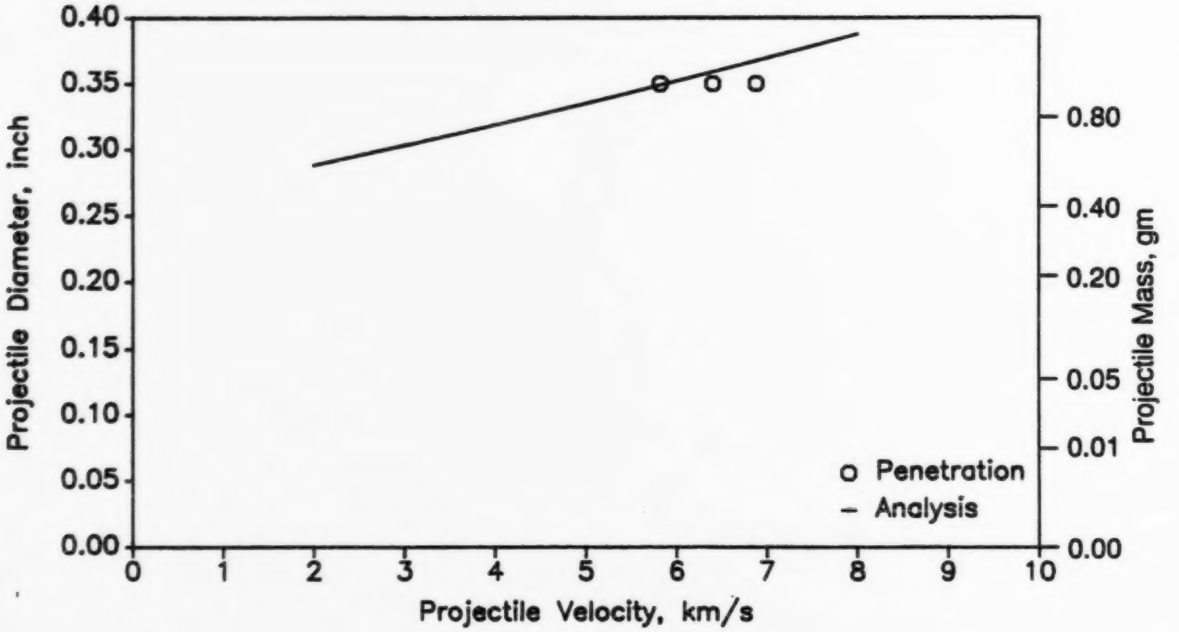

NAS8–36426 Task I Test Series 218
.040 inch Shield, .188 inch Wall
8 inch Spacing, MLI, 45 deg Angle

Lexan Projectile, Task I Test Series 225
.040 inch Shield, .125 inch Shield
4 inch Spacing, No MLI, 0 deg Angle

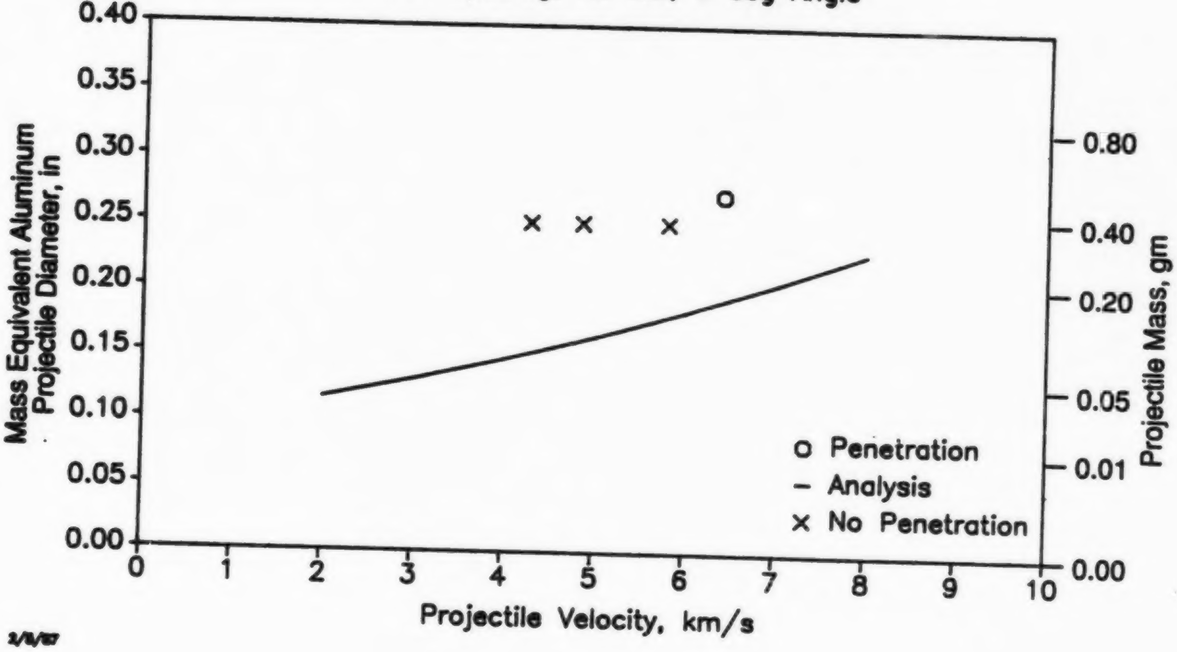

NAS8–36426 Task I Test Series 226
.032 inch Shield. .100 inch Wall
6 inch Spacing, MLI, 45 deg Angle

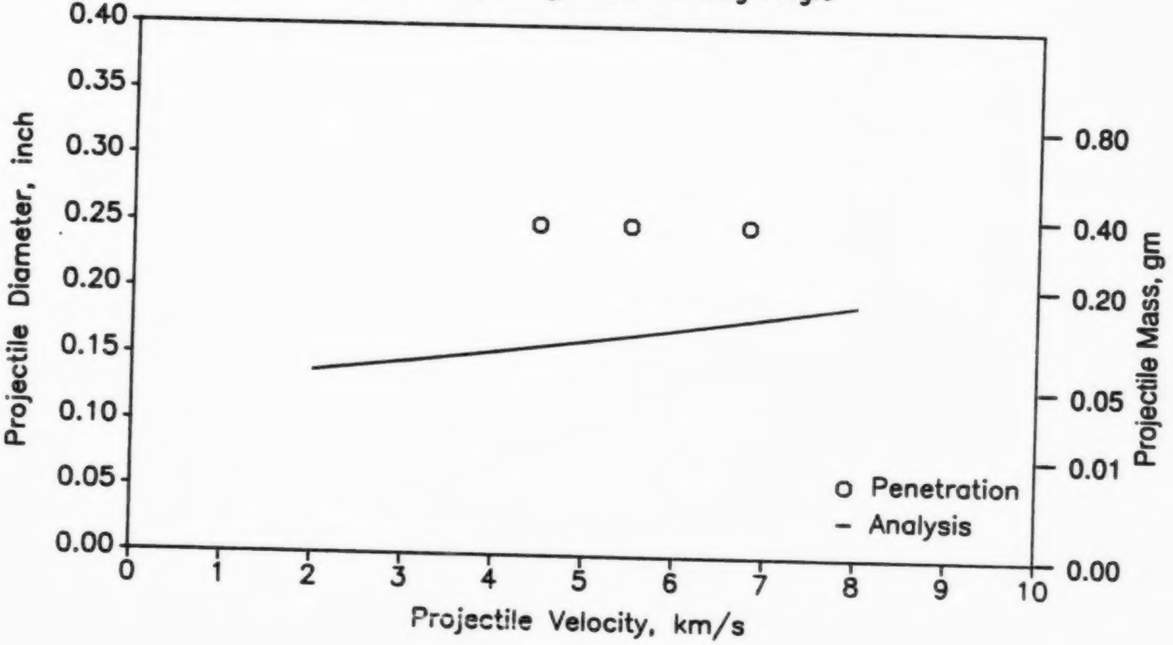

NAS8–36426 Task I Test Series 227
.032 inch Shield, .063 inch Wall
6 inch Spacing, MLI, 45 deg Angle

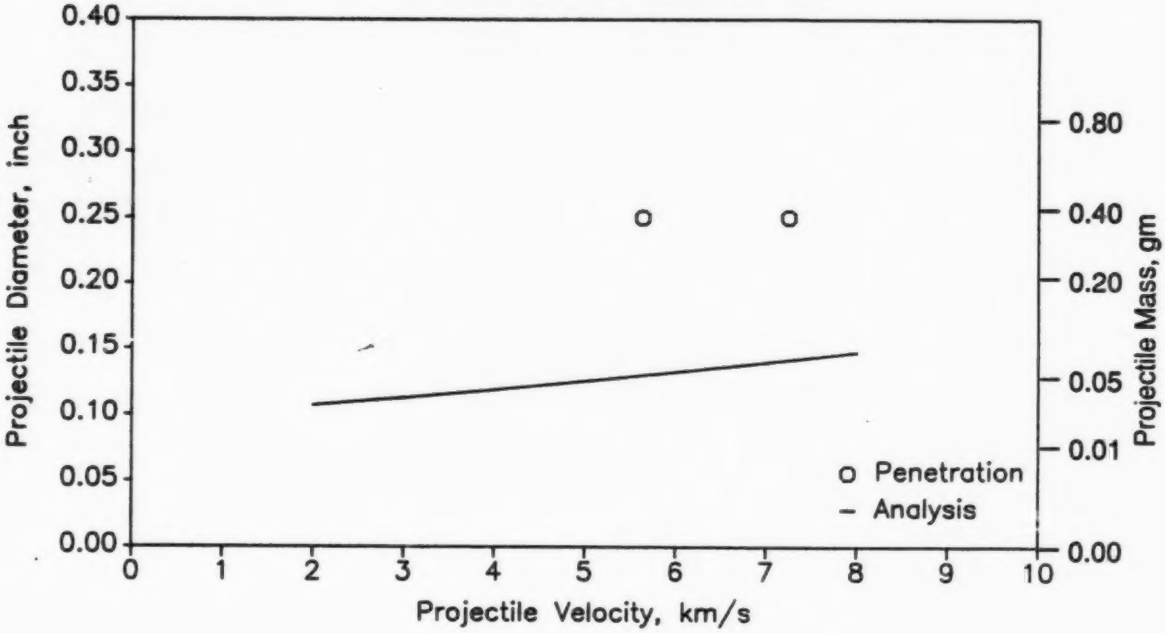

NAS8–36426 Task I Test Series 228
.032 inch Shield, .188 inch Wall
4 inch Spacing, No MLI, 0 deg Angle

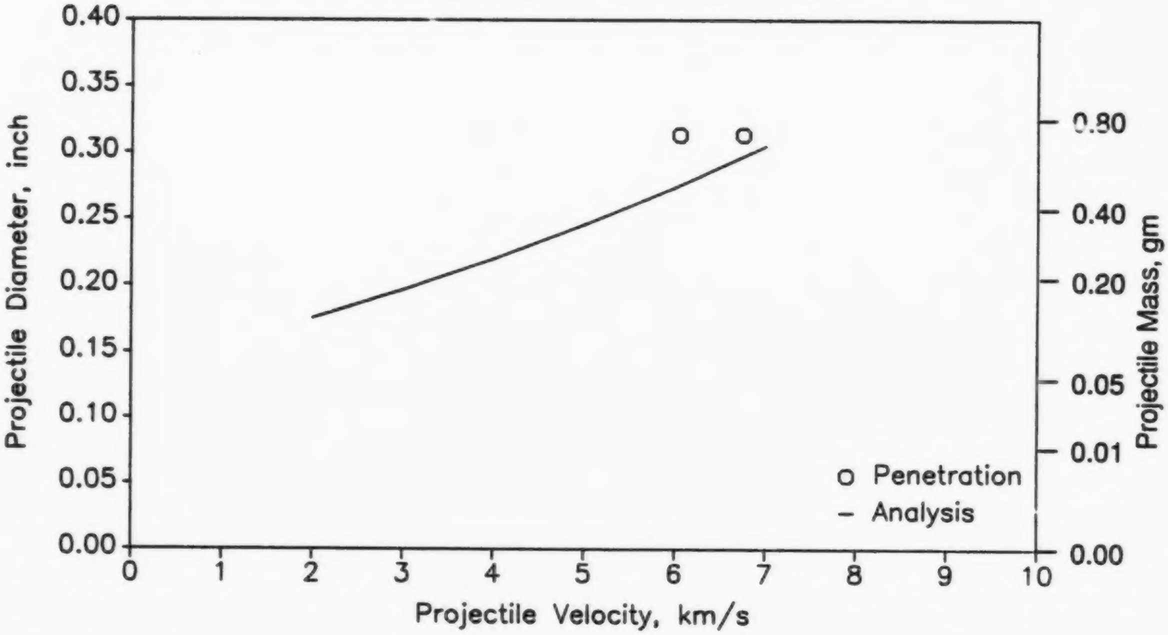

NAS8-36426 Task I Test Series 229
.080 inch Shield, .188 inch Wall
4 inch Spacing, MLI, 0 deg Angle

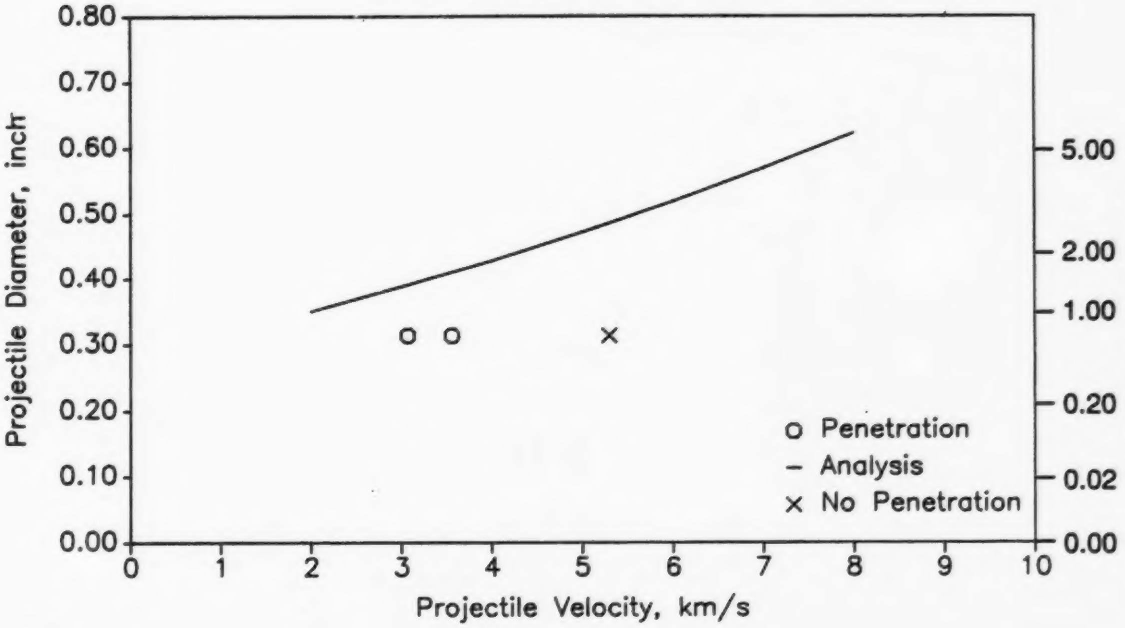

2/3/87